Methods in Molecular Biology 1293

Springer Protocols

Maria del Mar Vivanco *Editor*

Mammary Stem Cells

Methods and Protocols

Humana Press

METHODS IN MOLECULAR BIOLOGY

Series Editor
John M. Walker
School of Life and Medical Sciences
University of Hertfordshire
Hatfield, Hertfordshire, AL10 9AB, UK

For further volumes:
http://www.springer.com/series/7651

Mammary Stem Cells

Methods and Protocols

Edited by

Maria del Mar Vivanco

CIC bioGUNE, Technological Park of Bizkaia, Derio, Spain

Humana Press

Editor
Maria del Mar Vivanco
CIC bioGUNE
Technological Park of Bizkaia
Derio, Spain

ISSN 1064-3745 ISSN 1940-6029 (electronic)
Methods in Molecular Biology
ISBN 978-1-4939-2518-6 ISBN 978-1-4939-2519-3 (eBook)
DOI 10.1007/978-1-4939-2519-3

Library of Congress Control Number: 2015939081

Springer New York Heidelberg Dordrecht London

Printed on acid-free paper

Humana Press is a brand of Springer
Springer Science+Business Media LLC New York is part of Springer Science+Business Media (www.springer.com)

Preface

The concept of stem cells was first postulated more than a century ago, and over the last few years it has become a focus of interest and discussion even in nonscientific circles. The fact that this book is dedicated to Mammary Stem Cells reflects the attention that these cells have recently received and, as a consequence, many of the variety of approaches that researchers are using to investigate their properties and function are discussed here. Studying stem cells from the healthy mammary gland may not appear as relevant as the intriguing work presently being carried out with adult stem cells from other tissues, such as the heart or the nervous system, which epitomizes the great hope and potential for regenerative medicine in the future. However, understanding the role that stem cells play during development and in the physiology of the mammary gland is not only interesting in its own right but also essential to understand the molecular mechanisms underlying the alterations that lead to breast cancer, particularly when considering the hypothesis that the molecular basis of tumorigenesis is a stem/progenitor cell gone awry. Thus, the identification of normal and breast cancer stem cells more than a decade ago has offered a new vision of this heterogeneous disease and new hopes for its prognosis and treatment.

The collection of chapters in this book aims to guide the researcher interested in mammary stem cells, to isolate them and characterize them, at various different levels. Max Wicha, one of the protagonists in the field, opens the book with an extensive introduction to the subject that takes us from the nineteenth century to the current state of the art and a look into the future implications of targeting these cells in the clinic. Mammary cell lineage specification occurs during embryogenesis and thus Chapter 2 presents a protocol that allows the study of progenitor cells during embryonic mammary development ex vivo. The following two chapters provide guidance and experimental details that should help a researcher to start isolating stem cells using fluorescent-activated cell sorting. Once the stem/progenitor cells have been identified and isolated, there is a wide variety of methods to study them. Omics techniques are quickly becoming very informative tools, and there are three chapters that discuss DNA and mRNA sequencing, as well as proteomics techniques to assist in profiling cells in a more efficient manner. Chapter 8 focuses on lentiviral cell transduction, which provides an invaluable method to stably modify gene expression and facilitate functional studies. Transplantation studies have been considered the gold standard to demonstrate normal and cancer stem cell potential, and there are two chapters that provide detailed protocols to investigate mammary gland development and tumorigenesis by taking advantage of the mammary fat pads of mice. A more recent addition to the experimental alternatives to study stem cells is in vivo lineage tracing, which allows the researcher to track cell fate in situ, and this is discussed in detail in Chapter 11. Cancer stem cells not only function as tumor initiating cells but also can be implicated in resistance to therapy and disease dissemination. The finding that these cells display properties that allow them to establish themselves in a different environment is investigated in two chapters, which aim to follow stem cells from their initial niche to the new microenvironment at their metastasis site, to study their metastatic re-initiation capabilities and to establish an experimental system that allows monitoring of the survival, dormancy, and proliferation of

disseminated cancer cells. Finally, the last chapters are striking examples of how scientists are reaching out into other areas, from biology to physics and mathematics and back to biomedicine.

I hope that this book, by including some of the most basic techniques and exciting new developments, will help members of the scientific community new to the field to explore the behavior of stem cells and to learn how to tackle them. This knowledge should guide the design of new and complimentary strategies to be applied in the clinic with the final aim of fighting breast cancer.

Derio, Spain ***Maria del Mar Vivanco***

Contents

Contributors

Renée van Amerongen • *Section of Molecular Cytology, Swammerdam Institute for Life Sciences, University of Amsterdam, Amsterdam, The Netherlands*

Ana M. Aransay • *Genome Analysis Platform, CIC bioGUNE & CIBERehd, Derio, Spain*

Enrique J. Arenas • *Oncology Program, Institute for Research in Biomedicine (IRB-Barcelona), Barcelona, Spain*

L.M. Arendt • *Developmental, Molecular, and Chemical Biology Department, Sackler School of Graduate Biomedical Sciences, Tufts University School of Medicine, Boston, MA, USA; Raymond and Beverly Sackler Laboratory for the Convergence of Biomedical, Physical and Engineering Sciences, Molecular Oncology Research Institute, Tufts Medical Center, Boston, MA, USA; Department of Comparative Biosciences, School of Veterinary Medicine, University of Wisconsin-Madison, Madison, WI, USA*

Ebrahim Azizi • *Department of Internal Medicine, University of Michigan, Ann Arbor, MI, USA*

Laura Barcena • *Genome Analysis Platform, CIC bioGUNE, Derio, Spain*

Fariba Behbod • *Pathology and Laboratory Medicine, University of Kansas Medical Center, Lawrence, Kansas City, USA*

René B.H. Braakman • *Department of Medical Oncology, Erasmus MC Cancer Institute, University Medical Center Rotterdam, Rotterdam, The Netherlands; Postgraduate School of Molecular Medicine, Erasmus University Medical Center, Rotterdam, The Netherlands; Center for Translational Molecular Medicine, Eindhoven, The Netherlands*

Steven A. Carr • *Broad Institute of MIT and Harvard, Cambridge, MA, USA*

Shawn G. Clouthier • *Department of Internal Medicine, University of Michigan, Ann Arbor, MI, USA*

Yadwinder Deol • *Department of Internal Medicine, University of Michigan, Ann Arbor, MI, USA*

Marie-Ange Deugnier • *Centre de Recherche, UMR144, CNRS, Institut Curie, PSL Research University, Paris, France*

Gabriela Dontu • *Stem Cell Group, Guy's Hospital, King's College London School of Medicine, London, UK; Research Oncology, Division of Cancer Studies, Guy's Hospital, King's College London, London, UK*

Marisa M. Faraldo • *Centre de Recherche, UMR144, CNRS, Institut Curie, PSL Research University, Paris, France*

Sylwia Gawrzak • *Oncology Program, Institute for Research in Biomedicine (IRB-Barcelona), Barcelona, Spain*

Philipp Getto • *Fachrichtung Mathematik, Institut fur Analysis, TU Dresden, Dresden, Germany; Basque Center for Applied Mathematics (BCAM), Bilbao, Spain*

Marina A. Glukhova • *Centre de Recherche, UMR144, CNRS, Institut Curie, PSL Research University, Paris, France*

Roger R. Gomis • *Oncology Program, Institute for Research in Biomedicine (IRB-Barcelona), Barcelona, Spain; Institució Catalana de Recerca i Estudis Avançats (ICREA), Barcelona, Spain*

Aintzane Gonzalez-Lahera • *Genome Analysis Platform, CIC bioGUNE & CIBERehd, Derio, Spain*

Marc Guiu • *Oncology Program, Institute for Research in Biomedicine (IRB-Barcelona), Barcelona, Spain*
Beatrice A. Howard • *Division of Breast Cancer Research, Breakthrough Breast Cancer Research Centre, The Institute of Cancer Research, London, UK*
Richard Iggo • *Bergonié Cancer Institute, University of Bordeaux, Bordeaux, France*
Oihana Iriondo • *CIC bioGUNE, Technological Park of Bizkaia, Derio, Spain*
Naoko Kogata • *Division of Breast Cancer Research, Breakthrough Breast Cancer Research Centre, The Institute of Cancer Research, London, UK*
Eric Kuhn • *Broad Institute of MIT and Harvard, Cambridge, MA, USA*
Charlotte Kuperwasser • *Developmental, Molecular, and Chemical Biology Department, Sackler School of Graduate Biomedical Sciences, Tufts University School of Medicine, Boston, MA, USA; Raymond and Beverly Sackler Laboratory for the Convergence of Biomedical, Physical and Engineering Sciences, Molecular Oncology Research Institute, Tufts Medical Center, Boston, MA, USA*
Roderick Y.H. Lim • *Biozentrum and The Swiss Nanoscience Institute, University of Basel, Basel, Switzerland*
Suling Liu • *School of Life Sciences, University of Science and Technology of China, Hefei, China*
Ming Luo • *Department of Internal Medicine, University of Michigan, Ann Arbor, MI, USA*
Nuria Macias-Camara • *Genome Analysis Platform, CIC bioGUNE, Derio, Spain*
Tommaso De Marchi • *Department of Medical Oncology, Erasmus MC Cancer Institute, Erasmus University Medical Center, Rotterdam, The Netherlands; Postgraduate School of Molecular Medicine, Erasmus University Medical Center, Rotterdam, The Netherlands*
Anna Marciniak-Czochra • *Interdisciplinary Center for Scientific Computing and BIOQUANT, Institute of Applied Mathematics, Heidelberg University, Heidelberg, Germany*
Rebecca Marlow • *Breakthrough Breast Cancer Research Unit, Guy's Hospital, King's College London School of Medicine, London, UK*
Sunitha Nagrath • *Department of Chemical Engineering, University of Michigan, Ann Arbor, MI, USA*
Milica Pavlovic • *Oncology Program, Institute for Research in Biomedicine (IRB-Barcelona), Barcelona, Spain*
Marija Plodinec • *Biozentrum and The Swiss Nanoscience Institute, University of Basel, Basel, Switzerland*
Miriam Rábano • *CIC bioGUNE, Technological Park of Bizkaia, Derio, Spain*
Elodie Richard • *Bergonié Cancer Institute, University of Bordeaux, Bordeaux, France*
José Schneider • *Facultad de Ciencias de la Salud, Universidad Rey Juan Carlos, Madrid, Spain*
Anieta M. Sieuwerts • *Department of Medical Oncology, Erasmus MC Cancer Institute, University Medical Center Rotterdam, Rotterdam, The Netherlands; Postgraduate School of Molecular Medicine, Erasmus University Medical Center, Rotterdam, The Netherlands; Center for Translational Molecular Medicine, Eindhoven, The Netherlands*
Arzu Umar • *Laboratory of Breast Cancer Genomics and Proteomics, Department of Medical Oncology, Erasmus MC Cancer Institute, University Medical Center Rotterdam, Rotterdam, The Netherlands; Postgraduate School of Molecular Medicine, Erasmus University Medical Center, Rotterdam, The Netherlands; Center for Translational Molecular Medicine, Eindhoven, The Netherlands*
María d.M. Vivanco • *CIC bioGUNE, Technological Park of Bizkaia, Derio, Spain*
Max S. Wicha • *Department of Internal Medicine, University of Michigan, Ann Arbor, MI, USA*
A. Wronski • *Developmental, Molecular and Chemical Biology Department, Sackler School of Graduate Biomedical Sciences, Tufts University School of Medicine, Boston, MA, USA; Raymond and Beverly Sackler Laboratory for the Convergence of Biomedical, Physical and Engineering Sciences, Molecular Oncology Research Institute, Tufts Medical Center, Boston, MA, USA*

Chapter 1

Breast Cancer Stem Cells: Current Advances and Clinical Implications

Ming Luo, Shawn G. Clouthier, Yadwinder Deol, Suling Liu, Sunitha Nagrath, Ebrahim Azizi, and Max S. Wicha

Abstract

There is substantial evidence that many cancers, including breast cancer, are driven by a population of cells that display stem cell properties. These cells, termed cancer stem cells (CSCs) or tumor initiating cells, not only drive tumor initiation and growth but also mediate tumor metastasis and therapeutic resistance. In this chapter, we summarize current advances in CSC research with a major focus on breast CSCs (BCSCs). We review the prevailing methods to isolate and characterize BCSCs and recent evidence documenting their cellular origins and phenotypic plasticity that enables them to transition between mesenchymal and epithelial-like states. We describe in vitro and clinical evidence that these cells mediate metastasis and treatment resistance in breast cancer, the development of novel strategies to isolate circulating tumor cells (CTCs) that contain CSCs and the use of patient-derived xenograft (PDX) models in preclinical breast cancer research. Lastly, we highlight several signaling pathways that regulate BCSC self-renewal and describe clinical implications of targeting these cells for breast cancer treatment. The development of strategies to effectively target BCSCs has the potential to significantly improve the outcomes for patients with breast cancer.

Key words Cancer stem cells (CSCs), Breast cancer, Circulating tumor cells (CTCs), Phenotypic plasticity, Patient-derived xenograft (PDX)

1 Introduction

The mammary epithelium is mainly composed of two distinct lineages: an inner layer of luminal epithelial cells and an outer layer of basal/myoepithelial cells. At puberty, the rudimentary mammary epithelial trees, under the influence of sex hormones including estrogen and progesterone, expand considerably to form an elaborate branching network terminating in small lobular structures called terminal ductal lobular units (TDLU, for women) [1, 2]. In late pregnancy, the epithelium compartment attains maximal development, and luminal epithelial cells in TDLU undergo robust proliferation and differentiation to form lobular-alveolar buds called

Maria del Mar Vivanco (ed.), *Mammary Stem Cells: Methods and Protocols*, Methods in Molecular Biology, vol. 1293,
DOI 10.1007/978-1-4939-2519-3_1,

secretory alveoli that produce milk during lactation [3]. After weaning, these lobular-alveolar structures regress with massive apoptosis, and the mammary glands remodel to a virgin-like state for the next pregnancy cycle [3, 4]. The dynamic features of the mammary gland strongly suggest the existence of stem-like cells with the mammary epithelium. Indeed, early transplantation studies using mouse mammary fat pad segments as well as retroviral labeling of mammary epithelial cells revealed that the mammary epithelium is maintained by a multipotent mammary stem cell compartment [5, 6]. Recent prospective isolation and characterization of mammary stem cells and progenitor populations in the mouse [7–10] and human [11–15] mammary gland provide further evidence that the mammary epithelium is organized in a hierarchical manner, and that a single mammary stem cell (MaSC), which resides in the basal/myoepithelial layer, can functionally reconstitute a mammary gland by giving rise to differentiated progenies through various lineage-restricted progenitor cells [8, 9, 16].

Despite a longstanding relationship between tumorigenesis and stem cell biology, it is only recently that advances in stem cells biology have enabled direct testing of this hypothesis. Only recently, John Dick's team provided the first evidence that human acute myeloid leukemia is organized as a hierarchy that originates from a primitive hematopoietic cell with self-renewal capacity [17]. Breast cancer, analogous to the hierarchical organization of the normal mammary epithelium, is also characterized as a highly heterogeneous disease. The heterogeneity of breast cancers is manifested by their classification into a number of distinct subtypes, each with a characteristic transcriptome and molecular expression signature [16]. There is now substantial evidence that breast cancer is hierarchically organized and driven by a small fraction of tumor cells that display stem cell properties [18–20]. This small population of breast cancer stem cells (BCSCs), also termed breast cancer initiating cells, were first identified among solid tumors by virtue of their expression of the cell surface markers $EpCAM^+$, $CD24^-$, and $CD44^+$ [21]. As few as 100 cells bearing this phenotype were able to produce tumors in immune deficient NOD/SCID mice, whereas over 100-fold greater cells that did not bear this phenotype was non-tumorigenic. Furthermore, tumors generated from $EpCAM^+CD24^-CD44^+$ BCSCs recapitulated the cell type heterogeneity of the initial tumor with a small fraction of tumor cells express the same stem-like signature, while the majority of bulk tumor cells do not. More recently, it has been shown that both normal and malignant breast stem cells express high level of the enzyme aldehyde dehydrogenase (ALDH) as assessed by the Aldefluor assay (Stem Cell Technologies, Inc., Vancouver, British Columbia, Canada). Moreover, ALDH1 expression serves as a predictor of poor clinical outcome in breast cancers [22]. Interestingly, the $EpCAM^+CD24^-CD44^+$ and $ALDH^+$ populations across different

subtypes of breast cancers identify anatomically distinct BCSCs with respective EMT (epithelial-to-mesenchymal transition) and MET (mesenchymal-to-epithelial transition) gene expression profiles, and they dynamically transition between the mesenchymal and epithelial states reflective of their normal counterparts in the mammary epithelial hierarchy [23].

The cancer stem cell (CSC) hypothesis and the prospective isolation and identification of a small fraction of highly tumorigenic cells with stem cell properties in leukemia, breast cancers and subsequently from a wide variety of other malignancies including that of the brain [24], prostate [25, 26], colon [27, 28], pancreas [29], liver [30, 31], lung [32], and head and neck [33] in the past decade has led to a paradigm shift in terms of how cancers form, progress and relapse. In this chapter, we provide a historical review and current state of knowledge on CSCs with a major focus on BCSCs, especially regarding the prevailing methods to isolate and characterize these cells, their potential cellular origin and phenotypic plasticity, and the role of BCSCs in promoting metastasis and treatment resistance of breast cancer. We also highlight the use of circulating tumor cells (CTCs) and patient-derived xenograft (PDX) models in preclinical breast cancer research, the main signaling pathways regulating BCSC self-renewal, and potential therapeutic approaches and clinical implications of targeting these cells for breast cancer treatment.

2 Stemness as a Concept in Cancer Biology

2.1 CSC Model as a Cellular Mechanism of Carcinogenesis and Tumor Heterogeneity

Although oncology researchers have only recently began to probe cancers for tumor stem cells, the concept of stem-driven carcinogenesis dates back to the middle of the nineteenth century [34]. The German pathologist Rudolf Virchow proposed in 1855 that cancer arises from newly activated embryonic-like cells resident in a once dormant state in mature tissue [34–36]. More than 150 years later direct evidence for the existence and importance of CSCs in tumor biology emerged. For years, clinicians and research scientists have recognized that the behavior of metastatic cancers is highly reminiscent of that of stem cells. However, CSCs could not be identified until specific cell surface protein markers became available for distinguishing a rare population of cells present in acute myeloid leukemia [17]. These CSCs resident in the peripheral blood of patients with leukemia were found to be capable of initiating leukemia—at approximately 1 in every 250,000 cells—when transferred into immune-compromised mice. Moreover, subsequent analysis of populations of leukemia-initiating cells from various subtypes of the disease indicated that these cells are primitive, in other words, they are most closely related to nascent hematopoietic blood-forming cells rather than to more

differentiated, function-specific blood cells. The identification of leukemia-initiating cells subsequently fostered attempts to isolate and characterize CSCs in solid tumors. Particularly, during the past decade stem cell-like populations have been identified in benign and malignant tumors of the breast, colon, brain, pancreas, liver, prostate, head and neck, and many other tissues and in melanoma [21, 22, 24–33, 37–41]. The inability to identify reliable markers capable of reliably discriminating CSCs was a major impediment to progress within this field particularly when there is ample evidence that a presumptive CSC population exists for many tissue malignancies. In other cancers in which CSCs remain to be identified, researchers are beginning to investigate known stem cell markers in the various cancer cell populations in an effort to derive novel targeted therapeutics. Through this approach solid evidence supporting the role of CSCs in various cancers has materialized in recent years. These findings provide strong supporting rationale in favor of the hypothesis that a stem/early primitive progenitor cell gone awry could explain the molecular basis of tumorigenesis.

The reemergence and establishment of the CSC model as a cellular mechanism to probe tumor heterogeneity represents one of the major advances in cancer biology over the past decade. The CSC model of tumorigenesis is fundamentally different from the classic stochastic or clonal evolution model, which proposes that tumors arise via random mutation and clonal selection. According to the stochastic model, all cells within a tumor have equal possibility to acquire genetic mutations necessary to drive tumor initiation and growth. Random accumulation of genomic abnormities may lead to the generation of divergent, but coexisting tumor cell clones, which may account for intratumoral heterogeneity. However, this view of tumorigenesis is hard to reconcile with recent discoveries that only a small fraction of tumor cells harboring a "tumor initiating signature" can efficiently generate secondary tumors that recapitulate the same heterogeneous cell populations as the initial tumor. Distinct from the stochastic model, the CSC hypothesis postulates that, in the breast as well as other tissues, cancer arises from stem-like cells with dysregulated self-renewal capability. Based on this model, cancer is derived from cells harboring tumorigenic mutations and/or epigenetic modifications, which endow deregulated self-renewal capacity in these cells. Tumorigenic mutations and/or epigenetic modifications are more likely to occur and accumulate in tissue stem cells and/or their early progenitor cells due to their relatively long lifespan, leading to formation of CSCs. Alternatively, these genetic and epigenetic aberrations could hit more terminal differentiated cell populations, leading to a dedifferentiation process and endowing these cells with stem cell properties. In both scenarios, CSCs are at the top of the hierarchy to drive tumor initiation, growth, and progression. Like their normal counterparts, being able to self-renew and differentiate are two

hallmarks of CSCs regardless of their cellular origins. The self-renewal process drives tumor initiation and growth, while differentiation helps to generate the bulk tumor cells and maintain tumor cell heterogeneity.

2.2 CSCs Are Not Necessarily Rare

Several studies have questioned the rarity of tumor cells with stem cell properties and tumor-initiating capacity as well as the xenotransplantation assay used to assess these cell populations. A recent publication by Sean Morrison's group suggested that melanoma cells did not in fact follow a stem cell model [42]. Therein they discovered through the use of a highly immune-compromised NOD/SCID Interleukin-2 Receptor gamma chain deficient (IL-2Rγ$^{-/-}$) mouse model that tumor-initiating cell frequency rose dramatically (up to 25 % versus one in a million when using conventional NOD/SCID mice). The IL-2Rγ$^{-/-}$ NOD/SCID (NSG) mice lack NK function and are less able to reject tumor xenografts than the parental NOD/SCID mice. Another study supported Morrison's contention that melanoma does not arise from stem cells. Using the H3K4 demethylase JARID1B as a biomarker, Roesch and colleagues characterized a small subpopulation of slow-cycling melanoma cells that cycle with doubling times of more than 4 weeks within the rapidly proliferating main tumor population [43]. Knockdown of JARID1B led to an initial acceleration of tumor growth followed by exhaustion, suggesting that the JARID1B-positive subpopulation was essential for continuous tumor growth. Furthermore, JARID1B negative cells could become positive and a single melanoma cells irrespective of selection were found to be tumorigenic, suggesting that melanoma heterogeneity and maintenance are a dynamic process mediated by a temporarily distinct subpopulation [43]. However, this study used only established melanoma cell lines rather than primary tumors. Using primary melanoma cells as well as melanoma cell lines, Fang et al. showed that melanomas can contain a subpopulation of stem-like cells that contribute to heterogeneity and tumorigenesis [41]. Recently, Weissman's lab further demonstrated that human neural crest nerve growth factor receptor CD271 enriched for tumor initiating cells and transplantation of isolated CD271^{+}, but not CD271^{-}, melanoma cells into engrafted human skin or bone in T-, B-, and natural-killer-deficient *Rag2*$^{-/-}$γc$^{-/-}$ mice resulted in melanoma and metastasized [44]. Besides CD271 as a marker for melanoma CSCs, recently the expression of ALDH1 has been shown to enrich human melanoma stem cells [45] suggesting that tumorigenic cancer stem cells do exist in human melanomas. Additional CSC research will undoubtedly shed more light on this line of inquiry.

Similar to melanomas, CSCs may not necessarily constitute a minor component of the tumor in other tissue malignancies. Kelly et al. (2007) showed that, when lymphoma and leukemia of mouse

origin are transplanted into histocompatible mice, a very high frequency (at least 1 in 10) of the tumor cells can seed tumor growth, suggesting that the low frequency of tumor-sustaining cells observed in xenotransplantation studies may reflect the limited ability of human tumor cells to adapt to growth in a foreign mouse environment [46]. In breast cancer, poorly differentiated and high-grade tumors displayed higher content of BCSCs than did low-grade well-differentiated tumors such as luminal breast cancers. In terms of ALDH marker expression, the basal breast carcinoma cell lines contain a higher content of Aldefluor-positive cells compared to luminal breast cancer cell lines [47]. Moreover, ALDH1 expression in human breast cancer tissues is associated with poor clinical outcome [22] and the content of ALDH1-positive cancer stem cells also predict engraftment of primary human breast tumors in NOD/SCID mice [48]. Using transcriptional profile of PKH26-label-retaining mammary epithelial cells (human MaSC signature), a recent study also supported the notion that the heterogeneous phenotypical and molecular traits of human breast cancers are a function of their CSC content [49]. Thus, in high-grade or advanced stages of breast tumors, the pool of BCSCs is greatly increased and they may not represent the minor population of cells found in the early-staged tumors.

3 Isolation and Identification of BCSCs

In order to study the basic attributes of CSCs, it is necessary to first identify, isolate, purify, and characterize these cells by employing techniques that enable one to distinguish them from the bulk tumor cell population. This objective remains extremely challenging because CSCs often constitute a small fraction of the total cell population of a tumor and may express the same cell surface markers as their more differentiated counterparts. A major challenge in the field today is to define specific CSC markers that are not expressed on differentiated bulk tumor cells. Nevertheless, the functional characteristics of CSCs including self-renewal capability and differentiation potential can be exploited by various in vitro and in vivo assays in order to identify and characterize this important cell population. Among the most useful techniques for identification and enrichment of BCSCs are side population (SP) dye exclusion, specific expression of cell surface markers, aldehyde dehydrogenase activity, tumorsphere culture and label-retention assays such as PKH staining. The putative BCSCs enriched by these techniques can be further validated functionally by the serial transplantation assay in vivo to evaluate their tumorigenic and self-renewal potential.

Dye exclusion relies on the observation that stem cells, as opposed to differentiated cells, have the ability to efflux lipophilic

dyes including Rhodamine or Hoechst owing to their increased expression of the ATP-binding cassette transporter proteins such as ABCG2/BCRP1. This dye exclusion activity results in a so-called SP fraction that can be further quantitated by flow cytometry [50]. Several studies have demonstrated that the SP component is enriched in cells capable of recreating the whole cell population [51]. These observations suggest that the SP fraction may contain stem cells capable of recapitulating a tumor. To date, SP cells have been found in bone marrow, normal solid tissues, tumors, and various cancer cell lines [52, 53]. In human and mouse mammary epithelial cells, SP cells have been reported to contain stem/progenitor cell compartment [54–57]. SP cells have also been identified in different subtypes of human breast cancer cells, which display a more tumorigenic phenotype than the cells do not readily efflux vital dyes [52, 58–60].

Another useful tool for identifying CSCs including BCSCs is flow cytometry utilizing expressed cell surface antigens. In breast and pancreatic cancers, the cell surface markers CD44 and CD24 are commonly used to define a population enriched in CSCs [21, 29, 61, 62]. The $CD24^{-}CD44^{+}$ BCSCs cells possess the ability to self-renew and to differentiate when injected into the mammary fat pad of NOD/SCID mice, resulting in engrafted mammary tumor formation and progression [21]. Although the $CD24^{-}CD44^{+}$ phenotypic markers have been extensively used to isolate BCSCs in different cancer subtypes especially basal-like tumors [63], a recent study showed that both $CD24^{-}CD44^{+}$ and $CD24^{+}CD44^{+}$ cell populations in ERα–negative breast tumors are tumorigenic in murine xenograft models, and a third population of tumor-initiating cells enriched in $CD44^{+}CD49f^{hi}CD133/2^{hi}$ subset displays heightened tumorigenicity and self-renewal in vivo, and the capacity to give rise to functional and molecular heterogeneity [64]. The use of cell surface markers CD49f (α6 integrin) and CD29 (β1 intergrin) together with CD24 (heat stable antigen) or EpCAM (epithelial specific antigen), have been shown to enrich for mammary stem/progenitors in the mouse and human mammary gland [8, 9, 13]. In breast cancer, elevated CD49f expression is associated with reduced survival [65] and knockdown of its partner CD104 decreases in vivo tumorigenicity [66]. Thus, $CD49f^{+}$, combined with $CD44^{+}CD24^{-/low}$ expression signature, may better identify and enrich BCSCs in different breast cancer subtypes.

BCSCs can also be segregated from mixed cell populations using the Aldefluor assay which relies upon aldehyde dehydrogenase (ALDH) activity [67]. ALDH is an enzyme responsible for the oxidation of intracellular aldehydes; it plays a vital role in stem cell differentiation via retinoic acid metabolism [68, 69]. The commercially available Aldefluor kit (StemCell Technologies, Inc., Vancouver, British Columbia, Canada) contains a BODIPY-aminoacetaldehyde (BAAA) substrate labeled

with a fluorochrome that is converted into BODIPY-aminoacetate (BAA) by ALDH catabolism [68]. Cells expressing high ALDH activity have brighter fluorescence and can be enumerated on a standard cytometer when DEAB (an inhibitor of the enzymatic reaction) is used as the isotype control for FACS analysis. The Aldefluor assay has been used for both murine and human stem/progenitor populations in many different cancers. Those cancers known to harbor an Aldefluor positive population with stem properties include acute myeloid leukemia [70], breast [22, 47], lung [71], colon [72, 73], head and neck [38], prostate [74], and others. ALDH immunohistochemistry on a number of isoforms can readily identify CSCs within formalin-fixed, paraffin-embedded tissues with the ALDH1-A1 and ALDH1-A3 isoforms being the most preferentially expressed [22]. The combination of Aldefluor positivity with other unique stem cell surface markers such as $CD133^+$ and $CD24^-CD44^+$ has been shown to further label and locate ovarian CSCs and BCSCs in their respective tumor tissue slides [39, 47].

BCSCs can subsequently be sorted and assayed for clonogenic potential in vitro and tumorigenicity in vivo by xenotransplantation using immune-compromised mice. The latter is the gold standard for assessing BCSC activity. Tumorsphere assays have also been frequently used to examine stem/progenitor activity in vitro for many cancers including breast cancer, glioblastoma and other tissue malignancies. Tumorspheres are generated by plating cells in a petri dish or flask under low attachment, serum-free conditions supplemented with B27, hydrocortisone, insulin, fibroblast growth factor (FGF), and epidermal growth factor (EGF) [75]. Those few cells that self-renew under this anchorage-independent condition divide and form tumorspheres. Notably, cells isolated from tumorspheres exhibit multi-lineage differentiation potential when given serum and extracellular matrix such as collagen [75].

A more recent method to characterize CSCs in vitro is the cell membrane label-retaining assay. This assay uses the PKH fluorescent dye series, which consist of a fluorophore attached to a peptide backbone that irreversibly binds to the lipid bilayer of cell membranes [76]. The PKH67/PKH26 dyes that irreversibly bound to the lipid bilayer on cell membranes get equally partitioned among daughter cells during cell division; thus the intensity decreases in an exponential manner with each round of cell cycle [77]. Stem cells including CSCs are usually maintained via an asymmetric self-renewal process, where a stem cell and a daughter cell are formed. Following asymmetric cell division, the stem cell enters a quiescent state, while the daughter cell (known as the transient amplifying cell) undergoes rapid proliferation and differentiation. As a result, the stem cell retains the PKH dye and can thus be identified and isolated by flow cytometry. This method has, for example, been used to label murine hematopoietic stem cells [78];

it has also been used to track the homing of short- and long-term repopulating cells in bone marrow [79] and to detect labeled cells by fluorescence microscopy [80]. The use of PKH dye label-retaining mammosphere assay has recently been used to identify both normal MaSCs and BCSCs [49, 81]. In these studies, normal or malignant mammary epithelial cells were stained with PKH26, grown in primary and secondary mammosphere culture, and subsequently dissociated and sorted for PKH high, low, or negative cell populations. These distinct cell populations were further tested for mammary epithelial repopulating or tumorigenic capacities, and as expected, only the $PKH26^{high}$ cell population was found to enrich for stem cell activities [49, 81]. This method is useful for labeling cells of interest, but these dyes can inadvertently be transferred to surrounding cells confounding results [82]. Therefore, the technique of PKH dye exclusion is most useful when combined with another stem cell characterization assays to validate stem cell phenotypes.

4 Cellular Origins and Phenotypic Plasticity of BCSCs

4.1 BCSCs Transition Between EMT- and MET-Like States

In primary breast xenografts, the $CD24^{-}CD44^{+}$ and $ALDH^{+}$ BCSCs identify minimally overlapping, largely separate cell populations, with each capable of initiating tumors in NOD/SCID mice [22]. However, whether these different phenotypic populations identify distinct or independent BCSCs in the tumor remains an interesting question. Recently, using gene expression profiling of $ALDH^{+}$ and $CD24^{-}CD44^{+}$ BCSCs isolated across different subtypes of human breast cancer tissues together with multi-marker immunofluorescence including CD24, CD44 and ALDH1, it was determined that $CD24^{-}CD44^{+}$ and $ALDH^{+}$ cell populations identify anatomically distinct BCSCs with distinct EMT and MET gene-expression profiles respectively. The EMT-like $CD24^{-}CD44^{+}$ BCSCs are primarily quiescent and localized at the tumor invasive front, while the MET-like BCSCs expressing ALDH1 are recycling, proliferative cells located mainly in the central part of primary tumors [23]. Importantly, the epithelial and mesenchymal states of BCSCs are not static; instead they display a cellular plasticity allowing them to transit between the EMT and MET states [23]. The interconversion of BCSCs from the EMT-like (which is $EpCAM^{-}CD49f^{+}$ that expresses the stem cell markers $CD24^{-}CD44^{+}$) and MET-like (which is $EpCAM^{+}CD49f^{+}$ that expresses the CSC marker ALDH) state, as illustrated in Fig. 1, has been shown to be regulated by microRNA networks including EMT-inducing mir-9, mir-100, mir-221, and mir-155 as well as MET-inducing mir-200, mir-205, and mir-93 [83].

These studies, together with the findings that distinct microRNAs regulate the transition of BCSCs between the $CD24^{-}CD44^{+}$

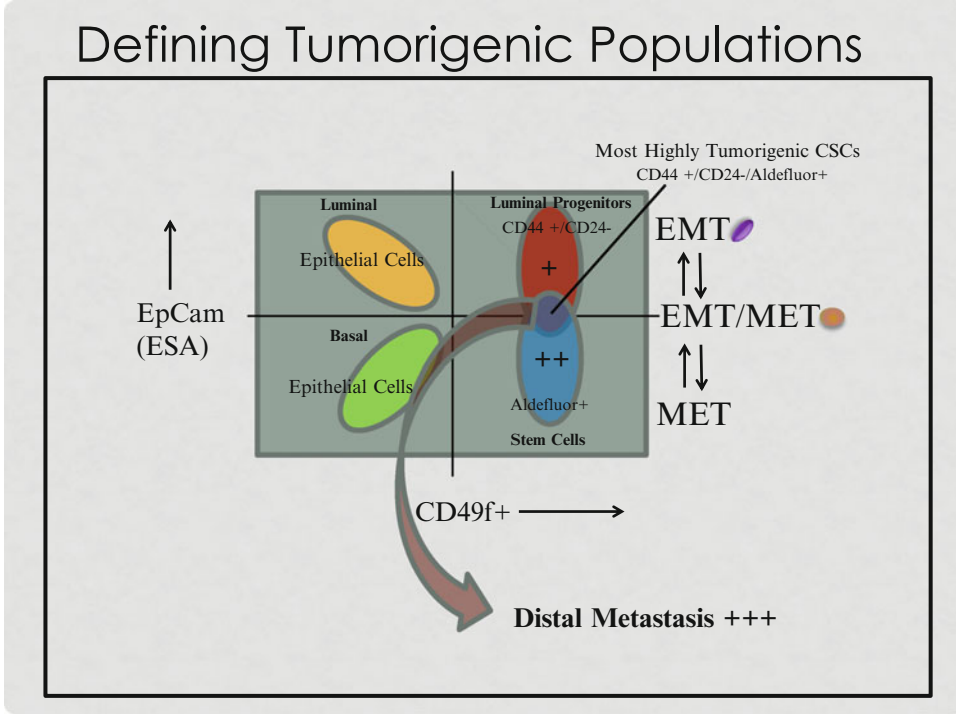

Fig. 1 Breast cancer stem cells can exist in at two interchangeable states, one EMT-like (EpCAM$^-$ CD49f$^+$ that expresses the stem cell markers CD44$^+$ CD24$^-$) and a MET-like population (which is EpCAM$^+$ CD49f$^+$ and expresses the CSC marker ALDH). These stem cells states are interconvertible and are regulated by microRNAs

and ALDH$^+$ phenotypes [83, 84], led to a hypothetical model (Fig. 2) highlighting the role of different BCSC states in tumor growth and metastasis. As illustrated in Fig. 2a, the CD24$^-$CD44$^+$ BCSCs exist in an EMT-like state that are E-cadherin and EpCAM negative, Vimentin positive, and relatively quiescent, whereas the MET-like ALDH+ BCSCs are cycling, and E-cadherin and EpCAM positive, and Vimentin negative. The transition between these states is most likely dictated by the tumor microenvironment. For example, TGF-β generated in the tumor milieu can induce EMT by downregulation of epithelial markers such as E-cadherin and upregulation of EMT-inducing factors, such as Twist and Snail [85–87]. Both the inflammatory immune response [87] and the hypoxic tumor environment [88] have also been reported to induce EMT in cancers. On the other hand, BMP signaling has been reported to induce MET via induction of miR-205 and the miR-200 family of microRNAs that are key regulators of MET [89].

The demonstration that BCSCs exist in two interchangeable epithelial and mesenchymal states also helps define a model of how BCSCs drive primary tumor growth and metastasis. As illustrated in Fig. 2b, in primary breast cancer, the CD24$^-$CD44$^+$ mesenchymal-like BCSCs mediate the tumor invasion toward the basal membrane

surrounding the tumor and into the blood, where they survive due to their intrinsic quiescence and anoikis resistance. After extravasation of the blood circulation system, these mesenchymal-like BCSCs form micro-metastasis in distant organs, where tumor microenvironment in the remote sites induces MET, which is required for BCSC self-renewal and generation of macro-metastasis. The plasticity of BCSCs from a quiescent mesenchymal state to a proliferative epithelial-like state plays a critical role for these cells to establish sizable metastatic nodules in distant organs. Indeed, there is increasing experimental evidence to suggest that such transition, termed colonization, is essential for development of successful macrometastasis [90]. For example, using a spontaneous squamous cell carcinoma mouse model, Tsai et al. recently demonstrated that turning off Twist1 to allow reversion of EMT is essential for disseminated tumor cells to proliferate and form metastases [91].

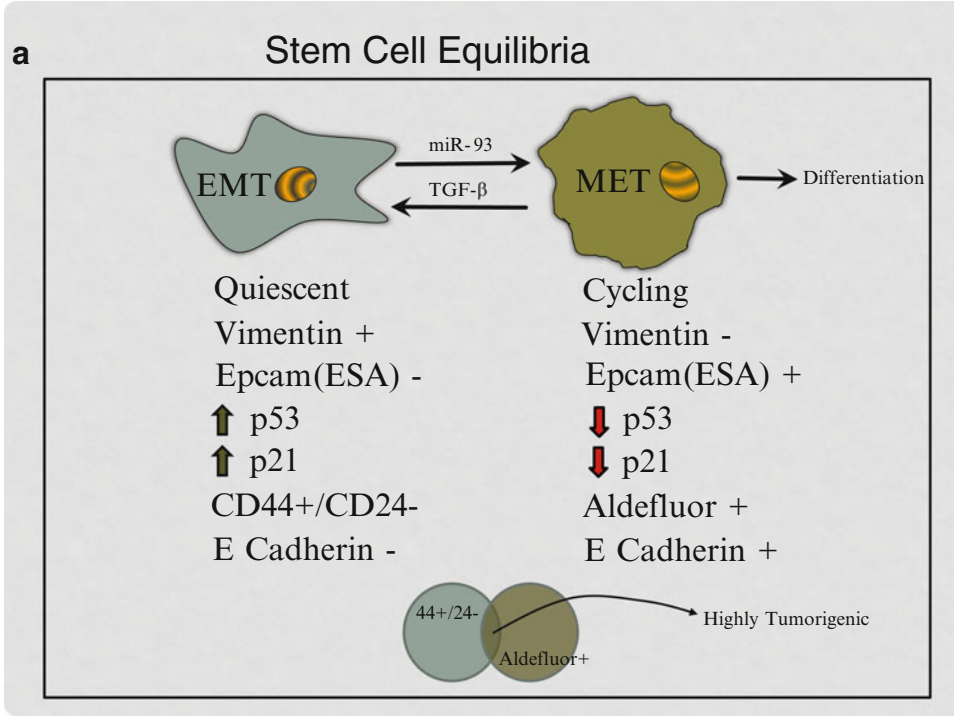

Fig. 2 (**a**) Breast cancer stem cells may exist in an EMT-like state (that are relatively quiescent, E cadherin and ESA negative, Vimentin positive and expresses the stem cell markers $CD44^{+}$ $CD24^{-}$) or MET-like states (that are cycling, E cadherin and ESA positive, Vimentin negative and expresses the stem cell marker ALDH+). A small fraction of stem cells express both EMT and MET markers and these appear to be the most highly tumorigenic population of cancer stem cells. (**b**) BCSCs located inside the tumor mass exist chiefly as MET cells which are highly proliferative and ALDH+. In contrast, EMT CSCs are located at the tumor invasive front and are characterized by $CD44^{+}$ $CD24^{-}$ markers. EMT cells are highly invasive and mediate metastasis. An intermediary CSC state ($CD44^{+}$ $CD24^{-}$ $ALDH^{+}$) that is highly proliferative with invasive potential also resides inside the tumor

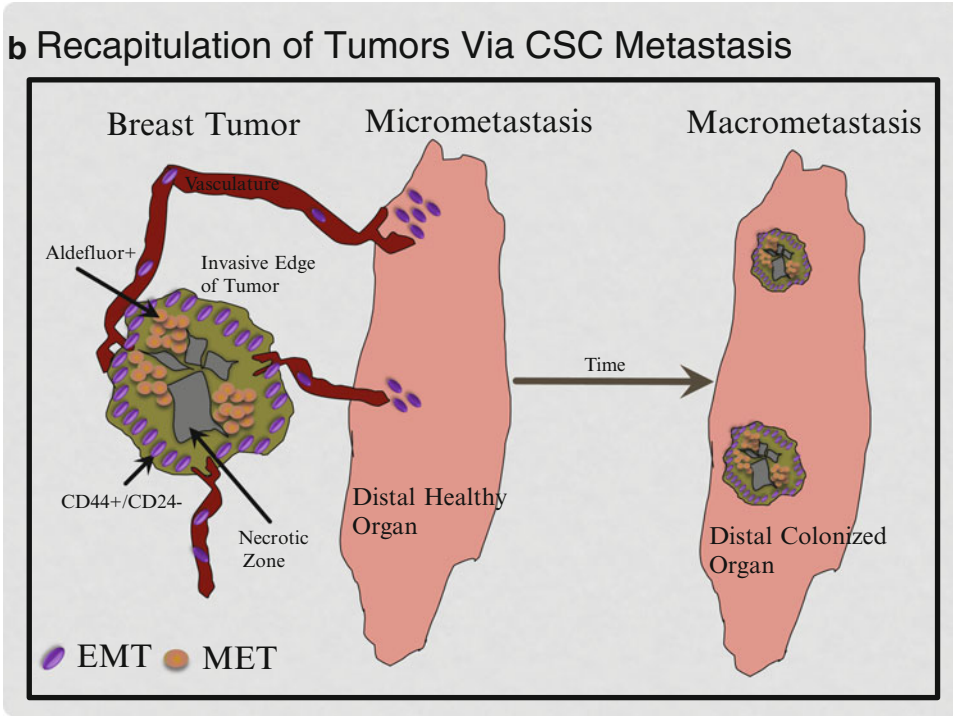

Fig. 2 (continued)

In another study, Ocaña et al. demonstrated that temporal loss of the EMT inducer Prrx1 is required for cancer cells to form lung macrometastasis [92]. In breast cancer, the content of $CD24^{-}CD44^{+}$ BCSCs in the primary tumor correlates with increased risk of distant metastasis. However, distant metastases formed from these tumors frequently show a higher differentiation rate compared to the primary tumor, as manifested by increased expression of the luminal epithelial marker CD24 [11]. Similarly, in mouse model of breast cancer driven by *MMTV-PyMT* oncogene, it has been shown that $CD90^{+}$ circulating tumor cells are responsible for lung metastasis, however, the proportion of $CD90^{+}$ tumor cells decreases again in differentiating and growing metastatic nodules [93]. Furthermore, reexpression of miR-200 family members and subsequently epithelial differentiation was found to promote metastatic colonization of breast cancer cells [94]. Most recently, specific expression of Id1 gene in breast cancer cells undergone EMT has been shown to induce MET through antagonism of Twist1, and this phenotypic switching is required for metastatic colonization in the lung [95].

4.2 Cell Origins of BCSCs and Breast Tumorigenesis

Breast cancers are highly heterogeneous with several distinct subtypes characterized by their distinct histological and molecular expression features. These include luminal breast cancers that express steroid hormone receptors including estrogen receptor (ER)

and progesterone receptor (PR); HER2 positive breast cancers characterized by amplification of the *ErbB2* gene; and basal breast cancers that are triple negative (TN) for the expression of ER, PR, and HER2. Clinically, the classification of breast cancers into these major molecular subtypes greatly facilitates the use of treatment strategies and helps predict treatment response and prognostic relevance. Recent advancement in global gene expression profiling of breast cancers have further subdivided this heterogeneous disease into six different subtypes, including luminal A, luminal B, HER2 overexpressing, basal-like, claudin-low, and normal breast-like [96–99]. The existence of these distinct breast cancer subtypes suggests that mammary oncogenesis may be derived from different cellular origins in the mammary epithelial hierarchy. Alternatively, different subtypes of breast cancers may arise from a common precursor in the mammary epithelium, but different oncogenic events play a major role in determining the distinct tumor subtype.

An intriguing finding from recent gene expression profiling is that, both the $CD24^{-}CD44^{+}$ and $ALDH^{+}$ BCSC subsets isolated in different subtypes of primary breast cancers exhibit a remarkable similarity in their patterns of gene expression, although whole-tumor gene expression profiles are distinct across different subtypes [23]. This finding, coupled with the knowledge that BCSCs transit between the EMT and MET states, suggests a potential common cell of origin for BCSCs across different breast cancer subtypes. Previous studies suggested a potential common cell origin for breast cancer cells that are resistant to chemotherapy [100, 101]. In these studies, gene expression pattern of primary tumors obtained from breast cancer patients after treatment with docetaxel showed a similar genetic profile, irrespective of their original histological phenotype [100]. Furthermore, it has been shown that molecular profile of breast tumors obtained after chemotherapy closely resembles the gene expression profile of untreated $CD24^{-}CD44^{+}$ BCSCs [101]. This BCSC signature was found in TN and hormone sensitive breast cancers treated with neoadjuvant chemotherapy and endocrine therapy respectively [101]. This study suggested that hormone-sensitive luminal breast cancers also contain a subpopulation of mesenchymal-like $CD24^{-}CD44^{+}$ BCSCs, which are hormone-resistant and are enriched following neoadjuvant endocrine therapy.

The relationship between different BCSC populations and their corresponding normal counterparts in the mammary epithelial hierarchy remains controversial. In women carrying *BRCA1* germ line mutations, the relative proportion of $EpCAM^{-}CD49f^{hi}$ basal epithelial cells that containing basal stem cells was shown to be decreased, whereas the proportion of $EpCAM^{+}CD49f^{+}$ luminal progenitor cells increased. This aberrant luminal progenitor cell population also showed increased clonogenic activity compared to non-*BRCA1* mutation carriers. Moreover, genome-wide

transcriptome analyses of different subtypes of breast cancers as well as different mammary epithelial subpopulations in human *BRCA1* mutation carriers revealed that the luminal progenitor gene signature was most strongly associated with the basal subtype of breast cancer, while the basal/mammary stem cell signature was correlated to tumors classified as Normal-like and Claudin-low subtypes [13]. These studies, although suggested aberrant luminal progenitors as the cell origin of *BRCA1* basal breast cancer, could not directly demonstrate a cell origin of *BRCA1* mutation-associated basal breast cancers. Using a mouse model carrying conditional *BRCA1* alleles, Molyneux et al. have further demonstrated that *BRCA1* basal-like breast cancer originates from luminal epithelial progenitors but not from basal mammary stem cells [102]. In this study, specific deletion of *BRCA1* in luminal progenitor cells by *Blg-Cre* led to mammary tumors that are predominantly high grade invasive ductal carcinomas of no special type (IDC-NST), which closely phenocopies human basal *BRCA1* tumors. In contrast, cell-type specific deletion of *BRCA1* in basal stem/myoepithelial compartment by *K14-Cre* generated tumors that are predominantly malignant adenomyoepitheliomas. Several other studies using mouse models and isolated mammary epithelial cell populations also indicated that basal stem cells and mature luminal epithelial cells are not important targets for tumor initiation, but rather luminal progenitor cells are emerging as key players in breast tumorigenesis [103, 104].

Although the aforementioned studies strongly suggest luminal progenitor cells as the origin of basal breast cancer, the relationship of between BCSCs and the stem/progenitor cells in the normal mammary gland remains to be defined. Recent lineage tracing studies of the mouse mammary gland suggested that distinct basal and luminal stem cells give rise to cells restricted to the basal and luminal lineage respectively under normal developmental conditions [105]. However, transplantation of the basal $CD24^{med}CD49f^{hi}$ and luminal $CD24^{hi}CD49f^{low}$ populations into cleared mammary fat pad of recipient mice induces their plasticity and enables either of the stem cell populations to regenerate an entire mammary epithelial tree [106]. The existence of distinct luminal and basal stem cells in the mouse mammary gland prompted us to evaluate if distinct luminal and basal stem cells with regenerative capability exist in the human mammary tissue, and if these stem cell populations are reflective of the $ALDH^+$ and $CD24^-CD44^+$ BCSCs isolated in different subtypes of breast cancers. Indeed, recent studies have demonstrated that the human mammary gland displays a similar hierarchy organization, containing functional luminal stem cells located in the terminal lobules that are $EpCAM^+CD49f^+ALDH^+$, and basal stem cells located in the mammary ducts that are $CD24^-CD44^+EpCAM^-CD49f^+$ [23]. Interestingly, in the luminal compartment, only $EpCAM^+CD49f^+ALDH^+$ luminal stem cells,

which constitute 6 % of total $EpCAM^+CD49f^+$ population, have high colony-forming activity and generate ductal/alveolar structures in 3D Matrigel [23]. These studies suggest that ALDH serves as a functional marker of the luminal stem cells and the self-renewing/proliferative state of $ALDH^+$ luminal stem cells may increase their susceptibility to carcinogenic mutations, making them a logical cell of origin for breast cancer. This notion was supported by studies showing that expansion of lobules containing ALDH1-expressing cells is associated with loss of heterozygosity in *BRCA1* mutation carriers [107]. These studies also suggest that it is the luminal stem cells instead of luminal progenitors that are involved in the tumorigenesis of *BRCA1* basal breast cancer.

The studies from Liu et al. together with recent observations of luminal progenitor cells as the key players in breast tumorigenesis led to a model of breast oncogenesis in which luminal stem cells serve as a common cell origin of breast cancers, but distinct oncogenic events dictate the individual tumor subtype. For example, loss of *BRCA1* or *BRCA1* mutation in the luminal stem cells promotes their tumorigeneis leading to the so-called basal breast cancer. However, further oncogenic events, such as loss of P53 and Pten, may drive EMT and promote the mesenchymal-like claudin-low phenotype. The EMT process could also be induced by the tumor microenvironment, leading to the mesenchymal-like claudin-low phenotype. On the other hand, oncogenic mutations such as the PIK3CA and HER2 amplification in luminal stem cells may promote the luminal and HER2 phenotype respectively.

5 BCSCs and Treatment Resistance

5.1 BCSCs Are Associated with Treatment Resistance

Current antitumor strategies are mainly aimed at shrinking tumor mass by targeting the rapidly proliferating bulk tumor cells. These therapeutic strategies, albeit effective in reducing the size of primary tumors, frequently fail to eradicate advanced tumors and are associated with tumor relapse. The CSC hypothesis suggests that conventional antitumor strategies targeting rapidly proliferating cells may fail to target CSCs that divide infrequently in the tumor. A plethora of studies have indicated that BCSCs are relatively resistant to both ionizing radiation and chemotherapy [108–111] in cultured breast cancer cell lines, in primary mammary tumor cells derived from different mouse models of human breast cancer [112–114], and in patient derived tumor xenografts in mice [109, 115, 116].

The intrinsic resistance of BCSCs to neoadjuvant chemotherapy in the clinical setting has also been documented in a number of studies. Using primary breast cancer cells isolated from tumors treated with neoadjuvant chemotherapy and those resected

from chemotherapy-naive patients, Yu and colleagues examined mammosphere forming activity as well as $CD24^{-}CD44^{+}$ BCSC content in corresponding tumor samples. This study revealed a 14-fold increase in mammosphere forming activity (5.8 % vs. 0.4 %) and eightfold increase in $CD24^{-}CD44^{+}$ enriched population (74 % vs. 9 %) after neoadjuvant chemotherapy [115]. The intrinsic resistance of BCSCs to neoadjuvant chemotherapy was also reported in paired breast cancer core biopsies obtained from 31 patients before and after 12 weeks of treatment with docetaxel or doxorubicin/cyclophosphamide [117]. This study revealed that the percentage of $CD24^{-}CD44^{+}$ BCSCs and tumorsphere forming activity in the residual tumor tissues significantly increased following neoadjuvant chemotherapy. Interestingly, in a separate group of patients with HER2 amplification, treatment with HER2 and EGFR inhibitor Lapatinib following chemotherapy did not increase, but rather slightly decreased the content of $CD24^{-}CD44^{+}$ BCSCs as well as tumorsphere forming activity [117]. Since HER2 overexpression has been show to drive BCSC activity [118], this clinical study suggests that strategies combining BCSC targeting agents (e.g., Trastuzumab and Lapatinib) with conventional chemotherapy hold the potential to overcome BCSC associated treatment resistance and achieve better therapeutic outcomes.

BCSCs can also be enriched by virtue of their expression of ALDH activity and ALDH1 expression in human breast tumors is associated with poor prognosis [22]. Consistent with this observations, a clinical study examining ALDH1 expression in a cohort of primary breast cancer samples treated with sequential paclitaxel and epirubicin-based chemotherapy revealed that ALDH1 positivity was significantly associated with a low pathological complete response (pCR) rate and resistance to the therapy [119]. This study suggests that ALDH1 positive BCSCs also share the properties of resistance to conventional chemotherapy.

5.2 Mechanisms Involving Treatment Resistance in BCSCs

5.2.1 BCSCs with Enhanced Drug Efflux Activity

One mechanism that has been described to explain the innate resistance of BCSCs to neoadjuvant chemotherapy is the elevated efflux activity found in BCSCs. In the mouse mammary gland, a population of long-term BrdU label retaining cells has been shown to enrich for stem cell antigen-1 (Sca-1) and Hoechst dye-effluxing "side population" properties associated with increased regenerative potential when transplanted into the cleared mammary fat pads of host mice [57]. SP cells with stem/progenitor activity have also been identified in human mammary tissue which constitute 0.2–5.0 % of the total cell population [54–56]. Transcriptional profiling of mammary gland SP cells has revealed an upregulation of genes associated with multidrug resistance [120]. BCSCs, like the normal mammary stem/progenitor cells, may share this "side population" property and thus contribute to their intrinsic capacity for multidrug resistance. Indeed, SP cells have been identified in

different subtypes of human breast cancer cells, which display a more tumorigenic phenotype than the cells do not readily efflux vital dyes [52, 58–60]. These studies further identified an increased expression of ABC transporter genes, especially the breast cancer resistance protein BCRP (also named as ABCG2) and the multi-drug resistance protein 1 (also named ABCB1), in the SP cells that containing BCSC activities. The expression of ABC transporter proteins in BCSCs suggests that these cells play important roles in development of drug resistance in breast cancer. Interestingly, the SP phenotype was found to be more prevalent in luminal subtype of breast cancer cells compared to the triple negative (ER–, PR–, and HER2–) subtype, and HER2 expression, which specifically upregulates $ALDH^+$ luminal BCSCs [121], was significantly correlated with the occurrence of SP phenotype [60]. The strong association of SP phenotype with luminal BCSCs may contribute to the increased resistance of chemotherapy found in $ALDH1^+$ breast cancers [119].

5.2.2 ALDH Enzymatic Activity Expressing in BCSCs Directly Involves in Drug Resistance

Aldehyde dehydrogenases (ALDH) are a family of NAD(P)-dependent enzymes involved in detoxifying a wide variety of endogenous and exogenous aldehydes [122]. Mounting evidence suggests that ALDH activity can be utilized either alone or in combination with different cell surface markers to identify CSCs in a wide varieties of tissue malignancies including leukemia [70] and solid tumors, ranging from those of the breast [22], colon [72, 73], bladder [123], prostate [74], lung [71], pancreas [124], head and neck [38], ovary [125], and melanoma [45]. Recent studies have indicated that ALDH enzymes can directly regulate resistance of cancer cells to many cytotoxic drugs. The role of ALDH in drug resistance was first observed for the alkylating agent, cyclophosphamide. Overexpression of the ALDHA1 gene resulted in a significant increases in cyclophosphamide resistance in transduced L1210 and U937 cells [126] and K562 leukemic cell lines [127]. Conversely, downregulation of ALDH1A1 by antisense RNA resulted in increased sensitivity of tumor cells to 4-hydroperoxycyclophosphamide (4-HC), an active derivative of cyclophosphamide [128]. Overexpression of ALDH1 has been observed in many drug resistant cancer cell lines as well as in patients with drug resistant cancers including breast cancer [119, 129]. In a retrospective study, ALDHA1 activity was significantly higher in breast cancer metastatic cells, which developed resistance to cyclophosphamide, compared with sensitive cells [130]. Most recently, Croker and Allan showed that $ALDH^{hi}CD44^+$ BCSCs isolated from MDA-MB-231 and MDA-MB-468 cell lines are more resistant to chemotherapy (doxorubicin/paclitaxel) or radiotherapy than $ALDH^{lo}CD44^-$ cells, and that inhibiting ALDH activity through all-trans retinoic acid (ATRA) or the specific ALDH inhibitor diethylaminobenzaldehyde (DEAB) sensitizes

$ALDH^{hi}CD44^{+}$ BCSCs to treatment [131]. Together, these studies strongly suggests that ALDH activity expressed in BCSCs plays an important role in mediating BCSC resistance to conventional cancer therapy, and inhibitors of ALDH enzymes may serve as potential therapeutic agents to prevent treatment resistance in breast cancer.

5.2.3 BCSCs Exhibit Low Reactive Oxygen Species Levels and Radioresistance

Increased production of reactive oxygen species (ROS) has long been described as a critical mediator of radiation and chemotherapy induced cytotoxicity to cancer cells by inducing DNA damage such as single-stranded and double-stranded breaks [132–134]. In neural stem cells (NSCs) and hematopoietic stem cells (HSCs), protection from oxidative stress is critical for the maintenance of their self-renewal [135–137], and mice deficient in ATM kinase or *FoxO1*, *FoxO3*, and *FoxO4* transcription factors exhibit elevated ROS levels in the HSC compartment which result in a rapid extinction of HSCs [136, 138, 139]. Similar to the paradigm found in NSCs and HSCs, a recent study by Diehn et al. convincingly demonstrated that human and mouse BCSCs, similar to their normal tissue counterparts, have increased expression of free radical scavenging systems and maintain low levels of ROS that result in less DNA damage and radioprotection [114], providing a possible explanation for tumor recurrence after radiation therapy. These findings also suggest that the self-renewal potential of CSCs in different tumor tissues may be exquisitely sensitive to ROS levels, and this liability might represent a CSC "Achilles' heel" for future therapeutic exploitation to eliminate these lethal seeds of cancer. Indeed, pharmacological depletion of ROS scavengers in BCSCs markedly decreases their clonogenicity and results in radiosensitization [114]. Accordingly, treatment of human acute myeloid leukemia (AML) with parthenolide, a naturally occurring compound that induces ROS, effectively targets AML stem and progenitor cells for apoptosis [140].

5.2.4 BCSCs Have Enhanced DNA-Damage Repair Responses

A number of studies have suggested that resistance to chemo or radiation therapy observed in CSCs or tumor-initiating cells is mediated by altered DNA damages responses. The Ataxia Telangiectasia Mutated (ATM) gene maintains genomic stability by activating a key cell-cycle checkpoint response to DNA damage, telomeric instability or oxidative stress. In glioblastoma following radiation, increased activation of ATM kinase pathway has been reported in $CD133^{+}$ CSCs, contributing to tumor radioresistance through preferential activation of the DNA damage checkpoint response and an increase in DNA repair capacity [141]. Blocking the checkpoint kinases Chk1 and Chk2 led to enhanced killing of CSCs by ionizing radiation [141], suggesting that pharmacological approaches targeting DNA damage checkpoint kinases may overcome this intrinsic resistance. The enhanced ATM signaling activity

in $CD24^{-}CD44^{+}$ BCSCs compared to non $CD24^{-}CD44^{+}$ tumor cells following radiation was also found in breast cancer cell lines and primary human breast cancer cells [142], and treatment with an ATM inhibitor effectively decreased the radiation resistance of $CD24^{-}CD44^{+}$ BCSCs [142], suggesting that targeting ATM signaling may provide a new tool to abolish the radiation resistance of BCSCs. In mouse models of breast cancer, BCSCs deficient in p53 showed accelerated DNA repair activity, as well as high levels of Akt and Wnt signaling [143] and pharmacological inhibition of the Akt pathway by perifosine, an Akt inhibitor, reduced the content of BCSCs in the p53 null tumor and sensitized BCSCs to radiation treatment [143].

6 BCSCs and Tumor Metastasis

In human breast cancer tissues, one of the first identified markers to enrich BCSCs was CD44, a transmembrane glycoprotein serving as a major adhesion molecule and receptor for the extracellular matrix especially extracellular glycosaminoglycan hyaluronic acid [144]. CD44 and its alternative splicing variants have been shown to form co-receptor complexes with various receptor tyrosine kinases to modulate diverse cellular signaling events and regulate cell proliferation, migration, and invasion [144–148]. In line with these studies, expression of CD44 in breast cancer cells has been demonstrated to potentiate the adherence of cancer cells to bone marrow endothelial cells [149] and promotes bone metastasis by enhancing tumorigenicity, cell motility, and hyaluronan production [150]. Besides a direct role in promoting tumor cell motility, CD44 has been implicated to play a role in EMT, a process critical for embryogenesis but abnormally activated during cancer metastasis and recurrence. In a recent study, Brown et al. demonstrated that a shift in CD44 expression from variant isoforms (CD44v) to the standard isoform (CD44s) was essential for mammary epithelial cells to undergo EMT, and was required for the formation of breast tumors that display EMT characteristics in mice [151]. The role of CD44 in promoting EMT and mammary tumorigenesis is in agreement with another report showing that EMT generates cells with stem cell properties [61]. The nature of $CD44^{+}$ BCSCs as the cells undergo EMT strongly suggests these cells are likely to play critical role in tumor metastasis.

The increased expression of the cell adhesion/invasion molecule CD44 in BCSCs suggests that these cells not only play important roles in tumor initiation (by definition, BCSCs are highly tumorigenic cells when implanted into immunodeficient mice), but also act as major players for tumor progression and metastasis. Indeed, several other cell adhesion molecules including CD29 (β1 integrin), CD49f (α6 integrin), and CD61 (β3 integrin) are later

identified to enrich both normal and malignant mammary stem/progenitor cells [8, 9] in human and mouse mammary epithelium. In mouse breast cancer model derived by *MMTV-PyMT* oncogene, the subset of tumor cells defined by $CD24^{+}CD29^{hi}CD61^{+}$ is not only highly tumorigenic but also has significantly higher motility as shown in Boyden chamber assay [152].

In contrast to elevated expression of adhesion molecules including CD44, CD29, and CD49f in BCSCs, another marker of BCSCs is the negative or low expression of heat stable antigen, CD24 [21]. Interestingly, high levels of CD24 expression have been shown to suppress CXCR4 activity [153], whereas the CXCL12/CXCR4 signaling axis has been implicated in trafficking of breast cancer cells to sites of metastasis [154]. The negative or low expression of CD24 in BCSCs may enable these cells to have high CXCL12/CXCR4 signaling activity and facilitate their metastatic spreading and ability to colonize distant organs.

In addition to the roles of BCSC markers in regulation of cancer cell migration, invasion and metastasis, the $CD24^{-}CD44^{+}$ BCSCs isolated from a variety of breast cancer lines have been shown to express higher levels of inflammatory cytokines and proteins associated with invasion and bone metastasis, including IL-1α, IL-6, IL-8, and urokinase plasminogen activator [155]. Recent gene profiling studies also suggested that BCSCs possess an "invasiveness" gene signature that is associated with decreased metastasis-free survival [156]. In support of these findings, Balic et al. have demonstrated that micrometastasis isolated from the bone marrow of early-stage breast cancer patients are highly enriched for the cells displaying the $CD24^{-}CD44^{+}$ BCSC phenotype [157]. Using human-in-mouse breast cancer orthotopic models combined with noninvasive imaging techniques, Liu et al. further showed that $CD24^{-}CD44^{+}$ BCSCs isolated from human breast tumors are involved in spontaneous metastasis [158]. Recent studies of CTCs in breast cancer blood samples also revealed that these CTCs share a BCSC phenotype [159].

Although BCSCs were initially identified with an $EpCAM^{+}CD24^{-}CD44^{+}$ phenotype [21], subsequently it was determined that human normal and malignant mammary epithelial cells with increased ALDH activity have mammary stem/progenitor properties [22]. In breast carcinomas, high ALDH activity identifies the tumorigenic cell fraction, capable of self-renewal and of generating tumors which recapitulate the heterogeneity of the parental tumor [22]. ALDH1 expression represents the first independent prognostic marker to predict metastasis and poor patient outcome in inflammatory breast cancer (IBC), an angio-invasive form of breast cancer associated with a high incidence of early nodal and systemic metastasis [160]. $ALDH^{+}$ cells as assessed by Aldefluor assay from various mammary carcinoma cell lines also

display increased invasive characteristics as well as an increased ability to metastasize following intra-cardiac injection in NOD/SCID mice [161].

The properties of two BCSC states, including their invasive capacity assessed by Matrigel invasion assay, have recently been characterized [23]. These studies demonstrate that MET-like $ALDH^+$ BCSCs are proliferative, while EMT-like $CD24^-CD44^+$ BCSCs are more dormant in cell cycling. Within the two BCSC populations, $CD24^-CD44^+$ cells were significantly more invasive than $ALDH^+$ cells and cells that displayed all three stem cell markers have the greatest invasive capacity. These findings support the proposed model (Fig. 2b) in which EMT BCSCs that are found at the tumor invasive front enter the blood circulation where ultimately they may metastasize to distant sites. These micro-metastases are non-proliferative and remain dormant until they are induced into a transitional state to convert back to an MET "self-renewing" phenotype which can generates additional BCSCs as well as the more differentiated cells which form the tumor bulk. This model is further supported by studies which have demonstrated that both CTCs as well as disseminated tumor cells (DTCs) in the bone marrow of breast cancer patients show significant increase in the $CD44^+/CD24^{-/low}$ cell population that are non-proliferative [155, 157]. One of the characteristics of EMT BCSCs is very low or absent expression of the epithelial marker EpCAM. Therefore, using anti-EpCAM antibodies to capture CTCs in methods such as the CellSearch™ assay may miss important populations of CTCs which display an EMT phenotype. The importance and implications of CTCs as well as alternative CTC capture technologies are discussed below.

7 Circulating Tumor Cells (CTCs)

7.1 Clinical Importance of Circulating BCSCs

More than 100 years ago, CTCs were first described by Thomas Ashworth, an Australian physician. In 1889, Steve Paget proposed "the seed and soil hypothesis" that explains the existence of cross talk between the seed (cancer cells) and the soil (microenvironment of distant organ) during the process of metastasis [162]. Prior to distant organ metastasis, cancer cells must route from primary tumor tissue to the blood stream. These so called CTCs have been documented to be enriched in CSCs [163–165]. Fortunately, most of cancer cells that enter the bloodstream from a primary tumor die as a consequence of shear force or anoikis, or are eliminated by the immune system. Therefore, only a small number of CTCs survive to extravasate to a distant organ. Successfully disseminated cancer cells may either grow to form metastatic colonies or remain dormant for many years [164].

Initially most studies focused on identifying CTCs of an epithelial phenotype [166, 167], but subsequent studies revealed that CTCs consist of several subpopulations including CSCs with different characteristics. Overall, the concept of a noninvasive liquid biopsy to explore mechanisms involved in metastasis makes CTCs an active area of cancer research. In xenograft models, metastasis initiating cells (MICs) within the CTCs have been shown to be CD44 positive. These $CD44^+$ MICs also have been demonstrated to express other markers such as MET and CD47 [158]. In a cohort study, it has been reported that the number of CTCs with an $EpCAM^+/CD44^+/MET^+/CD47^+$ expression profile increased with the clinical progression without significant alterations in the bulk CTC numbers [168]. These findings that CD47 and MET are expressed in both MIC-containing CTCs and metastatic disease may have implications for developing new therapies. In another animal study, it was demonstrated that $EpCAM^-/ALDH1^+/CD45^-$ CTCs isolated from blood sample of breast cancer patients were capable of metastasizing to brain and lung tissues of recipient mice [169]. These CTCs showed a $HER2^+/EGFR^+/HPSE^+/Notch1^+$ gene expression profile that are enriched in brain metastasis. They further showed that these EpCAM-negative breast cancer CTCs with overexpression profile of brain metastasis markers increased brain metastatic capabilities and frequency. These data on metastatic potential of EpCAM-negative CTCs may explain the reason for undetectable CTCs by the CellSearch™ (Veridex LLC) method in a majority of breast cancer patients who developed brain metastasis [169].

Recent studies suggest that the CTCs and primary tumors may display different phenotypes which may reflect tumor evolution as well as differential expression of markers. In a serial CTCs monitoring study in human breast cancer, mesenchymal cells were found to be highly enriched in patients' CTCs. These isolated CTCs demonstrated expression of TGFβ pathway components and the FOXC1 transcription factor [170]. Interestingly, the same study showed that changes in the CTCs content and type in serial blood samples was correlated with primary response to therapy followed by resistance and finally disease progression.

It has been reported that HER2 plays a prominent regulatory role in the breast CSCs [118]. Moreover, in luminal breast cancers, HER2 may be selectively expressed in CSCs in the absence of HER2 gene amplification [121]. These findings might account for the reports of detection of HER2 expressing CTCs isolated from blood sample of women with HER2 "negative" breast cancers [171]. This can also explain the surprising observation that the clinical benefit of HER2 blockade in the adjuvant setting may be extended to woman whose breast tumors do not display HER2 gene amplification. In an artificial neural network (ANN) analysis of CTCs from metastatic breast cancer (MBC) patients, a linear increase of

risk of death was reported with increasing CTC counts across a panel of molecularly different tumor subtypes [172]. However, the CTCs prognostic effect was less evident in the HER2+ patients following targeted therapy [172]. These findings support the concept that the number of CTCs along with the biologic characteristics may have prognostic significance.

7.2 Isolation Methods for Characterization of CTCs

A wide variety of methods has been developed to isolate and characterize CTCs. Most of these techniques are either based on immunodetection of surface markers on CTCs or size and morphology of cancer cells. Of these approaches, immunoaffinity based capture devices are more widely used for CTC isolation. In these methods, distinct antibodies are used against surface markers that are expressed exclusively on tumor cells but not present on the blood cells. Anti-EpCAM antibody is the most commonly used antibody for isolation of CTCs. In these techniques, the antibody may be chemically tethered to magnetic beads or a capture surface, ultimately allowing isolation of CTCs. These immunoaffinity based techniques which are highly specific for CTCs isolation have demonstrated the prognostic, monitoring, and molecular diagnostic potentials of CTCs. Immunocapture systems have evolved from the macroscale operation to a host of microfluidic devices being developed today.

A successful example of macroscale immunocapture system is the CellSearch™ (Veridex LLC), which is FDA approved for use with metastatic breast [164], colon [173], and prostate cancer patients [174]. The antibody in this system is raised against an epithelial surface marker, EpCAM, allowing for the separation of epithelial cancer cells from the blood. A study on blood samples from metastatic patients, patients with nonmalignant disease and healthy volunteers showed the ability of CellSearch to detect as few as 2 CTCs/7.5 ml blood in 36 % of metastatic patients versus only 0.3 % of healthy and nonmalignant samples [175]. Despite being sufficiently robust for FDA approval, the CellSearch™ system lacks high purity, recovery and sensitivity that new and improved cell capture systems need to be developed. Considering the advantages of minimized footprint, cost, and reagent expenditures coupled with a library of well-documented fabrication methods [176], it is not surprising that the field of CTC research turned to microfluidics. Microfluidic devices have been used for biological analysis in the form of "labs-on-a-chip" for the polymerase chain reaction (PCR), molecular separation, and immunosensing [177, 178] through the construction of systems with small scale mixers, pumps, reservoirs, and valves [179].

Microfluidics first appeared in field of CTC isolation in 2007 with the introduction of the CTC-chip [167]. The main advantages of this device include isolation of viable cells for further potential downstream analysis, and the ability to use the whole

blood without further processing. This device has been used in the clinical setting by processing 116 samples with CTCs detected in 99 % (115 of 116) of patient samples. The immunocapture-based microfluidic CTC separation devices have been further engineered with respect to capture antibodies, geometries, and materials. The circular posts in the CTC-chip have been developed in the geometrically enhanced differential immunocapture (GEDI) chip [180]. In addition, the use of the transparent and inexpensive PDMS bonded to a transparent glass slide facilitates imaging that allows on-chip FISH (fluorescence in situ hybridization). Polymers that are cheap and easy to pattern and mold can also be used as a capture substrate in microfluidic devices such as high-throughput microsampling unit (HTMSU) [181] and the "Herringbone-chip" [182]. More recently, a novel nanomaterial graphene oxide (GO) patterned onto a silicon capture surface and conjugated with anti-EpCAM antibody that yielded both high CTC capture efficiency and unprecedented purity has been developed [183].

Although immunoaffinity techniques have the advantage of high specificity, they are limited to only isolate cells with the specified antigens. Therefore, these methods may not be appropriate for isolating all different types of CSCs at the same time from whole blood due to lack of unique surface marker that can distinguish CSCs from hematopoietic cells. Considering these limitations, researchers have focused on development of "label–free" isolation methods based on the biophysical properties of the CTCs including membrane potential, dielectric properties, size of cancer cells relative to blood cells, and their difference in adhesion preferences.

In order to move away from immunoaffinity based isolation methods, researchers focused on size based technologies to isolate CTCs derived from solid tumors that are large enough to be distinguished from blood cells. Size based filtration methods have emerged [184, 185] in which the cells are passed through pores etched in membranes, physically retaining larger cells on the top of the membrane. In this respect, an efficient membrane microfilter device was made of parylene-C for the isolation of prostate cancer cells from whole blood [186]. Moreover, researchers used two-layer membranes to filter viable prostate and breast cancer cells [187]. Two problems associated with size based methods when increasing volumes of blood are (1) easy clogging and (2) the requirement for diluting whole blood before filtering. To address these issues, a microfluidic filtration system consisting of a serpentine channel interconnected with two outer filtrate channels with rectangular apertures was developed which could isolate breast cancer cells spiked into whole blood with 50–90 % recovery rate [188]. Despite improved processing speed as compared to immunoaffinity capture methods, the volume of

blood sample that can be processed without sacrificing efficiency and purity is still limited. Different approaches have been used to improve high throughput analysis of blood samples that are based on shape, geometry and distribution of microchannels [189–191]. Inertial sorting has been coupled with both positive and negative cell sorting in the CTC-iChip [192]. In this case, as with the negative sorting approach that does not require labeling of the CTCs, researchers can isolate cells from multiple cancers and phenotypes. Although these inertial microfluidics based techniques offer high throughput and sensitivity, they suffer from a lack of sufficient specificity of isolated cells. An array of precisely spaced posts has been introduced to capture cells that are not flexible enough to travel through the gaps. These cancer cells were shown to have $CD44^{+}/CD24^{-}/claudin^{low}$ gene expression pattern and tumor initiating capacity [193]. Because of the flexibility of blood cells, this approach can be used as a secondary enrichment step following CTC separation from the blood using other label-free methods. Despite these limitations in microfluidic devices, this class of techniques offers the ideal platform for the label-free isolation of CSCs within the CTCs.

Future methods for CTC capture will aim to solve these problems, ideally increasing the specificity, yield, and throughput. These approaches will in all likelihood take the direction of integrated modules that allow the advantages of multiple techniques and the use of nanomaterials. Integrated devices such as the CTC-iChip use both inertial and immunomagnetic sorting, making feasible the selection of cells of multiple tissue types, stages, and transitional phenotypes. These devices can integrate preprocessing into the device and increase throughput while simultaneously increasing the populations of cells targeted.

The ultimate goal of CTC isolation and characterization is to achieve maximal clinical utility. Therefore, it is essential for the isolation technologies to provide consistent results optimized for yield and purity. More importantly, the isolated CTCs should represent the heterogeneity of the primary tumor cells as well as the alterations necessary to allow the disseminated cells to survive within the blood circulation and finally form metastases at secondary sites. The sensitivity and specificity of isolation methods are key factors to isolate CTCs that are free from blood cells to allow useful downstream experiments. Furthermore, the quantity of isolated CTCs is important for functional analysis and meaningful biological assays. Currently the clinical utility of CTCs is hindered by the low number of CTCs, and hence, the ability to process larger volume of blood sample can change this paradigm. To achieve these goals, isolation methods should be rapid and be able to provide reliable data with respect to the number and cellular phenotypes of CTCs to predict the disease status and treatment response.

8 Patient Derived Xenograft Models for Cancer Stem Cell Research

Despite marked progress in our understanding of cancer biology, the translation of research findings into new therapies for cancer remains an enormous barrier with a failure rate of about 90 % for new oncology drugs in the clinical settings. Part of this high failure rate is due to the lack of in vivo preclinical models that authentically reflect patient tumor biology. Historically, in vivo experimental therapeutic research has been largely dependent on either genetically engineered mouse models, or "xenograft" transplantation models, wherein established human cancer cell lines are transplanted into immune-compromised host mice. These models, although useful and informative, only partially recapitulates the primary tumors in patients. To overcome these limitations, use of patient derived xenograft (PDX) models through engraftment of actual tumor tissues into immune-deficient mice is increasing in cancer biology and preclinical drug testing. These tumor xenografts generally retain the morphology, cellular heterogeneity, genetic background and molecular expression profiles of the original patient tumors. In addition, serial passage and expansion of patient tumors through immune-deficient murine hosts permits ongoing propagation of tumor lines and the study of tumor biology without subjecting PDX tumor cells to the stressful and compromising culture conditions encountered in vitro.

Early attempts to establish human primary breast cancer tissue xenografts used athymic (nude) mice that lack T cell immunity or NOD/SCID mice that lack both T- and B-cell function but retain innate cellular immunity. However, a technical hurdle frequently presented in these studies is the low engraftment rate and the difficulty to maintain the transplantable tumor xenografts over time. The use of "humanized" NOD/SCID mice by introducing an immortalized human fibroblast cell line into the mammary fat pad before transplantation has greatly increased the efficiency to establish PDX models of human breast cancer [194]. Using primary tumor cells transplanted orthotopically in humanized cleared fat-pad of NOD/SCID mice, many serially transplantable tumor xenotransplants have been established. For example, our group has established several widely used xenotransplants derived from independent human breast cancers including MC1, UM1, UM2, and UM3. The $ER^-PR^-ErbB2^-$ MC1 and $ER^+PR^+ErbB2^-$ UM2 xenotransplants were derived from metastatic tumors of pleural effusion and ovarian metastasis respectively, while the UM1 and UM3 were from $ER^-PR^-ErbB2^-$ primary tumors [22]. Taking advantage of these PDX models, Ginestier et al. (2007) showed that the Aldefluor-positive tumor cell population isolated from human breast tumors xenografts has CSC properties [22].

The development and use of PDX models represents the gold standard to assess tumor stem cell activities. Although BCSCs can be propagated in vitro through non-adherent culture conditions, these culture conditions cannot recapitulate the tumor microenvironment in vivo. Tumor xenograft assays in mice measure not only tumorigenic activity but also the self-renewal and maintenance of tumor stem cell component presented in the original tumor. In the landmark study, Al Hajj et al. (2007) transplanted a number of patient tumors into the thoracic mammary fat-pad of etoposide- and estrogen-pretreated NOD/SCID mice and successfully identified a tumorigenic subpopulation in breast cancers with stem cell activities [21]. More recently, Liu et al. established additional models from primary and metastatic tumors, with the majority of these PDXs generating lung micrometastases [158].

In contrast to the use of immortalized human fibroblast cell line to "humanized" NOD/SCID mice, Derose et al. (2011) have showed that implantation of human mesenchymal stem cells (MSCs) with tumor transplants into cleared fat pad of NOD/SCID mice increased tumor growth and stability of the tumor grafts by promoting angiogenesis [195]. These studies of PDX models are in line with the studies of Liu et al. (2011) who demonstrated that $ALDH^+$ stem cells in patient breast tumors are regulated by MSCs, and co-transplantation of MSCs via intratibial injection accelerated tumor growth by increasing the breast CSC population [161]. Besides the frequently utilized NOD-SCID mice, use of SCID/Beige and NSG mice that lack T-cell, B-cell, and NK cell function for xenotransplantation has been proved to increase the efficiency to establish tumor xenografts of human breast cancers. Recently, Michael Lewis' team at Baylor College in Houston established a large cohort of 32 stably transplantable xenograft lines in SCID/Beige and NSG mice. These tumor xenograft lines represent different breast cancer subtypes including triple negative ($ER^-PR^-HER2^-$), HER2-positive ($ER^-PR^-HER2^+$), ER-positive ($ER^+PR^-HER2^-$), ER/PR double positive ($ER^+PR^+HER2^-$), and triple-positive ($ER^+PR^+HER2^+$), and provide a renewable, quality-controlled tissue resource for preclinical studies to investigate treatment response and metastasis [196]. In another study, Charafe-Jauffret et al. (2013) have also established primary breast tumor-derived xenografts in NSG mice that encompass the main diversity of human breast cancers and retain the major clinicopathologic features of primary tumors [48]. In this study, 20 PDXs were established from 74 primary breast tumors with an engraftment rate of 27 %, and 13 PDX lines were successfully maintained through serial passages with a transplantable rate of 17.5 %. Interestingly, successful engraftment of patient tumor was found to correlate with the presence of $ALDH^+$ BCSCs,

which predicted poor prognosis in patients. The correlation of ALDH+ BCSC content with increased tumor engraftment rate is in agreement with a number of other studies showing that high grade TNBCs and metastatic tumors (which contain higher BCSC content) have higher graft take rates than low grade ER+ luminal tumors [196–200]. These studies have further strengthened a critical role of BCSCs in initiating and maintaining tumor growth.

Endocrine therapy has proven very successful and yet only 50 % of all estrogen receptor-positive breast cancers respond to endocrine therapies [201]. Recent development of PDX models of hormone-driven breast cancer has provided a valuable assay to study hormone dependence and resistance of luminal breast cancers. Historically, tumor xenograft strategies for hormone-driven luminal breast cancers have generated limited success. This is largely due to fact that luminal tumors inherently have lower pathological grades and slower growth rates. Recent efforts focusing on generation of ER-positive luminal tumors has increased the number of stable luminal PDXs. DeRose and colleagues established four luminal B PDXs with co-transplantation of human MSCs [195]. Cottu et al. (2012) established a panel of eight luminal breast carcinoma xenografts by engrafting 423 tumors including 314 ER+ tumors, with a tumor take rate of 2.5 %, which is much lower than for non-luminal tumors (2.5 vs. 24.7 %, $P < 0.0001$). Histological and immunohistochemical studies on patient's tumors and xenografts revealed striking similarities in the tumor morphology as well as in the expression level of ER, PR, and HER2. In addition, six luminal models had different sensitivities to hormone therapy, thus exhibiting heterogeneity similar to what is observed in the clinic [202]. Kabos et al. (2012) recently described the development and characterization of five transplantable luminal ER^+ breast cancer xenografts, derived from both primary untreated tumors and late stage metastases. Four of the tumor xenografts were found to be estrogen-dependent and tamoxifen or estrogen withdrawal abrogated estrogen-dependent growth [203]. Interestingly, examination of the BCSC population in the five ER^+ PDX models revealed that tumor xenografts from untreated primary tumors generally contained low $CD24^{-/low}CD44^+$ BCSCs. In contrast, xenograft derived from late stage metastases contained a significant higher $CD24^{-/low}CD44^+$ population [203]. These studies further evidenced an important role of BCSCs in promoting tumor metastasis in luminal tumors.

PDX models of human breast cancer are increasingly used in preclinical study to evaluate the impact of potential breast cancer therapies to eliminate BCSCs. Ginestier et al. (2010) demonstrated that reparixin, a small-molecule inhibitor of the IL8 receptor CXCR1, has the potential to selectively target BCSCs. Administration of reparixin together with Docetaxel, but not

Docetaxel alone, selectively decreased BCSC population in tumor xenografts from three different patients (MC1, UM2, and UM3) and reduced tumor growth and metastasis [204]. The signal transducer and activator of transcription 3 (Stat3) serves as an oncogene activated in many cancers including breast, prostate, lung, head and neck and colon, liver, pancreas, and multiple myeloma [205–207]. Dave et al. (2012) recently showed that targeting the SH2 domain of Stat3 with a novel small molecule inhibitor decreased the percentage of cells expressing BCSC markers ($CD24^{-/low}CD44^{+}$ and $ALDH^{+}$) and mammosphere formation in phospho-Stat3 overexpressing human breast cancer xenografts in SCID-beige mice [208]. Moreover, treatment of Stat3 inhibitor plus docetaxel resulted in a fourfold improvement in recurrence-free survival relative to docetaxel alone in the chemo-resistant tumor model [208]. These findings provide a strong impetus for the development of selective Stat3 inhibitors to target BCSCs in phospho-Stat3 overexpressing breast cancers.

The delta-like 4 ligand (DLL4) is an important component of the Notch pathway and contributes to stem cell self-renewal and vascular development. Previous studies have indicated that inhibition of DLL4 resulted in broad spectrum antitumor activity in cancer cell line-based xenograft models [209–211]. Using specific antibodies targeting DLL4, Hoey et al. (2009) demonstrated that specifically inhibiting human DLL4 in the tumor xenograft models, either alone or in combination with the chemotherapeutic agent irinotecan, reduced CSC frequency, as shown by flow cytometric and in vivo tumorigenicity studies [212]. In another study, treatment with a gamma secretase inhibitor, GSI, has been shown to reduce BCSCs in MC1 and other tumorgrafts by inhibition of the Notch pathway [213]. In addition, treatment with GSI enhanced efficacy of docetaxel and reduced BCSCs [213]. Using PDX model of breast cancer, effect of erythropoietin (EPO) on sensitivity of chemotherapy on BCSCs was also evaluated. EPO administration counteracted the effects of chemotherapeutic agents on BCSC-derived orthotopic tumor xenografts and promoted metastatic progression both in the presence and in the absence of chemotherapy treatment. This suggested that EPO acts directly on BCSC by activating specific survival pathways, resulting in BCSC protection from chemotherapy and enhanced tumor progression [214]. Taken together these studies suggest that PDX models of human breast cancers, which recapitulate the complexity and heterogeneity of patient tumors, have the advantages that more accurately reflect human breast cancer biology than other existing models. These PDX models also have great potential to facilitate the next phase of drug discovery designed to target BCSCs, and ultimately cure this disease.

9 Key Signaling Pathways Regulating the Self-Renewal of CSCs

Several signal transduction pathways such as Wnt, Notch, and Hedgehog and molecules such as Bmi-1 are known to regulate self-renewal pathways in normal stem cells, while in CSCs these pathways are normally dysregulated due to accumulated mutations and epigenetic changes. Understanding the signaling pathways through which CSCs regulate their self-renewal and maintenance and hence tumor growth and metastasis is important for developing targeted therapies to abrogate CSCs. Conventional cancer therapies normally target aberrant pathways in the rapidly proliferating bulk tumor cells, but often spare the CSCs leading to tumor recurrence and metastasis. Therefore, the design of new therapies must be based on targeting the signaling pathways that affect both CSCs as well as bulk tumor cells. Here, we discuss the main pathways that are involved in CSC self-renewal along with their potential therapeutic implications.

9.1 Hedgehog Signaling Pathway

Hedgehog (Hh) is a family of secreted ligands including Sonic, Indian, and Desert which activate Gli transcription factors through interaction with HIP1, Ptch-1, and Ptch-2. Hh signaling regulates body pattern formation, cell proliferation, cell fate determination, and stem/progenitor cell maintenance [215]. Increased expression of Bmi-1 as well as the Hh pathway components Ptch1, Gli1, and Gli2 has been shown in $CD24^{-}CD44^{+}$ BCSCs compared to non-stem cells [216]. Moreover, overexpression of the Hh target Gli2 in human mammary stem/progenitor cells enriched in mammosphere culture produces ductal hyperplasias when these cells are implanted into the humanized fatpads of NOD-SCID mice [216]. These studies indicate that the hedgehog pathway and Bmi-1 play important roles in regulating self-renewal of normal and tumorigenic MaSC/progenitor cells.

Initially, the Hh pathway was targeted using cyclopamine, a steroidal alkaloid that downregulates Gli1 by binding to Smo and hence suppressing the growth of breast cancer cells [217]. Subsequently, new Hh inhibitors have been developed by chemically modifying cyclopamine [218]. At present, GDC-0449 (Vismodegib, trade name: Erivedge), the first Hh pathway inhibitor approved by FDA [219], is undergoing clinical trials in combination with the Notch signaling inhibitor RO4929097 (a gamma-secretase inhibitor, GSI) for metastatic breast cancers where tumors cannot be surgically removed (http://clinicaltrials.gov/). It would be particularly interesting to see the effect of these Hh inhibitors on CSCs as the Hh pathway may be activated in CSCs in response to chemotherapy or during recurrence. Since Hh signaling also imparts chemoresistance [220], the most effective cancer therapy would likely include a Hh inhibitor along with cytotoxic chemotherapy.

9.2 Notch Signaling

Notch signaling involves four homologous transmembrane receptors Notch1-4. Upon binding to their cognate ligands (Delta, Delta-like, Jagged1, and Jagged2), the intracellular domain (ICD) of Notch is cleaved which then translocates into the nucleus to activate its target genes. Notch signaling has emerged as a key regulator involving stem cell maintenance, cell-fate specification, and differentiation [221] and dysregulated Notch signaling has been implicated in a number of human malignancies [222, 223]. In a MMTV mouse model, expression of an activated Notch-related int-3 transgene was shown to interfere with cell differentiation and induce neoplastic transformation in the mammary gland [224]. In a recent study, knockdown of the canonical Notch effector Cbf-1 in MaSC-enriched population was found to increase stem cell activity whereas constitutive Notch signaling specifically targeted luminal progenitor cells for expansion, leading to hyperplasia and tumorigenesis [225]. In human breast cancers, coexpression of JAG1 and NOTCH1 is associated with poor overall survival [226]. In ESA^+ $CD24^-CD44^+$ BCSCs, Notch-4 and Notch-1 activity was found to be eight-fold and four-fold higher respectively compared to the differentiated bulk tumor cells [227]. Expectedly, pharmacologic or genetic inhibition of Notch1 or Notch4 reduced stem cell activity in vitro and reduced tumor formation in vivo [227]. Elevated Notch-1 signaling also contributes to drug resistance as downregulation of Notch-1 signaling in human breast cancer cells increases chemosensitivity to doxorubicin and docetaxel [228].

Several important oncogenic pathways such as ErbB2, Jak/Stat, TGF-β, NF-κB, Wnt, and Hedgehog interact with the Notch pathway [229]. For example, ErbB2 has been shown to induce Notch-1 activity through Cyclin D1 induction [230]. Combined treatment of DAPT, a Notch inhibitor with ErbB2 inhibitor Lapatinib effectively targets stem/progenitor cells both in vitro and in vivo in breast ductal carcinoma in situ (DCIS) [231]. Another study showed that Notch-1 signaling is decreased in ErbB-2 overexpressing SKBR3, BT474 and MCF7/HER2 cells and that HER2-targeted therapies using trastuzumb or lapatinib reactivated Notch-1 and rendered them sensitive to GSIs [232]. These studies suggest that combined treatment of GSI with HER2 targeted therapies may be more beneficial and could potentially reverse the resistance of HER2 targeted therapies especially in CSCs. The Wnt pathway also interacts with Notch through Wnt/TCF target Jagged-1, a Notch ligand, and Mel-18, a negative regulator of Bmi-1. Knockdown of Mel-18 has been shown to enhance the self-renewal of BCSCs whereas its overexpression inhibited the number and self-renewal activity of BCSCs. Mel-18 blockade upregulated Jagged-1 expression and consequently activated the Notch pathway [233]. The activation of Notch activity further activates the Hedgehog pathway and increases expression of Ptch

and Gli [216]. Together these studies suggest that treatments aimed at molecules that affect multiple stem cell pathways could present a novel strategy for targeted therapies.

9.3 HER2 Signaling

Recent studies have indicated an association between HER2 and ALDH1 BCSC marker expression [118]. In clinical setting, one-third of HER2$^+$ patients do not respond to HER2-targeting agents such as trastuzumab and further resistance could develop after long term treatments. This resistance has been attributed to loss of PTEN, somatic mutations of PI3K, truncation of extracellular domain of HER2, engagement of alternate signaling pathways, alterations in antibody binding to HER2, loss of the apoptotic response, and evasion of the immunomodulatory effects conferred by trastuzumab [234, 235]. Korkaya et al. (2009) mechanistically demonstrated the role of the PI3K/AKT pathway in BCSC regulation whereby AKT activation upregulates the WNT pathway through phosphorylation of GSK-3β and β-catenin on Ser552 leading to localization of β-catenin to the nucleus [236]. Therefore, targeting AKT pathway may be an additional approach to target the BCSCs. In support of this notion, Perifosine, an AKT inhibitor, effectively reduced BCSCs in tumor xenografts [236].

In HER2$^+$ breast cancers, the combination of a PI3K inhibitor with trastuzumab is known to be effective to overcome trastuzumab resistance [237, 238]. Another approach to overcome the resistance to HER2 therapy is to target downstream nodes of PI3K/AKT pathway. It has been shown that blockade of mTOR downstream of HER2 with everolimus (a TORC1 inhibitor) in combination with trastuzumab and a taxane resulted in significant clinical response in metastatic HER2$^+$ breast cancers [239]. Recently, a study by Chakrabarty et al. (2013) demonstrated that combined treatment of the pan-PI3K inhibitor, XL147, and trastuzumab reduced proliferation and triggered apoptosis of trastuzumab resistant breast cancer cells [240]. Further, the CSC fraction within trastuzumab-resistant cells was also reduced both in vivo and in vitro [240], providing the proof of principle that HER2 is involved in stem cell maintenance. Recently, Ithimkain et al. (2013) demonstrated that HER2 is selectively expressed in and regulates self-renewal of CSC population in ER$^+$, HER2$^-$ luminal breast cancers [121]. In addition, HER2 expression is increased in luminal tumors grown in mouse bone xenografts, as well as in breast cancer bone metastases as compared with matched primary tumors. This increased expression of HER2 in luminal tumor grown in bone xenografts was mediated by receptor activation of NF-κB (RANK)-ligand in the bone microenvironment [121].

9.4 Wnt Pathway

The Wnt family is a group of secreted glycoproteins that binds to the protein complex of Frizzled and low density lipoprotein receptor related protein 5 or 6 (LRP5 or LRP6). Downstream of LRP5/LRP6 is GSK3β which phosphorylates β-catenin leading

to its ubiquitin-mediated degradation. Activation of the Wnt pathway phosphorylates GSK3β and hence stabilizes β-catenin which then translocates to the nucleus activating several oncogenes such as ID2, MMP7, and c-Myc [241]. The noncanonical Wnt pathway is known to act through Rho family small GTPase, calcium and protein kinase A signaling. The Wnt pathway regulates cell fate determination in several tissues including the mammary gland [242]. In LRP5 knockout mammary glands, very few stem or progenitor cells were present compared to wild type mammary glands [243]. Activation of Wnt signaling and its components have been implicated in variety of cancers including breast [244–247]. A recent study further indicated that increased expression of stemness gene Sox2, by activating the Wnt signaling pathway, promotes resistance in breast cancer cells [248].

Transgenic mice overexpressing Wnt-1 in mammary glands were enriched for epithelial cells expressing progenitor cell markers keratin 6 and Sca1 and tumors that developed in these mice contained cells expressing keratin 6 [249]. This suggests that mammary stem cells and/or progenitors may be the targets for oncogenesis by Wnt pathway. Furthermore, the transforming activity of Wnt effectors was shown to be correlated with their ability to induce accumulation of mammary progenitor cells [250]. The AKT/β-catenin pathway is also activated by antiangiogenic agents such as sunitinib and bevacizumab which drives CSCs expansion through HIF1 alpha [251]. Targeting of the Wnt pathway could be achieved by several approaches. For example, methylation-associated silencing of SFRP1 was shown to inhibit Wnt signaling in breast cancer [252]. In breast cancer cell lines including MCF7, HuL100 and SKBR3, incubation with Wnt1 monoclonal antibody has been used to inhibit Wnt-1 signaling and induce apoptosis [253]. The redundancy between different ligands may suggest that antibody directed Wnt inhibition would not be a successful approach. However, since some cancers have been shown to rely heavily on specific Wnt isoforms, it may be a viable approach in those cancers. For tumors which do not rely on specific Wnt, the use of pan-Wnt inhibitor may be more efficacious. A recent study demonstrated that a soluble ligand binding domain of Fzd8, Fzd8-CRD-Fc, inhibited autocrine Wnt signaling in vitro, as well as in multiple xenograft models [254].

9.5 Regulation of BCSCs by Tumor Microenvironment

The tumor microenvironment involves diverse elements including cancer cells, fibroblasts, endothelial cells, inflammatory cells, and MSCs. Since the tumor microenvironment plays a pivotal role in regulating stem cells; it has been collectively called the stem cell niche [255]. The tumor microenvironment, through paracrine interactions or cytokine networks, may activate the signal transduction pathways described above to regulate CSCs. It has been shown that MSCs recruited from breast stroma or bone marrow [161, 256] interact with BCSCs through cytokine loops involving

IL-6 and CXCL7 stimulating the self-renewal of BCSCs [161]. It has been reported that estrogen signaling in the ERα⁺ non-stem cell compartment stimulates the proliferation of cells within the ERα⁻ stem cell compartment [257]. Similarly, in luminal breast cancers, estrogen signaling expands the pool of ERα⁻ BCSCs through a paracrine FGF/FGFR/Tbx3 signaling which was inhibited by tamoxifen [258].

Circulating markers of inflammation such as serum C-reactive protein (CRP) and amyloid A (SAA) have been shown to correlate with increased risk of breast cancer recurrence in women after primary therapy [259]. Inflammation is known to be mediated by IL6, IL8, IL-1β, and many other cytokines [260]. Gene profiling studies conducted by our group suggested a role of IL8 in promoting tumor stemness in breast cancer cell lines [47]. Indeed, blockade of IL8 signaling through Reparixin, a small molecular inhibitor of the IL-8 receptor CXCR1, has been shown to selectively target BCSCs both in vitro and in breast cancer xenografts, leading to significantly inhibited tumor growth and metastasis [204]. Reparixin is currently being evaluated in a Phase 2 clinical trial at The University of Michigan. In another recent study, Chakrbarty et al. (2013) showed that the combined treatment of Trastuzumab resistant cells with trastuzumab and PI3K inhibitor, XL147, reduced the CSC stem cell population by inhibiting IL-8 [240].

Besides IL8, several preclinical studies have shown that IL6 expression is associated with tumorigenicity and treatment resistance in breast cancer cells [261, 262]. An epigenetic switch involving NF-κB, Lin28, Let-7 MicroRNA, and an IL6 feedback loop has been reported to link inflammation to mammary epithelial cell transformation [263]. Korkaya et al. (2012) further showed that trastuzumab resistant PTEN knockout breast cancer cell lines had an activated IL6 inflammatory feedback loop leading to expansion of the EMT-like CSCs [264]. This suggests that in addition to the NF-κB, IL6 could also serve as a molecular target to eliminate BCSCs. The Stat3 protein plays a central role in relaying extracellular signals initiated by cytokines and growth factors [205, 265]. Therefore, in addition to IL6 targeting, inhibition of Stat3 could serve as an alternative therapeutic strategy. In ALDH⁺ and ALDH⁺/CD44⁺/CD24⁻ BCSCs, higher level of phosphorylated Stat3 (P-STAT3, Y705) compared to bulk tumor cell populations has been demonstrated [266]. Furthermore, a novel Stat3 inhibitor, LLL12, suppresses ALDH⁺ and ALDH⁺/CD44⁺/CD24⁻ BCSCs in vitro and inhibits tumor growth in mouse xenograft and mammary fat pad models in vivo [266]. Thus, Stat3 may represent a target for therapeutic intervention in BCSCs and inhibition of constitutive Stat3 signaling may provide a novel therapeutic approach.

9.6 Regulation of BCSCs by MicroRNAs

Recently, MicroRNAs (miRNAs or Mirs) have emerged as master regulators of stem cell pathways. Mir93 expression has been associated with downregulating TGFβ signaling along with multiple

stem cell regulatory genes including JAK-1, STAT3, AKT3, SOX4, EZH1, and HMGA2 and thus inhibiting stem cell populations [83]. Yu et al. (2007) cell demonstrated that breast tumor initiating cells (TICs) and differentiated cells have low and high levels of let-7 expression respectively [115]. Let-7 overexpression in TICs reduced mammosphere formation in vitro and tumor formation and metastasis in NOD/SCID mice [115]. The same group further showed that miR-30 decreases BCSCs through ubiquitin-conjugating enzyme 9 (UBC9) and integrin β3 [267]. The genomic analysis between BCSCs and bulk cancer cells identified 37 Mirs differentially expressed with miR200c-141, miR-200b-200a-429, and Mir 183-96-182 downregulated in human BCSCs, normal human and murine stem cells. MiR200c expression decreased clonal expansion of breast cancer cells by targeting BMI both in vitro and in vivo [268]. Thus, targeting of Mirs could provide a better approach for eliminating BCSCs since a single Mir could affect multiple pathways.

10 Therapy Implications of CSC-Targeted Approaches

10.1 Cancer Treatment and Prognosis: Why a New Paradigm Is Necessary

Cancer is a leading cause of disease-related mortality worldwide [269]. According to the World Health Organization there were more than 1.6 million new cases of breast cancer in 2010, a dramatic increase as compared to 640,000 cases reported in 1980 [270]. Better early detection methods are unlikely to fully account for such a dramatic rise in incidence in three decades. Over this timeframe progress in the treatment of advanced forms of the most common cancers including those of the breast have shown modest gains in terms of survival metrics. In stark contrast, spectacular advancements have been achieved in the fields of genetics and stem cell biology to characterize and understand the molecular mechanisms that foster cancer. These innovations hold the potential to transform cancer treatment only as long as this growing detailed understanding of the molecular basis of cancer can be translated into clinical benefits. Molecular analyses of tumors reveal a far greater genetic complexity leading to more variation in the pathways that drive tumor growth and metastasis than heretofore recognized. The discovery of genes directly linked to cancer and the molecular pathways influenced by these genes has allowed scientists to draw more precise maps of cancer progression and tautologies. Future drug development efforts will need to put to use this novel understanding to focus targeted therapies that tackle cancer-specific events with unparalleled precision. Currently, the overall 5-year survival rate for all cancers, relative to the anticipated survival from a comparable cohort of people without cancer is 65 % [271]. Statistics like these are sobering, albeit survival and recurrence

rates following diagnosis vary greatly and mostly as a function of cancer type and stage at detection. For example, the relative survival rate 5 years following diagnosis of melanoma is greater than 90 % whereas that of cancers of the brain and nervous system is about 35 % [272]. Once a cancer has metastasized, the survival rate declines dramatically. When melanoma is diagnosed at the localized stage, 99 % of patients will survive beyond 5 years. However survival rates drop to 65 % for those diagnosed with regionally metastasized melanoma and to 15 % for those whose melanoma has spread to distant sites [272]. Once a cancer has been diagnosed, conventional treatments vary according to cancer type and severity. Resection, radiotherapy, and systemic treatments such as chemotherapy or hormone therapy represent traditional approaches designed to remove or eradicate rapidly dividing cancer cells [97, 273, 274]. These methods all have limitations for clinical use. Cancer surgeons may not be able to fully remove all of the tumor tissue due to its location, extent of spreading or degree of intercalation with healthy tissue. Radiation and chemotherapy are inherently nonspecific cytotoxic strategies that result in extensive collateral damage to healthy tissue despite their targeting rapidly dividing cancer cells. Recently, several new immune modulating agents that target specific proteins implicated in cancer molecular pathways have been developed for clinical use. These include trastuzumab, a HER2-targeting monoclonal antibody in breast cancer [275], bevacizumab which targets VEGF in colorectal and lung cancer [276], erlotnib and gefitinib which target epidermal growth factor receptor (EGFR) in lung cancer [277], imatinib which targets BCR-ABL in CML [278], and panitumumab and cetuximab which target EGFR in colorectal cancer [276]. These agents demonstrate that a targeted approach is feasible, but they are most often effective only in patients who display specific subclasses of the respective cancers, hence justifying the efforts to develop more personalized medicine. Furthermore, patients can become resistant to these therapies and most systemic immune treatments are only moderately successful unless the cancer is localized. With few exceptions, these agents fail to provide significant clinical benefit at the advanced metastatic stage of the disease. Therefore, a new paradigm is needed for the treatment of resistant and advanced disease. CSC-directed therapies offer the possibility for disease remission without recurrence. In the final section we discuss implications of the CSC hypothesis, supporting evidence for CSC clinical trials and perspectives on how CSCs could impact the development of future cancer therapy.

10.2 Clinical Implications of CSCs

The presence of and the molecular events triggered by CSCs within tumors has important implications for the development of cancer-targeting therapeutics. The CSC hypothesis suggests that tumor regrowth following traditional resection and/or chemo/radio

approaches can be arrested if the repopulating cells are destroyed with a selective CSC targeting agent. This is fundamentally important because CSCs are generally found to be more aggressive, invasive and prone to promote metastasis than the bulk tumorigenic cells [83]. Aldefluor$^+$ cells from mammary carcinoma cell lines display increased invasive characteristics as well as an increased ability to metastasize following intra-cardiac injection in NOD/SCID mice [161]. Similarly, Balic et al. observed an increase in the CD24$^-$CD44$^+$ breast CSC population in bone marrow metastases in patients with breast carcinomas [157]. As a result, targeting of the CSC clinically could lead to a reduction in metastasis. CSCs are presumed to be responsible for both the radiation- and chemotherapeutic-resistance commonly observed in many cancers [116]. Since stem cells are quiescent and typically cells with slower cycles than differentiated cells, stem cells are intrinsically more resistant to cell cycle altering chemotherapeutic drugs [279]. CSCs also possess a high level of drug transporters and particularly exporters such that the intracellular effective chemotherapuetic concentrations in these cells is lower than in differentiated cells resulting in the apparent decreased overall efficacy of the chemotherapeutic agent administered. Furthermore, the activity of the enzyme ALDH is high in CSCs, and this enzyme has been demonstrated to metabolize certain common chemotherapeutic drugs including cyclophosphamide into forms of metabolites with lower cytotoxicity [69]. To maximize the clinical benefits of drugs that target CSCs, these drugs should thus be used in combination with radiation or standard chemotherapy since CSC-targeting agents are typically not designed to clear the vast majority of differentiated bulk tumor cells and complications from tumor burden alone might adversely complicate patient prognosis. Because the CSC subpopulation of a tumor often constitutes a minor portion of the tumor mass, novel methods need to be implemented such as new trial designs for accurately measuring success and outcome of CSC-targeting agents. Current clinical trials use the so-called RECIST (Response Evaluation Criteria in Solid Tumors) criteria to measure tumor shrinkage. However, tumor regression frequently fails to correlate with improved survival rates [280]. CSC treatment alone would not be expected to elicit major reductions of the parameters that are measured using the RECIST evaluation criteria [19, 280]. CSC clinical trials thus need to be designed to directly measure the effect that the new drug under investigation has on CSCs. This objective could be met by conducting neo-adjuvant CSC trials. For example, CD24$^-$CD44$^+$ breast CSCs have been observed to increase after chemotherapy, however combination therapy using BCSC targeting agent such as HER2 and EGFR inhibitor Lapatinib with chemotherapy prevented the increase of BCSCs [117]. A similar outcome could also be accomplished by providing the CSC-targeting agent prior to surgery followed by a CSC biomarker

profiling step performed on selected patient biopsies. Practically, cells from these very biopsies could be grown as tumorspheres in order to determine not only a drug's ability to target CSCs but also which signaling pathways are involved. For effectively destroying CSCs, it is necessary to understand how the various signaling pathways of these cells interact to regulate CSC-specific processes of growth, renewal, differentiation and apoptosis. The Notch, Hedgehog, HER-2/PI3K/Akt/ PTEN, p53 and Wnt signaling pathways have been shown to regulate normal and malignant stem cells [236, 281]. Notably, inhibitors of Notch, Hedgehog, Akt and Wnt targeting agents have been developed by several pharmaceutical companies [19, 282, 283]. Emerging evidence suggests that microRNAs (miRNAs) may play a pivotal role in regulating the genes that control self-renewal, differentiation and division of normal stem and CSC signaling pathways [83].

11 Future Perspectives

The critical roles of CSCs in tumor initiation, progression and recurrence has sparked enormous interest among oncology researchers to explore key signaling pathways that regulate their self-renewal and to develop novel therapeutic strategies to eradicate these lethal seeds of cancer. The combination of conventional cancer therapies together with specific CSC targeted therapies brings the promise of eradicating a cancer with no possibility of recurrence. Yet, a multitude of surmountable barriers exist before CSC therapeutics can be fully deployed and clinical benefits derived. First and foremost, close cooperation between industry and academia is urgently needed to foster early stage drug discovery, biomarker characterization, unique animal model generation, target/pathway validation and clinical trial translation. As the field is less than a decade old, more basic CSC research is prerequisite to comprehensive understanding of the molecular basis of disease and the signaling pathways underlying each cancer and unique disease subtype. Another chief impediment to CSC therapeutic development is the exceptionally high cost to translate promising basic science discoveries in stem cell biology into meaningful clinical interventions. The lack of federal mechanisms large enough to support highly innovative research is at present a significant deterrent to translational science. New funding mechanisms must be developed to bring together academic researchers, disease foundations, donors, philanthropists, angel investors, government sponsors and industry stakeholders. Since existing RECIST criteria are not suitable endpoints for CSC trials [19], novel trial designs are vitally important at this juncture.

The most promising CSC therapeutic agents to date that target Notch, Hedgehog, Wnt, NFkB, Her2, Pten, Akt, Stat3, IL6R,

CXCR1 and many other CSC self-renewal pathways afford ample opportunities for new partnerships and trials. Dual or multiple pathway inhibitors will be at a significant advantage since many cancers appear to be driven by multiple cellular regulators. Novel separation methods and characterization assays for better discrimination and quantification of CSCs are desperately needed. Imaging methods either ultrasonic, magnetic resonance or conventional microscopy-based are needed to better visualize CSCs before and after treatment to assess patient response. In addition, partnerships working toward CTC capture and characterization, nanoparticle delivery mechanisms and improvement of devices capable of sensitizing CSCs to chemotherapy and/or radiation clearance (e.g., low temperature hyperthermia induction) may be of great use in the fight against cancer in the near term. Similarly, business ventures that are able to develop clinical trial protocols capable of clearly elucidating CSC therapeutic targeting is urgently needed. Stem cell targeting approaches that can be co-administered with conventional debulking agents are most apt to quickly gain regulatory approval and yield the best results. Especially promising approaches would be those that take advantage of unique cell cycling aspects, apoptosis programs, epigenetics, miRNA regulation of EMT/MET states or other features of tumor initiating cells that would spare normal stem cells and the bodies' innate regenerative capabilities.

References

1. Sternlicht MD et al (2006) Hormonal and local control of mammary branching morphogenesis. Differentiation 74(7):365–381
2. Hinck L, Silberstein GB (2005) Key stages in mammary gland development: the mammary end bud as a motile organ. Breast Cancer Res 7(6):245–251
3. Hennighausen L, Robinson GW (2005) Information networks in the mammary gland. Nat Rev Mol Cell Biol 6(9):715–725
4. Smalley M, Ashworth A (2003) Stem cells and breast cancer: a field in transit. Nat Rev Cancer 3(11):832–844
5. Kordon EC, Smith GH (1998) An entire functional mammary gland may comprise the progeny from a single cell. Development 125(10):1921–1930
6. Smith GH (1996) Experimental mammary epithelial morphogenesis in an in vivo model: evidence for distinct cellular progenitors of the ductal and lobular phenotype. Breast Cancer Res Treat 39(1):21–31
7. Asselin-Labat ML et al (2007) Gata-3 is an essential regulator of mammary-gland morphogenesis and luminal-cell differentiation. Nat Cell Biol 9(2):201–209
8. Stingl J et al (2006) Purification and unique properties of mammary epithelial stem cells. Nature 439(7079):993–997
9. Shackleton M et al (2006) Generation of a functional mammary gland from a single stem cell. Nature 439(7072):84–88
10. Sleeman KE et al (2006) CD24 staining of mouse mammary gland cells defines luminal epithelial, myoepithelial/basal and non-epithelial cells. Breast Cancer Res 8(1):R7
11. Shipitsin M et al (2007) Molecular definition of breast tumor heterogeneity. Cancer Cell 11(3):259–273
12. Villadsen R et al (2007) Evidence for a stem cell hierarchy in the adult human breast. J Cell Biol 177(1):87–101
13. Lim E et al (2009) Aberrant luminal progenitors as the candidate target population for basal tumor development in BRCA1 mutation carriers. Nat Med 15(8):907–913
14. Eirew P et al (2008) A method for quantifying normal human mammary epithelial stem

cells with in vivo regenerative ability. Nat Med 14(12):1384–1389
15. Keller PJ et al (2011) Defining the cellular precursors to human breast cancer. Proc Natl Acad Sci U S A 109:2772–2777
16. Visvader JE (2009) Keeping abreast of the mammary epithelial hierarchy and breast tumorigenesis. Genes Dev 23(22): 2563–2577
17. Bonnet D, Dick JE (1997) Human acute myeloid leukemia is organized as a hierarchy that originates from a primitive hematopoietic cell. Nat Med 3(7):730–737
18. Wicha MS, Liu S, Dontu G (2006) Cancer stem cells: an old idea—a paradigm shift. Cancer Res 66(4):1883–1890, discussion 1895-6
19. Liu S, Wicha MS (2010) Targeting breast cancer stem cells. J Clin Oncol 28(25): 4006–4012
20. Charafe-Jauffret E et al (2008) Cancer stem cells in breast: current opinion and future challenges. Pathobiology 75(2):75–84
21. Al-Hajj M et al (2003) Prospective identification of tumorigenic breast cancer cells. Proc Natl Acad Sci U S A 100(7):3983–3988
22. Ginestier C et al (2007) ALDH1 is a marker of normal and malignant human mammary stem cells and a predictor of poor clinical outcome. Cell Stem Cell 1(5):555–567
23. Liu S et al (2014) Breast cancer stem cells transition between epithelial and mesenchymal states reflective of their normal counterparts. Stem Cell Reports 2(1):78–91
24. Singh SK et al (2004) Identification of human brain tumour initiating cells. Nature 432(7015):396–401
25. Collins AT et al (2005) Prospective identification of tumorigenic prostate cancer stem cells. Cancer Res 65(23):10946–10951
26. Patrawala L et al (2006) Highly purified CD44+ prostate cancer cells from xenograft human tumors are enriched in tumorigenic and metastatic progenitor cells. Oncogene 25(12):1696–1708
27. O'Brien CA et al (2007) A human colon cancer cell capable of initiating tumour growth in immunodeficient mice. Nature 445(7123): 106–110
28. Ricci-Vitiani L et al (2007) Identification and expansion of human colon-cancer-initiating cells. Nature 445(7123):111–115
29. Li C et al (2007) Identification of pancreatic cancer stem cells. Cancer Res 67(3):1030–1037
30. Ma S et al (2007) Identification and characterization of tumorigenic liver cancer stem/progenitor cells. Gastroenterology 132(7): 2542–2556
31. Ma S et al (2010) MiR-130b Promotes CD133(+) liver tumor-initiating cell growth and self-renewal via tumor protein 53-induced nuclear protein 1. Cell Stem Cell 7(6): 694–707
32. Kim CF et al (2005) Identification of bronchioalveolar stem cells in normal lung and lung cancer. Cell 121(6):823–835
33. Prince ME et al (2007) Identification of a subpopulation of cells with cancer stem cell properties in head and neck squamous cell carcinoma. Proc Natl Acad Sci U S A 104(3): 973–978
34. Mukherjee S (2010) The emperor of all maladies: a biography of cancer. 1st Scribner hardcover ed, vol 14. Scribner, New York, NY, p 571, 8 p. of plates
35. Huntly BJ, Gilliland DG (2005) Cancer biology: summing up cancer stem cells. Nature 435(7046):1169–1170
36. Sell S (2004) Stem cell origin of cancer and differentiation therapy. Crit Rev Oncol Hematol 51(1):1–28
37. Xu Q et al (2009) Isolation of tumour stem-like cells from benign tumours. Br J Cancer 101(2):303–311
38. Clay MR et al (2010) Single-marker identification of head and neck squamous cell carcinoma cancer stem cells with aldehyde dehydrogenase. Head Neck 32(9):1195–1201
39. Silva IA et al (2011) Aldehyde dehydrogenase in combination with CD133 defines angiogenic ovarian cancer stem cells that portend poor patient survival. Cancer Res 71(11): 3991–4001
40. Krishnamurthy S et al (2010) Endothelial cell-initiated signaling promotes the survival and self-renewal of cancer stem cells. Cancer Res 70(23):9969–9978
41. Fang D et al (2005) A tumorigenic subpopulation with stem cell properties in melanomas. Cancer Res 65(20):9328–9337
42. Quintana E et al (2008) Efficient tumour formation by single human melanoma cells. Nature 456(7222):593–598
43. Roesch A et al (2010) A temporarily distinct subpopulation of slow-cycling melanoma cells is required for continuous tumor growth. Cell 141(4):583–594
44. Boiko AD et al (2010) Human melanoma-initiating cells express neural crest nerve growth factor receptor CD271. Nature 466(7302):133–137
45. Luo Y et al (2012) ALDH1A isozymes are markers of human melanoma stem cells and potential therapeutic targets. Stem Cells 30(10):2100–2113

46. Kelly PN et al (2007) Tumor growth need not be driven by rare cancer stem cells. Science 317(5836):337
47. Charafe-Jauffret E et al (2009) Breast cancer cell lines contain functional cancer stem cells with metastatic capacity and a distinct molecular signature. Cancer Res 69(4):1302–1313
48. Charafe-Jauffret E et al (2013) ALDH1-positive cancer stem cells predict engraftment of primary breast tumors and are governed by a common stem cell program. Cancer Res 73(24):7290–7300
49. Pece S et al (2010) Biological and molecular heterogeneity of breast cancers correlates with their cancer stem cell content. Cell 140(1):62–73
50. Bunting KD (2002) ABC transporters as phenotypic markers and functional regulators of stem cells. Stem Cells 20(1):11–20
51. Hadnagy A et al (2006) SP analysis may be used to identify cancer stem cell populations. Exp Cell Res 312(19):3701–3710
52. Hirschmann-Jax C et al (2004) A distinct "side population" of cells with high drug efflux capacity in human tumor cells. Proc Natl Acad Sci U S A 101(39):14228–14233
53. Kondo T, Setoguchi T, Taga T (2004) Persistence of a small subpopulation of cancer stem-like cells in the C6 glioma cell line. Proc Natl Acad Sci U S A 101(3):781–786
54. Clarke RB et al (2005) A putative human breast stem cell population is enriched for steroid receptor-positive cells. Dev Biol 277(2): 443–456
55. Alvi AJ et al (2003) Functional and molecular characterisation of mammary side population cells. Breast Cancer Res 5(1):R1–R8
56. Clayton H, Titley I, Vivanco M (2004) Growth and differentiation of progenitor/stem cells derived from the human mammary gland. Exp Cell Res 297(2):444–460
57. Welm BE et al (2002) Sca-1(pos) cells in the mouse mammary gland represent an enriched progenitor cell population. Dev Biol 245(1): 42–56
58. Patrawala L et al (2005) Side population is enriched in tumorigenic, stem-like cancer cells, whereas ABCG2+ and ABCG2- cancer cells are similarly tumorigenic. Cancer Res 65(14):6207–6219
59. Britton KM et al (2012) Breast cancer, side population cells and ABCG2 expression. Cancer Lett 323(1):97–105
60. Nakanishi T et al (2010) Side-population cells in luminal-type breast cancer have tumour-initiating cell properties, and are regulated by HER2 expression and signalling. Br J Cancer 102(5):815–826
61. Mani SA et al (2008) The epithelial-mesenchymal transition generates cells with properties of stem cells. Cell 133(4):704–715
62. Marotta LL et al (2011) The JAK2/STAT3 signaling pathway is required for growth of CD44CD24 stem cell-like breast cancer cells in human tumors. J Clin Invest 121(7): 2723–2735
63. Honeth G et al (2008) The CD44+/CD24- phenotype is enriched in basal-like breast tumors. Breast Cancer Res 10(3):R53
64. Meyer MJ et al (2010) CD44posCD49 fhiCD133/2hi defines xenograft-initiating cells in estrogen receptor-negative breast cancer. Cancer Res 70(11):4624–4633
65. Friedrichs K et al (1995) High expression level of alpha 6 integrin in human breast carcinoma is correlated with reduced survival. Cancer Res 55(4):901–906
66. Lipscomb EA et al (2005) The alpha6beta4 integrin maintains the survival of human breast carcinoma cells in vivo. Cancer Res 65(23):10970–10976
67. Chute JP et al (2006) Inhibition of aldehyde dehydrogenase and retinoid signaling induces the expansion of human hematopoietic stem cells. Proc Natl Acad Sci U S A 103(31): 11707–11712
68. Storms RW et al (1999) Isolation of primitive human hematopoietic progenitors on the basis of aldehyde dehydrogenase activity. Proc Natl Acad Sci U S A 96(16):9118–9123
69. Ludeman SM (1999) The chemistry of the metabolites of cyclophosphamide. Curr Pharm Des 5(8):627–643
70. Cheung AM et al (2007) Aldehyde dehydrogenase activity in leukemic blasts defines a subgroup of acute myeloid leukemia with adverse prognosis and superior NOD/SCID engrafting potential. Leukemia 21(7): 1423–1430
71. Sullivan JP et al (2010) Aldehyde dehydrogenase activity selects for lung adenocarcinoma stem cells dependent on notch signaling. Cancer Res 70(23):9937–9948
72. Huang EH et al (2009) Aldehyde dehydrogenase 1 is a marker for normal and malignant human colonic stem cells (SC) and tracks SC overpopulation during colon tumorigenesis. Cancer Res 69(8):3382–3389
73. Carpentino JE et al (2009) Aldehyde dehydrogenase-expressing colon stem cells contribute to tumorigenesis in the transition from colitis to cancer. Cancer Res 69(20): 8208–8215
74. van den Hoogen C et al (2010) High aldehyde dehydrogenase activity identifies tumor-initiating and metastasis-initiating cells in

human prostate cancer. Cancer Res 70(12): 5163–5173

75. Dontu G et al (2003) In vitro propagation and transcriptional profiling of human mammary stem/progenitor cells. Genes Dev 17(10): 1253–1270
76. D'Angelo RC, Wicha MS (2010) Stem cells in normal development and cancer. Prog Mol Biol Transl Sci 95:113–158
77. Kusumbe AP, Bapat SA (2009) Cancer stem cells and aneuploid populations within developing tumors are the major determinants of tumor dormancy. Cancer Res 69(24): 9245–9253
78. Hendrikx PJ et al (1996) Homing of fluorescently labeled murine hematopoietic stem cells. Exp Hematol 24(2):129–140
79. Lanzkron SM, Collector MI, Sharkis SJ (1999) Homing of long-term and short-term engrafting cells in vivo. Ann N Y Acad Sci 872:48–54, discussion 54-6
80. Askenasy N, Farkas DL (2002) Optical imaging of PKH-labeled hematopoietic cells in recipient bone marrow in vivo. Stem Cells 20(6):501–513
81. Cicalese A et al (2009) The tumor suppressor p53 regulates polarity of self-renewing divisions in mammary stem cells. Cell 138(6): 1083–1095
82. Lassailly F, Griessinger E, Bonnet D (2010) "Microenvironmental contaminations" induced by fluorescent lipophilic dyes used for noninvasive in vitro and in vivo cell tracking. Blood 115(26):5347–5354
83. Liu S, Clouthier SG, Wicha MS (2012) Role of microRNAs in the regulation of breast cancer stem cells. J Mammary Gland Biol Neoplasia 17(1):15–21
84. Liu S et al (2012) MicroRNA93 regulates proliferation and differentiation of normal and malignant breast stem cells. PLoS Genet 8(6):e1002751
85. Thiery JP (2003) Epithelial-mesenchymal transitions in development and pathologies. Curr Opin Cell Biol 15(6):740–746
86. Yang J et al (2004) Twist, a master regulator of morphogenesis, plays an essential role in tumor metastasis. Cell 117(7):927–939
87. Wu Y et al (2009) Stabilization of snail by NF-kappaB is required for inflammation-induced cell migration and invasion. Cancer Cell 15(5):416–428
88. Yang MH et al (2008) Direct regulation of TWIST by HIF-1alpha promotes metastasis. Nat Cell Biol 10(3):295–305
89. Samavarchi-Tehrani P et al (2010) Functional genomics reveals a BMP-driven mesenchymal-to-epithelial transition in the initiation of somatic cell reprogramming. Cell Stem Cell 7(1):64–77
90. Brabletz T (2012) To differentiate or not: routes towards metastasis. Nat Rev Cancer 12(6):425–436
91. Tsai JH et al (2012) Spatiotemporal regulation of epithelial-mesenchymal transition is essential for squamous cell carcinoma metastasis. Cancer Cell 22(6):725–736
92. Ocana OH et al (2012) Metastatic colonization requires the repression of the epithelial-mesenchymal transition inducer Prrx1. Cancer Cell 22(6):709–724
93. Malanchi I et al (2012) Interactions between cancer stem cells and their niche govern metastatic colonization. Nature 481(7379):85–89
94. Korpal M et al (2011) Direct targeting of Sec23a by miR-200s influences cancer cell secretome and promotes metastatic colonization. Nat Med 17(9):1101–1108
95. Stankic M et al (2013) TGF-beta-Id1 signaling opposes Twist1 and promotes metastatic colonization via a mesenchymal-to-epithelial transition. Cell Rep 5(5):1228–1242
96. Herschkowitz JI et al (2007) Identification of conserved gene expression features between murine mammary carcinoma models and human breast tumors. Genome Biol 8(5):R76
97. Perou CM et al (2000) Molecular portraits of human breast tumours. Nature 406(6797): 747–752
98. Sorlie T et al (2001) Gene expression patterns of breast carcinomas distinguish tumor subclasses with clinical implications. Proc Natl Acad Sci U S A 98(19):10869–10874
99. Sotiriou C et al (2003) Breast cancer classification and prognosis based on gene expression profiles from a population-based study. Proc Natl Acad Sci U S A 100(18): 10393–10398
100. Chang JC et al (2005) Patterns of resistance and incomplete response to docetaxel by gene expression profiling in breast cancer patients. J Clin Oncol 23(6):1169–1177
101. Creighton CJ et al (2009) Residual breast cancers after conventional therapy display mesenchymal as well as tumor-initiating features. Proc Natl Acad Sci U S A 106(33): 13820–13825
102. Molyneux G et al (2010) BRCA1 basal-like breast cancers originate from luminal epithelial progenitors and not from basal stem cells. Cell Stem Cell 7(3):403–417
103. Proia TA et al (2011) Genetic predisposition directs breast cancer phenotype by dictating progenitor cell fate. Cell Stem Cell 8(2):149–163

104. Keller PJ et al (2012) Defining the cellular precursors to human breast cancer. Proc Natl Acad Sci U S A 109(8):2772–2777
105. Van Keymeulen A et al (2011) Distinct stem cells contribute to mammary gland development and maintenance. Nature 479(7372): 189–193
106. Jeselsohn R et al (2010) Cyclin D1 kinase activity is required for the self-renewal of mammary stem and progenitor cells that are targets of MMTV-ErbB2 tumorigenesis. Cancer Cell 17(1):65–76
107. Liu S et al (2008) BRCA1 regulates human mammary stem/progenitor cell fate. Proc Natl Acad Sci U S A 105(5):1680–1685
108. Lagadec C et al (2010) Survival and self-renewing capacity of breast cancer initiating cells during fractionated radiation treatment. Breast Cancer Res 12(1):R13
109. Phillips TM, McBride WH, Pajonk F (2006) The response of CD24(-/low)/CD44+ breast cancer-initiating cells to radiation. J Natl Cancer Inst 98(24):1777–1785
110. Karimi-Busheri F et al (2010) Senescence evasion by MCF-7 human breast tumor-initiating cells. Breast Cancer Res 12(3):R31
111. Fillmore CM, Kuperwasser C (2008) Human breast cancer cell lines contain stem-like cells that self-renew, give rise to phenotypically diverse progeny and survive chemotherapy. Breast Cancer Res 10(2):R25
112. Shafee N et al (2008) Cancer stem cells contribute to cisplatin resistance in Brca1/p53-mediated mouse mammary tumors. Cancer Res 68(9):3243–3250
113. Woodward WA et al (2007) WNT/beta-catenin mediates radiation resistance of mouse mammary progenitor cells. Proc Natl Acad Sci U S A 104(2):618–623
114. Diehn M et al (2009) Association of reactive oxygen species levels and radioresistance in cancer stem cells. Nature 458(7239): 780–783
115. Yu F et al (2007) let-7 regulates self renewal and tumorigenicity of breast cancer cells. Cell 131(6):1109–23
116. Zielske SP et al (2011) Ablation of breast cancer stem cells with radiation. Transl Oncol 4(4):227–233
117. Li X et al (2008) Intrinsic resistance of tumorigenic breast cancer cells to chemotherapy. J Natl Cancer Inst 100(9):672–679
118. Korkaya H et al (2008) HER2 regulates the mammary stem/progenitor cell population driving tumorigenesis and invasion. Oncogene 27(47):6120–6130
119. Tanei T et al (2009) Association of breast cancer stem cells identified by aldehyde dehydrogenase 1 expression with resistance to sequential Paclitaxel and epirubicin-based chemotherapy for breast cancers. Clin Cancer Res 15(12):4234–4241
120. Behbod F et al (2006) Transcriptional profiling of mammary gland side population cells. Stem Cells 24(4):1065–1074
121. Ithimakin S et al (2013) HER2 drives luminal breast cancer stem cells in the absence of HER2 amplification: implications for efficacy of adjuvant trastuzumab. Cancer Res 73(5): 1635–1646
122. Sladek NE (2003) Human aldehyde dehydrogenases: potential pathological, pharmacological, and toxicological impact. J Biochem Mol Toxicol 17(1):7–23
123. Su Y et al (2010) Aldehyde dehydrogenase 1 A1-positive cell population is enriched in tumor-initiating cells and associated with progression of bladder cancer. Cancer Epidemiol Biomarkers Prev 19(2):327–337
124. Kim MP et al (2011) ALDH activity selectively defines an enhanced tumor-initiating cell population relative to CD133 expression in human pancreatic adenocarcinoma. PLoS One 6(6):e20636
125. Landen CN Jr et al (2010) Targeting aldehyde dehydrogenase cancer stem cells in ovarian cancer. Mol Cancer Ther 9(12): 3186–3199
126. Magni M et al (1996) Induction of cyclophosphamide-resistance by aldehyde-dehydrogenase gene transfer. Blood 87(3): 1097–1103
127. Moreb J et al (1996) Overexpression of the human aldehyde dehydrogenase class I results in increased resistance to 4-hydroperoxycyclophosphamide. Cancer Gene Ther 3(1):24–30
128. Moreb JS et al (2000) Expression of antisense RNA to aldehyde dehydrogenase class-1 sensitizes tumor cells to 4-hydroperoxycyclophosphamide in vitro. J Pharmacol Exp Ther 293(2):390–396
129. Sun QL et al (2011) Comparative proteomic analysis of paclitaxel sensitive A549 lung adenocarcinoma cell line and its resistant counterpart A549-Taxol. J Cancer Res Clin Oncol 137(3):521–532
130. Sladek NE et al (2002) Cellular levels of aldehyde dehydrogenases (ALDH1A1 and ALDH3A1) as predictors of therapeutic responses to cyclophosphamide-based chemotherapy of breast cancer: a retrospective study. Rational individualization of

oxazaphosphorine-based cancer chemotherapeutic regimens. Cancer Chemother Pharmacol 49(4):309–321

131. Croker AK, Allan AL (2012) Inhibition of aldehyde dehydrogenase (ALDH) activity reduces chemotherapy and radiation resistance of stem-like ALDHhiCD44(+) human breast cancer cells. Breast Cancer Res Treat 133(1):75–87
132. Ward JF (1985) Biochemistry of DNA lesions. Radiat Res Suppl 8:S103–S111
133. Powell S, McMillan TJ (1990) DNA damage and repair following treatment with ionizing radiation. Radiother Oncol 19(2):95–108
134. Kryston TB et al (2011) Role of oxidative stress and DNA damage in human carcinogenesis. Mutat Res 711(1–2):193–201
135. Smith J et al (2000) Redox state is a central modulator of the balance between self-renewal and differentiation in a dividing glial precursor cell. Proc Natl Acad Sci U S A 97(18):10032–10037
136. Ito K et al (2004) Regulation of oxidative stress by ATM is required for self-renewal of haematopoietic stem cells. Nature 431(7011): 997–1002
137. Ito K et al (2006) Reactive oxygen species act through p38 MAPK to limit the lifespan of hematopoietic stem cells. Nat Med 12(4): 446–451
138. Tothova Z et al (2007) FoxOs are critical mediators of hematopoietic stem cell resistance to physiologic oxidative stress. Cell 128(2):325–339
139. Miyamoto K et al (2007) Foxo3a is essential for maintenance of the hematopoietic stem cell pool. Cell Stem Cell 1(1):101–112
140. Guzman ML et al (2005) The sesquiterpene lactone parthenolide induces apoptosis of human acute myelogenous leukemia stem and progenitor cells. Blood 105(11):4163–4169
141. Bao S et al (2006) Glioma stem cells promote radioresistance by preferential activation of the DNA damage response. Nature 444(7120): 756–760
142. Yin H, Glass J (2011) The phenotypic radiation resistance of CD44+/CD24(-or low) breast cancer cells is mediated through the enhanced activation of ATM signaling. PLoS One 6(9):e24080
143. Zhang M, Atkinson RL, Rosen JM (2010) Selective targeting of radiation-resistant tumor-initiating cells. Proc Natl Acad Sci U S A 107(8):3522–3527
144. Ponta H, Sherman L, Herrlich PA (2003) CD44: from adhesion molecules to signalling regulators. Nat Rev Mol Cell Biol 4(1): 33–45
145. Cheng C, Yaffe MB, Sharp PA (2006) A positive feedback loop couples Ras activation and CD44 alternative splicing. Genes Dev 20(13):1715–1720
146. Orian-Rousseau V et al (2002) CD44 is required for two consecutive steps in HGF/c-Met signaling. Genes Dev 16(23):3074–3086
147. Sherman LS et al (2000) CD44 enhances neuregulin signaling by Schwann cells. J Cell Biol 150(5):1071–1084
148. Bourguignon LY et al (1997) Interaction between the adhesion receptor, CD44, and the oncogene product, p185HER2, promotes human ovarian tumor cell activation. J Biol Chem 272(44):27913–27918
149. Draffin JE et al (2004) CD44 potentiates the adherence of metastatic prostate and breast cancer cells to bone marrow endothelial cells. Cancer Res 64(16):5702–5711
150. Hiraga T, Ito S, Nakamura H (2013) Cancer stem-like cell marker CD44 promotes bone metastases by enhancing tumorigenicity, cell motility, and hyaluronan production. Cancer Res 73(13):4112–4122
151. Brown RL et al (2011) CD44 splice isoform switching in human and mouse epithelium is essential for epithelial-mesenchymal transition and breast cancer progression. J Clin Invest 121(3):1064–1074
152. Kouros-Mehr H et al (2008) GATA-3 links tumor differentiation and dissemination in a luminal breast cancer model. Cancer Cell 13(2):141–152
153. Schabath H et al (2006) CD24 affects CXCR4 function in pre-B lymphocytes and breast carcinoma cells. J Cell Sci 119(Pt 2):314–325
154. Cojoc M et al (2013) Emerging targets in cancer management: role of the CXCL12/CXCR4 axis. Onco Targets Ther 6: 1347–1361
155. Sheridan C et al (2006) CD44+/CD24– breast cancer cells exhibit enhanced invasive properties: an early step necessary for metastasis. Breast Cancer Res 8(5):R59
156. Liu R et al (2007) The prognostic role of a gene signature from tumorigenic breast-cancer cells. N Engl J Med 356(3):217–226
157. Balic M et al (2006) Most early disseminated cancer cells detected in bone marrow of breast cancer patients have a putative breast cancer stem cell phenotype. Clin Cancer Res 12(19):5615–5621
158. Liu H et al (2010) Cancer stem cells from human breast tumors are involved in spontaneous metastases in orthotopic mouse models. Proc Natl Acad Sci U S A 107(42): 18115–18120

159. Theodoropoulos PA et al (2010) Circulating tumor cells with a putative stem cell phenotype in peripheral blood of patients with breast cancer. Cancer Lett 288(1):99–106
160. Charafe-Jauffret E et al (2010) Aldehyde dehydrogenase 1-positive cancer stem cells mediate metastasis and poor clinical outcome in inflammatory breast cancer. Clin Cancer Res 16(1):45–55
161. Liu S et al (2011) Breast cancer stem cells are regulated by mesenchymal stem cells through cytokine networks. Cancer Res 71(2): 614–624
162. Lianidou ES, Markou A (2011) Circulating tumor cells in breast cancer: detection systems, molecular characterization, and future challenges. Clin Chem 57(9):1242–1255
163. Murray NP et al (2012) Redefining micrometastasis in prostate cancer: a comparison of circulating prostate cells, bone marrow disseminated tumor cells and micrometastasis—implications in determining local or systemic treatment for biochemical failure after radical prostatectomy. Int J Mol Med 30(4):896–904
164. Cristofanilli M et al (2005) Circulating tumor cells: a novel prognostic factor for newly diagnosed metastatic breast cancer. J Clin Oncol 23(7):1420–1430
165. Joosse SA, Pantel K (2013) Biologic challenges in the detection of circulating tumor cells. Cancer Res 73(1):8–11
166. Maheswaran S et al (2008) Detection of mutations in EGFR in circulating lung-cancer cells. N Engl J Med 359(4):366–377
167. Nagrath S et al (2007) Isolation of rare circulating tumour cells in cancer patients by microchip technology. Nature 450(7173): 1235–1239
168. Baccelli I et al (2013) Identification of a population of blood circulating tumor cells from breast cancer patients that initiates metastasis in a xenograft assay. Nat Biotechnol 31(6): 539–544
169. Zhang L et al (2013) The identification and characterization of breast cancer CTCs competent for brain metastasis. Sci Transl Med 5(180):180ra48
170. Yu M et al (2013) Circulating breast tumor cells exhibit dynamic changes in epithelial and mesenchymal composition. Science 339(6119):580–584
171. Pestrin M et al (2012) Final results of a multicenter phase II clinical trial evaluating the activity of single-agent lapatinib in patients with HER2-negative metastatic breast cancer and HER2-positive circulating tumor cells. A proof-of-concept study. Breast Cancer Res Treat 134(1):283–289
172. Giordano A et al (2011) Artificial neural network analysis of circulating tumor cells in metastatic breast cancer patients. Breast Cancer Res Treat 129(2):451–458
173. Cohen SJ et al (2009) Prognostic significance of circulating tumor cells in patients with metastatic colorectal cancer. Ann Oncol 20(7):1223–1229
174. Olmos D et al (2009) Circulating tumour cell (CTC) counts as intermediate end points in castration-resistant prostate cancer (CRPC): a single-centre experience. Ann Oncol 20(1): 27–33
175. Allard WJ et al (2004) Tumor cells circulate in the peripheral blood of all major carcinomas but not in healthy subjects or patients with nonmalignant diseases. Clin Cancer Res 10(20):6897–6904
176. Whitesides GM (2006) The origins and the future of microfluidics. Nature 442(7101): 368–373
177. Khandurina J et al (2000) Integrated system for rapid PCR-based DNA analysis in microfluidic devices. Anal Chem 72(13):2995–3000
178. Erickson D et al (2004) Electrokinetically controlled DNA hybridization microfluidic chip enabling rapid target analysis. Anal Chem 76(24):7269–7277
179. Haeberle S, Zengerle R (2007) Microfluidic platforms for lab-on-a-chip applications. Lab Chip 7(9):1094–1110
180. Gleghorn JP et al (2010) Capture of circulating tumor cells from whole blood of prostate cancer patients using geometrically enhanced differential immunocapture (GEDI) and a prostate-specific antibody. Lab Chip 10(1):27–29
181. Adams AA et al (2008) Highly efficient circulating tumor cell isolation from whole blood and label-free enumeration using polymer-based microfluidics with an integrated conductivity sensor. J Am Chem Soc 130(27): 8633–8641
182. Stott SL et al (2010) Isolation of circulating tumor cells using a microvortex-generating herringbone-chip. Proc Natl Acad Sci U S A 107(43):18392–18397
183. Yoon HJ et al (2013) Sensitive capture of circulating tumour cells by functionalized graphene oxide nanosheets. Nat Nanotechnol 8(10):735–741
184. Lin HK et al (2010) Portable filter-based microdevice for detection and characterization of circulating tumor cells. Clin Cancer Res 16(20):5011–5018
185. Vona G et al (2004) Impact of cytomorphological detection of circulating tumor cells in patients with liver cancer. Hepatology 39(3): 792–797

186. Zheng S et al (2007) Membrane microfilter device for selective capture, electrolysis and genomic analysis of human circulating tumor cells. J Chromatogr A 1162(2):154–161
187. Zheng S et al (2011) 3D microfilter device for viable circulating tumor cell (CTC) enrichment from blood. Biomed Microdevices 13(1):203–213
188. Kuo JS et al (2010) Deformability considerations in filtration of biological cells. Lab Chip 10(7):837–842
189. Zhou J, Papautsky I (2013) Fundamentals of inertial focusing in microchannels. Lab Chip 13(6):1121–1132
190. Bhagat AA, Kuntaegowdanahalli SS, Papautsky I (2008) Continuous particle separation in spiral microchannels using Dean flows and differential migration. Lab Chip 8(11):1906–1914
191. Hou HW et al (2013) Isolation and retrieval of circulating tumor cells using centrifugal forces. Sci Rep 3:1259
192. Ozkumur E et al (2013) Inertial focusing for tumor antigen-dependent and -independent sorting of rare circulating tumor cells. Sci Transl Med 5(179):179ra47
193. Zhang W et al (2012) Microfluidics separation reveals the stem-cell-like deformability of tumor-initiating cells. Proc Natl Acad Sci U S A 109(46):18707–18712
194. Kuperwasser C et al (2004) Reconstruction of functionally normal and malignant human breast tissues in mice. Proc Natl Acad Sci U S A 101(14):4966–4971
195. DeRose YS et al (2011) Tumor grafts derived from women with breast cancer authentically reflect tumor pathology, growth, metastasis and disease outcomes. Nat Med 17(11):1514–1520
196. Zhang X et al (2013) A renewable tissue resource of phenotypically stable, biologically and ethnically diverse, patient-derived human breast cancer xenograft models. Cancer Res 73(15):4885–4897
197. Marangoni E et al (2007) A new model of patient tumor-derived breast cancer xenografts for preclinical assays. Clin Cancer Res 13(13):3989–3998
198. Beckhove P et al (2003) Efficient engraftment of human primary breast cancer transplants in nonconditioned NOD/Scid mice. Int J Cancer 105(4):444–453
199. Bergamaschi A et al (2009) Molecular profiling and characterization of luminal-like and basal-like in vivo breast cancer xenograft models. Mol Oncol 3(5–6):469–482
200. du Manoir S et al (2013) Breast tumor PDXs are genetically plastic and correspond to a subset of aggressive cancers prone to relapse. Mol Oncol 8:431–43
201. Clarke R et al (2001) Cellular and molecular pharmacology of antiestrogen action and resistance. Pharmacol Rev 53(1):25–71
202. Cottu P et al (2012) Modeling of response to endocrine therapy in a panel of human luminal breast cancer xenografts. Breast Cancer Res Treat 133(2):595–606
203. Kabos P et al (2012) Patient-derived luminal breast cancer xenografts retain hormone receptor heterogeneity and help define unique estrogen-dependent gene signatures. Breast Cancer Res Treat 135(2):415–432
204. Ginestier C et al (2010) CXCR1 blockade selectively targets human breast cancer stem cells in vitro and in xenografts. J Clin Invest 120(2):485–497
205. Turkson J, Jove R (2000) STAT proteins: novel molecular targets for cancer drug discovery. Oncogene 19(56):6613–6626
206. Redell MS, Tweardy DJ (2005) Targeting transcription factors for cancer therapy. Curr Pharm Des 11(22):2873–2887
207. Chen Z, Han ZC (2008) STAT3: a critical transcription activator in angiogenesis. Med Res Rev 28(2):185–200
208. Dave B et al (2012) Selective small molecule Stat3 inhibitor reduces breast cancer tumor-initiating cells and improves recurrence free survival in a human-xenograft model. PLoS One 7(8):e30207
209. Noguera-Troise I et al (2006) Blockade of Dll4 inhibits tumour growth by promoting non-productive angiogenesis. Nature 444(7122):1032–1037
210. Ridgway J et al (2006) Inhibition of Dll4 signalling inhibits tumour growth by deregulating angiogenesis. Nature 444(7122):1083–1087
211. Scehnet JS et al (2007) Inhibition of Dll4-mediated signaling induces proliferation of immature vessels and results in poor tissue perfusion. Blood 109(11):4753–4760
212. Hoey T et al (2009) DLL4 blockade inhibits tumor growth and reduces tumor-initiating cell frequency. Cell Stem Cell 5(2):168–177
213. Schott AF et al (2013) Preclinical and clinical studies of gamma secretase inhibitors with docetaxel on human breast tumors. Clin Cancer Res 19(6):1512–1524
214. Todaro M et al (2013) Erythropoietin activates cell survival pathways in breast cancer stem-like cells to protect them from chemotherapy. Cancer Res 73(21):6393–6400
215. Ingham PW, McMahon AP (2001) Hedgehog signaling in animal development: paradigms and principles. Genes Dev 15(23):3059–3087

216. Liu S et al (2006) Hedgehog signaling and Bmi-1 regulate self-renewal of normal and malignant human mammary stem cells. Cancer Res 66(12):6063–6071
217. Kubo M et al (2004) Hedgehog signaling pathway is a new therapeutic target for patients with breast cancer. Cancer Res 64(17):6071–6074
218. Tremblay MR et al (2008) Semisynthetic cyclopamine analogues as potent and orally bioavailable hedgehog pathway antagonists. J Med Chem 51(21):6646–6649
219. Robarge KD et al (2009) GDC-0449-a potent inhibitor of the hedgehog pathway. Bioorg Med Chem Lett 19(19):5576–5581
220. Olive KP et al (2009) Inhibition of Hedgehog signaling enhances delivery of chemotherapy in a mouse model of pancreatic cancer. Science 324(5933):1457–1461
221. Chiba S (2006) Notch signaling in stem cell systems. Stem Cells 24(11):2437–2447
222. Roy M, Pear WS, Aster JC (2007) The multifaceted role of Notch in cancer. Curr Opin Genet Dev 17(1):52–59
223. Radtke F, Raj K (2003) The role of Notch in tumorigenesis: oncogene or tumour suppressor? Nat Rev Cancer 3(10):756–767
224. Jhappan C et al (1992) Expression of an activated Notch-related int-3 transgene interferes with cell differentiation and induces neoplastic transformation in mammary and salivary glands. Genes Dev 6(3):345–355
225. Bouras T et al (2008) Notch signaling regulates mammary stem cell function and luminal cell-fate commitment. Cell Stem Cell 3(4): 429–441
226. Reedijk M et al (2005) High-level coexpression of JAG1 and NOTCH1 is observed in human breast cancer and is associated with poor overall survival. Cancer Res 65(18): 8530–8537
227. Harrison H et al (2010) Regulation of breast cancer stem cell activity by signaling through the Notch4 receptor. Cancer Res 70(2): 709–718
228. Zang S et al (2010) RNAi-mediated knockdown of Notch-1 leads to cell growth inhibition and enhanced chemosensitivity in human breast cancer. Oncol Rep 23(4):893–899
229. Olsauskas-Kuprys R, Zlobin A, Osipo C (2013) Gamma secretase inhibitors of Notch signaling. Onco Targets Ther 6:943–955
230. Lindsay J et al (2008) ErbB2 induces Notch1 activity and function in breast cancer cells. Clin Transl Sci 1(2):107–115
231. Farnie G et al (2013) Combined inhibition of ErbB1/2 and Notch receptors effectively targets breast ductal carcinoma in situ (DCIS) stem/progenitor cell activity regardless of ErbB2 status. PLoS One 8(2):e56840
232. Osipo C et al (2008) ErbB-2 inhibition activates Notch-1 and sensitizes breast cancer cells to a gamma-secretase inhibitor. Oncogene 27(37):5019–5032
233. Won HY et al (2012) Loss of Mel-18 enhances breast cancer stem cell activity and tumorigenicity through activating Notch signaling mediated by the Wnt/TCF pathway. FASEB J 26(12):5002–5013
234. Rexer BN, Arteaga CL (2013) Optimal targeting of HER2-PI3K signaling in breast cancer: mechanistic insights and clinical implications. Cancer Res 73(13):3817–3820
235. Nagata Y et al (2004) PTEN activation contributes to tumor inhibition by trastuzumab, and loss of PTEN predicts trastuzumab resistance in patients. Cancer Cell 6(2):117–127
236. Korkaya H et al (2009) Regulation of mammary stem/progenitor cells by PTEN/Akt/beta-catenin signaling. PLoS Biol 7(6):e1000121
237. Junttila TT et al (2009) Ligand-independent HER2/HER3/PI3K complex is disrupted by trastuzumab and is effectively inhibited by the PI3K inhibitor GDC-0941. Cancer Cell 15(5): 429–440
238. Serra V et al (2008) NVP-BEZ235, a dual PI3K/mTOR inhibitor, prevents PI3K signaling and inhibits the growth of cancer cells with activating PI3K mutations. Cancer Res 68(19):8022–8030
239. Andre F et al (2010) Phase I study of everolimus plus weekly paclitaxel and trastuzumab in patients with metastatic breast cancer pretreated with trastuzumab. J Clin Oncol 28(34): 5110–5115
240. Chakrabarty A et al (2013) Trastuzumab-resistant cells rely on a HER2-PI3K-FoxO-survivin axis and are sensitive to PI3K inhibitors. Cancer Res 73(3):1190–1200
241. Klaus A, Birchmeier W (2008) Wnt signalling and its impact on development and cancer. Nat Rev Cancer 8(5):387–398
242. Logan CY, Nusse R (2004) The Wnt signaling pathway in development and disease. Annu Rev Cell Dev Biol 20:781–810
243. Badders NM et al (2009) The Wnt receptor, Lrp5, is expressed by mouse mammary stem cells and is required to maintain the basal lineage. PLoS One 4(8):e6594
244. Bafico A et al (2004) An autocrine mechanism for constitutive Wnt pathway activation in human cancer cells. Cancer Cell 6(5): 497–506
245. Klopocki E et al (2004) Loss of SFRP1 is associated with breast cancer progression and

poor prognosis in early stage tumors. Int J Oncol 25(3):641–649

246. Nagahata T et al (2003) Amplification, up-regulation and over-expression of DVL-1, the human counterpart of the Drosophila disheveled gene, in primary breast cancers. Cancer Sci 94(6):515–518
247. Nakopoulou L et al (2006) Study of phospho-beta-catenin subcellular distribution in invasive breast carcinomas in relation to their phenotype and the clinical outcome. Mod Pathol 19(4):556–563
248. Piva et al (2014) Sox2 promotes tamoxifen resistance in breast cancer cells. EMBO Mol Med 6:66–79
249. Li Y et al (2003) Evidence that transgenes encoding components of the Wnt signaling pathway preferentially induce mammary cancers from progenitor cells. Proc Natl Acad Sci U S A 100(26):15853–15858
250. Liu BY et al (2004) The transforming activity of Wnt effectors correlates with their ability to induce the accumulation of mammary progenitor cells. Proc Natl Acad Sci U S A 101(12):4158–4163
251. Conley SJ et al (2012) Antiangiogenic agents increase breast cancer stem cells via the generation of tumor hypoxia. Proc Natl Acad Sci U S A 109(8):2784–2789
252. Yang ZQ et al (2009) Methylation-associated silencing of SFRP1 with an 8p11-12 amplification inhibits canonical and non-canonical WNT pathways in breast cancers. Int J Cancer 125(7):1613–1621
253. He B et al (2004) A monoclonal antibody against Wnt-1 induces apoptosis in human cancer cells. Neoplasia 6(1):7–14
254. DeAlmeida VI et al (2007) The soluble wnt receptor Frizzled8CRD-hFc inhibits the growth of teratocarcinomas in vivo. Cancer Res 67(11):5371–5379
255. Albini A, Sporn MB (2007) The tumour microenvironment as a target for chemoprevention. Nat Rev Cancer 7(2):139–147
256. Karnoub AE et al (2007) Mesenchymal stem cells within tumour stroma promote breast cancer metastasis. Nature 449(7162):557–563
257. Asselin-Labat ML et al (2010) Control of mammary stem cell function by steroid hormone signalling. Nature 465(7299):798–802
258. Fillmore CM et al (2010) Estrogen expands breast cancer stem-like cells through paracrine FGF/Tbx3 signaling. Proc Natl Acad Sci U S A 107(50):21737–21742
259. Pierce BL et al (2009) Elevated biomarkers of inflammation are associated with reduced survival among breast cancer patients. J Clin Oncol 27(21):3437–3444
260. Coussens LM, Werb Z (2002) Inflammation and cancer. Nature 420(6917):860–867
261. Sansone P et al (2007) IL-6 triggers malignant features in mammospheres from human ductal breast carcinoma and normal mammary gland. J Clin Invest 117(12): 3988–4002
262. Conze D et al (2001) Autocrine production of interleukin 6 causes multidrug resistance in breast cancer cells. Cancer Res 61(24): 8851–8858
263. Iliopoulos D, Hirsch HA, Struhl K (2009) An epigenetic switch involving NF-kappaB, Lin28, Let-7 MicroRNA, and IL6 links inflammation to cell transformation. Cell 139(4):693–706
264. Korkaya H et al (2012) Activation of an IL6 inflammatory loop mediates trastuzumab resistance in HER2+ breast cancer by expanding the cancer stem cell population. Mol Cell 47(4):570–584
265. Germain D, Frank DA (2007) Targeting the cytoplasmic and nuclear functions of signal transducers and activators of transcription 3 for cancer therapy. Clin Cancer Res 13(19): 5665–5669
266. Lin L et al (2013) Evaluation of STAT3 signaling in ALDH+ and ALDH+/CD44+/CD24– subpopulations of breast cancer cells. PLoS One 8(12):e82821
267. Yu F et al (2010) Mir-30 reduction maintains self-renewal and inhibits apoptosis in breast tumor-initiating cells. Oncogene 29(29): 4194–4204
268. Shimono Y et al (2009) Downregulation of miRNA-200c links breast cancer stem cells with normal stem cells. Cell 138(3):592–603
269. World Health Organization (2012) Cancer Fact Sheet N297. http://publications.cancerresearchuk.org/downloads/product/CS_REPORT_WORLD.pdf
270. Phend C (2011) Breast cervical cancer kill 625,000 women each year. (3/25/12). http://abcnews.go.com/Health/breast-cervical-cancers-rise-globally/story?id=14529241
271. National Cancer Institute. Surveillance epidemiology and end results: SEER stat fact sheets. Accessed 31 Mar 12. http://seer.cancer.gov/
272. American Cancer Society. Cancer facts and figures 2012. Accessed 31 Mar 12. http://www.cancer.org/research/cancerfactsstatistics/cancerfactsfigures2012/

273. Perez EA et al (2010) HER2 and chromosome 17 effect on patient outcome in the N9831 adjuvant trastuzumab trial. J Clin Oncol 28(28):4307–4315
274. Recht A et al (1996) The sequencing of chemotherapy and radiation therapy after conservative surgery for early-stage breast cancer. N Engl J Med 334(21):1356–1361
275. Slamon DJ et al (2001) Use of chemotherapy plus a monoclonal antibody against HER2 for metastatic breast cancer that overexpresses HER2. N Engl J Med 344(11):783–792
276. Hedge SR, Sun W, Lynch JP (2008) Systemic and targeted therapy for advanced colon cancer. Expert Rev Gastroenterol Hepatol 2(1):135–149
277. Silvestri GA, Rivera MP (2005) Targeted therapy for the treatment of advanced non-small cell lung cancer: a review of the epidermal growth factor receptor antagonists. Chest 128(6):3975–3984
278. Sherbenou DW, Druker BJ (2007) Applying the discovery of the Philadelphia chromosome. J Clin Invest 117(8):2067–2074
279. Sakariassen PO, Immervoll H, Chekenya M (2007) Cancer stem cells as mediators of treatment resistance in brain tumors: status and controversies. Neoplasia 9(11):882–892
280. Brekelmans CT et al (2007) Tumour characteristics, survival and prognostic factors of hereditary breast cancer from BRCA2-, BRCA1- and non-BRCA1/2 families as compared to sporadic breast cancer cases. Eur J Cancer 43(5):867–876
281. Korkaya H, Wicha MS (2007) Selective targeting of cancer stem cells: a new concept in cancer therapeutics. BioDrugs 21(5): 299–310
282. Houston S (2011) Stemming the tide. ChemistryWorld.org. http://www.rsc.org/chemistryworld/restricted/2011/September/StemmingTheTide.asp
283. Markey K (2009) Firms seek to prove cancer stem cell hypothesis. Bio Market Trends. 29(18). http://www.genengnews.com/gen-articles/firms-seek-to-prove-cancer-stem-cell-hypothesis/3066/

Chapter 2

A Protocol for Studying Embryonic Mammary Progenitor Cells During Mouse Mammary Primordial Development in Explant Culture

Naoko Kogata and Beatrice A. Howard

Abstract

Embryonic explant culture is a powerful technique to observe tissue morphogenesis ex vivo, and is particularly useful for monitoring embryonic mammary gland development. It has been established that mammary cell lineage specification occurs during embryogenesis, although much remains to be elucidated with respect to how this occurs. During mammary specification, mammary progenitor cells are formed. Embryonic mammary development can proceed and be monitored in embryonic explant culture. Studies using explant culture will greatly enhance our understanding of the cellular mechanisms that regulate embryonic mammary primordial development and mammary progenitor cell specification. We present a protocol for culturing explants from mid-gestation mouse embryos so that morphogenetic processes and mammary epithelial progenitor cells can be studied during embryonic mammary development ex vivo.

Key words Embryonic explant culture, Embryonic mammary progenitor cell, Mammary primordium, Mammary-forming region, *s-SHIP-GFP* reporter mice

1 Introduction

The mammary gland is a skin appendage as the organ originates from local thickening of the epidermis at the mammary-forming region that first appears in the mid-gestation mouse embryo [1]. The thickened epidermis is called the mammary placode and subsequently assembles into an epithelial spheroidal cell cluster, which are present as five pairs of mammary buds by embryonic day (E) 12 in C57Bl6/J (B6) mice. The mammary bud epithelium together with the associating mesenchyme is known as the mammary primordium, which plays a pivotal role in regulating the morphogenesis of the mammary gland via tissue interactions. Lineage tracing studies have shown that embryonic mammary epithelial cells give rise to both basal and luminal postnatal mammary epithelial cells [2, 3]. The embryonic mammary epithelial cells also exhibit

Maria del Mar Vivanco (ed.), *Mammary Stem Cells: Methods and Protocols*, Methods in Molecular Biology, vol. 1293,
DOI 10.1007/978-1-4939-2519-3_2,

ability to self-renew, when assessed by limiting-dilution transplantation assays [4]. Self-renewing multi-potential mammary stem cells are found at a higher incidence in embryonic compared to adult mammary tissue. Some markers that are highly expressed in mammary epithelial stem cell-enriched populations in the adult are also expressed by the embryonic mammary epithelium; one example, Keratin 14 is shown expressed in embryonic mammary primordia (Fig. 1). Embryonic mammary progenitor cell behavior is receiving increasing interest since their study may pave the way to understand mechanisms in breast cancer initiation and progression.

The formation of the primary mammary placode is thought to be driven predominantly by epithelial progenitor cell migration rather than epithelial mitosis [5, 6]. This early mammary developmental phase (E10-E13) is highly distinct from the subsequent stages of placode enlargement, which mainly rely on increased mitosis from E13.5-stage onwards [5]. Excellent methods exist for ex vivo culture of microdissected murine mammary buds from E13-13.5 stages [7, 8]. To date, robust methodology to study cellular dynamics and molecular mechanisms of initial mammary placode assembly remains to be established. Here, we describe a novel protocol for embryonic mammary placode formation in cultured flank explants, based on traditional Trowell-style ex vivo organoid culture that has been optimized for study of the earliest stages of mammary placode development [9]. We also discuss fluorescent-reporter mouse models that may be suitable for labelling and monitoring the formation and expansion of mammary epithelial progenitor cells during embryonic explant culture. The advantage of using a reporter strain of mice for the short isoform of the protein SH2 domain-containing 5′-inositol phosphatase (*s-SHIP*)-*GFP*, which expresses EGFP specifically in epithelial stem cell lineage, is highlighted.

2 Equipment and Materials

2.1 Preparation of Culture Medium

1. Small water bath.
2. Sterilization Box (FST, Heidelberg, Germany, cat no. 20810-01).
3. Hydrophilic and autoclavable filter membranes (Sigma, St. Louis, MO, cat. no. P9699-100EA).
4. Two Cell Cavity slides (Hawksley, Lancing, Sussex, UK, cat. no. 2CS000).

Fig. 1 (continued) cells in embryonic mammary tissue. Mammary primordium 3 from E11.0 *s-SHIP-GFP* embryonic explant cultured for 24 h (**a**), mammary primordium 3 in E12.5 *s-SHIP-GFP* (**b**, **c**) and mammary gland 4 in E16.5 B6 (**d**) were examined by whole-mount immunostaining

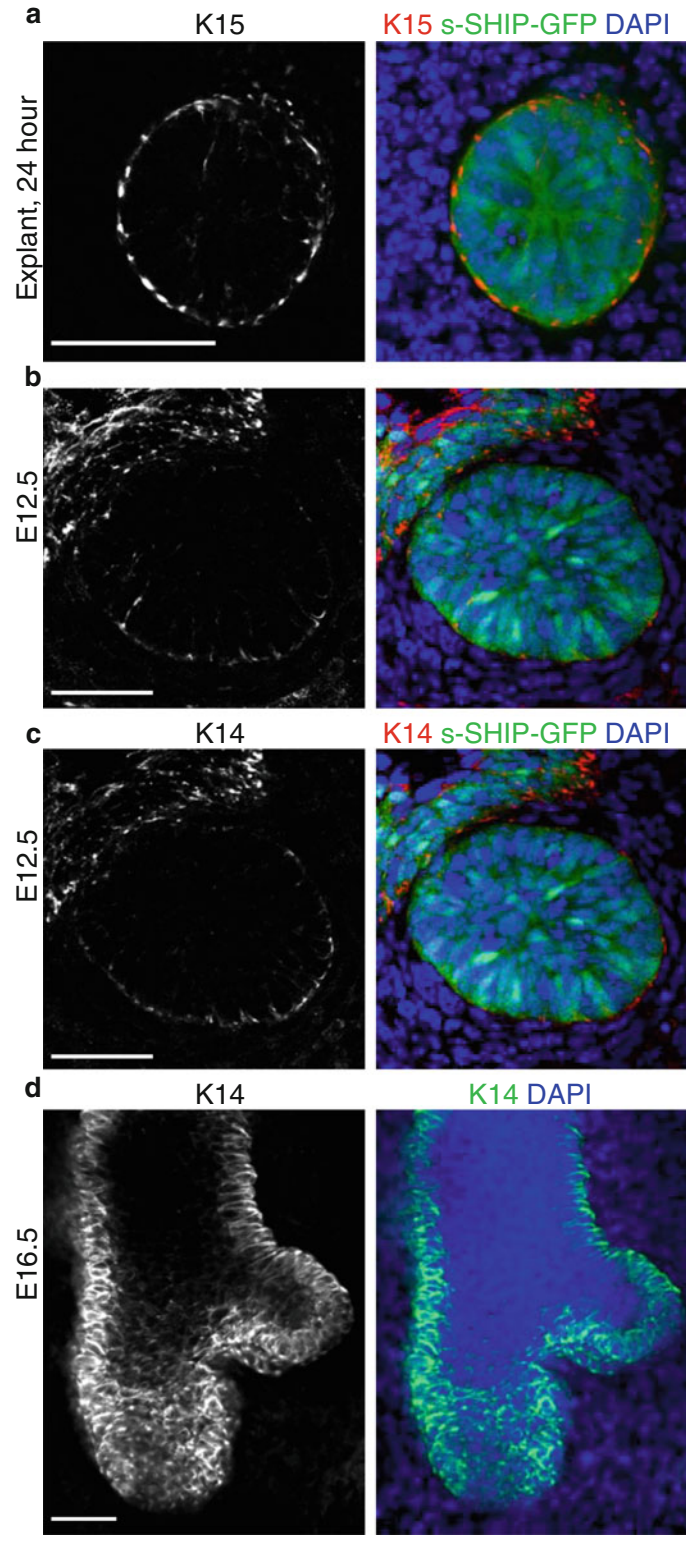

Fig. 1 Examples of mammary epithelial marker expression in embryonic mammary tissue in vivo and ex vivo. Keratin 15 (K15) and keratin 14 (K14) co-expression with s-SHIP-GFP shows the localisation of presumptive mammary basal stem

5. 0.2 μm hydrophilic syringe filter.
6. 50 mL syringe.
7. 50 mL plastic tube.
8. Micropipetter and disposable tips.
9. KSOM medium: EmbryoMax® KSOM Embryo Culture Medium (1×), Powder, w/o Phenol Red (Millipore, Watford, Hartfordshire, UK).
10. L-Ascorbic acid.
11. EmbryoMax® Ultra Pure Water, sterile.
12. (Optional) Any supplements, growth factors, and inhibitors to be studied for effect on mammary primordial development.

2.2 Dissection of Embryo Flank

1. Stereomicroscope for dissecting embryo flank (e.g., Leica MZ16 from Leica microsystems, Milton Keynes, Bucks, UK).
2. Uplight fluorescent microscope (e.g., Leica DM5000B) equipped with a color CCD camera (e.g., Leica DFC 500) and an image acquisition software (e.g., Leica Application Suite ver. 2.8.1).
3. Desired mouse strain (*see* **Note 1**).
4. Sterilized DPBS (Dulbecco's PBS), with Calcium and Magnesium.
5. 10 cm diameter plastic petri dishes.
6. Dissection Scissors (FST, cat. no.14084-08).
7. Dumont #5 forceps (FST, cat. no. 11251-20).
8. Wecker Spring Scissors (FST, cat. no. 15010-11).
9. Round-head microspatula.
10. Tübingen Spring Scissors (FST, cat. no. 15003-08).

2.3 Embryonic Explant Culture

1. CO_2 Incubator for tissue culture use, equilibrated to 37 °C, 5 % CO_2 atmosphere.
2. Falcon 60 mm Centre Well Organ Culture dish (VWR International, Lutterworth, Leicestershire, UK, cat. no. 353037).
3. Nunc Square BioAssay Dishes.

3 Methods

All materials and equipment should be sterile. However, experimental procedures may be carried out in the normal laboratory atmosphere instead of under a laminar flow cabinet. In this manner, we have never experienced contamination within 2 days of organ culture.

3.1 Preparation of Materials and Equipment for Explant Culture

1. Set up matings of suitable mouse strains to obtain pregnant female mice. Vaginal plug monitoring after the pairing is performed on daily basis and the morning of the day the plug is considered as E0. We describe here the procedure using *s-SHIP-GFP* reporter mice [10] (*see* **Note 1**).
2. Autoclave filter membranes and sterilize cavity slides using Sterilization Box.
3. Add 1.33 mL of EmbryoMax pure water into a 100 mg vial of L-Ascorbic acid to make 75 mg/mL Ascorbic acid stock solution. Store 100 μl aliquots at −20 °C for single-use purpose.
4. The KSOM medium is provided as a dry powder format with sterile diluent. Reconstitute the medium by adding exact 50 mL of sterile diluent into a vial of powdered medium (*see* **Note 2**).
5. Incubate the medium in a water bath at 37 °C for 15 min, with occasionally rocking the vial upside down for a few times to gently mix the media.
6. Pass the medium through a 0.2 μm syringe filter attached to a 50 mL syringe and collect the filtered medium in 50 mL tube. The filtered medium can be kept as 10 mL aliquots at 4 °C for up to 1 week.
7. Prepare the priming medium by adding L-Ascorbic acid solution into the KSOM medium at a 1:1,000 dilution (75 μg/mL final), just prior to dissect embryos (*see* **Note 3**). 9 mL of the priming medium is enough to set up five embryos in each organ culture dish. Investigator's choice of additives, i.e., culture supplement, growth factors, immobilized antibodies, and chemical inhibitors, can be included in the priming medium.

3.2 Dissection of Embryo Flanks

1. Sacrifice plugged female mouse in the morning, 11 days after the plug was observed (*see* **Note 4**). Dissect out the whole uterus carefully using Dissection scissors and forceps (Fig. 2a).
2. Transfer the uterus into a petri dish filled in cold DPBS. Carefully make a small cut parallel to muscle fiber alignment of the uterus using a Wecker Spring Scissors so that the conceptus containing the intact embryo inside will slowly slide out from the uterus (Fig. 2b). Take care to do this in this manner otherwise embryos will be squeezed by high contractile force generated from the uterus and may be damaged. Repeat this **step 1** at a time to collect all concepti.
3. Using two Dumont forceps, separate yolk sac containing embryo from the Reichert's membrane, the umbilical vessels and placenta (Fig. 2c). Carefully tear yolk sac and then the vitelline vessels to isolate embryo intact (Fig. 2d). Hereafter, do not damage surface epithelium around the mammary-forming region, the thoracic and inguinal region between

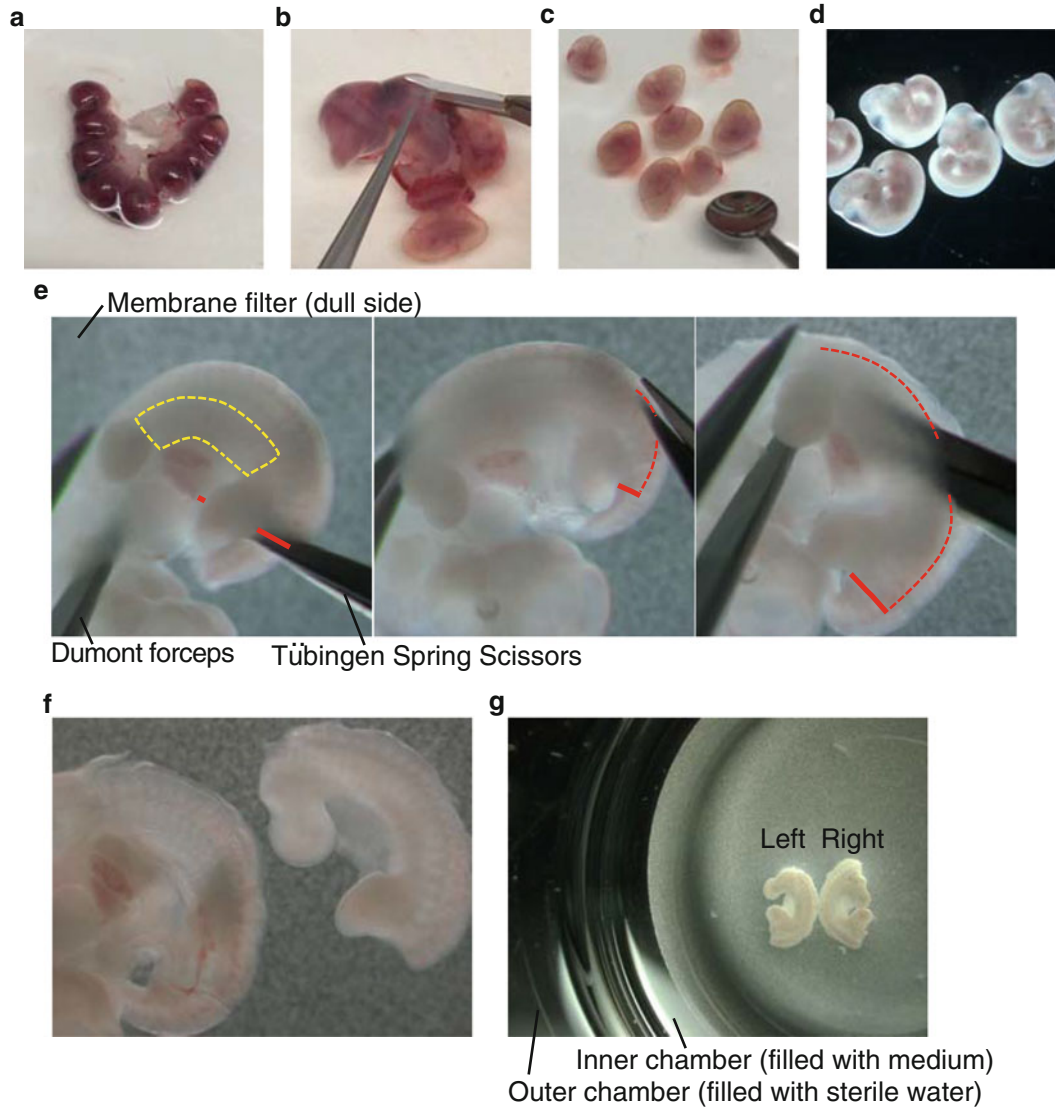

Fig. 2 Dissection of embryo flanks that mammary progenitor cells around mammary-forming region. (**a**) The whole uterus dissected out from plugged female on the morning of E11.0. (**b**) Making a cut alongside the uterine smooth muscle to isolate each conceptus-containing embryo in the yolk sac. (**c**) Embryos in yolk sacs cleared of Reichert's membrane, the umbilical vessels and placenta. (**d**) Intact embryos after removal of yolk sacs and the vitelline vessels. (**e**) Sequential steps of dissecting embryo flank. *Red solid line* indicates the first cut made at the lower side of a hindlimb, and *red dotted line* indicates a sequential incision to extract the flank from the embryo. Mammary-forming region is shown as *yellow-dotted area* which contains mammary progenitor cells. (**f**) A dissected embryonic flank and an embryo body which will be dissected to extract flank. (**g**) Both left and right embryonic flanks placed on a membrane in Organ Culture dish, which is ready for photograph fluorescent images and incubation

forelimb and hindlimb where the mammary epithelial progenitor cells reside in embryo. Also make sure that the embryo is entirely soaked in DPBS in order to keep it hydrated at all times.

4. Next, examine the stage of mammary placode formation. Inspect the distribution of mammary epithelial progenitor cells over mammary-forming region by checking fluorescence under fluorescent microscope. Typical distribution of *s-SHIP-GFP*-positive mammary progenitor cells is shown in Fig. 3a. Embryos in which any mammary placode had not formed yet are suitable to use and should proceed to embryonic flank dissection, if researcher wishes to observe mammary placode 3 formation. Embryos which have already formed mammary placode 3 can be used to study the formation of mammary placode 2 and 4. Local progenitor cell migration is thought to a major driver of initial mammary placode formation [5, 6], which is disturbed by sample dehydration and scratches or other damage to the epidermis (Fig. 3b). Damaged samples should be excluded from culture as they will not develop mammary placodes.
5. Transfer embryos using microspatula into a petri dish filled with fresh ice-cold DPBS and keep them on ice until dissection (*see* **Note 5**).
6. Prepare organ culture dish: place 1.5 mL of the priming medium or medium containing growth factors or inhibitors in the center reservoir of Centre Well Organ Culture dish. Add approximately 2 mL of sterile water in the outer reservoir of dish for humidifying purpose. Pre-incubate the dish within small water bath or in CO_2 incubator.
7. Preparations for flank dissection: Filter membranes have a dull surface on one side and a shiny surface on the other side. Soak suitable number of membranes with the dull side upward in a petri dish filled with DPBS. Prepare another petri dish filled with DPBS, containing one cavity slide and one hydrated membrane with the dull side facing upward at outer area of the slide.
8. Dissect embryonic flanks (Fig. 2e): Transfer one embryo onto the membrane; this makes dissection easier as the dull surface of the membrane prevents embryo moving around in DPBS. Cut tail off at the bottom side of the hindlimb using Tübingen Spring Scissors, while firmly holding the embryo head with a Dumont forceps. Insert Tübingen Spring Scissors from the incision, and gradually expand a lengthwise cut toward the top of forelimb on both dorsal and ventral side so that embryonic flank including both limbs (Fig. 2f). Again, pay great attention not to disrupt epidermis of mammary-forming region during dissection. Turn the remaining embryo and repeat

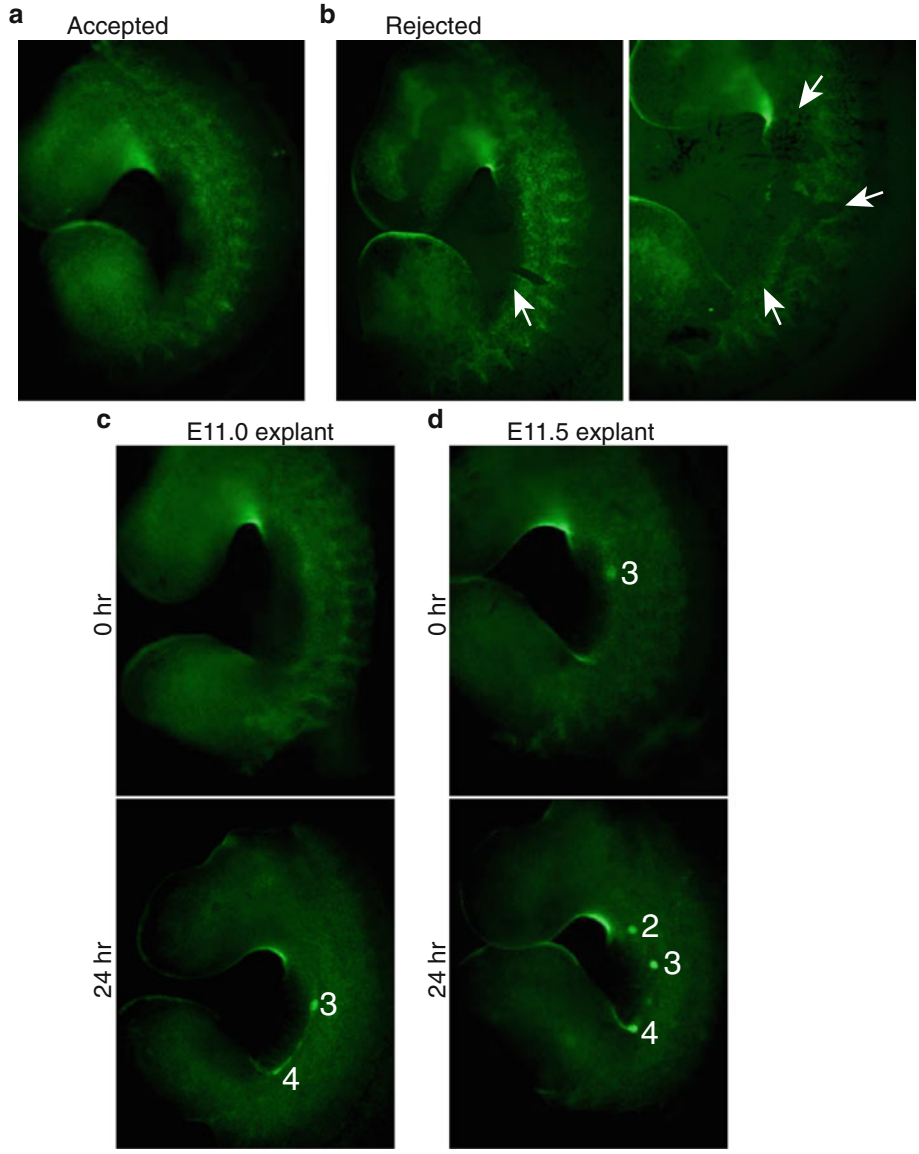

Fig. 3 Examples of E11.0 embryonic flanks that are suitable and unsuitable for use in mammary placode culture. (**a**) GFP photographs of embryonic flank displaying typical distribution of *s-SHIP-GFP*-positive mammary progenitor cells at E11.0. (**b**) Damaged embryonic flanks should be excluded from further experimental use. *Arrows* indicate damage on epidermis. (**c**) Typical result of E11.0 embryonic explant culture photographed at 0 h and 24 h, showing de novo mammary placode 3 formation. Mammary placode is numbered in images. (**d**) Typical result of E11.5 embryonic explant culture photographed at 0 h and 24 h, showing de novo mammary placode 2 and 4 formation

for the other side of embryonic flank. Assemble the isolated flanks in the center of membrane.

9. Bring one Organ Culture dish filled with culture medium out from incubator. Using a Dumont forceps, move the membrane with the flanks on a cavity slide (make sure the flanks are still completely soaked in DPBS). Slowly lift the membrane with the flanks using a Dumont forceps from the cavity slide, so that surface tension at the air–liquid interface is gradually reduced and flank stays put. Gently place the membrane with flanks on the center chamber of Organ Culture dish without making any bubbles (Fig. 2g). The size difference between the membrane and the center chamber allows some medium to escape to the upside of membrane. Gently rock the Culture dish to enhance embryonic flank merging with medium. Finally, the flanks should be placed at the interface of air–liquid, but should neither be floating nor completely submerged in the medium.
10. Repeat **steps 7–9** for the remaining embryos (*see* **Note 5**).

3.3 Embryonic Explant Culture

1. Photograph GFP image of *s-SHIP-GFP* embryonic explant as 0 h.
2. After imaging, incubate embryonic flanks in humidified 5 % CO_2 incubator. Check explants 3 h after incubation and gently rock the culture dish for a few times to rehydrate explants with medium if necessary. Photograph GFP image of *s-SHIP-GFP* embryonic explant at 24 h as generally mammary placode is formed by that time. Typical results of de novo mammary placode 3 and mammary placode 2, 4 are shown in Fig. 3c, d, respectively. A comparison of mammary progenitor cell mitosis in different explant culture medium is shown in Fig. 4.

4 Notes

1. Mammary placode is morphologically visible under the stereomicroscope from only E11.5 onward in B6 mice. Use of a suitable model mouse expressing a fluorescent protein in mammary progenitor cells is highly recommended for this protocol. The distribution of those cells not only can be traced at several time-points during culture but also will be a good indicator to judge whether each sample is suitable for culture. *s-SHIP-GFP* mice developed in the Rohrschneider laboratory is so far the most characterized model to study mammary epithelial stem and progenitor cells [10], which express EGFP in a variety of epithelial stem cell lineages. We routinely cross this strain with mouse models of interest, including gene-targeted mice to study gene function in mammary placode formation.

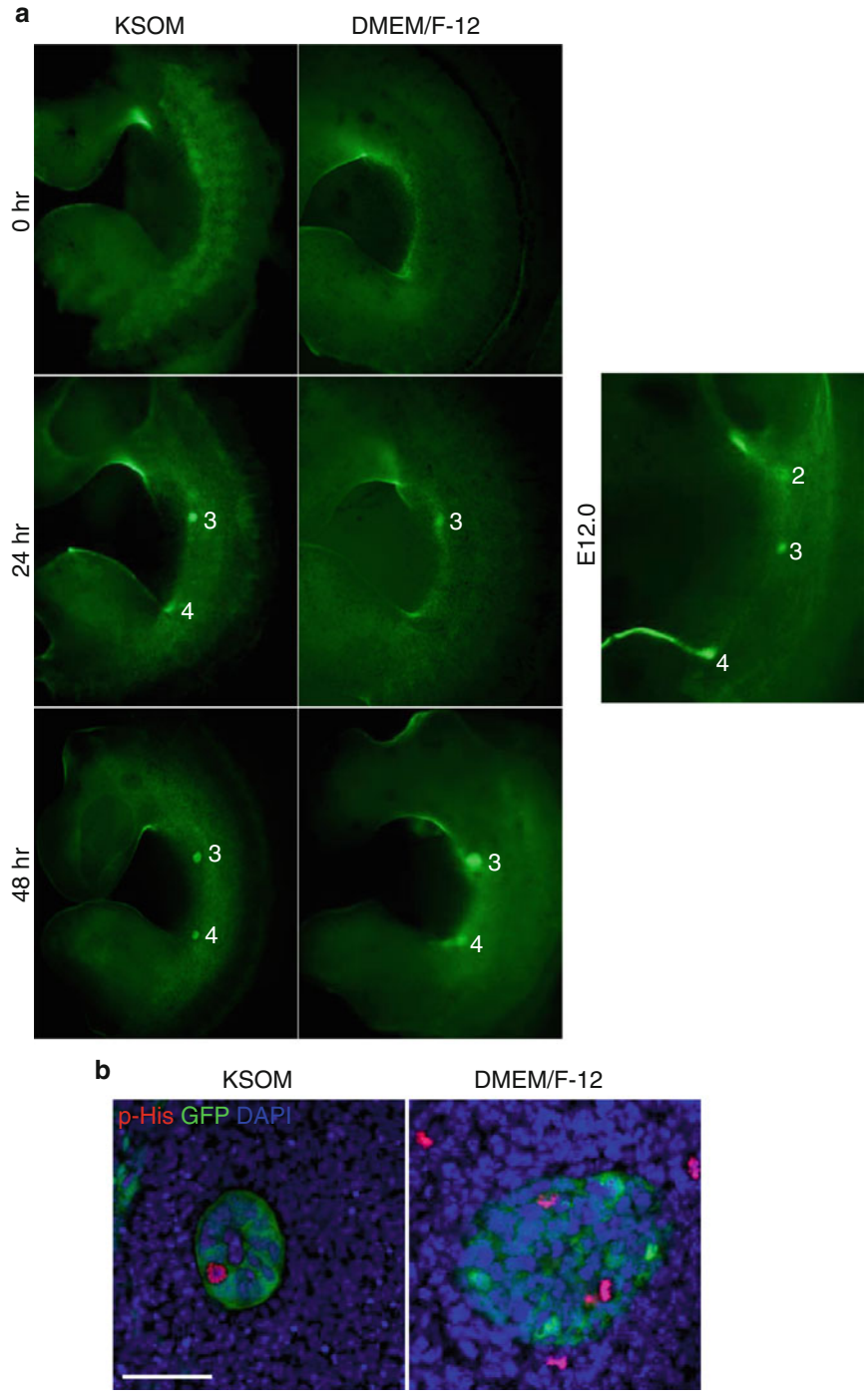

Fig. 4 Comparison of mammary progenitor cell mitosis in different explant culture medium. (**a**) GFP images of E11.0 embryonic explants cultured with either KSOM medium or DMEM/F-12 medium. Explant cultured with KSOM develops mammary placode 3 comprising compacted cells within 24 h. Mammary placode 3 developed in DMEM/F-12 at 24 h is rather faint when compared to that in KSOM and E12.0 mammary placode, and develops further into an abnormally large mammary placode after 48 h. Mammary placode is numbered in images. (**b**) Phospho-Histone 3 staining on E11.0 explant mammary placode cultured for 24 h. Note that explant culture using DMEM/F-12 medium facilitates mammary progenitor cell mitosis, which is consistent with increased size in mammary placode (**a**). Scale, 50 μm

Wnt signalling-reporter models, listed below, are also favorable for studying embryonic mammary gland development:

Axin2CreERT2 mice [3] (*B6.129(Cg)-Axin2tm1(cre/ERT2) Rnu/J*) available from The Jackson Laboratory, Maine, USA. This model is expected to label mammary epithelial progenitor cells during embryonic mammary placode formation when bred to reporter mice harboring *Cre-loxP*–inducible fluorescent protein gene, for example, B6;129-Gt(ROSA) 26Sortm1Joe/J from The Jackson Laboratory.

ins-TOPEGFP mice [11] (*B6;CBA-Tg(Axin2-d2EGFP)5Cos/Mmnc*, stock number 015749-UNC) available from Mutant Mouse Regional Resource Centers at The Jackson Laboratory.

TCF/Lef:H2B-GFP mice [12] (*Tg(TCF/Lef1-HIST1H2BB/EGFP)61Hadj/J*) available from The Jackson Laboratory.

2. Accurate measurement when withdrawing the diluent is required for optimal medium performance with precise pH and osmolality.
3. In our experience, the success of explant culture is highly influenced by L-Ascorbic acid that is rapidly oxidized and expires under in vitro circumstance. L-Ascorbic acid is essential for the synthesis and hydration of various extracellular matrix components (i.e., Collagen).
4. If researcher wishes to observe mammary placode 3 formation in explant culture, 7–8 AM is an ideal time to start collect embryos in B6 background as at this time they will not have developed any mammary placode. To study the formation of mammary placode 2 and 4, researcher can collect embryos between 10 AM–1 PM as mammary placode 3 is forming and the others will follow shortly.
5. Ex vivo whole embryos often progress through the stages of mammary formation rapidly and develop the mammary placode within 2–4 h. Therefore, the dissection of embryonic flanks should be performed as speedily as possible, ideally within 2 h. Keep embryos to be dissected on ice in order to prevent the developmental progress of placode formation from occurring prior to starting culture of the embryonic explant.

Acknowledgement

This work was funded by Breakthrough Breast Cancer Research.

References

1. Propper AY, Howard BA, Veltmaat JM (2013) Prenatal morphogenesis of mammary glands in mouse and rabbit. J Mammary Gland Biol Neoplasia 18(2):93–104. doi:10.1007/s10911-013-9298-0
2. Van Keymeulen A, Rocha AS, Ousset M, Beck B, Bouvencourt G, Rock J, Sharma N, Dekoninck S, Blanpain C (2011) Distinct stem cells contribute to mammary gland development and maintenance. Nature 479(7372):189–193. doi:10.1038/nature10573
3. van Amerongen R, Bowman AN, Nusse R (2012) Developmental stage and time dictate the fate of Wnt/beta-catenin-responsive stem cells in the mammary gland. Cell Stem Cell 11(3):387–400. doi:10.1016/j.stem.2012.05.023
4. Makarem M, Kannan N, Nguyen LV, Knapp DJ, Balani S, Prater MD, Stingl J, Raouf A, Nemirovsky O, Eirew P, Eaves CJ (2013) Developmental changes in the in vitro activated regenerative activity of primitive mammary epithelial cells. PLoS Biol 11(8):e1001630. doi:10.1371/journal.pbio.1001630
5. Balinsky BI (1950) On the prenatal growth of the mammary gland rudiment in the mouse. J Anat 84(3):227–235
6. Balinsky BI (1952) I.—On the developmental processes in mammary glands and other epidermal structures. Earth Environ Sci Trans R Soc Edinb 62(01):1–31. doi:10.1017/S0080456800009224
7. Kratochwil K, Schwartz P (1976) Tissue interaction in androgen response of embryonic mammary rudiment of mouse: identification of target tissue for testosterone. Proc Natl Acad Sci U S A 73(11):4041–4044
8. Voutilainen M, Lindfors PH, Mikkola ML (2013) Protocol: ex vivo culture of mouse embryonic mammary buds. J Mammary Gland Biol Neoplasia 18(2):239–245. doi:10.1007/s10911-013-9288-2
9. Trowell OA (1959) The culture of mature organs in a synthetic medium. Exp Cell Res 16(1):118–147
10. Rohrschneider LR, Custodio JM, Anderson TA, Miller CP, Gu H (2005) The intron 5/6 promoter region of the ship1 gene regulates expression in stem/progenitor cells of the mouse embryo. Dev Biol 283(2):503–521. doi:10.1016/j.ydbio.2005.04.032, S0012-1606(05)00270-8 [pii]
11. Moriyama A, Kii I, Sunabori T, Kurihara S, Takayama I, Shimazaki M, Tanabe H, Oginuma M, Fukayama M, Matsuzaki Y, Saga Y, Kudo A (2007) GFP transgenic mice reveal active canonical Wnt signal in neonatal brain and in adult liver and spleen. Genesis 45(2):90–100. doi:10.1002/dvg.20268
12. Hadjantonakis AK, Papaioannou VE (2004) Dynamic in vivo imaging and cell tracking using a histone fluorescent protein fusion in mice. BMC Biotechnol 4:33. doi:10.1186/1472-6750-4-33, 1472-6750-4-33 [pii]

Chapter 3

FACS Sorting Mammary Stem Cells

Oihana Iriondo, Miriam Rábano, and María d.M. Vivanco

Abstract

Fluorescent-activated cell sorting (FACS) represents one of the key techniques that have been used to isolate and characterize stem cells, including cells from the mammary gland. A combination of approaches, including recognition of cell surface antigens and different cellular activities, has facilitated the identification of stem cells from the healthy mammary gland and from breast tumors. In this chapter we describe the protocol to use FACS to separate breast cancer stem cells, but most of the general principles discussed could be applied to sort other types of cells.

Key words FACS, Immunostaining, Sorting, Stem cells, Cell surface antigens

1 Introduction

For decades researchers have been taking advantage of the specific presence of a particular combination of cell surface antigens to identify and isolate stem cells using fluorescent-activated cell sorting (FACS). Following pioneering work in the 1970s, hematopoietic stem cells (HSCs) were the first tissue-specific stem cells to be purified and characterized [1]. Isolation of HSCs and progenitor cells has served as a template for the isolation of adult stem cells from different tissues.

The striking regenerative capacity of the mammary gland, which undergoes dramatic changes during puberty, pregnancy, lactation, and involution, had been considered indicative of the presence of a pool of stem cells that are able to maintain the tissue architecture of the mammary gland. Support for the presence of stem cells in the human breast emerged from transplantation [2] and X chromosome inactivation studies [3]. Further evidence for the presence of stem cells originated from studies based on in vitro analyses of FACS-sorted mammary epithelial cells exhibiting distinct phenotypes. These were based on combinations of markers from differentiated breast cells. The differentiated epithelial cells that form the mammary epithelium, luminal, and myoepithelial

Maria del Mar Vivanco (ed.), *Mammary Stem Cells: Methods and Protocols*, Methods in Molecular Biology, vol. 1293,
DOI 10.1007/978-1-4939-2519-3_3,

cells can be identified by their expression of various cell surface proteins. The expression of epithelial membrane antigen (EMA, also known as MUC-1) and epithelial specific antigen (ESA or EpCAM) is characteristic of luminal cells, while common acute lymphoblastic leukemia antigen (CALLA or CD10) represents a myoepithelial cell surface marker. Two putative mammary progenitors were proposed based on the morphology and marker expression of colonies grown at low clonal density in culture, $EMA^{+}CALLA^{-}ESA^{+}$ cells as candidate alveolar progenitors and $EMA^{+/\mp}CALLA^{\mp/+}ESA^{+}$ as bipotent ductal progenitors [4]. Additionally, $EMA^{-}ESA^{+}$ cells within the epithelium lineage were suggested as precursor cells of terminal duct lobular units in the human breast [5]. Adopting approaches to identify stem cells in the human breast based on the knowledge of HSCs, and the observation that only EMA and CALLA were shown to separate the luminal and myoepithelial cell types, respectively, to high purity using FACS [6], double-positive (DP) and double-negative (DN) cells for EMA and CALLA were shown to generate mixed colonies containing both luminal and myoepithelial cells from a single cell and, therefore, represent candidate multipotent stem cells [7]. When defined by another combination of cell surface markers, $CD49f^{hi}ESA^{-/low}$, a subset of human breast cells showed mammary regenerative capacity in vivo [8, 9].

Reinforcing the cancer stem cell (CSC) hypothesis, which proposes that tumors arise from transformed normal stem cells, CSCs that exhibit a $CD44^{+}CD24^{-/low}Lin^{-}$ phenotype demonstrated to form tumors in the mammary fat pad of immunocompromised mice. Furthermore, this tumorigenic population could be serially passaged to generate new tumors containing additional $CD44^{+}CD24^{-/low}Lin^{-}$ tumorigenic cells, as well as the phenotypically diverse mixed populations of non-tumorigenic cells present in the initial tumor [10]. This finding supports the hypothesis that mammary tumors are initiated in mutated stem cells, or by more differentiated cells that acquire stem cell-like properties. Importantly, the presence of $CD44^{+}CD24^{-/low}Lin^{-}$ cells within the tumors of breast cancer patients is significantly associated with poor prognosis, shorter disease-free interval, and overall survival [11, 12], suggesting that the presence and frequency of the CSC population have prognostic relevance. It is particularly noteworthy that other phenotypes, also identified by FACS, have contributed to support the association between the presence of tumor cells with a CSC phenotype and patient prognosis. Increased aldehyde dehydrogenase activity was found to identify malignant mammary stem cells and to correlate with poor clinical outcome [13]. Furthermore, it was shown that poorly differentiated tumors contain more CSCs than well-differentiated tumors [14, 15]. The corollary of the presence of cells with a CSC phenotype within the tumor is that these properties may facilitate the development of

resistance to current therapies and lead to enrichment of breast CSCs. Indeed, increases in the proportion of cells with CSC features have been described after radiotherapy [16], chemotherapy [17, 18], and tamoxifen treatment [19]. These findings highlight the need to consider CSCs as targets of novel and complementary forms of therapy.

2 Materials

1. TrypLE™.
2. Phosphate-buffered saline (PBS) without calcium and magnesium.
3. Staining buffer: PBS, 1 % bovine serum albumin (BSA). Weigh 1 g BSA and add PBS to a volume of 100 ml. Dissolve by stirring and filter using 0.2 μm pore size filter. Store at 4 °C.
4. Blocking buffer: PBS, 40 % FBS.
5. FACS Flow: PBS, 1 % BSA, 25 mM Hepes pH 7, 5 mM EDTA. Weigh 1 g BSA and add 2.5 ml Hepes 1 M pH 7, 1 ml EDTA 0.5 M, and 96.5 ml PBS. Dissolve, filter, and store as in previous step.

3 Methods

3.1 Setting Up the Experiment (Antibody Selection and Titration)

Several protocols for flow cytometric analyses have been published and, to date, the way the results are reported is still inconsistent and often unclear. For a recent discussion on data reporting guidelines the reader can refer to [20].

1. Direct vs. indirect staining: Protocols for direct staining are simpler and less time consuming than those for indirect staining. Under some circumstances, indirect staining can be useful because it amplifies the signal. However, background noise can also be increased in indirect staining.
2. Selection of fluorochromes: Take into account the following factors when choosing the fluorochromes to be used in an experiment: (a) know your instrument. The combinations of the fluorochromes to be used in the experiment depend on the type and number of lasers and filters. (b) Try to minimize the spectral overlap among the different fluorochromes (*see* **Note 1**). (c) Use high-efficiency fluorochromes to detect antigens with low expression levels (*see* **Note 2**).
3. Titration (**steps 3**–**7**): Stain a mixture of cells containing cells that express and cells that do not express the antigen of interest with the different antibody concentrations to be tested (*see* **Note 3**). Follow the same protocol that you will use for the experiment.

4. Select the population of interest using the standard gating strategy (see below).
5. In a mono-dimensional histogram, set two gates, one for the negative population and another one for the positive population, and request the median fluorescence intensity (MFI) of each population (*see* **Note 4**).
6. For each sample, calculate the signal-to-noise ratio dividing MFIpos by MFIneg.
7. Draw a scatterplot of concentration vs. signal-to-noise ratio and choose the concentration that gives the maximum ratio (*see* **Note 5**).
8. Compensation controls: In order to calculate compensations, you will need unstained cells and cells single-stained with each of the fluorochromes used in the experiment (*see* **Note 6**).

3.2 Cell Preparation

1. Prepare a single-cell suspension from primary tissue or cultured cells (*see* **Note 7**).
2. Count cells (*see* **Note 8**).
3. Add PBS to wash the cells.

3.3 Cell Staining

Unless otherwise specified, carry out all procedures at 4 °C. Use the same exact procedure for compensation controls, FMO controls, and samples.

1. Centrifuge cell suspension at $400 \times g$ for 5 min.
2. Discard the supernatant and add blocking buffer. Resuspend cells and incubate for 15 min at room temperature (*see* **Note 9**).
3. Wash by adding staining buffer on top of the blocking buffer, mix by pipetting, and centrifuge at $400 \times g$ for 5 min. Discard the supernatant.
4. Add staining buffer to a final concentration of 2.5×10^6 cells per ml, and distribute cells in the wells of a conical bottom 96-well plate (Vee bottom), 100 μl per well (*see* **Note 10**).
5. Centrifuge at $800 \times g$ for 5 min and discard supernatant (*see* **Note 11**).
6. Add the primary antibodies diluted in staining buffer, in a total volume of 100 μl per well (*see* **Note 12**). In this case, cell concentration would be 2.5×10^6 cells per ml (*see* **Note 13**).
7. Incubate for 30 min at 4 °C. Cover the plate with aluminum foil to protect from light if using fluorescence-conjugated primary antibodies (*see* **Note 14**).
8. Add 100 μl staining buffer on top of the diluted antibodies, mix by pipetting, and centrifuge at $800 \times g$ for 5 min. Discard the supernatant.

9. Add 200 μl staining buffer, resuspend by pipetting, and centrifuge at 800 × *g* for 5 min. Discard the supernatant.
10. For indirect staining of cells, repeat **steps 7–9** with a fluorochrome-conjugated appropriate secondary antibody (*see* **Note 15**).
11. Resuspend cells in FACS Flow (*see* **Note 16**).
12. Add the cell viability dye to the appropriate controls and to all the samples and incubate as indicated by the manufacturer.

3.4 Setting Up for Sorting

Start the FACS sorter following the recommendations of the manufacturer. Ideally, by the time cells are stained the FACS sorter should be clean and ready to use.

1. Start up the computer and the cytometer, as indicated by the manufacturer.
2. Install the appropriate size nozzle (use the 100 μm nozzle when sorting breast epithelial cells or breast cancer cells).
3. Use the recommended fluorescent beads to calculate the drop delay (*see* **Note 17**).
4. Install the chosen collection device and test the formation of side streams.
5. If available, temperature control option should be used (*see* **Note 18**).
6. Adjust the area scaling for FSC and the lasers to be used.
7. Adjust the FSC threshold to eliminate the debris from the analysis.

3.5 Analysis and Sorting

1. Calculate compensations: Acquire the unstained control and gate the population of interest in the SSC-A vs. FSC-A plot. Acquire all single-stained control tubes, check the gates corresponding to the positive populations, and calculate compensations (*see* **Notes 19** and **20**).
2. Use cells stained with the viability dye to gate the population of interest (Fig. 1).
3. Acquire the FMO controls and set the gates that will define the positive and negative populations (Fig. 2).
4. Acquire the sample and gate the populations to be sorted.
5. Select the sort precision mode of interest, if available.
6. Start sorting. During sorting, make sure that abort rates are low, to maximize the yield.
7. Once sorting is finished, it is recommended to evaluate the efficiency of the sorting. Take a sample of sorted cells, add the viability dye, and incubate and acquire them using the same

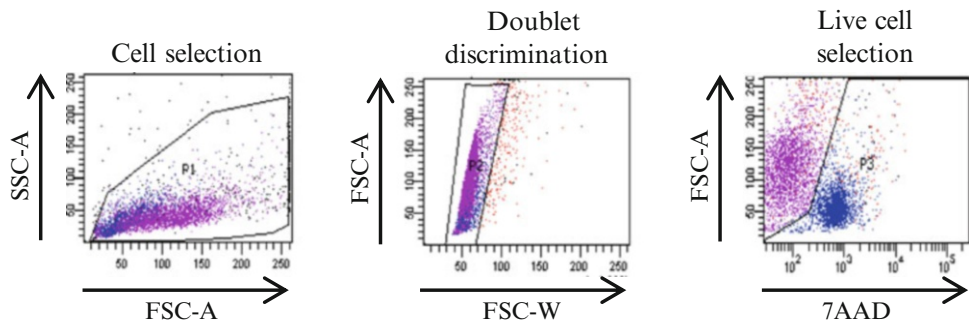

Fig. 1 From the general population (*left*) select single cells (*middle*) and live cells with intact membrane (*right*)

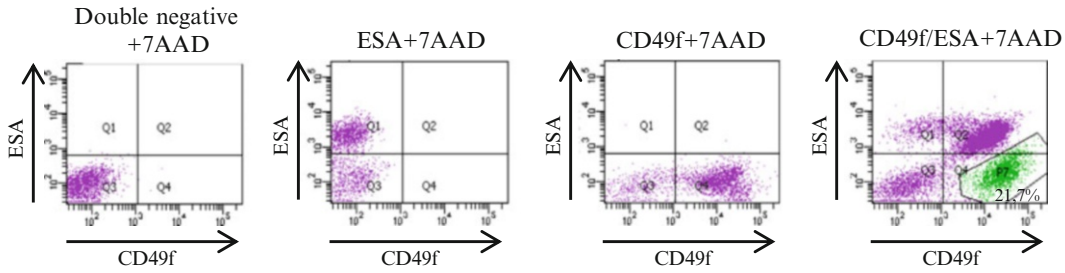

Fig. 2 For a CD49f/ESA staining adjust gates for CD49f using cells stained with anti-ESA antibody and 7AAD, and set gates for ESA using cells stained with anti-CD49f antibody and 7AAD

conditions as in the sorting (same PMT voltages, same flow rate, etc.). This will provide information about the purity of the sorted population and viability of sorted cells.

4 Notes

1. Careful selection of appropriate antibodies, fluorochromes, and controls, as well as titration of antibodies, is absolutely essential for the success of any FACS analysis and sorting experiment. Time used in this first step is time well invested. Spectral overlaps of the fluorochromes used in flow cytometry can be found in different online resources (see for example http://www.bdbiosciences.com/research/multicolor/spectrum_viewer/index.jsp).
2. See for example http://www.bdbiosciences.com/documents/Multicolor_Fluorochrome_Guide.pdf. Choose the weakest fluorochrome for the biggest population and, conversely, the strongest fluorochrome for the smallest cell population

or for weakly expressed antigens. Although the use of FITC-conjugated antibodies is very extended, substituting FITC for Alexa-488 is another option. Both fluorochromes have similar excitation and emission spectra and brightness, but FITC is very sensitive to changes in pH.

3. The objective is to find the concentration of the antibodies with which the signal-to-noise ratio is maximum. If the concentration of the antibody is too low, positive cells could remain unstained, while excess of antibody could increase unspecific binding. Both situations would lead to a lower separation between negative and positive cells. Start with the recommended antibody concentration given by the manufacturer, and do two or threefold serial dilutions.
4. You will need to adjust the gates with each sample.
5. An alternative option is to use the stain index to select the optimum concentration of an antibody, because it also considers the dispersion (W) of the negative population. Stain index = (MFIpos-MFIneg)/W.
6. When the available biological material is scarce, BD™ Compbeads can be used. However, whenever possible, using the same cells as in the experiment is recommended. Fluorescence minus one (FMO) controls should be used for gating, mainly as the number of fluorochromes in an experiment increases. FMO controls contain all the fluorochromes in the experiment except for the one that is being measured. An isotypic control conjugated with the fluorochrome being measured can also be added. The isotypic controls should match with the specific antibody in terms of concentration, fluorochrome-to-antibody ratio (F/P ratio), and isotype.
7. When working with primary cells, it is important to start with a pure preparation of mammary epithelial cells. We use the same protocol as described in [7] for normal breast tissue and [21] for breast tumor samples. When using cells isolated from primary tissue or cell culture, the use of mechanic and/or enzymatic dissociation will be necessary. However, aggressive treatments should be avoided, since they could alter the antigens to be detected. In addition, some cell surface antigens are sensitive to trypsin. Therefore, the use of gentle cell dissociation reagents, such as TrypLE™, is recommended.
8. Always stain more (ideally a minimum of 100,000) cells than the number that you are planning to record, because a percentage of cells is lost during the staining procedure.
9. Depending on the specificity of the antibodies, this step can be omitted.

10. Depending on the number of cells to be stained, staining could be carried out in conical tubes or in 96-well plates.
11. Depending on the cells we are using, it may be necessary to centrifuge cells to a lower speed than indicated. The speed that allows a satisfactory recovery of the cells, without compromising cell viability, should be selected.
12. It is recommended to pre-dilute the antibodies in staining buffer in Eppendorf or 15 ml conical tubes. For example, if a CD24-PE/CD44-APC double staining is being performed, prepare four tubes, each one with a single antibody (twice as concentrated as the desired final concentration). Then add 50 μl of diluted IgG-PE and 50 μl of diluted IgG-APC to a well for the DN control, 50 μl of diluted IgG-APC and 50 μl of diluted CD24-PE to a well for the CD24 control, 50 μl of diluted IgG-PE and 50 μl of diluted CD44-APC to a well for the CD44 control, and 50 μl of diluted CD24-PE and 50 μl of diluted CD44-APC to the wells that will be double stained. If the number of wells to double stain is high, preparing a premix containing both specific antibodies could be useful.
13. The optimal cell concentration may vary depending on cell type (i.e., primary cells vs. cell lines). Small variations in cell concentration do not influence the staining. If a considerable increase in cell concentration is required, tests should be done to ensure that staining intensity is not compromised.
14. The duration and the temperature of the incubation can vary depending on the antibodies. Shorter incubations should be enough when they are done at room temperature, but this could increase the unspecific staining. When the incubation is long, incubation with the antibodies can be done on a rocker to avoid the deposition of cells.
15. When a combination of direct and indirect staining is used, care should be taken to avoid cross-reactivity. If the fluorescent-conjugated antibodies originate from the same species as the unconjugated primary antibody they could be recognized by the fluorescent secondary antibody. In order to prevent that from happening, follow the next procedure: (a) Incubate with unlabelled primary antibody. Wash twice. (b) Incubate with fluorescent secondary antibody. Wash twice. (c) Block any unreacted sites on the secondary antibodies using IgGs or serum from the same species as the primary antibodies. Wash twice. (d) Incubate with labeled primary antibody. Wash twice.
16. Optimum cell concentration for sorting will vary depending on cell type. Mainly when the duration of the sorting is expected to be long, it is recommended to concentrate the sample as much as possible, but making sure that the chosen

concentration does not result in cell aggregation. Higher cell concentrations will shorten the sorting, increasing the viability of sorted cells. In addition, increased number of sorted cells can be obtained at a lower flow rate. Lower flow rates result in lower coefficient of variation (CV), allowing a better separation between positive and negative signals, and positive signals of different intensities.

17. The drop delay is the period of time elapsing from the moment at which the cell of interest is detected at the interrogation point to the moment the droplet containing this cell of interest is charged at the droplet break-off point, so that it is correctly sorted.
18. Temperature is one of the factors that influence viability of sorted cells. The optimum temperature can vary depending on cell type, but we usually sort the mammary epithelial cells at 4 °C. Other factors that affect cell viability are sheath pressure, duration of cell sorting, and collection medium.
19. Cells that are positive for each fluorochrome should be at least as bright as anything that will be acquired in the experiment.
20. Depending on their emission spectra, the fluorescence emitted by a fluorochrome can be detected in a detector designed to measure signal from another fluorochrome. This is called spillover. The objective of compensation is to eliminate the signal from a given fluorochrome from other channels where it is also detected. For example, to calculate the compensation necessary to correct the spillover of an FITC-stained sample in the PE channel, record cells stained with the FITC-conjugated antibody, and modify the PE-%FITC value so that the median florescence in the PE channel is the same for FITC-positive and FITC-negative cells. Then repeat the same procedure for every combination of fluorochromes. It is important that PMT voltages used for compensation must be the same as the PMT voltages that will be used for the sorting experiment. Depending on the sorter used, the compensations could be done automatically by the software program.

Acknowledgement

This work was supported by grants from the Institute of Health Carlos III (PI11/02251), the Departments of Education (PI2009-7) and Health (2010-111060), and the Department of Industry, Tourism and Trade (Etortek) of the Government of the Autonomous Community of the Basque Country.

References

1. Spangrude GJ, Heimfeld S, Weissman IL (1988) Purification and characterization of mouse hematopoietic stem cells. Science 241(4861): 58–62
2. Smith GH, Medina D (1988) A morphologically distinct candidate for an epithelial stem cell in mouse mammary gland. J Cell Sci 90(Pt 1):173–183
3. Tsai YC et al (1996) Contiguous patches of normal human mammary epithelium derived from a single stem cell: implications for breast carcinogenesis. Cancer Res 56(2):402–404
4. Stingl J et al (2001) Characterization of bipotent mammary epithelial progenitor cells in normal adult human breast tissue. Breast Cancer Res Treat 67(2):93–109
5. Gudjonsson T et al (2002) Isolation, immortalization, and characterization of a human breast epithelial cell line with stem cell properties. Genes Dev 16(6):693–706
6. O'Hare MJ et al (1991) Characterization in vitro of luminal and myoepithelial cells isolated from the human mammary gland by cell sorting. Differentiation 46(3):209–221
7. Clayton H, Titley I, Vivanco M (2004) Growth and differentiation of progenitor/stem cells derived from the human mammary gland. Exp Cell Res 297(2):444–460
8. Eirew P et al (2008) A method for quantifying normal human mammary epithelial stem cells with in vivo regenerative ability. Nat Med 14(12):1384–1389
9. Lim E et al (2009) Aberrant luminal progenitors as the candidate target population for basal tumor development in BRCA1 mutation carriers. Nat Med 15(8):907–913
10. Al-Hajj M et al (2003) Prospective identification of tumorigenic breast cancer cells. Proc Natl Acad Sci U S A 100(7):3983–3988
11. Shipitsin M et al (2007) Molecular definition of breast tumor heterogeneity. Cancer Cell 11(3):259–273
12. Liu R et al (2007) The prognostic role of a gene signature from tumorigenic breast-cancer cells. N Engl J Med 356(3):217–226
13. Ginestier C et al (2007) ALDH1 is a marker of normal and malignant human mammary stem cells and a predictor of poor clinical outcome. Cell Stem Cell 1(5):555–567
14. Pece S et al (2010) Biological and molecular heterogeneity of breast cancers correlates with their cancer stem cell content. Cell 140(1): 62–73
15. Vivanco M (2010) Function follows form: defining mammary stem cells. Sci Transl Med **2**(31): 31ps22
16. Phillips TM, McBride WH, Pajonk F (2006) The response of CD24(−/low)/CD44+ breast cancer-initiating cells to radiation. J Natl Cancer Inst 98(24):1777–1785
17. Li X et al (2008) Intrinsic resistance of tumorigenic breast cancer cells to chemotherapy. J Natl Cancer Inst 100(9):672–679
18. Creighton CJ et al (2009) Residual breast cancers after conventional therapy display mesenchymal as well as tumor-initiating features. Proc Natl Acad Sci U S A 106(33): 13820–13825
19. Piva M et al (2014) Sox2 promotes tamoxifen resistance in breast cancer cells. EMBO Mol Med 6(1):66–79
20. Alexander CM et al (2009) Separating stem cells by flow cytometry: reducing variability for solid tissues. Cell Stem Cell 5(6):579–583
21. Simoes BM et al (2011) Effects of estrogen on the proportion of stem cells in the breast. Breast Cancer Res Treat 129(1):23–35

Chapter 4

Side Population

Fariba Behbod and Maria d.M. Vivanco

Abstract

The side population (SP) assay has been utilized as a method for isolation and characterization of normal and cancer stem cells from a variety of tissues. However, the SP phenotype may not be a common property of all stem cells. This chapter reviews the principle and potential pitfalls of the SP assay with an emphasis on mammary gland SP cell analysis.

Key words Side Population (SP), Fluorescence-activated cell sorter (FACS), Stem cells, Hoechst 33342, Breast cancer resistance protein (BCRP1/ABCG2)

1 Introduction

Many years ago, flow cytometric analysis of hematopoietic cells first showed that Hoechst dye exclusion defines a side population (SP) of stem cells for the hematopoietic system [1, 2]. Later on it was postulated that the SP might represent a universal stem cell phenotype [2]. Indeed, human and mouse breast epithelial SP cells were identified and demonstrated that they constitute an undifferentiated subpopulation that can differentiate to form ductal and lobular structures as well as myoepithelial and luminal epithelial cell types [3, 4].

The side population (SP) assay is based on the ability of cells to efflux the Hoechst dye by the ATP-binding cassette (ABC) family of transporter proteins located on their surface membrane. The SP phenotype was first described by Goodell and colleagues in 1996, using mouse bone marrow cells. Their group showed that the bone marrow SP cells were highly enriched in functional hematopoietic stem cell activity [1]. In fact, the bone marrow SP cells could be further enriched in stem cell activity by combining SP with other known cell surface markers such as $CD117^{+}SCA^{-}1^{+}Lin^{-}Thy1^{lo}$. SP assay involves staining the cells using Hoechst dye 33342, followed by FACS analysis. Cells that efflux the dye appear on the left side of a FACS analysis panel and are referred to as SP cells. Cells that

Maria del Mar Vivanco (ed.), *Mammary Stem Cells: Methods and Protocols*, Methods in Molecular Biology, vol. 1293,
DOI 10.1007/978-1-4939-2519-3_4,

retain the dye appear on the right side and are referred to as non-SP cells. The ABC transporters, responsible for Hoechst dye efflux, belong to a superfamily of membrane transporters that use ATP for transport of various xenobiotics and endogenous compounds, i.e., folate, heme, and porphyrin to the outside of the cell. The ABC transporters, ABCB1 (P-glycoprotein, MDR1), ABCC1-5 (MRP1-5), and ABCG2 (BRCP1) are the major contributors to the SP phenotype [5]. The contribution of specific transporters to the SP phenotype may be different in various tissues. For example, in the mouse mammary glands, Bcrp1 (Abcg2), Mdr1a (Abcb1a) and 1b (Abcb1b) are the major contributors to the SP phenotype, whereas in the bone marrow, Bcrp1 is the major contributor to the SP phenotype [6].

Since the introduction of SP as a hematopoietic stem cell phenotype, the assay has been adopted as a method for the isolation of stem cells from many organ systems including umbilical cord blood, skeletal muscle, kidney, mammary glands, and lungs [5]. However, several studies have demonstrated that the SP phenotype may not be a common property of all stem cells [5, 7–9]. Indeed, SP phenotype has been demonstrated in the differentiated cells of many organs including small intestine, liver, kidney, brain endothelial cells, blood–brain barrier, blood–testis barrier, and mammary gland alveolar cells [5, 10]. Interestingly, Bcrp1 is expressed at low levels in virgin mammary glands; however, its expression is highly upregulated in late pregnancy and lactation. This may not be surprising since Bcrp1 as well as other members of the ABC transporters play a role in protection against the cytotoxic agents and drugs by limiting toxin/drug entry into certain tissues and promoting their elimination into bile, urine and milk.

The first functional proof that cancer stem cells and normal stem cells share a common phenotype came from the studies by John Dick and colleagues in 1994 [11]. By limiting dilution transplantation, this group showed that a rare population of leukemia cells, referred to as leukemia initiating cells or stem cells (LSC), were capable of recapitulating the original patient's leukemia in SCID mice. LSC shared similar surface markers as the normal hematopoietic stem cells ($CD34^+CD38^-$). However, the remaining subpopulations, $CD34^+CD38^+$ and $CD34^-$ fractions, did not contain this property. The knowledge that SP cells may define a subpopulation of cancer stem cells capable of effluxing chemotherapeutic agents raised awareness in their possible role as the underlying cause of cancer relapse and chemotherapy resistance. Indeed, many studies have shown SP cells to be enriched in tumorigenic potential and the SP phenotype to correlate with poor patient outcome [12–14]. However, similar to normal stem cells, SP cells may not represent an enriched population of cancer stem cells in all tumor types. Therefore, it is imperative to evaluate SP cells, derived from various tissues or tumors, for stem cell and or cancer stem cell activity/function, i.e.,

by limiting dilution transplantation, differentiation assays, colony formation assays, etc.

The SP phenotype may be regulated by many growth factors, signaling pathways, and miRNAs [15]. For example, in the hematopoietic system, SP phenotype is acquired/reactivated in Lin^- cells upon interactions with mesenchymal stromal cells through VLA-4/α4β1 integrin and DC44 [16]. Furthermore, an integrin-dependent activation of SP phenotype in acute myeloid leukemia circulating blasts may play a role in adhesion mediated chemotherapy resistance [16]. Another group showed that transforming growth factor-β treatment of LX2 cells, a hepatic stellate cell line, decreased the SP fraction in a dose-dependent manner [17]. By utilizing three non-small-cell lung cancer cell lines (A549, NCI-H460, H460) as well as a colon cancer cell line (LoVo), Liu and colleagues demonstrated that glucose induces a reversible upregulation of SP fraction through ATP mediated suppression of AMPK and activation of the Akt pathways [18]. Furthermore, BCRP transcription is under regulation by a number of transcription factors that bind to the cis and trans regulatory elements in the BCRP promoter. These include hypoxia-inducible factor 1 (Hif-1α), estrogen receptor, progesterone receptor isoform β, Gli, Nrf2, SP1 and SP2 among others (reviewed in ref. [15]). Additionally, a number of miRNAs, i.e., miR-519c, miR-520h, and miR-328, bind to the 3′ UTR of BCRP gene and negatively regulate the translation of BCRP protein [19–21].

Hoechst 33342 is a fluorescent dye that is taken up by all living cells through passive diffusion. While all cells uptake the dye, efflux is through an active energy-driven process requiring the expression of a sufficient number of ABC transporters [5]. SP resolution requires a flow cytometer equipped with an ultraviolet (UV) laser. Hoechst may be excited with non-UV wavelengths as well. However, optimal resolution is only achieved with the traditional UV sources [5]. SP or Hoechst profile may be visualized in two distinct channels, the Hoechst blue (450/50 nm band-pass filter) and the Hoechst Red (675/20 nm long-pass filter).

Since many factors can affect the SP phenotype (i.e., glucose concentration, stress, and hypoxia) every effort must be taken to maintain consistency in the procedure in order to obtain reproducible results. In doing so, it must be noted that the number of contaminating cells, i.e., red blood cells, endothelial cells, can affect the dye equilibrium with the cells of interest. As discussed previously, more than one member of the ABC transporters may contribute to the SP phenotype in some tissues. Additionally, different cells within the same tissue may express different members of the ABC transporters. There are a number of ABC transporter inhibitors available with specificity towards distinct ABC family members. For example, verapamil and cyclosporine A inhibit ABCB1 while fumitremorgin C (FTC) is highly specific for ABCG2 [5]. Others such as imatinib

are nonspecific. Therefore, a Hoechst and transporter inhibitor dose–response curve should be performed simultaneously. Some tissues may require the use of more than one transporter inhibitor to completely eliminate the SP phenotype.

2 Materials

1. TrypLE™ Select (Life Technologies).
2. Phosphate Buffered Saline (PBS).
3. Medium: Dulbecco's Modified Eagle Medium (DMEM) medium containing 10 % Fetal Bovine Serum (FBS).
4. Hoechst 33342.
5. Verapamil (dissolved in ethanol).
6. TO-PRO-3.
7. FACS Flow: PBS, 1 % BSA, 25 mM Hepes, pH 7, 5 mM EDTA. Weigh 1 g BSA and add 2.5 ml Hepes 25 mM, pH 7, 1 ml EDTA 5 mM, and 96.5 ml PBS. Dissolve, filter, and store at 4 °C.

3 Methods

3.1 Hoechst 33342 Staining of Cells

1. Prepare a single cell suspension from primary tissue or cultured cells (*see* **Note 1**).
2. Ensure that no contaminating cells are included (*see* **Note 2**).
3. Plan to have three conditions per experiment: control, with Hoechst 33342 dye, and with dye plus inhibitor (*see* **Note 3**).
4. Put 1×10^6 cells/ml in pre-warmed DMEM medium containing 8 % FCS in each Eppendorf tube (*see* **Note 4**).
5. Add Hoechst 33342 to a final concentration of 5 μg/ml (*see* **Note 5**).
6. Add 20 μM verapamil to the control tube containing inhibitor (*see* **Note 6**).
7. Incubate cells for exactly 90 min at 37 °C with occasional agitation (*see* **Note 7**).
8. Centrifuge cells at $450 \times g$ for 5 min at 4 °C.
9. Wash cells by resuspension in cold DMEM containing 8 % FBS.
10. Centrifuge cells at $450 \times g$ for 5 min at 4 °C.
11. Resuspend in 1 ml of DMEM medium containing 8 % FBS.
12. Add 2 μM TO-PRO-3 to the samples to exclude dead cells for the FACS analysis (*see* **Note 8**).

13. Keep cells on ice at all times after staining with the Hoechst 33342 dye.
14. If required, after incubation with the Hoechst 3342 dye, cells can be labeled for cell surface antigens (*see* **Note 9**).

3.2 Analysis and Sorting

1. Start the FACS sorter following the recommendations of the manufacturer and be ready to start the sort.
2. Cells were analyzed and sorted using a FACSVantage SE flow cytometer using Cell Quest software (Becton Dickinson) (*see* **Note 10**).
3. Exclude dead cells by TO-PRO-3 fluorescence (Fig. 1).
4. Measure Hoechst 33342 fluorescence at both 424/44 nm and above 670 nm (split by a 610 nm short-pass dichroic mirror), both from UV excitation (*see* **Note 11**).
5. Sort cells (*see* **Note 12**) either into tubes, onto poly-L-lysine-coated slides, or into culture plates, depending on the type of analysis to be performed.
6. Characterize the cells as required.

4 Notes

1. When working with primary cells, it is important to start with a pure preparation of single mammary epithelial cells. The various methods of solid tissue digestion can affect the SP phenotype. The readers are referred to a recent review on leading methods used for mammary gland digestion and the benefits of the different approaches before choosing an appropriate method [22]. The cells to be analyzed must be viable and in a single cell suspension (no cell clumps). This is particularly important for solid tissues that require enzymatic and mechanical digestion to generate single cells. When using cells isolated from primary tissue or cell culture, the use of mechanic and/or enzymatic dissociation will be necessary. However, aggressive treatments should be avoided, since they could alter the antigens to be detected. In addition, some cell surface antigens are sensitive to trypsin. Therefore, the use of gentle cell dissociation reagents, such as TrypLE, is recommended.
2. Since some stromal cells also express the SP phenotype, the simultaneous use of antibodies to exclude stromal cell specific surface markers needs to be considered. These include endothelial cells (CD31), hematopoietic cells (CD45 and or lineage cocktail), and fibroblasts (CD140a). Please note that some laboratories exclude fibroblasts from their SP analysis while others do not. This is because CD140a may also be expressed by some epithelial cells.

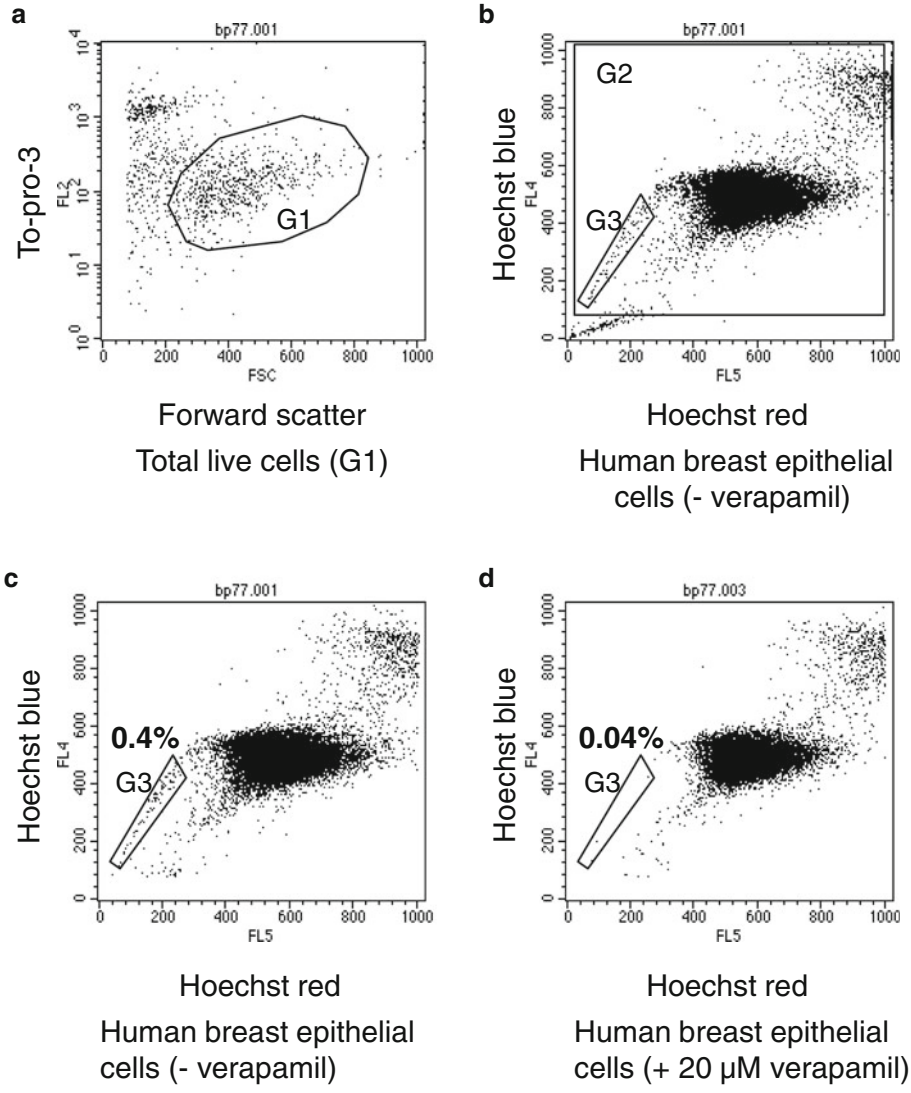

Fig. 1 Identification of human mammary SP cells and the influence of verapamil, a multidrug-resistant (mdr) inhibitor, on these cells. (**a**) The total live cell population was again selected (G1) to exclude dead cells from the analysis. (**b**) A second gate (G2) was applied to remove persisting debris. (**c**) SP cells are indicated by G3. (**d**) Addition of 20 μM verapamil resulted in a tenfold reduction in SP cells

3. Selection of inhibitor: we used verapamil (or Ko143, see below) but there are others available (i.e., GF120918). The important thing to take into account is that it is essential to choose a specific inhibitor to demonstrate that the SP observed is due to the activity of the membrane pump. Thus, BCRP1 is inhibited by Ko143, an analogue of the fungal toxin fumitremorgin C, which is a potent and specific inhibitor of BCRP (Allen et al., 2002), and therefore represents a better control than verapamil (Fig. 2).

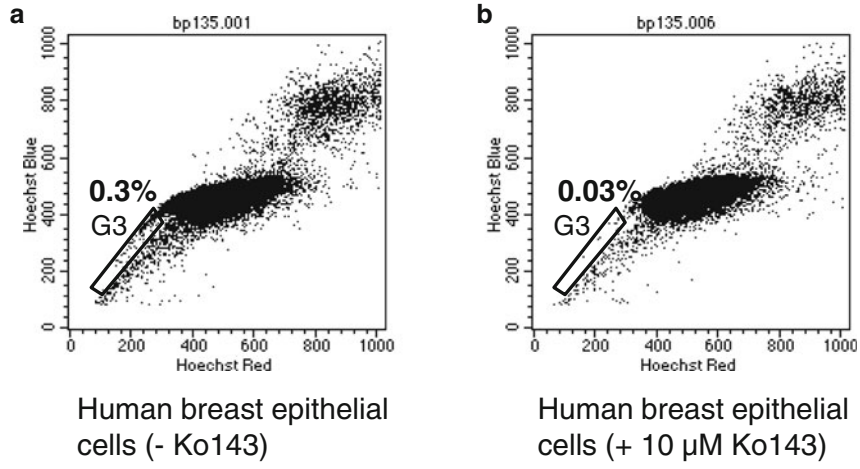

Fig. 2 Influence of Ko143, a specific BCRP inhibitor, on human mammary SP cells. (**a**) The presence of SP cells (G3) on incubation of human breast epithelial cells with Hoechst 33342. (**b**) Addition of 10 μM Ko143 resulted in a tenfold reduction in the side population. SP and non-SP cells were gated as described in Fig. 1

4. Another important factor is keeping a constant cell concentration, i.e., 1×10^6 live cells per ml in order to keep the equilibrium between the dye and the intracellular compartment. It is essential to count the cells and keep the ratio cell number/dye concentration constant.
5. The SP phenotype is influenced by the Hoechst dye concentration. A low concentration may result in unsaturated Hoechst staining and the appearance of a false SP population. A standard Hoechst concentration is 5 μg/ml for bone marrow. However, this concentration may be higher for solid tissues such as muscle and skin (up to 20 μg/ml). A Hoechst saturation response curve and cellular toxicity curve will need to be performed in order to obtain an optimal dye concentration where the percentage of SP remains stable. Importantly, the Hoechst staining needs to be combined with a transporter inhibitor in order to confirm the specificity of the dye efflux. The staining time (usually 90–120 min) may also be optimized for the tissue of interest. Dye incubation can be performed in a 37 °C shaking incubator. However, the washes, centrifugation, antibody staining, and data acquisition should be carried out in cold at 4 °C and in the dark in order to preserve the SP profile. It should also be kept in mind that Hoechst is toxic, and cell viability may be a confounding factor when comparing stem cell activity of SP to non-SP subpopulations following sorting.
6. Depending on the cell type used verapamil may be toxic to the cells. For example, at the concentration used verapamil is more

toxic to mouse mammary SP cells than to bone marrow cells or human mammary SP cells.

7. This is a very sensitive assay and the target population is very small (often less than 1 %). Therefore, it is important to be as consistent as possible in each step. We recommend setting a timer and agitating the samples every 15 min to ensure homogenous staining and increase reproducibility.
8. Since dead cells appear in the SP region, the use of a dead cell exclusion assay, i.e., TO-PRO-3 iodide or LIVE/DEAD Fixable Dead Cell Stain, is critical to exclude the dead cells from the SP analysis.
9. In order to characterize the SP cell population further, it may be interesting to label cells with surface antigens to examine potential overlap among different stem cell phenotypes. At this point, cells could be labeled for the cell surface antigens CD49f, ESA (or any other) and BCRP.
10. The FACSVantage SE flow cytometer is equipped with an argon laser (488 nm excitation), a HeNe laser (633 nm excitation) and a multi-line UV laser (334–364 nm excitation). TO-PRO-3 is excited by the HeNe laser. Cells incubated with Hoechst 33342 were visualized using the UV laser. Hoechst 33342 fluorescence was measured at both 424/44 nm (Hoechst blue) and above 670 nm (Hoechst red). A 610 nm short pass dichroic mirror was used to separate the emission wavelengths. Both Hoechst red and Hoechst blue fluorescence are shown on a linear scale.
11. Because Hoechst dye binds cellular DNA, aneuploidy, and cell cycle status can affect Hoechst/SP profile. Therefore, there may be a distinct SP tail for aneuploid cancer cells vs. the normal diploid cells. In this case, it will be important to adjust the SP gate according to the ploidy of the cells.
12. As it is the case after any type of staining, sorting at the lowest pressure and maintaining the cells at 4 °C will increase the viability of the sorted cells.

Acknowledgement

The authors thank K99/R00 Pathway to Independence Award: 5R00CA127462-06 (F Behbod) and the Institute of Health Carlos III (PI11/02251), the Departments of Education (PI2009-7) and Health (2010-111060), and the Department of Industry, Tourism and Trade (Etortek) of the Government of the Autonomous Community of the Basque Country (MdM Vivanco) for financial support.

References

1. Goodell MA et al (1996) Isolation and functional properties of murine hematopoietic stem cells that are replicating in vivo. J Exp Med 183(4):1797–1806
2. Zhou S et al (2001) The ABC transporter Bcrp1/ABCG2 is expressed in a wide variety of stem cells and is a molecular determinant of the side-population phenotype. Nat Med 7(9):1028–1034
3. Alvi AJ et al (2003) Functional and molecular characterisation of mammary side population cells. Breast Cancer Res 5(1):R1–R8
4. Clayton H, Titley I, Vivanco M (2004) Growth and differentiation of progenitor/stem cells derived from the human mammary gland. Exp Cell Res 297(2):444–460
5. Golebiewska A et al (2011) Critical appraisal of the side population assay in stem cell and cancer stem cell research. Cell Stem Cell 8(2):136–147
6. Jonker JW et al (2005) Contribution of the ABC transporters Bcrp1 and Mdr1a/1b to the side population phenotype in mammary gland and bone marrow of mice. Stem Cells 23(8):1059–1065
7. Kubota H, Avarbock MR, Brinster RL (2003) Spermatogonial stem cells share some, but not all, phenotypic and functional characteristics with other stem cells. Proc Natl Acad Sci U S A 100(11):6487–6492
8. Triel C et al (2004) Side population cells in human and mouse epidermis lack stem cell characteristics. Exp Cell Res 295(1):79–90
9. Iwatani H et al (2004) Hematopoietic and nonhematopoietic potentials of Hoechst(low)/side population cells isolated from adult rat kidney. Kidney Int 65(5):1604–1614
10. Jonker JW et al (2005) The breast cancer resistance protein BCRP (ABCG2) concentrates drugs and carcinogenic xenotoxins into milk. Nat Med 11(2):127–129
11. Lapidot T et al (1994) A cell initiating human acute myeloid leukaemia after transplantation into SCID mice. Nature 367(6464):645–648
12. Wouters J et al (2013) The human melanoma side population displays molecular and functional characteristics of enriched chemoresistance and tumorigenesis. PLoS One 8(10):e76550
13. Britton KM et al (2012) Breast cancer, side population cells and ABCG2 expression. Cancer Lett 323(1):97–105
14. Mukhopadhyay P et al (2013) Heterogeneity of functional properties of clone 66 murine breast cancer cells expressing various stem cell phenotypes. PLoS One 8(11):e78725
15. Natarajan K et al (2012) Role of breast cancer resistance protein (BCRP/ABCG2) in cancer drug resistance. Biochem Pharmacol 83(8):1084–1103
16. Malfuson JV et al (2014) SP/drug efflux functionality of hematopoietic progenitors is controlled by mesenchymal niche through VLA-4/CD44 axis. Leukemia 28(4):853–864
17. Kim JB et al (2014) Side population in LX2 cells decreased by transforming growth factor-beta. Hepatol Res 44(2):229–237
18. Liu PP et al (2014) Metabolic regulation of cancer cell side population by glucose through activation of the Akt pathway. Cell Death Differ 21(1):124–135
19. To KK et al (2009) Escape from hsa-miR-519c enables drug-resistant cells to maintain high expression of ABCG2. Mol Cancer Ther 8(10):2959–2968
20. Wang F et al (2010) hsa-miR-520h downregulates ABCG2 in pancreatic cancer cells to inhibit migration, invasion, and side populations. Br J Cancer 103(4):567–574
21. Pan YZ, Morris ME, Yu AM (2009) MicroRNA-328 negatively regulates the expression of breast cancer resistance protein (BCRP/ABCG2) in human cancer cells. Mol Pharmacol 75(6):1374–1379
22. Smalley MJ et al (2012) Isolation of mouse mammary epithelial subpopulations: a comparison of leading methods. J Mammary Gland Biol Neoplasia 17(2):91–97

Chapter 5

Single-Cell Genome and Transcriptome Processing Prior to High-Throughput Sequencing

Ana M. Aransay, Laura Barcena, Aintzane Gonzalez-Lahera, and Nuria Macias-Camara

Abstract

Single-cell genome and transcriptome characterizations will probe to be decisive within the stem cells research, especially to describe appropriately the genetic impact of the diverse stem cells populations that are present in each organism. In the present chapter, we describe in detail how to prepare sequencing libraries out of single cells, for whole genome DNA and mRNA sequencing.

Key words Single-cell genome, Single-cell transcriptome, Sequencing library, High-throughput sequencing (HTS)

1 Introduction

Stem cells characterization at whole genome level has been one of the hottest scientific issues during the last few years, especially if single-cell studies were considered. In parallel, high-throughput sequencing (HTS) technologies [1, 2] have progressed very rapidly since the first HTS sequencer was in the market in 2004, as well as all the protocols related to DNA and RNA sample processing previous to be massively read, which is making feasible this evolution. Recently, the possibility of sequencing the genome and transcriptome of single-cells is transforming the field of stem cells genomics. This is a so much trendy topic, that Nature Methods Journal [3] has nominated the sequencing of DNA and RNA of single cells the "Method of the Year 2013."

These procedures allow studies of cell diversity in an organ or tissue depending on its location, details of cell development and differentiation, tumor evolution as well as many other important biological processes that determine the healthy status of a living organism. However, due to the polymerase amplification step that is considered in these protocols, we should be aware that, at the

Maria del Mar Vivanco (ed.), *Mammary Stem Cells: Methods and Protocols*, Methods in Molecular Biology, vol. 1293,
DOI 10.1007/978-1-4939-2519-3_5,

moment, the information we can get out of them is between 40 to 70 % accurate, since some genome regions are difficult or impossible to replicate with these protocols. Consequently, several adjustments should be made to rich 97–100 % precision for whole genome information, and thus, several laboratories [4] are working hard to develop other strategies to achieve an unbiased amplification of the genome or transcriptome obtained from a single cell. This issue will be totally overcome when third and fourth generation HTS technologies show their potential on processing tiny amounts of nucleic acids.

This chapter brings up clue steps within the preparation of single-cell total DNA and mRNA before sequencing, focused specially in Illumina Inc.'s library procedures, since it is the most world-wide used HTS technology (http://omicsmaps.com/stats), but applicable to many other sequencing strategies.

2 Materials

Before starting any procedure, it is important to arrange the purchasing of all the kits accordingly to the needs, and take into account that all solutions should be prepared using ultrapure, PCR grade water (e.g., SIGMA 1000 cc, Cat. No. W-4502).

During all procedures, the user will require:

1. Filter tips.
2. Ice bucket.
3. 10 % bleach solution.
4. PCR grade Water (e.g., SIGMA 1000 cc, Cat. No. W-4502).
5. Sets of p1000, p200, p10, and p2 Pipettes. It is recommended to have a dedicated set of pipettes only for DNA library preparations and another set to manipulate RNA.
6. Vortexer.
7. Microcentrifuge.

2.1 Single-Cell Whole-Genome DNA Library Preparation

The materials and equipment for single-cell whole-genome DNA library preparation are:

1. REPLI-g Single Cell Kit (QIAGEN, Cat. No. 150343 for 24 reactions) with the following contents:

   REPLI-g sc DNA Polymerase (blue lid).

   REPLI-g sc Reaction Buffer (yellow lid).

   Buffer DLB (clear lid).

   Stop Solution (red lid).

PBS sc 1× (clear lid) (*see* **Note 3**).

DTT, 1M (lilac lid).

H_2O sc.

2. Qubit® dsDNA Broad Range (BR) Assay kit (Life Technologies) applicable to concentrations from 2 to 1,000 ng, (Cat. No. Q32850 for 100 samples or Q32853 for 500 samples, based on an assay volume of 200 μl).
3. Qubit® dsDNA High sensitivity (HS) Assay kit (Life Technologies) applicable to concentrations from 0.2 to 100 ng (Cat. No. Q32851 for 100 samples or Q32854 for 500 samples, based on an assay volume of 200 μl).
4. Nextera DNA sample preparation kit (Illumina Inc.) are available for 96 samples (Cat. No. FC-121-1031) and for 24 samples (FC-121-1030) and the associated reagents are:

   TDE1: Tagment DNA Enzyme.

   TD: Tagment DNA Buffer.

   RSB: Resuspension Buffer.

   NPM: Nextera PCR Master Mix.

   PPC: PCR Primer Cocktail.
5. Nextera DNA sample preparation Index Kit (Illumina Inc.) can be purchase with 96 indexes for 384 samples (Cat. No. FC-121-1012) or with 24 indexes for 96 samples (Cat. No. FC-121-1011).
6. KAPA library quantification kit (KAPA Biosystems, Cat. No. kk4824) whose contents are:

   KAPA SYBR FAST qPCR Master Mix (2×).

   KAPA SYBR FAST ROX Low (50×).

   KAPA SYBR FAST ROX High (50×).

   Library quantification DNA Standards 1–6.

   Library quantification Primer Premix (10×).
7. ZR96 DNA Clean&Concentrator™-5 (2×96 preps) from Zymo Research (Cat. No. D4023) includes:

   DNA Binding Buffer.

   DNA Wash Buffer (Ethanol must be added to this reagent prior to use as indicated on its label).

   DNA Elution Buffer.

   Zymo-Spin™ Columns.

   Collection Tubes.
8. Thin-wall, clear 0.5 ml PCR tubes, Axygen PCR-05-C tubes (VWR, Cat. No. 10011-830).

9. 0.2 ml PCR DNase and RNase-free tubes (Deltalab, Cat. No. 4094.1N).
10. 8-well PCR tubes (Durviz, Cat. No. RA0624).
11. 8-well PCR caps (Durviz, Cat. No. RA0452).
12. 96-well TCY plate (Bio-Rad, Cat. No. HSP-9601).
13. Plate, deep well 0.8 ml (MIDI) (Thermo Scientific, Cat. No. AB-0765).
14. 0.2 ml skirted 96-well PCR plate (Thermo Scientific, Cat. No. AB-0800).
15. Adhesive sealing sheets (Thermo Scientific, Cat. No. AB-0558).
16. Adhesive plate sheets (Thermo Scientific, Cat. No. AB-0580).
17. Sterile Troughs (Beckman-Coulter, Cat. No. 372788).
18. Pure molecular biology grade DNase and RNase-free Agarose powder.
19. Tris–acetate–EDTA (TAE) Solution 50× DNase, RNase and Protease free (the content of TAE buffer 1× is 40 mM Tris–acetate + 1 mM EDTA).
20. 6× Gel Loading Dye.
21. Lambda/*Hind*III, concentration 0.5 mg/ml (Biotools, Cat. No. 31.011).
22. 1 Kb DNA ladder, concentration 0.5 mg/ml (Biotools, Cat. No. 31.005).
23. Ethidium bromide (10 mg/ml).
24. High Sensitivity DNA Kit (Agilent Technologies, Cat. No. 5067-4626).
25. AMPure XP Beads (Beckman Coulter: 5 ml, Cat. No. A63880 or 60 ml, Cat. No. A63881).
26. Fresh 80 % ethanol: prepare by mixing eight parts of absolute ethanol (for molecular biology, general supplier) and two parts of ultrapure, PCR grade water. Ethanol gets hydrated with the water molecules from the atmosphere, so it is really important to prepare the 80 % dilution as fresh as possible.
27. Tris–HCl pH 8.5.
28. Tween-20.
29. Thermal cycler, water bath, or heating block.
30. Centrifuge with 0.2 ml PCR tubes adaptors.
31. Qubit® 2.0 Fluorometer (Life Technologies, Cat. No. Q32866).
32. NanoDrop 2000 UV–Vis Spectrophotometer.
33. Horizontal agarose gel electrophoresis equipment.
34. UV Transilluminator.

35. Microplate Centrifuge.
36. 96-well thermal cycler (with heated lid).
37. Bioanalyzer 2100 Electrophoresis System (Agilent Technologies), which includes: Chip priming station (Cat. No. 5065-4401), IKA vortex mixer—Model MS3 (Cat. No. 5065-9966), and 16-pin bayonet electrode cartridge (Cat. No. 5065-4413).
38. High-speed microplate shaker.
39. Magnetic Stand-96 (Ambion, Cat. No. AM10027).

2.2 Single-Cell Whole-Genome mRNA Library Preparation

1. The SMARTer Ultra™ Low RNA Kit for Illumina Sequencing (Clontech, Cat. No. 634936), which consists of:

   "Advantage 2 PCR Kit" which contains:

   Advantage 2 Polymerase Mix.

   Advantage 2 PCR Buffer.

   Advantage 2 SA PCR Buffer.

   And "SMARTer Ultra Low RNA Kit" for Illumina Sequencing with:

   BOX 1:

   SMARTer II Oligonucleotide.

   Control Total RNA.

   BOX 2:

   3′ SMART CDS Primer II A

   IS PCR Primer.

   5× First-Strand Buffer (RNase-Free).

   dNTP Mix.

   DTT.

   SMARTScribe™ Reverse Transcriptase.

   Nuclease-Free water.

   RNase Inhibitor.

   Dilution Buffer.

   Purification Buffer.

2. Nextera XT DNA sample preparation kit (Illumina Inc.) is available for 96 samples (Cat. No. FC-131-1096) or for 24 samples (FC-131-1024). This kit contains:

   BOX 1

   ATM: Amplicon Tagment Mix, 96 RXN.

   TD: Tagment DNA Buffer.

   NPM: Nextera PCR Master Mix.

RSB: Resuspension Buffer.

LNA1: Library Normalization Additives 1.

LNW1: Library Normalization Wash 2.

HT1: Hybridization Buffer.

BOX 2:

NT: Neutralize Tagment Buffer.

LNB1: Library Normalization Beads 1.

LNS1: Library Normalization Storage Buffer 1.

3. Nextera XT DNA sample preparation Index Kit (Illumina Inc.) which can be purchase with 96 indexes for 384 samples (Cat. No. FC-131-1002) or with 24 indexes for 96 samples (Cat. No. FC-131-1001).
4. Illumina's library quantification is carried out with KAPA library quantification kit (KAPA Biosystems, Cat. No. KK4824) whose contents are:

   KAPA SYBR FAST qPCR Master Mix (2×).

   KAPA SYBR FAST ROX Low (50×).

   KAPA SYBR FAST ROX High (50×).

   Library quantification DNA Standards 1–6.

   Library quantification Primer Premix (10×).
5. DNA-OFF Solution (Takara Cat. No. 9036).
6. Thin-wall, clear 0.5 ml PCR tubes, Axygen PCR-05-C tubes (VWR, Cat. No. 10011-830).
7. 0.2 ml PCR DNase and RNase-free tubes (Deltalab, Cat. No. 4094.1N).
8. DNA LoBind Tube 1.5 ml (Eppendorf, Cat. No. 022431021).
9. 8-well PCR tubes (Durviz, Cat. No. RA0624).
10. 8-well PCR caps (Durviz, Cat. No. RA0452).
11. 96-well Axygen V-bottom Plate 500 μl (VWR, Cat. No. 47743-996).
12. MicroAmp Clean Adhesive Seal (Thermo Scientific, Cat. No. 4306311).
13. AMPure XP Beads (Beckman Coulter: 5 ml, Cat. No. A63880; 60 ml, Cat. No. A63881).
14. Absolute ethanol (for molecular biology).
15. High Sensitivity DNA Kit (Agilent, Cat. No. 5067-4626).
16. RNaseZAP® recommended for electrode decontamination (Ambion Inc., Cat. No. 9780).
17. Eight channel pipette: p20 and p200, one each.

18. Microplate centrifuge.
19. QuickSpin minicentrifuge for 1.5-ml tubes.
20. QuickSpin minicentrifuge for 0.2-ml tubes.
21. MagnaBot II Magnetic Separation Device (Promega, Cat. No. V8351).
22. Magnetic Stand-96 (Ambion, Cat. No. AM10027).
23. Bioanalyzer 2100 Electrophoresis System (Agilent Technologies), which includes: Chip priming station (Cat. No. 5065-4401), IKA vortex mixer—Model MS3 (Cat. No. 5065-9966), and 16-pin bayonet electrode cartridge (Cat. No. 5065-4413).
24. 96-well thermal cycler with heated lid.
25. High-speed microplate shaker.

3 Methods

The aim of this chapter is not to focus on detailed protocols for single-cell isolation, since this decision will depend very much on the characteristics of the starting material that is being studied, as well as the equipment available in the laboratory. However, we propose some references to the existing alternatives at the moment of writing:

- If complex and heterogeneous tissues are considered, whether fresh or frozen, researchers choose laser microdissection techniques [5–7].
- When target cells are not adherence-dependent, they can be suspended in specific liquid media, and then, the most affordable strategy to get single-cell aliquots is to proceed with serial dilutions in microtiter well plates.
- The previous aim can be also achieved by fluorescence activated cell sorting (FACS) cytometry [8] if the proper equipment and expertise are available.
- The company Fluidigm Corporation has developed a more specialized platform to isolate single cells and perform further steps to prepare total DNA or cDNA for HTS in a single-step, reducing significantly the variability caused by multi-platform and manipulation technical errors. This is the so-called "*C1™ Single-Cell Auto Prep System*", which is based on an innovative microfluidic technology. Additional details and protocols for this system can be found at http://www.fluidigm.com/c1-single-cell-auto-prep-system.html.

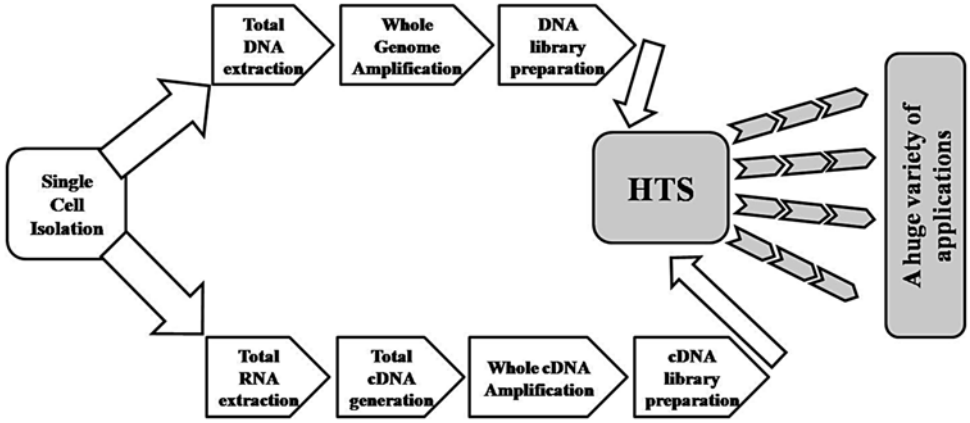

Fig. 1 Graphic display of the steps required from cell isolation to high-throughput sequencing (HTS) of single-cell DNA (Subheadings 3.1–3.6) or RNA (Subheadings 3.7–3.10)

Once the researcher has got single cells isolated, the following procedures for whole genome or transcriptome sequencing can be considered (Fig. 1).

3.1 Single-Cell Whole-Genome DNA Preparation for High-Throughput Sequencing

1. *See* **Notes 1** and **2** before starting any of the described procedures.
2. If collecting cells by micromanipulations or dilution, transfer a single cell in minimal 1× PBS volume to a PCR tube and complete to 4 μl with PBS sc buffer supplied within the kit. If collecting cells by FACS, collect single cell directly into 4 μl of PBS sc buffer (*see* **Notes** 3 and **4**).
3. Both DNA extraction from single-cell and whole-genome amplification are carried out in two sequential steps but in a single tube using *REPLI-g Single Cell Kit* (Qiagen, Cat. No.150343 for 24 samples or Cat. No. 150345 for 96 samples). This kit uses Phi-29 polymerase as well as buffers and reagents, for whole genome amplification, using Multiple Displacement Amplification, and allowing uniform amplification of whole genome.
4. Thaw REPLI-g sc Polymerase on ice and all other reagents (H_2O sc, REPLI-g sc Reaction Buffer, Buffer DLB, Stop Solution, PBS sc, and DTT) at room temperature (15–25 °C).
5. Add 500 μl H_2O sc to Buffer DLB (both provided with *REPLI-g Single Cell Kit*) mix thoroughly until totally dissolve and centrifuge briefly. It is important to take into account that once Buffer DLB is reconstituted, it can be stored only for 6 months at −20 °C, since it is pH-labile.
6. Vortex all buffers and reagents to ensure thorough mixing and spin them down.

7. Set a thermal cycler temperature to 65 °C and its heat lid temperature to 70 °C. A water bath or a heating block can also be used.
8. Prepare sufficient Buffer D2 for the total number of whole genome amplification reactions that will be carried out (3 μl Buffer D2/reaction). If performing fewer reactions than expected, store residual Buffer D2 at –20 °C, not longer than 3 months. For 12 reactions is required to mix:

3 μl of DTT 1M (provided with the kit)
33 μl of reconstituted Buffer DLB
36 μl Total volume of Buffer D2

9. Add 3 μl Buffer D2 (denaturation buffer) into the tube containing the 4 μl cell material. Mix carefully by flicking the tube and centrifuge briefly. Ensure that the cell material does not stick to the tube wall above the buffer line.
10. Incubate the samples in the thermal cycler previously set up at 65 °C, for 10 min.
11. After incubation, add 3 μl of Stop Solution and mix carefully by flicking the tube. Store on ice.
12. For each 10 μl of DNA denatured reaction (from previous step) prepare the following master mix (to prepare a master mix for multiple reactions, scale up according to the total number of reactions plus 10 %), combining in order, on ice:

9 μl	H_2O sc
29 μl	REPLI-g sc reaction buffer
2 μl	REPLI-g sc DNA polymerase (previously thawed on ice)
40 μl	Total reaction volume

13. Mix carefully by flicking the tube and centrifuge briefly. It is important to notice that once master mix is prepared, it should be kept on ice and used immediately upon addition of REPLI-g sc DNA Polymerase. If REPLI-g Reaction Buffer forms a precipitate, vortex for 10 s and spin down.
14. Program thermal cycler, water bath, or heating block and incubate samples:

    8 h at 30 °C

    3 min at 65 °C (to inactivate REPLI-g sc DNA Polymerase).

    If the same water bath or heating block is going to be used for both incubations, set its temperature to 65 °C after 30 °C incubation, and wait to start counting the 3 min until the proper temperature is reached.

15. Pulse-centrifuge and proceed to measure the concentration of the amplified DNA with Qubit 2.0 fluorometer (**steps 17–23**) and DNA integrity by agarose gel (**steps 24–32**) (*see* **Note 5**).
16. Store amplified DNA at 4 °C for short-term, or at −20 °C for long-term storage.
17. Quantification of total double-stranded DNA at this point should be done by fluorometric methods (*see* **Note 6**).
18. Set up 2 Assay Tubes (Axygen, Cat. No. PCR-05-C) for the standards and one tube for each user sample.
19. Prepare the Qubit Working Solution by diluting the Qubit reagent 1:200 in Qubit buffer. Prepare a master mix containing 200 μl of Working Solution for the two standards and all the samples that are being measured in parallel.
20. Prepare the Assay Tubes according to the table below:

    Standard Assay Tubes:

190 μl	Working solution
10 μl	Standard (from kit)
200 μl	Total reaction volume

    User Sample Assay Tubes:

180–199 μl	Working solution
1–20 μl	User sample
200 μl	Total reaction volume

21. Vortex all tubes for 2–3 s and spin down.
22. Incubate the tubes for 2 min at room temperature.
23. Insert the tubes in the Qubit® 2.0 Fluorometer and take readings.
24. Total amplified DNA integrity is evaluated by agarose gel electrophoresis. The DNA degradation level and RNA contamination determine the qualification of the DNA.
25. Prepare 1× TAE (Tris–acetate–EDTA) buffer by diluting the TAE 50× Solution.
26. Prepare 1 % agarose gel with ethidium bromide (final concentration 0.5 μg/ml), for higher resolution, following internal safety rules.
27. When the agarose gel is set, put it in the gel electrophoresis unit and fill the tank with 1× TAE Buffer to the maximum fill mark.
28. Load 6 μl of the 1 Kb DNA ladder mix (1 μl stock ladder + 1 μl 6× loading buffer + 4 μl double-distilled water) onto one lane of the gel.

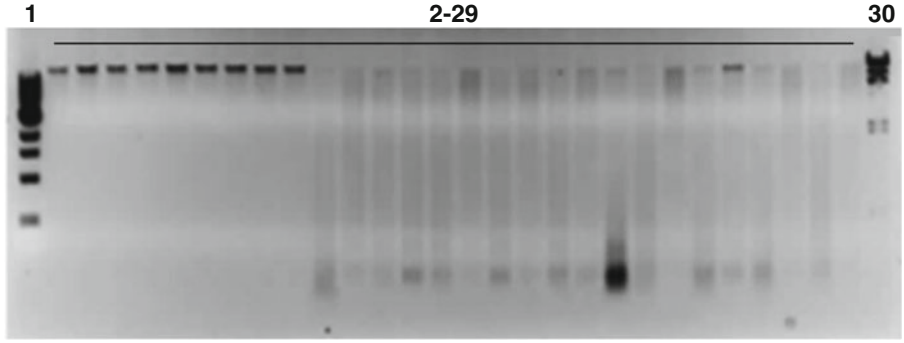

Fig. 2 1× TAE, 1 % agarose Gel picture including several examples of total DNA quality. *Lane 1*: 1 Kb DNA ladder. *Lane 30*: Lambda/*Hind*III ladder. *Lanes 2–29*: 50 ng DNA of each sample. On the gel, *lanes 2–10* show good DNA profiles; however, the rest of the samples have no clear bands, but obvious smears due to DNA degradation; therefore, samples 11–29 are degraded

29. Load 6 μl of the Lambda/*Hind*III ladder mix (1 μl stock ladder + 1 μl 6× loading buffer + 4 μl double-distilled water) onto one lane of the gel.
30. Load the samples (10 μl sample with 50 ng of DNA + 2 μl 6× gel loading buffer) onto the other lanes of the gel. Depending on each sample concentration, this aliquot will be prepared by dilution of the total amplified DNA samples to load only 50 ng.
31. Run gel at 100–120 V (depending on the distance between tank electrodes) for 1 h approximately.
32. View the gel on a UV transilluminator and interpret the quality of each assayed DNA (Fig. 2).

3.2 Total DNA Library Preparation

For Total genomic DNA library preparation from human or other complex genomes, Illumina Inc. has developed a new family of kits named Nextera. In case of single-cell DNA sequencing, Nextera DNA sample preparation kit (Cat. No. FC-121-1031 for 96 samples and Cat. No. FC-121-1030 for 24 samples) is recommended, and for small genomes such as bacteria and viruses, there is a special kit called Nextera XT Sample Prep Kit (Illumina Inc., Cat. No. FC-131-1096 for 96 samples and Cat. No. FC-131-1024 for 24 samples). Thus, these are the procedures that we recommend for single-cell genome sequencing.

1. Prepare a diagram with the order of the samples in a 96-well plate (*see* **Note 7**).
2. Normalize all amplified DNAs to 2.5 ng/μl.
3. Remove the TD, TDE1, and genomic DNA from −15 to −25 °C storage and thaw them on ice.
4. Mix all reagents gently by inverting the tubes 3–5 times and give a brief spin.

5. Random fragmentation of total DNA (*see* **Note 8**). All steps for this procedure are carried out at room temperature.
6. Label a new 96-well TCY plate (Bio-Rad, Cat. No. HSP-9601) "NET1" (Nextera Enrichment Tagmentation plate 1) with a smudge resistant pen.
7. Add 20 μl of Genomic DNA at 2.5 ng/μl (50 ng total) to each sample well of the "NET1" plate following the project diagram.
8. Calculate the total amount of TD Buffer needed for all the wells and divide it in an 8-well PCR strip tube, for using a multichannel pipette to dispense it into the "NET1" plate.
9. Add 25 μl of TD Buffer to every well containing Genomic DNA. Change tips between wells.
10. Add 5 μl of TDE1 to every well containing Genomic DNA with TD Buffer. Change tips between wells.
11. Using a multichannel pipette, mix by pipetting ten times. Change tips between samples.
12. Cover the plate with an adhesive sealing sheet (Thermo Scientific, Cat. No. AB-0558).
13. Centrifuge at 280×*g* at 20 °C for 1 min.
14. Place the "NET1" plate in a thermal cycler and run the following program:
    55 °C for 5 minutes.

    Hold at 10°C.

    Make sure that the thermal cycler's lid temperature is set to 70 °C during the incubation.
15. Before starting the tagmented DNA purification (*see* **Note 9**), remove RSB from −15 °C/−25 °C and thaw it at room temperature and add absolute ethanol to the DNA Wash Buffer following manufacturer's instructions.
16. While the tagmentation incubation is in progress, label a new MIDI plate (Thermo Scientific, Cat. No. AB-0765) as "NSP2" (Nextera Sample Plate 2) and add 180 μL of DNA Binding Buffer from ZR-96 DNA Clean & Concentrator™-5 kit (Zymo Research, Cat. No. D4023) to each well of the "NSP2" in which the samples of the "NET1" plate will be added. A multichannel pipette can be used if pouring DNA Binding Buffer into a trough.
17. Transfer 50 μl of each well of the "NET1" (tagmented DNA) plate to the corresponding well of the "NSP2" plate. Mix gently by pipetting. Change tips between samples.
18. Place the Zymo-Spin™ I-96 Plate on the Collection Plate (both included in ZR-96 DNA Clean & Concentrator™-5, Zymo Research, Cat. No. D4023).

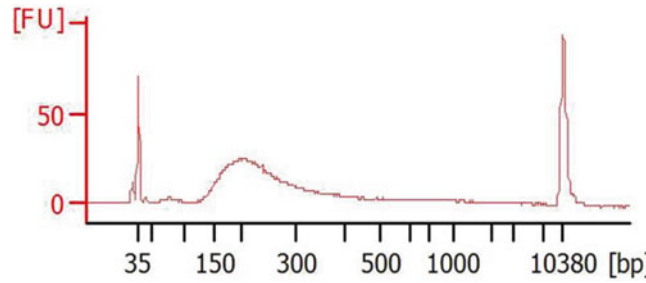

Fig. 3 Tagmented total DNA profile resolved in a 2100 Bioanalyzer (Agilent Technologies)

19. Using a multichannel pipette, transfer the sample mixture from the "NSP2" plate to the corresponding well of the Zymo-Spin™ I-96 Plate.
20. Centrifuge at 1,300×*g* at 20 °C for 2 min. Discard flow through. Here Illumina recommends the use of open top plate-holders for the centrifugation.
21. For washing the Zymo-Spin™ I-96 Plate, add 300 μl of prepared DNA Wash Buffer to each well containing sample. A multichannel can be use if pouring the buffer in a trough. Change tips between columns to avoid cross-contamination.
22. Centrifuge at 1,300×*g* at 20 °C for 2 min. Discard the flow through.
23. Repeat washing **steps 21** and **22**, for a total of two washes.
24. Centrifuge for an additional 2 min at 1,300×*g* at 20 °C to ensure no residual buffer is present.
25. Place the Zymo-Spin™ I-96 Plate on a new TCY plate (Bio-Rad, Cat. No. HSP-9601), labeled "NSP3" (Nextera Sample Plate 3).
26. Add 25 μl of RSB directly to the column matrix in each well.
27. Incubate the plate for 2 min at room temperature.
28. Centrifuge the plate at 1,300 ×*g* at 20 °C for 2 min.
29. Check the products of the tagmentation reaction by loading 1 μl of undiluted purified tagmented DNA on a High Sensitivity DNA Kit (Agilent Technologies, Cat. No. 5067-4626) and resolved in a 2100 Bioanlyzer as described in Subheading 3.9. This should produce a broad distribution of DNA fragments with a size range between 150 and 1,000 bp as shown in Fig. 3.

3.3 Library Enrichment

Library enrichment was adapted from Nextera DNA sample preparation guide, Part # 15027987 Rev. B. In this step the purified tagmented DNA is amplified. The PCR step also adds index 1 (i7) and index 2 (i5), as well as common adapters (P5 and P7) required for cluster generation and sequencing. Before starting library enrichment and to ensure high quality libraries, it is critical to use

full amount of recommended input DNA, as well as avoid adding extra PCR cycles. If less than a full set of libraries is pooled for sequencing, ensure that the correct index 1 (i7) and index 2 (i5) primers have been selected. For the proper selection of indexes depending on the multiplexing strategy, *see* **Note 10**.

1. Remove NPM, PPC, and the index primers from –15 °C/–25 °C storage. Thaw them on a bench to room temperature. Allow approximately 20 min to reach room temperature.
2. Gently invert the tubes 3–5 times to mix and give a brief spin.
3. Organize indexes according to the number of samples that are studied. If running 24 libraries *see* **Note 11** and for 96 libraries *see* **Note 12**.
4. Label a new 0.2 ml 96-well plate (Thermo Scientific, Cat. No. AB-0800) as "NAP1" (Nextera Amplification Plate 1).
5. Using a multichannel pipette, add 5 μl of index 2 primers (white caps) to each column of the "NAP1" plate. Change tips between columns.
6. Add 5 μl of index 1 primers (orange caps) to each row of the "NAP1" plate. Change tips between rows.
7. Change the original caps in the primers vials for new white or orange caps provided with the Illumina kit.
8. Remove all the index primer tubes from the working area and store them at –20 °C.
9. Add 15 μl of NPM to each well of the "NAP1" plate containing index primers. Change tips between samples.
10. Add 5 μl PPC to each well containing index primers and NPM. Change tips between samples.
11. Using a multichannel pipette, transfer 20 μl of purified tagmented DNA from "NSP3" plate to the corresponding well in the "NAP1" plate. Gently mix by pipetting. Change tips between samples.
12. Cover the "NAP1" plate with a seal.
13. Centrifuge at 280 × *g* at 20 °C for 1 min.
14. Perform a PCR using the following program (making sure that the thermocycler lid is heated to 100 °C during the incubation):

    72 °C for 3 min.

    98 °C for 30 s.

    5 (or the appropriate number) cycles of:

    98 °C for 10 s.

    63 °C for 30 s.

    72 °C for 3 min.

    hold at 10 °C.

15. Transfer the "NAP1" plate to the post-PCR area. SAFE STOPPING POINT!! If you are not planning to proceed immediately with the Enriched library cleanup step, the plate can be stored at 10 °C overnight or between 2 and 8 °C up to 2 days.

3.4 Enriched Library Cleanup

Enriched library cleanup was adapted from Nextera DNA sample preparation guide (Illumina Inc., Part# 15027987 Rev. B). This process aims to obtain DNA fragment size selection, in which very short fragments of the library population are removed. For appropriate use of AMPure XP Beads (Beckman Coulter: 5 ml, Cat. No. A63880; 60 ml, Part No. A63881) *see* **Note 13**.

1. Before starting Enriched library cleanup remove the AMPure XP Beads (Beckman Coulter: 5 ml, Cat. No. A63880 or 60 ml, Cat. No. A63881) from the 2–8 °C storage and allow them to reach room temperature for at least 30 min.
2. Prepare fresh 80 % ethanol.
3. Label a new deep well 0.8 ml MIDI (Thermo Scientific, Cat. No. AB-0765) plate "NAP2" (Nextera Amplification Plate2).
4. Centrifuge the "NAP1" plate at 280 × *g* at 20 °C for 1 min.
5. Transfer the PCR product from the "NAP1" plate to the corresponding well of the "NAP2" plate (50 μl). Change tips between samples.
6. Vortex the room-temperature AMPure XP beads to ensure a proper distribution of the beads in the solution. Transfer an appropriate volume of beads to a trough in order to use a multichannel pipette.
7. Add 30 μl of AMPure XP beads to each well containing sample of the "NAP2" plate. For 2 × 250 runs on the MiSeq, add 25 μl of AMPure XP beads to each well containing sample of the "NAP2" plate.
8. Mix gently by pipetting. Change tips between samples.
9. Incubate at room temperature on the bench for 5 min.
10. Place the "NAP2" plate on a magnetic stand (Ambion, Cat. No. AM10027) for 2 min, or until the supernatant has cleared.
11. With the "NAP2" plate on the magnetic stand, remove and discard the supernatant. Change tips between samples. If any beads are aspirated in the tips, dispense them back and wait for 2 more minutes on the magnetic stand, or until the supernatant has cleared.
12. With the "NAP2" plate on the magnetic stand, wash the beads adding 200 μl of 80 % ethanol to each sample well. Do not resuspend the beads.
13. Incubate the "NAP2" plate for 30 s on the magnetic stand, or until the liquid has cleared.

14. Carefully remove and discard the supernatant.
15. Repeat **steps 12–14** for a total of two ethanol washes. Ensure there is no ethanol excess in the well after the second ethanol wash.
16. Leave the "NAP2" plate on the magnetic stand air-drying for 15 min.
17. Remove the "NAP2" plate from the magnetic stand.
18. With a multichannel pipette, add 32.5 μl of RSB to each sample well of the "NAP2" plate.
19. Resuspend the AMPure XP beads joined to the targeted DNA by a gently pipetting.
20. Incubate at room temperature for 2 min.
21. Place the "NAP2" plate on the magnetic stand for 2 min or until the liquid appears clear.
22. Label a new 96-well TCY plate (Bio-Rad, Cat. No. HSP-9601) as "NLP" (Nextera Library Plate).
23. Transfer 30 μl of the supernatant from the "NAP2" plate to the new "NLP" plate. Make sure you are not taking any AMPure XP beads. Change tips between samples.
24. Seal the plate with an adhesive cover seal (Thermo Scientific, Cat. No. AB-0580). SAFE STOPPING POINT!! If you are not planning to proceed immediately with the libraries quality control and pooling, the plate can be stored at –15–25 °C.

3.5 Library Quality Control and Quantification

Before pooling and sequencing the libraries, quantification of each sample is needed.

1. The concentration of the libraries is measured by fluorometry (*see* Subheading 3.1, **steps 17–23**) for details on measurement by Qubit System (Applied Biosystems).
2. The fragment size range of each library is revised with Agilent High Sensitivity DNA chips (Cat. No. 5067-4626) in the Bioanalyzer 2100 Electrophoresis System (Agilent Technologies) (*see* Subheading 3.9 for details).
3. In addition, qPCR quantification is recommended with Illumina Library quantification kit of KAPA Biosystems (Cat. No. KK4824).
4. First, dilute libraries according to the previous measurements to a concentration within the rage of the KAPA Standards picomolarity (*see* **Note 14**).
5. Program the following steps in a Real-Time thermal cycler. These are the recommended conditions, but depending on the real-time thermal cycler used, some setup could be required

(make sure that the block lid is set to 100 °C during the whole incubation):

95 °C for 3 min.

40 cycles of:

95 °C for 30 s.

63 °C for 30 s.

72 °C for 30 s (Add Fluorescent reading point).

95 °C for 1 min.

55 °C for 1 min.

Melt Curve from 55 to 95 °C, increments of 0.5 °C every 10 s (Add plate reading point).

Hold at 10 °C.

6. Prepare a Master Mix of the following reagents for as many samples as you will study plus 10 %, taking into account that the volumes required for one sample are:

6 μl	ddH_2O
10 μl	2× KAPA SYBR FAST qPCR Master Mix
2 μl	(10×) Illumina Primer Premix
2 μl	Diluted DNA Template or Illumina DNA Standards
20 μl	Total volume per reaction

7. Use 2 μl of each sample dilution in triplicates to run the quantification qPCR.
8. Estimate each final library concentration according to their amplification threshold cycle (Ct) in relation to KAPA standards concentrations.

3.6 Pooling Libraries

Pooling libraries was adapted from Nextera DNA sample preparation guide (Illumina Inc., Cat. No. 15027987 Rev. B). This method explains how to mix up libraries in organized pools to be sequenced:

1. Before pooling the libraries of each project, label a new deep well 0.8 ml MIDI plate (Thermo Scientific, Cat. No. AB-0765) with an "NDP" barcode.
2. Only if multiplexing of libraries is taking into account, also label a new deep well 0.8 ml MIDI plate (Thermo Scientific, Cat. No. AB-0765) with an "NPP" barcode.
3. If the "NLP" plate was stored at −15 to −25 °C, thaw it at room temperature and centrifuge it at 280 × *g* at 20 °C for 1 min.
4. Remove the adhesive seal from the "NLP" plate.
5. Transfer 10 μl of sample library from the "NLP" plate to each corresponding well of the new "NDP" plate. Change tips between samples.

6. Normalize each sample in the "NDP" plate to 2 nM using Tris–HCl 10 mM, pH 8.5 with 0.1 % Tween 20. Depending on the library quantification, the volume in each well may vary from 10 to 100 μl.
7. Seal the "NDP" plate.
8. Vortex the plate on a shaker at 1,000 rpm for 2 minutes.
9. Centrifuge the "NDP" plate at 280 × *g* at 20 °C for 1 min.
10. Remove the adhesive seal.
11. Depending on the type of the libraries you want to generate, there are two options here: For non-multiplexed libraries, protocol stops here. Do one of the following: Proceed to cluster generation (following Illumina instructions, *see* **Note 15**) or seal the plate and store it at −15 to −25 °C. For multiplexed libraries, continue with the next step.
12. To make "NPP", transfer 5 μl from each sample of the "NDP" plate to the corresponding well of column 1 of the "NPP" plate following the experimental design established for each particular project (*see* **Note 7**).
13. Change tips and transfer 5 μl from each sample in column 2 of the "NDP" plate to column 1 of the "NPP" plate.
14. Repeat **step 13** as many times as the number of remaining sample columns in the "NDP" plate. Change tips between columns. The result will be a "NPP" plate with pooled libraries in column 1.
15. Seal the "NPP" plate and shake it at 1,800 rpm for 2 min.
16. Do one of the following: Proceed to cluster generation (following Illumina instructions, *see* **Note 15**) or seal the plate and store it between −15 and −25 °C.

3.7 mRNA Preparation from Single Cells

The Subheadings 3.7–3.10 describe the preprocessing of single-cell RNA prior to cDNA high-throughput sequencing. This procedure was adapted from SMARTer Ultra™ Low RNA Kit for Illumina Sequencing User Manual" (Clontech, number 120213). For first strand cDNA synthesis, and before starting the retrotranscription, there is no need for RNA extraction when starting from a single cell, but user should be sure that each cell is eluted in 1 μl of PBS.

1. *See* **Notes 1** and **2** before starting any of the described procedures.
2. Thaw Dilution Buffer and RNase Inhibitor at room temperature and place aside on ice.
3. Thaw master mix reagents for **step 8** from *SMARTer Ultra Low RNA Kit for Illumina Sequencing* (Clontech, Cat. No. 634936) and place aside on ice.

4. Prepare the following mix to obtain a stock solution of Reaction Buffer (scale-up as needed):

19 µl	Dilution Buffer
1 µl	RNase inhibitor
20 µl	Total final volume per sample

5. Dispense 2.5 µl of Reaction Buffer in each 0.2 ml RNase-free PCR tube of an 8-well strip, and add 1 µl of sample (*see* **Note 16**).
6. Place the samples on ice and add 1 µl of 3′ SMART CDS Primer A (12 µM) to each 0.2 ml RNase-free PCR tube. Gently vortex the tube(s) and spin briefly.
7. Incubate reactions at 72 °C for 3 min in a thermal cycler with lid heated at 100 °C.
8. Start preparing master mix for the next step at room temperature while previous incubation is running. The following steps are critical for first-strand cDNA synthesis and should not be delayed after the end of **step 7**.
9. In a DNA LoBind Tube 1.5 ml (Eppendorf Cat. No. 022431021) mix the following reagents in the order shown, for all the reactions that will be set plus one, at room temperature:

2 µl	5× First-strand buffer
0.25 µl	DTT (100 mM)
1 µl	dNTP mix (10 Mm)
1 µl	SMARTer IIA Oligonucleotide (12 µM)
0.25 µl	RNase inhibitor
1 µl	SMARTScribe reverse transcriptase (100 U/µl)
5.5 µl	Total volume per reaction

10. Mix well by gently vortexing and pulse-centrifuge. It is important to add SMARTScribe Reverse Transcriptase just prior to use.
11. Add 5.5 µl of Master Mix (**step 9**) to each reaction tube, mix by pipetting up and down and centrifuge briefly.
12. Place tubes in a thermal cycler and run the following program with heater lid set to 100 °C:

    42 °C for 90 min.

    70 °C for 10 min.
13. Centrifuge the tubes when incubation ends and continue with First-Strand cDNA purification.

Fig. 4 The top part of an inverted P20 or P200 tip holder is attached with tape to the Magnabot II Magnetic Separator Device (Promega, Cat. No. V8351). This procedure is extracted from "SMARTer Ultra Low RNA Kit for Illumina Sequencing User Manual" (Clontech)

14. Before starting purification of first strand cDNA, allow AMPure XP Beads (Beckman Coulter, 5 ml: Cat. No. A63880 or 60 ml: Cat. No. A63881) to reach room temperature for at least 30 min and vortex well (*see* **Note 13**). Ensure that there are no precipitates in the beads solution.
15. Then place the tubes in a device that you should set up as the one shown in Fig. 4.
16. Add 25 μl AMPure XP Beads to each sample. Set pipette to 35 μl and pipette up and down ten times to mix thoroughly. Incubate at room temperature for 8 min. It is important to pipette the beads slowly because they are viscous. Always check tips before discarding them.
17. After incubation, briefly spin down the tubes to collect any residual liquid on the tube wall. Place the tubes on the Promega MagnaBot II Magnetic Separation Device for 5 min or until liquid appears completely clear.
18. Leaving the samples on the Magnetic Separation Device, pipette out with p10 pipette and discard the solution, making sure that the beads are not disturbed. Leave the beads in the tube and check pipette filter tips before discarding them to ensure that there are no beads with the supernatant.
19. Spin tubes briefly and place them back in the Magnabot II Magnetic Separation Device for 2 min or until liquid is completely clear.
20. Using a p10 pipette, discard any residual liquid from the tubes again checking the tips very carefully.

3.8 Double Stranded cDNA Amplification and Purification

This Procedure was adapted from "SMARTer UltraTM Low RNA kit for Illumina Sequencing User Manual" number 120213.

1. Thaw Advantage 2 PCR Buffer, dNTP Mix (10 mM), IS PCR Primer (12 μM) and 50× Advantage 2 Polymerase Mix from *SMARTer Ultra Low RNA Kit for Illumina Sequencing* (Clontech, Cat. No. 634936) and place them aside on ice.
2. Prepare in a DNA LoBind Tube 1.5 ml a PCR Master Mix combining, in order, the following reagents volumes, for all reactions that are considered plus one:

5 μl	10× Advantage 2 PCR buffer
2 μl	dNTP mix (10 mM)
2 μl	IS PCR primer (12 μM)
2 μl	50× Advantage 2 polymerase mix
39 μl	Nuclease-free water
50 μl	Total volume per reaction

3. Vortex the tube containing the PCR Master Mix and centrifuge briefly.
4. Then add 50 μl of PCR Master Mix to each well containing DNA bound to the beads from Purification of first strand cDNA (Subheading 3.7, **step 20**). Mix well by vortexing and spin briefly.
5. Place the tubes in the thermal cycler with heated lid at 100 °C, and run the following program with the recommended number of cycles for 10 pg of Input amount (1 cell, 18 cycles)

   95 °C for 1 min.

   18 cycles of:

   95° for 15 s.

   65 °C for 30 s.

   68 °C for 6 min.

   72 °C for 10 min.

   Holds at 4 °C.
6. When PCR ends, follow the purification of ds-cDNA procedure in a POST-PCR area with AMPure XP Beads (*see* **Note 13**).
7. Prepare fresh 80 % ethanol.
8. Bring to room temperature AMPure XP Beads for at least 30 min and mix well.
9. Take a 96-well V-bottom plate (VWR Cat. No. 47743-996), cover it with MicroAmp Clean Adhesive Seal (AB Part No. 4306311) and uncover only the wells that are going to be used.

10. Add 90 μl of AMPure XP Beads to the wells that will contain the samples.
11. Transfer the entire PCR product including the AMPure XP Beads (from **step 5**) to the wells containing the 90 μl of AMPure XP Beads (from **step 10** above), and pipette up and down ten times to mix thoroughly.
12. Incubate at room temperature for 8 min to let the DNA bind to the beads.
13. Place the plate on the Ambion Magnetic Stand-96 (Ambion, Part No. AM10027) for 5 min or until the liquid appears completely clear.
14. Pipette out the supernatant and check pipette filter tips before discarding them to ensure that there are no beads within the collected supernatant.
15. Keep the 96-well plate on the Ambion Magnetic Stand-96 and add 200 μl of freshly prepared 80 % ethanol to each sample without disturbing the beads, and wait for 30 s. Then pipette out supernatant.
16. Repeat **step 15** one more time.
17. Seal the 96-well V-bottom plate with MicroAmp Clean Adhesive Seal and spin it down for 10 s.
18. Place the 96-well plate on the magnetic, stand 30 s and pipette out the remaining ethanol.
19. With the 96-well plate on the Ambion Magnetic Stand-96, let beads dry at room temperature for 3–5 min until beads appear dried (*see* **Note 17**).
20. Once the beads are dried, add 12 μl of Purification Buffer to cover the beads, and, afterwards, retire the 96-well plate from the magnetic and incubate it for 2 min to rehydrate beads.
21. Mix the beads by pipetting up and down for ten times or until beads are completely resuspended.
22. Put the 96-well plate back on the Ambion Magnetic Stand-96 for 1 min or until solution is completely clear.
23. Set pipette to 10 μl and transfer the supernatant that contain the purified cDNA from each well to a nuclease-free nonsticky tube labeled with sample information. SAFE STOPPING POINT!! Protocol can be stopped here storing samples at −20 °C.

3.9 cDNA Quality Control

Total cDNA for HTS should be non-degraded and free of contaminants that could inhibit subsequent reactions. For quantification of total cDNA using fluorometry, please refer to Subheading 3.1, **steps 17–23**. For qualification of total cDNA integrity the Bioanalyzer 2100 Electrophoresis System (Agilent Technologies) is used. For this particular purpose, the High Sensitivity DNA Kit

(Agilent, Cat. No. 5067-4626) is required. This kit contains chips and reagents designed for analysis of DNA fragments. Make sure that Bioanalyzer electrodes are clean (*see* **Note 18**).

1. To set up the Chip Priming Station, slide a new syringe into the hole of the lock adapter and screw it tightly to the chip priming station.
2. Adjust the base plate in position C (*see* Fig. 5).
3. Adjust the syringe clip in the lowest position (*see* Fig. 6).
4. Before preparing the gel–dye mix, allow the High Sensitivity DNA dye concentrate (blue-capped) and High Sensitivity DNA gel matrix (red-capped) to equilibrate to room temperature for 30 min (*see* **Note 19**).
5. Vortex the blue-capped vial with High Sensitivity DNA dye concentrate for 10 s and spin down. Make sure that the DMSO is completely thawed.
6. Pipette 15 μl of the blue-capped vial with High Sensitivity DNA dye concentrate into a red-capped High Sensitivity DNA gel matrix vial. Store the remaining dye concentrate at 4 °C in the dark again.
7. Cap the tube and vortex for 10 s. Visually inspect proper mixing of gel and dye.
8. Transfer the complete gel–dye mix to the top receptacle of a spin filter (included in the kit).
9. Place the spin filter in the included microcentrifuge tube and spin for 10 min at room temperature at 2,240 × *g* ± 20 %.
10. Discard the filter according to good laboratory practices. Label the tube containing dyed gel matrix including the date of prep-

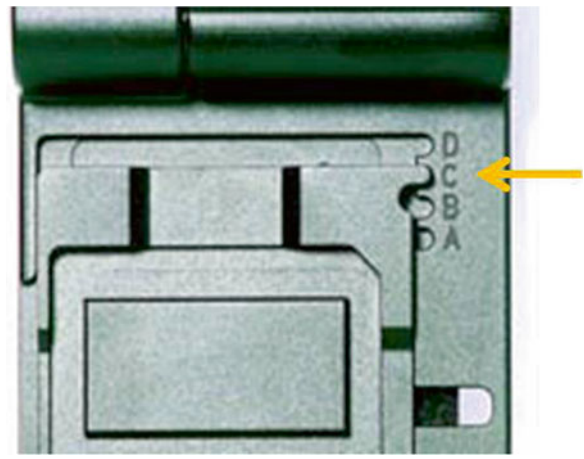

Fig. 5 Image of the base plate from the Chip Priming Station in position C of Bioanalyzer System (Agilent Technologies)

Fig. 6 Image of the syringe clip in the lowest position of Bioanalyzer System (Agilent Technologies)

aration. Each aliquot of gel–dye mix is sufficient for five chips. Protect the gel–dye mix from light and store it at 4 °C in the dark when it is not in use for more than 1 h. Use the gel–dye within 6 weeks of preparation.

11. Before loading the gel–dye mix into a chip, allow the gel–dye mix to equilibrate to room temperature for 30 min. Protect the gel–dye mix from light during this time.
12. Take a new High Sensitivity DNA chip out of its sealed bag and place it on the chip priming station (confirm that the chip priming station is in position C).
13. Pipette 9.0 μl of the gel–dye mix at the bottom of the well marked as G. When pipetting the gel–dye mix, make sure not to draw up particles that may sit at the bottom of the gel–dye mix vial. Insert the tip of the pipette to the bottom of the chip well when dispensing. This prevents a large air bubble forming under the gel–dye mix. Placing the pipette at the edge of the well may lead to poor results.
14. Make sure that the plunger of the syringe is set at 1 ml and then close the priming station. The lock of the latch will click when the priming station is closed correctly.

15. Press the plunger of the syringe down until it is held by the clip positioned at the lowest option.
16. Wait for exactly 60 s and then release the plunger with the clip release mechanism.
17. Wait for 5 s, then slowly pull back the plunger to the 1 ml position.
18. Open the chip priming station.
19. Pipette 9.0 μl of the gel–dye mix in each of the wells marked as G. Store the remaining gel–dye mix at 4 °C when it is not in use for more than 1 h.
20. For loading the High Sensitivity DNA Marker, pippette 5 μl of the High Sensitivity DNA marker (green-capped) into the well marked with the ladder symbol and into each of the 11 sample wells. Do not leave any well empty because the chip will not run properly.
21. For loading the ladder and samples, pipette 1 μl of each sample into wells 1–11 and 1 μl of High Sensitivity DNA ladder (yellow-capped), which should be kept on ice until stored at 4 °C, into the well marked with the ladder symbol. Unused wells must be filled with 1 μl of Purification Buffer (Subheading 3.8) in which the samples are diluted.
22. Put the chip horizontally in the IKA vortex mixer and vortex for 1 min at 2,400 rpm.
23. Run the chip within 5 min after preparation.
24. Open the lid of the Agilent 2100 Bioanalyzer instrument.
25. Place the chip carefully into the receptacle. The chip fits only one way.
26. Carefully close the lid, when the electrodes in the cartridge should fit into the wells of the chip.
27. The 2100 Expert software screen (*see* Fig. 7) indicates automatically that you have inserted a chip and closed the lid by displaying the chip icon at the top left of the Instrument context.
28. To start the Chip process, select the appropriate assay from the Assay menu, in this case, "High Sensitivity DNA assay" option (Fig. 7).
29. Enter sample information like sample names and comments in "Chip Summary" tab.
30. Accept the current File Prefix or modify it. Data will be saved automatically to a file with a name using the prefix you have just entered. At this time, you can also customize the file storage location and the number of samples that will be analyzed.

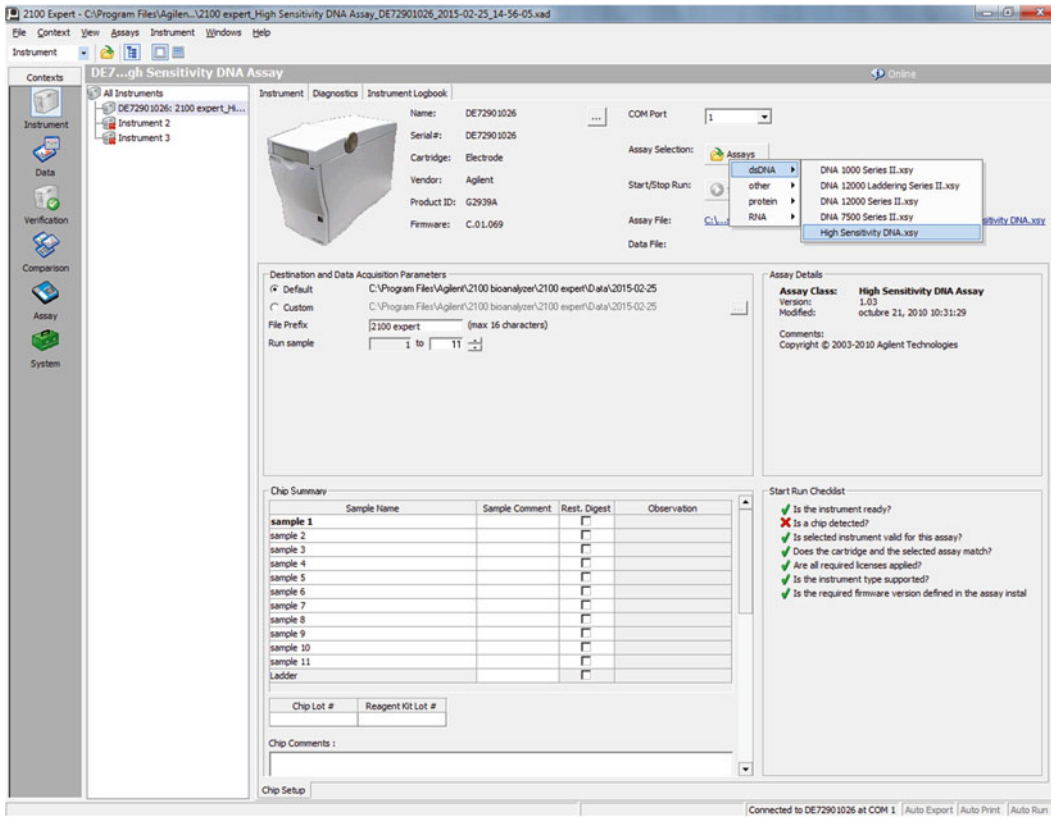

Fig. 7 Screen-shot of Bioanalyzer's 2100 Expert Software (Agilent Technologies) showing the assay selection that should be done in this procedure ("High Sensitivity DNA assay")

31. Click the Start button in the upper right of the window to start the chip. The incoming raw signals are displayed in the Instrument context.
32. After the chip run is finished, remove the chip from the receptacle of the Agilent 2100 Bioanalyzer instrument and dispose it according to good laboratory practices. Do not leave the chip in the Bioanalyzer after a run due to risk of electrode contamination after long periods of time (e.g., overnight).
33. Then slowly pour 350 μl RNase-free water through one of the wells of the Electrode Cleaner Chip.
34. Open the lid and place the Electrode Cleaner Chip in the Agilent 2100 Bioanalyzer's receptacle.
35. Close the lid and leave it closed for about 1 min.
36. Open the lid and remove the electrode cleaner.
37. Wait another 1 min to allow the water on the electrodes to evaporate before closing the lid.

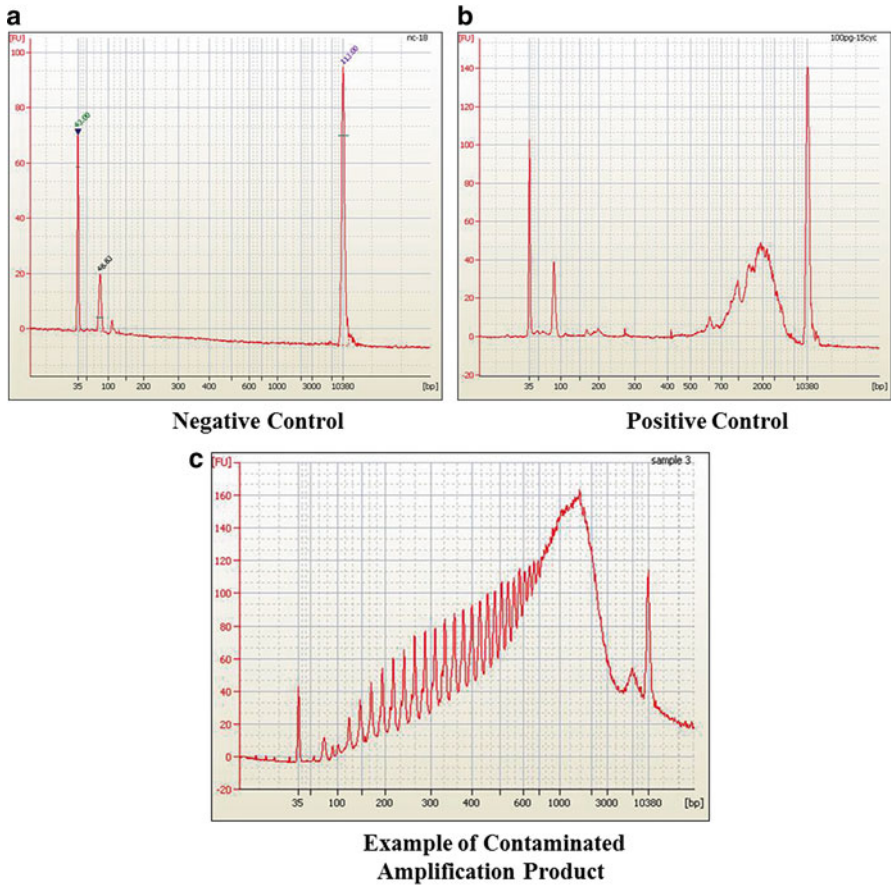

Fig. 8 2100 Bioanalyzer (Agilent Technologies) output electropherograms: (**a**) Example of non-RNA control cDNA library, (**b**) positive control cDNA library, or (**c**) contaminated amplification product obtained after cDNA synthesis and amplification

38. To interpret the results of cDNA integrity, one must compare the results of the samples and controls. Successful cDNA synthesis and amplification should yield no product in the negative control (Fig. 8a), and a distinct mountain spanning 400–9,000 bp and peaked at ~2,000 bp for the control RNA sample (Fig. 8b), yielding approximately 2–7 ng of cDNA (depending on the input). Contaminated samples will have a broader peak, and abnormally high yield (Fig. 8c).

3.10 cDNA Library Preparation

The procedure for library preparation of amplified total cDNA is equal to the described in Subheadings 3.2–3.6, but using *Nextera XT sample preparation kit* (Illumina Inc.), using as input 1 ng of purified cDNA (5 μl of 0.2 ng/μl dilution), tagmenting during 10 min instead of the 5 min is recommended in the protocol and with a library enrichment cycle as follows (*see* **Note 20**):

72 °C for 3 min.

95 °C for 30 s.

12 cycles of:

95 °C for 10 s.

55 °C for 30 s.

72 °C for 1 min.

72 °C for 5 min.

Hold at 10 °C.

4 Notes

1. General notes for good laboratory practice when performing PCR are as follow. Pre-PCR and Post-PCR Lab Procedures: PCR products can contaminate reagents, equipment and genomic DNA samples. To prevent that from happening there are some recommendations:
   - Physically separate PRE and POST PCR areas in the lab, ideally in two different rooms.
   - Keep the reagents for Pre-PCR and Post-PCR stored separately.
   - Use dedicated equipment for Pre-PCR and Post-PCR products as pipettes, centrifuges, heat blocks, etc., and never exchange them between processes.
   - It is highly recommended to clean all the supplies and surfaces with 0.5 % Sodium Hypoclorite (10 % bleach) before starting and after finishing daily work.
   - In addition, the use of DNAse/RNase-free supplies (tips, plates, tubes, strips, troughs, etc.) is compulsory for all the described procedures.
2. It is recommended to have a dedicated set of pipettes only for DNA library preparations and another set to manipulate total RNA before obtaining cDNA.
3. The *Repli-g Single Cell Kit* is not supplied with enough PBS sc to prepare serial dilutions of cell material, and therefore, the user should perform serial dilu*tions with a different* PBS buffer (general supplier) aliquot.
4. Optional: Control DNA sample is prepared by diluting a control DNA stock with 5 mM Tris–HCl (pH 8.0) to 1 ng/μl and subsequently to 15 pg/μl by taking 3 μl of 1 ng/μl preparation into 197 μl of 5 mM Tris–HCl (pH 8.0). Use 1 μl plus 3 μl of PBS sc buffer as if it were one more single-cell sample.

5. Be aware that the expected resulting product length is usually more than 10 Kbp, with a range between 2 and 100 Kbp, and with a concentration of approximately 40 μg per 50 μl of amplification reaction, but, depending on the quality of the input DNA, concentration may be lower. If using a negative (no-template) control, high-molecular-weight product can be generated by random extension of primer-dimers (10–40 μg per 50 μl). This DNA will not affect the quality of actual samples or specific downstream genetic assays.
6. Sample quality control is imperative since purity and integrity of DNA are critical for the overall success of HTS. Total DNA should be non-degraded and free of contaminants that could inhibit subsequent reactions. Appropriate quantification of double-strand DNA is made by specific fluorometric methods. Depending on the number of samples that are being handled, Quant-iT™ PicoGreen® dsDNA Assay Kit (Life technologies) or Qubit® 2.0 Fluorometer (Life technologies) methodologies can be chosen for accurate measurement of double-stranded-DNA concentration. Herein, we have described Qubit® 2.0 Fluorometer DNA concentration measurement for low to medium throughput projects. Qubit® Assay Kits provide concentrated assay reagent, dilution buffer, and prediluted standards. The assay is performed at room temperature, and the signal is stable for 3 h. It is important that the concentration of samples is inside of "assay range". This range is from 2 to 1,000 ng for the dsDNA Broad Range (BR) Assay and from 0.2 to 100 ng for the dsDNA High Sensitivity (HS) Assay. If it is possible, it is recommended to measure previously an aliquot of the samples with a NanoDrop (NanoDrop 2000 UV–Vis Spectrophotometer, Thermo Scientific). This way, one can approximate the samples to the required concentration range.
7. Before starting library preparations, it is compulsory to have ready a complete experimental design since the way in which the libraries will be prepared, indexed and pooled is decided depending on the aims of each particular HTS project.
8. During this step, total genomic DNA is tagmented (tagged and fragmented) by an engineered transposome, which also adds adapter sequences to the generated fragment ends. The steps described were adapted from Nextera DNA sample preparation guide, Part # 15027987 Rev. B. It is important that all steps are followed in the order described.
9. In this step, tagmented DNA is isolated from the Nextera transposome complex, which can bind tightly to the DNA and could interfere later on if not removed.
10. Low plexity pools indexing tip: Illumina's HTS systems use a green laser to read Gs and Ts and a red laser for As and Cs.

Thus, at every cycle of the index read, at least one nucleotide for each color channel should be present to avoid errors during the data generation. For more details about Illumina's libraries pooling guidelines visit: http://res.illumina.com/documents/products%5Ctechnotes%5Ctechnote_nextera_low_plex_pooling_guidelines.pdf.

11. If running 24 libraries, organize the index primers using the following arrangement: Arrange Index 1 (i7) primers (orange caps) in order horizontally, so N701 is in column 1 and N706 is in column 6. Arrange index 2 (i5) primers (white caps) in order vertically, so N501 is in row A and N504 is in row D. Record these positions on a lab tracking form.
12. For 96 libraries arrange the index primers using the following arrangement: Arrange Index 1 (i7) primers (orange caps) in order horizontally, so N701 is in column 1 and N712 is in column 12. Arrange index 2 (i5) primers (white caps) in order vertically, so N501 is in row A and N508 is in row H. Record these positions on a lab tracking form.
13. Handling Magnetic Beads:
    - Vortex until well resuspended and dispense an adequate volume in a trough with cap. The trough needs to be capped because you will need to vortex the beads before each addition to the samples without altering the original beads concentration.
    - After the addition of beads to the samples, mix them thoroughly by pipetting up and down ten times or until the solution appears homogeneous.
    - After the incubation of the mixes on the magnetic stand, beads bind to the wall of the well. Keep the plate on the magnetic stand for the time indicated in each protocol or until the solution appears clear and then aspirate the cleared supernatant slowly not to take beads with you. It is recommended the use of tips with thin ending.
14. For proper library quantification, it is necessary to have your sample concentrations within the range of the standard used for the standard curve. Illumina DNA standards for KAPA quantification kit are between 20 and 0.0002 pM. Therefore, based on the concentration estimated in the region table that can be exported from the Bioanalyzer 2100 Electrophoresis System (Agilent Technologies), one can estimate the required dilution of the obtained libraries.
15. If sequencing Nextera libraries with HiSeq2000/1000, HiScanSQ or GAIIx, you must be sure to use the TruSeq Dual Index Sequencing primer Boxes (Single read or paired End), Not required if sequencing with MiSeq System.

16. If using the positive control provided with the kit, add 1 μl of the diluted Control RNA that matches with the concentration of your test sample. In general, a single cell is supposed to contain 10 pg of total RNA. Dilute Control RNA in nuclease-free water. For negative control add 1 μl of Nuclease-free water.
17. You may see a tiny crack that indicates that the beads are dried. If you over-dried the beads there will be many cracks in the pellet. If you under-dried the beads, the DNA recovery rate will be lower because of the remaining ethanol.
18. It is highly recommended to clean the Bioanalyzer every month by decontaminating the electrodes with RNaseZAP. In order to do this, the following steps should be followed:
    - Slowly fill one of the wells of an electrode cleaner with 350 μl RNaseZAP.
    - Open the lid and place electrode cleaner in the Agilent 2100 Bioanalyzer.
    - Close the lid and leave it closed for about 1 min.
    - Open the lid and remove the electrode cleaner. Label the electrode cleaner and keep it for future use. You can reuse the electrode cleaner for 25 chips.
    - Slowly fill one of the wells of another electrode cleaner with 350 μl RNase-free water.
    - Place electrode cleaner in the Agilent 2100 Bioanalyzer.
    - Close the lid and leave it closed for about 10 s.
    - Open the lid and remove the electrode cleaner.
    - Wait another 10 s for the water on the electrodes to evaporate.
    - Repeat three or four times the previous five steps for a complete electrodes decontamination.
    - Close the lid and keep the water electrode cleaner for further use.
19. Be aware that High Sensitivity DNA Kit (Agilent, Cat. No. 5067-4626) components contain DMSO. Because the included dye binds to nucleic acids, it should be treated as a potential mutagen and used with appropriate care. It is important that all the reagents (except the ladder) are equilibrated to room temperature before starting the next step. While preparing the reagents at room temperature, protect the dye concentrate from light.
20. Although library preparation procedures are described in detail in the present chapter, we suggest the user to revise them within Illumina web (http://www.illumina.com/index-c.ilmn) since the HTS field is in continuous developing, and therefore, updates are introduced monthly.

Acknowledgements

We would like to thank Juan José Fuentes Nuño for his assistance on single-cell isolation procedure description. A.G.L. and some research expenses are partially supported by CIBERehd. A.M.A., N.M., A.G.L., L.B., and research expenses are supported by the Basque Country Government (Etortek Research Programs 2010/2014) and Bizkaia County's Innovation Technology Department.

References

1. Metzker ML (2010) Sequencing technologies – the next generation. Nat Rev Genet 11(1):31–46
2. Mardis ER (2011) A decade's perspective on DNA sequencing technology. Nature 470(7333): 198–203
3. Evanko D (2014) Method of the Year 2013. Nat Methods 11(1):1–112
4. Zong C et al (2012) Genome-wide detection of single-nucleotide and copy-number variations of a single human cell. Science 338(6114):1622–1626
5. Emmert-Buck MR et al (1996) Laser capture microdissection. Science 274(5289):998–1001
6. Nakamura N et al (2007) Laser capture microdissection for analysis of single cells. Methods Mol Med 132:11–18
7. Kuppers R, Schneider M, Hansmann ML (2013) Laser-based microdissection of single cells from tissue sections and PCR analysis of rearranged immunoglobulin genes from isolated normal and malignant human B cells. Methods Mol Biol 971:49–63
8. Fulwyler MJ (1965) Electronic separation of biological cells by volume. Science 150(3698): 910–911

Chapter 6

Shotgun Proteomics on Tissue Specimens Extracted with Acid Guanidinium-Thiocyanate-Phenol-Chloroform

René B.H. Braakman, Anieta M. Sieuwerts, and Arzu Umar

Abstract

Protein-containing organic fractions of acid guanidinium thiocyanate-phenol-chloroform-extracted tissues are an interesting source of proteins as this method is widely used for RNA extraction for gene expression analysis. However, due to difficulties in redissolving pelleted proteins from the organic phase, protein analysis has only been limitedly reported. Current shotgun mass spectrometry-based methods, however, require minute amounts of sample, and methods have been developed that allow SDS to be removed from an extraction buffer prior to protein digestion. The limited volume of starting material needed for shotgun proteomics facilitates redissolving proteins in SDS-containing buffers, allowing proteins to be readily extracted. Here we describe a protocol for an SDS-DTT-based extraction of proteins from the organic fraction of acid guanidinium-thiocyanate-phenol-chloroform-extracted tissues that remain after RNA isolation for shotgun MS analysis.

Key words Breast cancer, Sample preparation, Proteomics, Genomics, Acid guanidinium-thiocyanate-phenol-chloroform extraction

1 Introduction

Acid guanidinium thiocyanate-phenol-chloroform extraction (AGPC, commercially available as TRI reagent, TRIzol, RNA-Bee, RNAzol B, RNA STAT-60, etc.) is a commonly and widely used method for the extraction of RNA from both clinical tissue specimens and cell lines [1, 2]. Next to RNA, DNA and protein can also be recovered, and thus AGPC allows integrative analyses from fully identical material. As the method is widely used, archived organic DNA/protein fractions provide a rich source of samples for protein extraction that can be matched with gene expression data obtained from the same tissue. However, protein analysis, most notably shotgun proteomics, from AGPC fractions has only limitedly been reported [3–9]. In part, this is the result of difficulty in recovering proteins from the organic fraction. To recover proteins, usually an excess of a precipitating agent, such as acetone or

Maria del Mar Vivanco (ed.), *Mammary Stem Cells: Methods and Protocols*, Methods in Molecular Biology, vol. 1293,
DOI 10.1007/978-1-4939-2519-3_6,

isopropanol, is added, and precipitated proteins are pelleted through centrifugation. The pellet is then thoroughly washed and redissolved using a chaotrope or surfactant compatible with downstream analysis, such as urea or SDS. With the large amount of proteins (several milligrams) typically recovered from the organic fraction, the pellet will be large, dense, and difficult to redissolve. Several groups have attempted to improve resolubilization using minor variations of precipitation methods, resolubilization buffers and methods [6, 8–12] or avoiding precipitation by using dialysis [13]. For example, methanol-chloroform precipitation [14] has been reported to result in a less compact pellet, facilitating resolubilization in high concentrations of SDS [15]. For mass spectrometry-based proteomics an additional difficulty is that high concentrations of SDS will interfere with the downstream process of digestion, separation of peptides, and peptide ionization in the mass spectrometer [16–18]. Attempts to redissolve pelleted proteins in Rapigest, a mass spectrometry-compatible detergent, required the use of high-intensity ultrasound during the wash step of the pellet in order to disperse the pellet and increase its surface area [4, 5]. However, we could not consistently redissolve the pellet in a buffer with 0.1 % Rapigest, even when high-intensity ultrasound was applied. While SDS in high concentrations in the digestion buffer will interfere with downstream mass spectrometry (MS), several robust methods have been developed to remove SDS both prior to [19, 20] or after digestion [21] that challenge or outperform traditional in-solution digests [22, 23]. Furthermore, current quantitative MS-based proteomics approaches require input material in the low-microgram region, equivalent to just a few microliters of the organic fraction. Instead of focusing on the precipitation method or detergent for resolubilization, we attempted to scale the volume of the starting material down to reduce the pellet size to a volume that is readily dissolved in a buffer with a high concentration of SDS. We have found that a pellet corresponding to 50–100 μg of protein is consistently dissolved within 15 min of heating to 95 °C. To remove SDS, we have used a filter-assisted sample preparation (FASP) method, where SDS is displaced on an MWCO filter using high concentrations of urea [19, 24]. Next to SDS, any other minor low-molecular-weight contaminants that may interfere with digestion will be removed prior to the digestion step. FASP therefore matches well with samples extracted with AGPC. Furthermore, high-molecular-weight substances that may interfere with downstream peptide analysis remain on the filter after collection of the peptides. The result is a pure population of peptides that can be readily analyzed, or further processed, e.g., for fractionation or chemical labeling. Here we describe the procedure to precipitate proteins from AGPC-extracted breast cancer tissues and redissolve the protein pellet in an SDS-containing buffer, exchanging the buffer and digesting the proteins using the FASP method.

2 Materials

Prepare all solutions using MilliQ water and analytical grade reagents. Prepare and store all reagents at room temperature (unless indicated otherwise). Guanidinium thiocyanate, phenol, and chloroform are a health hazard if not handled properly. Avoid direct contact with the reagents, because contact to skin, eyes, or respiratory tract may cause chemical burns to the exposed area. Always work in a fume hood during AGPC extraction and wear a lab coat, gloves, and safety glasses. Redissolve (dithiothreitol) and alkylation (iodoacetamide) buffers are unstable and should be prepared just before use. Cleanup buffer should be used within a day. All reagents should be molecular biology grade certified to be free of DNases, RNases, and proteases.

1. RNA-Bee (Tel-Test, Inc.).
2. Chloroform (should not contain isoamyl alcohol or any other additives).
3. Ethanol.
4. Isopropyl alcohol.
5. Redissolve buffer: 4 % SDS, 100 mM DTT in 100 mM Tris/HCl pH 8.
6. Cleanup buffer: 8 M urea in 100 mM Tris/HCl pH 8.
7. Alkylation buffer: 50 mM iodoacetamide in cleanup buffer.
8. Digestion buffer: 50 mM tetraethyl ammonium bicarbonate in HPLC water.
9. Lys-C: 20 μg/mL in digest buffer.
10. Trypsin: 1 μg/μL in 50 mM acetic acid in HPLC water.
11. RNase/DNase-free tubes.
12. Protein LoBind tubes.
13. 30 kDa MWCO cutoff filters (Millipore Microcon or Sartorius Vivacon).

3 Methods

Carry out all procedures at room temperature unless otherwise specified. The AGPC procedure described below applies to RNA-Bee. Other brands may require a slightly different procedure; consult the manufacturer's instructions.

3.1 Patients and Tumor Tissue

Snap-frozen tumor tissues were used from our liquid N_2 biobank, which were selected based on high tumor percentage (based on invasive tumor cell nuclei as described before [25]). This study was approved by the Medical Ethics Committee of the Erasmus MC

Rotterdam, The Netherlands (MEC 02.953), and was performed in accordance to the Code of Conduct of the Federation of Medical Scientific Societies in the Netherlands. For experimental purposes, tissues were stored at −80 °C (midterm) or on dry ice (short term).

3.2 Tissue Cryostat Sectioning

1. Tissue cryostat sections are prepared in a properly cleaned cryostat (*see* **Note 1**).
2. Set the microtome blade at −23 °C and the tissue holder at −25 °C as a starting point, and adjust the temperature if needed.
3. Place deep-frozen tissue on the holder using Tissue-Tek mounting material but do not fully embed the tissue.
4. Cut 5 μm sections before and after sectioning for RNA and mount these 5 μm sections on regular glass slides for hematoxylin/eosin (HE) staining. These slides are kept at room temperature (overnight at 37 °C if desired) for drying prior to HE stain.
5. For RNA and subsequent protein isolation, prepare 10 × 30 μm sections (~30 mg) and place in chilled RNase/DNase-free tubes on dry ice.
6. Proceed with AGPC extraction directly or store prepared 30 μm tissue sections at −80 °C until downstream processing.

3.3 AGPC Extraction

1. Add 1 mL RNA-Bee to the frozen tissue sections (enough for up to 100 mg tissue).
2. Incubate for 12–15 min at room temperature. This includes the time to resuspend the solution by pipetting up and down through a 1 mL pipette tip with filter. Do not vortex (*see* **Note 2**).
3. Add exactly 150 μL chloroform to the homogenate (*see* **Note 3**).
4. Close tubes tightly and shake vigorously by hand for at least 20 s. Do not vortex (*see* **Note 2**).
5. Check if samples are completely homogenized; continue shaking for 10 s if this is not the case.
6. Allow samples to stand for 5 min at room temperature.
7. Centrifuge for 15 min 12,000 × *g* 4 °C.
8. Following centrifugation, the sample forms a lower blue phenol-chloroform phase, a white interphase, and an upper colorless aqueous phase. RNA remains exclusively in the aqueous phase whereas DNA and proteins are in the interphase and organic phase. The volume of the aqueous phase is about 50 % of the initial volume of RNA-Bee plus sample volume. Carefully transfer the aqueous phase to an RNase-free 1.5 mL tube and immediately proceed with RNA extraction. The organic (lower and inter) phase can be stored at −80 °C for at least a year until protein extraction.

3.4 Protein Isolation

1. Add 300 µL 100 % ethanol per 1 mL of AGPC solvent initially used for tissue extraction to the organic fraction.
2. Incubate at room temperature for 2–3 min, and then pellet DNA at 2,000 × g for 5 min at 4 °C.
3. Collect the phenol-ethanol supernatant and optionally proceed with DNA extraction from the remaining pellet according to the manufacturer's instructions.
4. Proceed with an aliquot of approximately 50 µL of the organic fraction for protein extraction.
5. Precipitate proteins by addition of 3 volumes of isopropanol, and incubate for 10 min at room temperature followed by centrifugation at 14,000 × *g* for 15 min at 4 °C.
6. Wash pellet twice with 500 µL 95 % ethanol, and air-dry for 10 min (*see* **Note 4**).
7. Redissolve and reduce proteins by adding 25 µL redissolve buffer and heating the sample to 99 °C for 15 min and agitation at 600 rpm (*see* **Note 5**).

3.5 FASP Digestion

FASP digestion of the protein pellet is performed according to Wiśniewski et al. [19] with minor modifications:

1. Dilute sample to 0.5 % SDS by addition of 175 µL cleanup buffer and load onto a 30 kDa MWCO filter (*see* **Notes 6** and **7**).
2. Spin at 14,000 × *g* for 15 min at 20 °C (*see* **Notes 8** and **9**).
3. Add 200 µL cleanup buffer to the filter and centrifuge once more.
4. Add 100 µL alkylation buffer to the filter.
5. Briefly agitate in a thermoblock at 600 rpm, and then incubate at room temperature for 20 min in the dark to alkylate proteins.
6. Centrifuge the filter at 14,000 × *g* for 10 min.
7. Wash by adding 100 µL cleanup buffer and centrifugation for 10 min at 14,000 × *g*. Repeat once.
8. Exchange the buffer by adding 100 µL digestion buffer and centrifugation for 10 min at 14,000 × *g*. Repeat once.
9. Replace collection tube with a fresh tube.
10. Add 1 µg lys C in 50 µL 50 mM TEAB and digest for 4 h in a wet chamber at 37 °C (*see* **Note 10**).
11. Add 2 µg trypsin in 2 µL 50 mM acetic acid, briefly agitate at 600 rpm, and continue digestion for another 16 h.
12. Spin at 14,000 × *g* for 15 min at 20 °C to collect peptides.
13. Add 50 µL digest buffer and spin at 14,000 × *g* for 15 min to maximize recovery.

14. Measure peptide concentration using a nanodrop UV spectrophotometer. A 1 mg/mL solution has 1.1 AU at 280 nm.

The sample can now be acidified for HPLC-MS analysis or can be further processed for, e.g., labeling and/or fractionation.

4 Notes

1. Make sure to clean the inside of the cryostat and the cutting blade with lint-free wipes instead of normal wipes. This is to avoid fibers sticking to your materials. Also, avoid using a hairbrush to place sections on the slides. In both cases, keratin contamination may be introduced that interferes with future proteomic applications. Use of steel needles and an antiroll plate is a good alternative. Also, use non-powdered, latex-free gloves, preferably nitrile.
2. Vortexing may not result in a clear phase separation and may result in shearing of DNA.
3. Higher volumes of chloroform increase the risk of concomitant DNA extraction.
4. There is no need to break up the pellet to facilitate solubilization; the pellet is small and will readily dissolve in SDS. Minor traces of interfering solvents will be removed downstream in the FASP procedure.
5. To obtain an indication of the total protein amount recovered from the organic fraction, process a 25 μL aliquot in parallel. Most accurate results are obtained using tryptophan fluorescence emission at 350 nm using an excitation wavelength of 295 nm. Alternatively, use a compatible colorimetric assay, e.g., Pierce 660 nm assay with detergent compatibility kit. A bicinchoninic acid (BCA) assay can be used when the pellet is dissolved in a buffer free of reducing agents; however minor traces of phenol will interfere and a more thorough washing may be required.
6. Filtration properties of Millipore Microcon 30 kDa MWCO filters vary between batches. It is recommended to test the performance of each batch using a standard cell or tissue lysate.
7. Occasionally a filter will leak due to a perforated or loose membrane. Leaking or damaged filters can be recognized by filters running completely dry between steps. Check for leakage prior to loading samples by applying 100 μL of urea buffer, centrifugation at 14,000 × *g*, and checking the volume that passed the filter after a minute. A leaking filter will run completely dry after a minute.
8. A too high loading of extracted proteins may result in clogging of the filters, resulting in longer flow-through times and

incomplete buffer exchange. Typically, up to 200 μg protein can be loaded on a Millipore Microcon 30 kDa MWCO filter.

9. These centrifugation times are normally sufficient to reduce the loaded volume down to approximately 10 μL between each step. Longer or shorter required centrifugation times indicate a too high sample amount or damaged filter, respectively.
10. The spin filter assembly is not airtight, and the sample will evaporate during prolonged incubation at 37 °C. Use a humidified chamber or oven in order to prevent evaporation during digestion.

Acknowledgements

This work was financially supported through the Center for Translational Molecular Medicine, Breast CARE (03O-104-06).

References

1. Chomczynski P, Sacchi N (1987) Single-step method of RNA isolation by acid guanidinium thiocyanate-phenol-chloroform extraction. Anal Biochem 162:156–159
2. Chomczynski P, Sacchi N (2006) The single-step method of RNA isolation by acid guanidinium thiocyanate-phenol-chloroform extraction: twenty-something years on. Nat Protoc 1:581–585
3. Lee FW-F, Lo SC-L (2008) The use of Trizol reagent (phenol/guanidine isothiocyanate) for producing high quality two-dimensional gel electrophoretograms (2-DE) of dinoflagellates. J Microbiol Methods 73:26–32
4. Kline KG, Frewen B, Bristow MR et al (2008) High quality catalog of proteotypic peptides from human heart. J Proteome Res 7:5055–5061
5. Kline KG, Wu CC (2009) MudPIT analysis: application to human heart tissue. Methods Mol Biol 528:281–293
6. Yamaguchi H, Hasegawa K, Esumi M (2013) Protein from the fraction remaining after RNA extraction is useful for proteomics but care must be exercised in its application. Exp Mol Pathol 95:46–50
7. Likhite N, Warawdekar UM (2011) A unique method for isolation and solubilization of proteins after extraction of RNA from tumor tissue using trizol. J Biomol Tech 22:37–44
8. Simões AES, Pereira DM, Amaral JD et al (2013) Efficient recovery of proteins from multiple source samples after TRIzol(®) or TRIzol(®)LS RNA extraction and long-term storage. BMC Genomics 14:181
9. Kirkland PA, Busby J, Stevens S, Maupin-Furlow JA (2006) Trizol-based method for sample preparation and isoelectric focusing of halophilic proteins. Anal Biochem 351:254–259
10. Young C, Truman P (2012) Proteins isolated with TRIzol are compatible with two-dimensional electrophoresis and mass spectrometry analyses. Anal Biochem 421:330–332
11. Nolan RL, Teller JK (2006) Diethylamine extraction of proteins and peptides isolated with a mono-phasic solution of phenol and guanidine isothiocyanate. J Biochem Biophys Methods 68:127–131
12. Man T-K, Li Y, Dang TA et al (2006) Optimising the use of TRIzol-extracted proteins in surface enhanced laser desorption/ionization (SELDI) analysis. Proteome Sci 4:3
13. Hummon AB, Lim SR, Difilippantonio MJ, Ried T (2007) Isolation and solubilization of proteins after TRIzol extraction of RNA and DNA from patient material following prolonged storage. Biotechniques 42:467–470, 472
14. Wessel D, Flügge UI (1984) A method for the quantitative recovery of protein in dilute solution in the presence of detergents and lipids. Anal Biochem 138:141–143
15. Chey S, Claus C, Liebert UG (2011) Improved method for simultaneous isolation of proteins and nucleic acids. Anal Biochem 411:164–166
16. Rundlett KL, Armstrong DW (1996) Mechanism of signal suppression by anionic

surfactants in capillary electrophoresis-electrospray ionization mass spectrometry. Anal Chem 68:3493–3497

17. Botelho D, Wall MJ, Vieira DB et al (2010) Top-down and bottom-up proteomics of SDS-containing solutions following mass-based separation. J Proteome Res 9:2863–2870
18. Proc JL, Kuzyk MA, Hardie DB et al (2010) A quantitative study of the effects of chaotropic agents, surfactants, and solvents on the digestion efficiency of human plasma proteins by trypsin. J Proteome Res 9:5422–5437
19. Wiśniewski JR, Zougman A, Nagaraj N, Mann M (2009) Universal sample preparation method for proteome analysis. Nat Methods 6:359–362
20. Antharavally BS, Mallia KA, Rosenblatt MM et al (2011) Efficient removal of detergents from proteins and peptides in a spin column format. Anal Biochem 416:39–44
21. Zhou J-Y, Dann GP, Shi T et al (2012) Simple sodium dodecyl sulfate-assisted sample preparation method for LC-MS-based proteomics applications. Anal Chem 84:2862–2867
22. Tanca A, Biosa G, Pagnozzi D et al (2013) Comparison of detergent-based sample preparation workflows for LTQ-Orbitrap analysis of the *Escherichia coli* proteome. Proteomics 13:2597–2607
23. León IR, Schwämmle V, Jensen ON, Sprenger RR (2013) Quantitative assessment of in-solution digestion efficiency identifies optimal protocols for unbiased protein analysis. Mol Cell Proteomics 12:2992–3005
24. Manza LL, Stamer SL, Ham A-JL et al (2005) Sample preparation and digestion for proteomic analyses using spin filters. Proteomics 5:1742–1745
25. Sieuwerts AM, Meijer-van Gelder ME, Timmermans M et al (2005) How ADAM-9 and ADAM-11 differentially from estrogen receptor predict response to tamoxifen treatment in patients with recurrent breast cancer: a retrospective study. Clin Cancer Res 11: 7311–7321

Chapter 7

Antibody-Based Capture of Target Peptides in Multiple Reaction Monitoring Experiments

Tommaso De Marchi, Eric Kuhn, Steven A. Carr, and Arzu Umar

Abstract

Targeted quantitative mass spectrometry of immunoaffinity-enriched peptides, termed immuno-multiple reaction monitoring (iMRM), is a powerful method for determining the relative abundance of proteins in complex mixtures, like plasma or whole tissue. This technique combines 1,000-fold enrichment potential of antibodies for target peptides with the selectivity of multiple reaction monitoring mass spectrometry (MRM-MS). Using heavy isotope-labeled peptide counterparts as internal standards ensures high levels of precision. Further, LC-MRM-MS selectivity allows for multiplexing; antibodies recognizing different peptides can be added directly to a single mixture without subjecting to interferences common to other multiple antibody protein assays. Integrated extracted ion chromatograms (XIC) of product ions from endogenous unlabeled "light" peptide and stable isotope-labeled internal standard "heavy" peptides are used to generate a light/heavy peak area ratio. This ratio is proportional to the amount of peptide in the digestion mixture and can be used to estimate the concentration of protein in the sample.

Key words Targeted mass spectrometry, MRM-MS, Protein quantification, Proteomics, Immunoaffinity enrichment

1 Introduction

Targeted mass spectrometry (MS) has made rapid advancements during the last decade and has begun to demonstrate the sensitivity and selectivity of highly developed immunoassays. These advancements make it possible to simultaneously measure concentration of 10s of proteins or more in a single biological sample (e.g., body fluid, tissue lysate) reproducibly [1–3]. Using a scan type called multiple reaction monitoring (MRM) (also referred to as selected reaction monitoring (SRM)) on a triple-quadrupole mass spectrometer (QqQ), mixtures of digested peptides derived from biological samples separated by nanoflow reversed-phase liquid chromatography (nano-RPLC) are detected and analyzed. Eluted peptides are ionized from liquid to the gas phase by a combination of applied voltage (typically 2,000 V in nanospray) and drying

Maria del Mar Vivanco (ed.), *Mammary Stem Cells: Methods and Protocols*, Methods in Molecular Biology, vol. 1293,
DOI 10.1007/978-1-4939-2519-3_7,

gases (N_2). Electrospray ionization generates gas-phase ions that are introduced into the mass spectrometer. In the first quadrupole (Q1) target ions are filtered and accelerated toward quadrupole two (Q2) which is set to a higher pressure and acts as a collision cell. Peptides are fragmented in Q2 by collision-induced dissociation (CID) and accelerated toward quadrupole three (Q3) which scans for the predetermined corresponding product ions. This transition ion, a Q3 detected mass of a peptide fragment that corresponds to a selected mass of a peptide precursor, is acquired in approximately 10 ms. Depending on the number of transition ions in a method and the chromatographic peak width, between 6 and 20 scans are collected for each transition. To confirm identification, typically 3–5 transition ions are monitored per peptide. To increase precision of quantification, stable isotope-labeled peptides, peptides containing an amino acid or acids with ^{13}C or ^{15}N (^{2}H is not preferred as chromatographic retention time is affected), can be synthesized and added to the mixture prior to nano-RPLC-MRM-MS analysis. This method, termed stable isotope dilution mass spectrometry (SID-MS), can account for variability in chromatographic retention time and ionization, which can be affected by variable amounts of background (peptidic and otherwise) in a mixture from run to run and sample to sample [4–8].

To determine the assay performance of each peptide, serial dilutions of concentration standard peptides are added to a background mixture of peptides prepared to mimic the expected matrix of the patient or study-derived sample. So-called reverse curves are curves comprising a variable concentration of stable isotope standard peptide and a fixed or singular concentration of corresponding unlabeled peptide is prepared to determine the lower limit of quantitation (LLOQ) and limit of detection (LOD) [9, 10]. This configuration, while generating measurements with a peak area ratio inverse to that of the intended "forward" measurement, reduces the interference that endogenous peptide can introduce. Depending on the analytes selected for MRM, background matrix of cell lysates or plasma may contain sufficient quantity of endogenous peptide to interfere with the determination of lower limits for the assay.

LC-MRM-MS-based techniques have proven useful for determining the relative amounts of proteins in a complex sample [1], but the sensitivity for analyte peptides present in lower abundance is also affected by high amounts of the background proteome derived from a complex sample. Therefore enrichment of target analytes is necessary to determine quantities of peptides present at lower concentrations (e.g., <1 μg/mL in plasma) [5, 8, 9]. Immunoaffinity enrichment of proteins from cell lysates, for example, is a well-established method for extracting the protein out of the mixture [11]. Recently, this methodology has been applied to the peptide-level enrichment using antibodies generated against

the analyte peptides from proteins of interest directly without a pre-enrichment step such as fractionation or depletion [12]. Anderson et al. were the first to describe the use of this approach coupled with SID-MRM-MS, and called it stable isotope standards and capture by anti-peptide antibodies (SISCAPA, [12]). Here we refer to the method by the more generic name of immunoMRM or iMRM. The antibodies used for peptide immunoaffinity enrichment are typically polyclonal [2, 3, 12, 13] but can also be generated as monoclonals [14]. Polyclonal antibodies are purified by peptide affinity chromatography from anti-sera generated by immunizing rabbits with KLH-conjugated peptides unique for a target protein that have been selected from MRM public repositories (e.g., SRM atlas, GPM) [15]. The most reliable method to obtain a peptide list to quantitate proteins in biological samples is to generate an in silico library from previous MS experiments using software packages such as Skyline [16]. Skyline is frequently used to generate a peptide library which can be derived from spectra that have been searched using Mascot [17] or Spectrum Mill (Agilent Technologies Inc., Santa Clara, CA). Peptide ion intensities can also be ranked in silico using the ESP algorithm [18]. Further selection of peptides with fragment ions best suited for MRM-MS can be made by matching the in silico digest of a target protein with previously generated MS/MS spectra. Generating an antibody of sufficient titer and affinity is also dependent on amino acid sequence of the peptide. Algorithms for determining the hydrophilicity of a section of peptide sequence within the context of the full-length protein sequence exist; however, specialized algorithms to rank the immunogenicity of single peptides are not currently available. To increase the success rate of antibody generation, rabbits are immunized in pairs with three to five peptides per protein [13]. To evaluate antibody affinity, stable isotope-labeled counterparts for peptides against which an antibody was generated are synthesized and purified from commercial sources (New England Peptide, Thermo, 21st Century Biochemicals). Antibody performance is then assessed by capture efficiency (percent of available peptide in a mixture) and LOD (from calibration curves). Immunoaffinity enrichment combined with high-sensitivity MRM-MS makes iMRM particularly well suited for quantifying analyte peptides (surrogates for relative abundance of protein) in complex samples, such as plasma, tissues, or cell lysates. Due to the selective properties of MRM-MS, antibodies can be used individually or within a multiplex without diminishing their performance [2, 19]. Linking antibodies onto protein G magnetic beads makes the assay more amenable to robotic automation and the potential to increase throughput and robustness. We herein describe a method for relative precise quantification of analyte peptides from breast cancer whole-tissue lysate samples through iMRM-MS (Fig. 1).

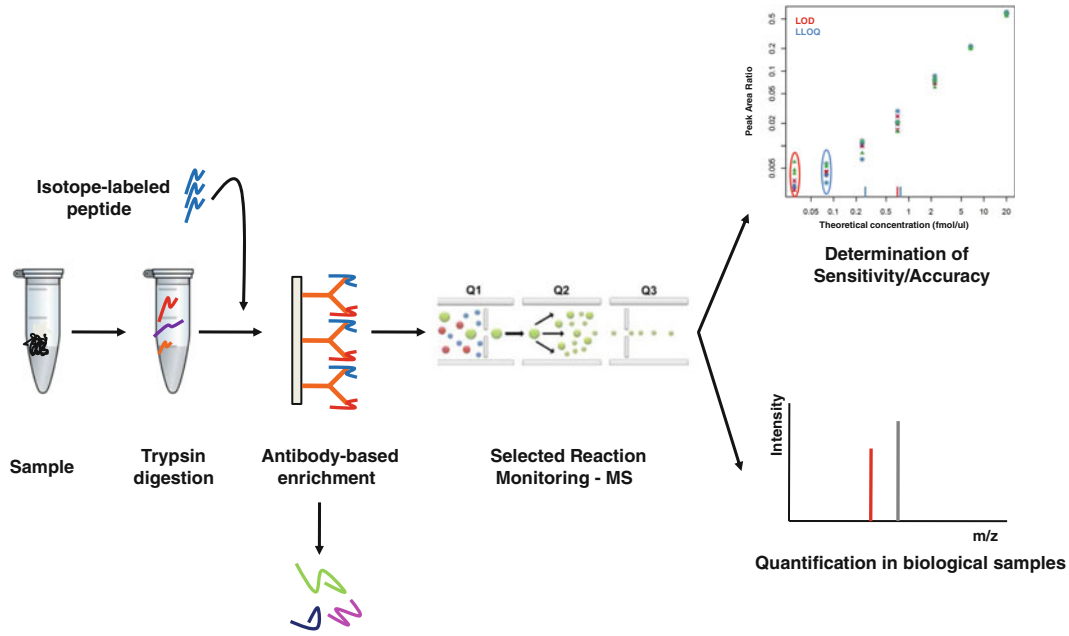

Fig. 1 Outline of an immuno-MRM experiment. Once target peptides have been selected, they are captured along with a known amount of their isotope-labeled counterpart through anti-peptide antibodies. Heavy and endogenous peptides are eluted and analyzed on a triple-quadrupole mass spectrometer in MRM mode. Capturing a fixed amount of endogenous peptide with decreasing concentrations of its isotope-labeled version enables determination of the limit of detection (LOD) and lower limit of quantitation (LLOQ) of the method. Quantification of target peptide/protein in biological samples is derived from peak area ratio (PAR) determination between endogenous peptide level and its heavy counterpart

2 Materials

2.1 Selection of Target Peptides

1. From either previous tandem MS experiments or public repositories select a minimum of two unique tryptic peptides per target protein (*see* **Note 1**).

2.2 Peptides and Antibody Buffers

1. Antibody wash solution 1: 1× PBS (137 mM NaCl, 2.7 mM KCl, 10 mM Na_2HPO_4-$2H_2O$, 2 mM KH_2PO_4)—0.03 % w/v CHAPS. Dissolve 300 mg of CHAPS in 1 L of 1× PBS.
2. Antibody wash solution 2: 0.1× PBS—0.03 % w/v CHAPS. Dilute 1× PBS 1:10 in HPLC-grade water and dissolve 300 mg of CHAPS in 1 L of 0.1× PBS.
3. Stable isotope-labeled (heavy) peptide high-concentration diluent: 30 % v/v ACN/0.1 % v/v FA. Dissolve 300 mL acetonitrile (ACN) and 10 mL formic acid (FA) in 1 L HPLC-grade water.

4. Stable isotope-labeled (heavy) peptide low-concentration diluent—MS blank buffer—Antibody elution buffer: 3 % v/v ACN/5 % v/v acetic acid (AcOH). Dissolve 30 mL ACN and 50 mL AcOH in 1 L HPLC-grade water (*see* **Note 2**).

2.3 Heavy Peptide Standard Stock Solutions and Mixtures

1. Heavy peptide high-concentration stocks: Prepare serial dilutions of heavy peptide stocks to a final concentration of 100 pmol/μL using 30 % ACN/0.1 % FA as diluent.
2. Combine equivalent volumes of heavy peptide high-concentration stocks in one tube. Do not dilute. Concentration depends on the number of peptides in the final mixture.
3. Heavy peptide low-concentration mixtures: Dilute the high-concentration stocks such that the final concentration is 100 fmol/μL; use 3 % ACN/5 % AcOH as diluent (*see* **Note 3**).

2.4 Anti-peptide Antibody Master-Mix Solutions

1. Antibody high-concentration mixture: Combine equivalent amounts of antibody stock solutions to a final concentration of 20 μg/mL for each antibody is. Use PBS 0.03 % CHAPS as diluent (*see* **Note 4**).
2. Antibody titration solutions: Prepare a serial dilution from the high-concentration antibody mixture into 1× PBS 0.03 % CHAPS to generate a series of final concentrations for each antibody per capture of 4, 2, 1, 0.5, 0.25, and 0.125 μg per 50 μL (*see* **Note 5**).

2.5 Cross-Linking Solutions

1. Cross-linking solution: 200 mM Triethanolamine (TEA) pH 8.5. Dissolve 10 mL of neat triethanolamine into 400 mL HPLC-grade water; adjust pH with 5 M HCl (*see* **Note 6**).
2. Cross-linking solution: 20 mM Dimethyl pimelimidate (DMP) in 200 mM TEA. Dissolve 1.03 g of DMP in 200 mL of 200 mM TEA.
3. Cross-linking quenching solution: 150 mM Monoethanolamine (MEA) pH 9.0: dissolve 3.15 mL of pure monoethanolamine in 400 mL HPLC-grade water; adjust pH with 5 M HCl.
4. Cross-linking washing solution: 5 % v/v AcOH/0.03 % w/v CHAPS: Dissolve 50 mL acetic acid and 30 mg of CHAPS in 1 L HPLC-grade water.
5. Resuspension buffer: 1× PBS/0.03 % w/v CHAPS/0.1 % w/v NaN_3. Dissolve 30 mg CHAPS and 1 g of NaN_3 in 1 L PBS (*see* **Note 7**).
6. Magnetic rack and KingFisher Flex Magnetic Particle Processor (Thermo Scientific, Rockford, IL USA).
7. MyOne Protein G 1 μm magnetic beads (Dynal/Invitrogen/Life Technologies/Thermo).

3 Methods

3.1 Antibody Cross-Linking Using KingFisher (Optional) (*See* Note 8)

1. Add volumes of protein G (ProG) magnetic beads into antibody mixes to a final bead:antibody ratio of 2:1 (μL to μg). Tumble mix solutions overnight at 4 °C (*see* **Note 9**).
2. Add 900 μL/well of cross-linking solution onto a 1 mL KingFisher plate (*see* **Note 10**).
3. Set KingFisher method as follows:
   - Plate 1: Antibody-bead solutions.
   - Plate 2: Cross-linking solution (900 μL/well), rinse 30′.
   - Plate 3: Cross-linking quenching solution (900 μL 150 mM MEA), rinse 30′.
   - Plate 4: Cross-linking washing solution (900 μL 5 % AcOH/0.03 % CHAPS), rinse 5′.
   - Plate 5: Cross-linking washing solution (900 μL 5 % AcOH/0.03 % CHAPS), rinse 5′.
   - Plate 6: PBS washing solution (900 μL PBS 0.03 % CHAPS), rinse 5′.
   - Plate 7: Resuspension buffer (900 μL PBS/0.03 % CHAPS/0.1 % NaN_3), rinse 5′.
   - Plate 8: Magnetic tip cover plate.
   - Note: Make sure that the volumes in the wells on plates 2–7 match the location of the volumes in the wells of plate 1.

3.2 Antibody Capture Efficiency Evaluation

1. Prepare a 1× PBS-0.03 % CHAPS stock solution. Resuspend the amount of digested lyophilized protein to target concentration per capture well as desired (e.g., cell lysates 100–500 μg/200 μL, plasma 10 μL equivalent = 600 μg/200 μL) in 1× PBS-0.03 % CHAPS-0.5 fmol/μL heavy mix (*see* **Note 11**).
2. Add 100 fmol heavy peptide (e.g., to final concentration of 0.5 fmol/μL for 200 μL). Transfer 200 μL of reconstituted background or sample in each well of a KingFisher 250 96-well plate. Add 50 μL of antibody mix to each well. Seal plate with aluminum adhesive foil and tumble mix plate overnight at 4 °C.
3. Set KingFisher magnetic particle processor method as follows:
   - Plate 1: Antibody capture plate.
   - Plate 2: Washing (250 μL/well), 1.5′ rinse.
   - Plate 3: Washing (250 μL 1× PBS/0.03 % CHAPS), 1.5′ rinse.
   - Plate 4: Washing (250 μL 0.1× PBS/0.03 % CHAPS), 1.5′ rinse.

- Plate 5: Elution (25 μL 3 % ACN/5 % AcOH), 5′ rinse (*see* **Note 12**).
- Plate 6: Bead collection (200 μL 1× PBS/0.03 % CHAPS/0.1 %NaN_3), 5′ rinse.
- Plate 7: Magnetic tip comb.
- NB: Make sure that the volumes in the wells on plates 2–6 match the location of the volumes in the wells of plate 1. Elution plate 5 solutions should be placed in a 96-well PCR plate.

4. Once KingFisher method has completed, remove elution plate 5 and place on a magnetic plate holder on wet ice (*see* **Note 13**).
5. Place a fresh 96-well PCR plate on wet ice and add 5 μL of 3 % ACN/5 % AcOH per well.
6. Using a multichannel pipet, transfer 25 μL of the supernatant from elution plate 5 into the fresh PCR plate.
7. Centrifuge plate briefly (30 s) to eliminate air bubbles and place plate onto autosampler for analysis on TQMS.
8. Analyze by MRM for preselected optimized transitions for light and heavy peptide masses by nano-RPLC-MRM-MS.
9. Export results file to Skyline to integrate data. Select optimal capture concentrations per each antibody (i.e., maximum heavy peptide signal, least noise).

3.3 Evaluation of Passenger Peptide

1. Prepare three replicates of antibody capture at a fixed antibody mix concentration. Add equivalent amounts of heavy peptide mix per each replicate capture. Depending on the type of background matrix prepared (digested cell lysate, tissue, or plasma) add 1:200 to 1:500 diluted background per each replicate capture (*see* **Note 11**).
2. Perform overnight capture and peptide elution as in **step 3**, Subheading 3.2.
3. Analyze on a triple-quadrupole MS instrument configured with nanoflow liquid chromatograph and autosampler.
4. Export results in Skyline and evaluate the presence of light peptide in captures with undiluted vs. diluted background.

3.4 Generation of Reverse Curve (Fig. 2)

1. Prepare serial dilutions of heavy peptide mixtures for a 7- or 8-point curve with concentrations from 0.3 to 200 fmol in 200 μL volume of 1× PBS/0.03 % CHAPS/100–500 μg background digested protein per capture. Include a comparable solution without heavy peptide. Mixtures may be made in bulk for total number of replicates (e.g., 600 μL for 3 replicates).
2. Transfer 200 μL into wells on a KingFisher 250-well plate.

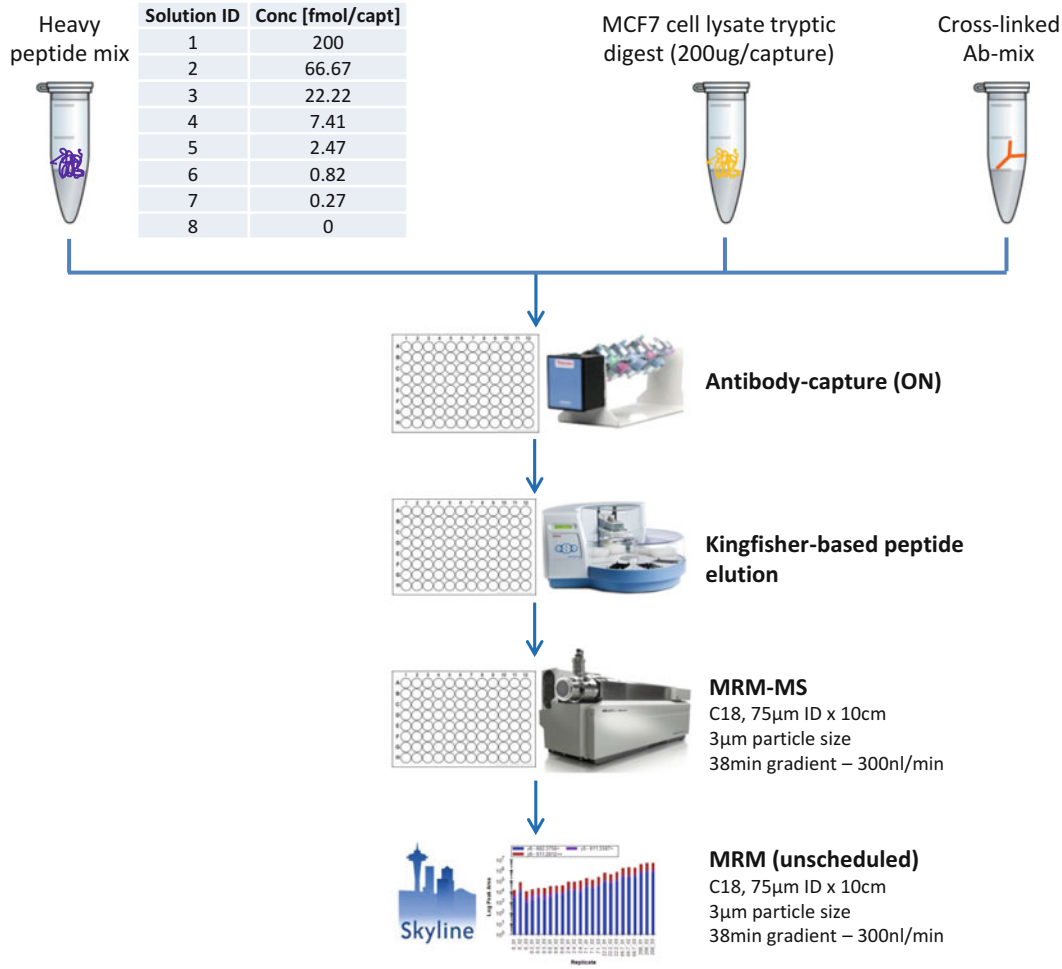

Fig. 2 Figure represents typical reverse curve experiment for determination of LOD/LLOQ of an iMRM assay. Heavy peptides are captured at different concentrations by antibodies in the presence of digested protein background (plasma or digested cell line proteins). Peptides are immunoaffinity enriched by tumble mixing 96-well plates overnight at 4 °C. Plates are transferred to the KingFisher magnetic particle handler the next day and peptides are eluted from the beads. MRM-MS is performed after transfer of captured peptides onto a new plate and results are imported and analyzed in Skyline

3. Based on capture efficiency data (*see* Subheading 3.2) prepare the antibody mix (cross-linked or non-cross-linked as desired) and add 50 µL of antibody mix to each well.
4. Cover with aluminum adhesive foil and tumble mix overnight at 4 °C.
5. Set KingFisher magnetic particle processor method as follows:
   - Plate 1: Antibody capture plate.
   - Plate 2: Washing (250 µL/well), 1.5′ rinse.

- Plate 3: Washing (250 μL 1× PBS/0.03 % CHAPS), 1.5′ rinse.
- Plate 4: Washing (250 μL 0.1× PBS/0.03 % CHAPS), 1.5′ rinse.
- Plate 5: Elution (25 μL 3 % ACN/5 % AcOH), 5′ rinse (*see* **Note 12**).
- Plate 6: Bead collection (200 μL 1× PBS/0.03 % CHAPS/0.1% NaN_3), 5′ rinse.
- Plate 7: Magnetic tip comb.
- NB: Make sure that the volumes in the wells on plates 2–6 match the location of the volumes in the wells of plate 1. Elution plate 5 solutions should be placed in a 96-well PCR plate.

6. Analyze on a triple-quadrupole MS instrument configured with nanoflow liquid chromatograph and autosampler.
7. Import results in a Skyline version containing QuaSAR (*see* **Note 14**). In the Result Grid tab fill in "SampleGroup" and "Concentration," which refer, respectively, to the sample replicate ID and to the concentration of the analyte. The "IS spike" file refers to the concentration of light peptide present in each capture. If a light version of each peptide is used then fill light peptide concentration in "IS spike," while fill in "1" if light peptide is not detected or not being used (area-only curve, not based on peak area ratio) (https://skyline.gs.washington.edu/labkey/announcements/home/software/Skyline/tools/thread.view?rowId=5436). QuaSAR analysis refers to an experiment in which only heavy peptides are used.
8. Perform a QuaSAR analysis, setting "Analyte" and "Standard" fields as heavy area and light area, respectively. Un-tick "Standard present" option if not using light peptides. Tick all options in the "Generate" submenu. LOD and LOQ of the method will be generated.
9. Export linear and log plots of concentration curves, tables of LOD and LOQ, and plots of CVs for all peptides in the group.

4 Notes

1. Target peptides to be analyzed in an iMRM experiment should be derived from trypsin digestion without missed cleavages, be unique to target protein, and not contain cysteine or methionine residues. Sequences containing serial arginine (R) or lysine (K) residues (e.g., RR or KK) would be cleaved randomly at one of the basic residues and the whole peptide would change in mass, making its detection and quantification problematic.

Nonunique peptides would make the quantitation less accurate, since their intensities would derive from different proteins, while sulfur-containing amino acids are targets for covalent modifications that could change the total molecular weight of the peptide. Therefore it is advised to select sequences, in which these are absent.

2. An aqueous solution containing a low percentage of organic solvent and a small percentage of acid is well suited to be used as a blank in MS experiments. Running blank solutions before and after each sample (duplicate/triplicate) would assess the presence of carryover but would not solve it. A sawtooth gradient with multiple ramps of high organic solvent concentration is advised to remove/minimize any carryover. Antibody affinity is optimal at neutral pH, based on a combination of noncovalent interactions. These interactions are removed or inhibited under acidic conditions ($pH < 2.5$) and the bound peptide is released from the antibody. A small amount of organic solvent (3 % ACN) aids in peptide solubility in the absence of matrix and antibody.
3. Preparation and dilution of heavy peptide mixtures reduce the need for potential additional freeze-thaw cycles of original stocks, thereby reducing the possibility of degradation of peptides. With these solutions it is possible to evaluate the capture efficiency of the anti-peptide antibodies, comparing a captured heavy peptide with its spiked-in counterpart.
4. CHAPS is a non-denaturing, nonionic detergent which makes it more amenable to downstream mass spectrometry. It is added primarily to keep magnetic beads from settling on the KingFisher magnetic bead handler. It also helps re-solubilize protein digests prepared under denaturing conditions (e.g., urea). Other detergents may be used to solubilize proteins prior to digestion, but additional detergent removal steps may be necessary to avoid irreversible binding onto C18 packing material as well as contaminating the mass spectrometer.
5. Typical concentration range for antibodies in immunopurification experiments varies between 0.5 and 2.0 μg per capture for polyclonal antibodies (lower for monoclonals), but in order to determine the optimal concentration for each antibody, a titration curve above and below that range should be prepared. Seven concentration levels from to 0.125 to 4 μg were chosen, but further considerations at the extremes are advised. To maintain antibody concentration at the low end (0.125 μg), use immediately after preparing dilution series and do not store for long periods of time. At the high end, depending on the number of antibodies in the multiplex, significant amounts of magnetic beads may be needed which could be nonspecifically lost during wash and elution steps on KingFisher.

The target volume for each capture is typically 250 μL per well—which consists of 200 μL 1× PBS, 0.03 % CHAPS, 2 μL 100 fmol/μL heavy mix, and 50 μL of antibody mix. Try not to exceed 300 μL per well in the KingFisher 96-well plates.

6. TEA is viscous and care should be used to accurately pipet volumes ensuring that mixing is complete once added to HPLC-grade water. Prepare DMP fresh and use immediately. pH of TEA and MEA solutions is critical (8.5 and 9.0, respectively). Use a pH meter when adjusting pH by addition of 5 M HCl.
7. Sodium azide (NaN_3) is a preservative and a bacteriostatic agent. Resuspending cross-linked antibody beads into a NaN_3-containing solution allows storage at 4 °C for several months or longer.
8. Protein G is the recommended ligand for binding antibodies derived from rabbit. It is a bacterial derived protein that binds the Fc of antibodies leaving the variable regions accessible to bind and release peptide epitopes. It is commercially available conjugated to agarose (Agarose Bead; ABT Technologies, Tampa, FL, USA), sepharose (Sepharose 4B®; Sigma-Aldrich Corporation, St. Louis, MO, USA), POROS (POROS®; Life Technologies, Foster City, CA, USA), and magnetic beads (Dynabeads®, Life Technologies, Foster City, CA, USA). Each bead has a different size. Magnetic beads were chosen to make the process more amenable to automation. Smaller bead sizes yield more surface area per volume of bead. In addition to analyte peptides, intact IgG will also elute from protein G under acidic conditions which can overload and foul the LC column used in nanoflow conditions (1 μg total capacity). Therefore, it is recommended to cross-link antibodies with DMP (in addition to the benefit of removing passenger peptides (*see* Subheading 3.3)) to reduce nonspecific background for reducing the overall signal in the mass spectrometer.
9. Optimal ratio of antibody to magnetic bead ranges from 1:1 to 1:10 (according to the manufacturer's specifications) depending on the antibody. Cross-linking after capture at different ratios to determine the optimal one is advised.
10. The maximum volume per well in a deep well plate (max volume 2 mL/well) is limited on the KingFisher to 0.9 mL. Volumes above 0.9 mL will exceed the capacity of the well with the magnetic head and tip comb inserted during mixing and transfer of magnetic beads. For these cases, use a magnet to readjust the final volume below 0.9 mL prior to cross-linking on KingFisher.
11. The choice of background material depends on the nature of the samples that have to be analyzed, while the amount to be added to each capture has to be determined experimentally.

The aforementioned capture was performed adding 500 μg of digested proteins from MCF7 breast cancer cell line to each capture. Generating a reverse curve in the presence of a background that best simulates the biological sample matrix and complexity will help determine the most representative LOD and LLOQ for the samples being analyzed. Each capture should be performed at least in triplicate. The concentration of nonspecific background peptides is proportional to the amount of antibodies used in each capture. These levels may vary intentionally (as in the titration experiment) or systematically (between a mock sample background and the real samples themselves). To minimize these effects on the analytical process, it is advised to cross-link antibodies onto magnetic beads.

12. Elution into small volumes (less than 50 μL) into the 250 KingFisher plates is not advised, Therefore elution plate 5 is a 150 μL 96-well PCR plate to increase the recovery from magnetic beads.
13. Small amounts of magnetic beads may elute with the captured peptides. A magnetic plate holder would allow transferring the supernatants from the PCR elution plate onto a fresh plate without transferring the beads as well. Putting the plate on ice decreases evaporation of organic solvents and preserves captured peptides during handling.
14. QuaSAR is a Skyline add-on which can be downloaded at https://brendanx-uw1.gs.washington.edu/labkey/announcements/home/software/Skyline/tools/thread.view?rowId=5436. And may not be available directly through Skyline without add-on.

Acknowledgements

This work was partially financed through the Center for Translational Molecular Medicine, Breast CARE project (030-104-06).

References

1. Addona T, Abbatiello SE, Schilling B, Skates SJ, Mani DR, Bunk DM, Spiegelman CH, Zimmerman LJ, Ham A-JL, Keshishian H, Hall SC, Allen S, Blackman RK, Borchers C, Buck CB, Cardasis HL, Cusack MP, Dodder NG, Gibson BW, Held JM, Hiltke T, Jackson A, Johansen EB, Kinsinger CR, Li J, Mesri M, Neubert TA, Niles RK, Pulsipher TC, Ransohoff D, Rodriguez H, Rudnick PA, Smith D, Tabb DL, Tegeler TJ, Variyath AM, Vega-Montoto LJ, Walhander A, Waldemarson S, Wang M, Whiteaker JR, Zhao L, Anderson NL, Fisher SJ, Liebler DC, Paulovich AG, Regnier FE, Tempst P, Carr SA (2009) Multi-site assessment of the precision and reproducibility of multiple reaction monitoring-based measurements of proteins in plasma. Nat Biotechnol 27:633–641
2. Kuhn E, Addona T, Keshishian H, Burgess M, Mani DR, Lee RT, Sabatine MS, Gerszten RE, Carr SA (2009) Developing multiplexed assays for troponin I and interleukin 33 in plasma by peptide immunoaffinity enrichment and targeted mass spectrometry. Clin Chem 55:1108–1117

3. Kuhn E, Whiteaker JR, Mani DR, Jackson A, Zhao L, Pope ME, Smith D, Rivera KD, Anderson L, Skates SJ, Pearson TW, Paulovich AG, Carr SA (2012) Interlaboratory evaluation of automated multiplexed peptide immunoaffinity enrichment coupled to multiple reaction monitoring mass spectrometry for quantifying proteins in plasma. Mol Cell Proteomics 11:1–14
4. Ossola R, Schiess R, Picotti P, Rinner O, Reiter L, Aebersold R (2011) Biomarker validation in blood specimens by selected reaction monitoring mass spectrometry of N-glycosites. Methods Mol Biol 728:179–194
5. Picotti P, Aebersold R (2012) Selected reaction monitoring-based proteomics: workflows, potential, pitfalls and future directions. Nat Methods 9:555–566
6. Liebler DC, Zimmermann LJ (2013) Targeted quantitation of proteins by mass spectrometry. Biochemistry 52:3797–3806
7. Ebhardt HA (2014) Selected reaction monitoring mass spectrometry: a methodology overview. Methods Mol Biol 1072:209–222
8. Keshishian H, Addona T, Burgess M, Kuhn E, Carr SA (2007) Quantitative, multiplexed assays for low abundance proteins in plasma by targeted mass spectrometry and stable isotope dilution. Mol Cell Proteomics 12: 2212–2229
9. Keshishian H, Addona T, Burgess M, Mani DR, Shi X, Kuhn E, Sabatine MS, Gerszten RE, Carr SA (2009) Quantification of cardiovascular biomarkers in patient plasma by targeted mass spectrometry and stable isotope dilution. Mol Cell Proteomics 10:2339–2349
10. Mani DR, Abbatiello SE, Carr SA (2012) Statistical characterization of multiple-reaction monitoring mass spectrometry (MRM-MS) assays for quantitative proteomics. BMC Bioinformatics 13:S9
11. Harlow E, Lane D (1999) Using antibodies: a laboratory manual. Cold Spring Harbor Laboratory Press, Cold Spring Harbor, NY, pp 321–325
12. Anderson NL, Anderson NG, Haines LR, Hardie DB, Olafson RW, Pearson TW (2004) Mass spectrometric quantitation of peptides and proteins using Stable Isotope Standards and Capture by Anti-Peptide Antibodies (SISCAPA). J Proteome Res 3:235–244
13. Whiteaker JR, Zhao L, Abbatiello SE, Burgess M, Kuhn E, Lim CW, Pope ME, Razavi M, Anderson NL, Pearson TW, Carr SA, Paulovich AJ (2011) Evaluation of large scale quantitative proteomics assay development using peptide affinity-based mass spectrometry. Mol Cell Proteomics 10:1–10
14. Schoenherr RM, Zhao L, Whiteaker JR, Feng L-C, Li L, Liu L, Liu X, Paulovich AG (2010) Automated screening of monoclonal antibodies for SISCAPA assays using a magnetic bead processor and liquid chromatography-selected reaction monitoring-mass spectrometry. J Immunol Methods 353(1–2):49–61
15. Deutsch EW, Lam H, Aebersold R (2008) PeptideAtlas: a resource for target selection for emerging targeted proteomics workflows. EMBO Rep 9:429–434
16. MacLean B, Tomazela DM, Shulman N, Chambers M, Gl F, Frewen B, Kern R, Tabb DL, Liebler DC, MacCoss MJ (2010) Skyline: an open source document editor for creating and analyzing targeted proteomics experiments. Bioinformatics 26:966–968
17. Perkins DN, Pappin DJ, Creasy DM, Cottrell JS (1999) Probability-based protein identification by searching sequence databases using mass spectrometry data. Electrophoresis 20:3551–3567
18. Fusaro VA, Mani DR, Mesirov JP, Carr SA (2009) Computational prediction of high responding peptides for development of targeted protein assays by mass spectrometry. Nat Biotechnol 27(2):190–198
19. Whiteaker JR, Zhao L, Lin C, Yan P, Wang P, Paulovich AG (2012) Sequential multiplexed analyte quantification using peptide immunoaffinity enrichment coupled to mass spectrometry. Mol Cell Proteomics. doi:10.1074/mcp.M111.015347

Chapter 8

Lentiviral Transduction of Mammary Epithelial Cells

Richard Iggo and Elodie Richard

Abstract

Lentiviral vectors are the workhorses of modern cell biology. They can infect a wide variety of cells including nondividing cells and stem cells. They integrate into the genome of infected cells leading to stable expression. It is easy to transduce 100 % of the cells in a culture and possible to infect cells simultaneously with multiple vectors, greatly facilitating studies on malignant transformation. We present simple protocols to produce and titrate lentiviral vectors, infect mammary epithelial cells, and check for contamination with replication-competent viruses.

Key words Lentivirus, Transfection, Infection

1 Introduction

Lentiviral vectors are convenient tools to express transgenes in a wide variety of cultured cells. At first glance it might seem somewhat risky to use vectors derived from HIV as basic research tools, but the labs that conceived them were aware of the risks and went to great lengths to make them safe [1–4]. Additional information on safety is given in **Notes 1** and **2**. Minimally, you should familiarize yourself with level 2 biosafety precautions and make the requisite declarations to the authorities before starting to work with lentiviral vectors.

Unlike transgenes in transfected DNA, transgenes in lentiviral vectors are immediately integrated stably into the genome of the target cell, greatly increasing the chance that they will be expressed stably. Unlike simple oncoretroviral or gamma retroviral vectors, lentiviral vectors can infect nondividing cells. The critical difference is that the cDNA produced by reverse transcription of lentiviral RNA is professionally imported into the nucleus, whereas cDNA from simple retroviruses must wait for the nuclear envelope to break down at mitosis to gain access to the chromosomes. This simplifies the protocol because it is not necessary to passage the target cells immediately after infection to make them divide.

Maria del Mar Vivanco (ed.), *Mammary Stem Cells: Methods and Protocols*, Methods in Molecular Biology, vol. 1293,
DOI 10.1007/978-1-4939-2519-3_8,

A second advantage is that titers tend to be higher and virus can be frozen with minimal loss of titer. The vectors are normally pseudotyped with vesicular stomatitis glycoprotein (VSV G), which broadens the tropism because it works by inducing fusion with the plasma membrane. This works well for mammary epithelial cells, which are normally easy to infect with VSV G pseudotyped lentiviral vectors.

2 Overall Strategy

The basic approach to make lentiviral vectors is to transfect 293T cells with a vector plasmid and two or three helper plasmids. The protocol below uses calcium phosphate transfection because it is cheap and highly effective in 293T cells. The transfection efficiency should be close to 100 %; if you find it difficult to achieve this, try commercial transfection reagents instead, such as Fugene (Promega).

3 Packaging Vectors

Most labs use so-called second-generation plasmids, in which one helper plasmid contains all the lentiviral helper genes and a second helper plasmid contains VSV G. Other than tat and rev, the lentiviral accessory genes (vif, vpr, vpu, and nef) are all deleted from the helper plasmids. In third-generation systems the lentiviral genes are split between two plasmids, with the gag, polymerase, protease, and integrase genes on one plasmid and rev on another. In this configuration the tat gene is deleted, which means the vector plasmid requires a tat-independent promoter. A plasmid expressing VSV G is still required, meaning a total of four plasmids must be transfected. The third-generation system is considered safer but the need to transfect an additional plasmid may reduce the titer. In practice, most users choose the second-generation psPAX2 and pMD2.G packaging vectors developed by the Naldini and Trono labs (Fig. 1a, b, Addgene 12259 and 12260).

4 Lentiviral Expression Vectors

There is a much wider choice of vector plasmids. In addition to deletion of all complete HIV genes, current vectors have partial replacement of the 5′-LTR by a heterologous promoter to make transcription in the packaging cell independent of tat; a deletion in the 3′-LTR to make both LTRs inactive as promoters after integration; and the presence of an RNase H-resistant central polypurine tract that primes reverse transcription and promotes nuclear import of

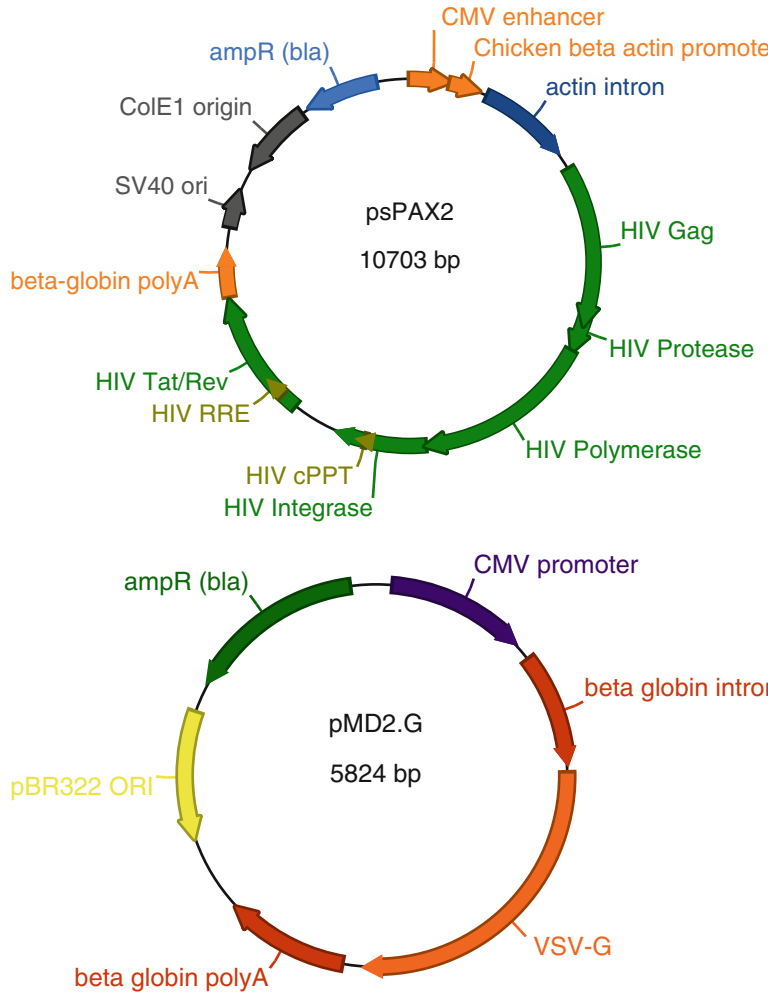

Fig. 1 Lentiviral plasmids. (**a**) psPAX2 contains the main lentiviral genes required for packaging: gag, protease, polymerase, integrase, tat, and rev. (**b**) pMD2.G expresses VSV glycoprotein, which replaces the normal envelope protein. VSV G fuses directly with the plasma membrane, allowing the viral particles to infect cells indiscriminately. (**c**) pSD-82 is a typical lentiviral expression vector. The genomic transcripts made in the packaging cells initiate at a hybrid RSV/HIV promoter. The RSV enhancer is deleted in integrated proviruses because the 3′-LTR is copied to the 5′-LTR during reverse transcription. There is a deletion removing the enhancer in the U3 region in the 3′-LTR. This deletion is copied to the 5′-LTR after reverse transcription to create integrated proviruses with defective promoters in both LTRs (a so-called self-inactivating or SIN vector). This means the first transcripts from the integrated proviruses initiate at the human PGK promoter. Since this is located after the packaging signal (psi), no transcripts from the integrated provirus can be packaged. The transgene, ESR1, is located between two Gateway attB sites and expressed from the human PGK promoter. The WPRE located after the attB2 site increases the level of the ESR1 RNA. The puromycin resistance gene is expressed from the murine PGK promoter. The viral RNAs all terminate in the 3′-LTR. It is important to delete polyA signals from the transgene to avoid cleaving the 3′-end off the genomic RNA that is packaged in the viral particles

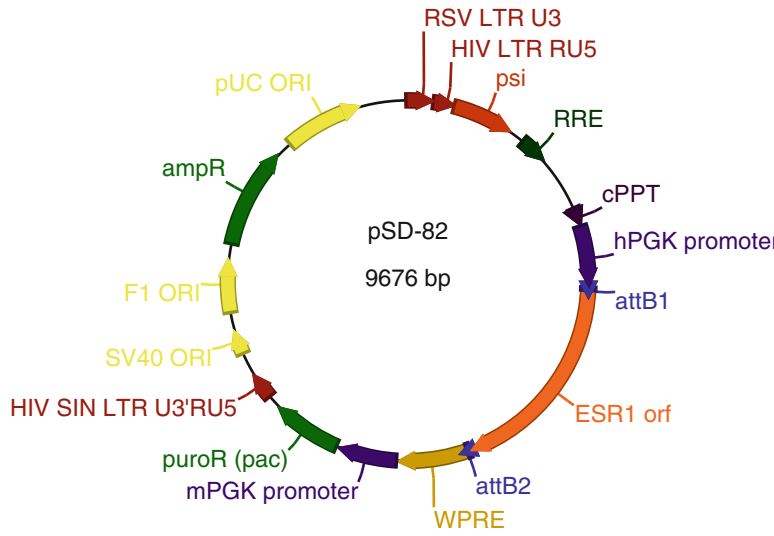

Fig. 1 (continued)

the preintegration complex. Many companies now sell lentiviral vectors but a cheap and convenient option for academic labs is to use vectors from Addgene. In addition to specific vectors that have been described in publications, Addgene contains an impressive collection of vectors deposited by Eric Campeau, many of which are based on the Gateway cloning system (http://www.addgene.org/Eric_Campeau/). The Campeau vectors systematically offer antibiotic resistance cassettes for puromycin, neomycin, hygromycin, blastomycin, and zeomycin, making it possible to select for multiple different vectors in the same cell. We have had difficulty selecting for hygromycin in primary mammary epithelial cells but the other markers all work well.

The choice of promoter is dictated by the propensity of some promoters to become silenced more easily than others (cellular promoters are often better than viral promoters), and by the characteristics of the cells transduced (PGK works well in mammary progenitors and stem cells). The vector we have used most extensively in mammary epithelial cells has a human PGK promoter driving the transgene and a mouse PGK promoter driving the puromycin resistance gene (*pac*) (Fig. 1c) [5]. Note that the vector contains a Woodchuck hepatitis virus RNA stability element (WPRE) between the two expression cassettes, so the WPRE is only present in the RNA produced by the promoter driving expression of the transgene. This is a good idea in the sense that it increases the chance of the transgene being expressed well, but careful titration of puromycin is required to avoid killing the cells if they are infected at single copy. Many of the Campeau vectors have the same promoters in the same configuration and express transgenes well in mammary epithelial cells.

5 Materials

5.1 Components for Lentiviral Production

293T/17 cells (ATCC CRL-11268).

Dulbecco's modified Eagle medium, 10 % FBS.

Phosphate-buffered saline.

0.05 % trypsin/EDTA.

TE buffer, pH 8.0.

DNase/RNase-free water.

Polylysine.

2.5 M $CaCl_2$, 18.4 g for 50 ml; filter sterilize (0.22 μm) and store aliquots at −20 °C.

2 M HEPES, 52.6 g for 100 ml; filter sterilize (0.22 μm) and store aliquots at −20 °C.

OptiMEM (Life Technologies); add 2 M HEPES to make OptiMEM 20 mM HEPES.

HEPES-buffered saline (2× HeBS, Sigma 51558—50 ml).

10 cm tissue culture dishes.

15 and 50 ml conical base tubes.

0.45 and 0.22 μm syringe filters.

Vivaspin 20 MWCO 100,000 (GE Healthcare #28-9323-63).

5 % CO_2, 37 °C incubator.

1 % Virkon (50 g sachets, Dupont).

70 % (v/v) ethanol.

Plasmids to make a simple GFP expression vector

pRRLSIN.cPPT.PGK-GFP.WPRE (classic GFP expression vector, Addgene 12252).

pMD2.G (for pseudotyping with VSV G protein, Addgene 12259).

psPAX2 (contains the main HIV-1 helper genes: Gag, Pol, Tat, and Rev, Addgene 12260).

Many other useful plasmids can be obtained from Addgene. *See* **Notes 3** and **4** for information on construction and production of plasmids. All plasmid maxipreps should be "endotoxin-free" (Qiagen EndoFree or Nucleobond Xtra EF). For convenience, adjust the concentration of plasmids to 1 mg/ml.

5.2 Components for Titration of Viruses

Target cells (e.g., MCF7 cells).

Cell culture medium (RPMI 10 % FCS for MCF7 cells).

Viral suspension.

Phosphate-buffered saline.

0.05 % trypsin/EDTA.

6-Well plates.

FACS tubes (polypropylene).

5 % CO_2, 37 °C incubator.

5.3 Components for Isolation of Mammary Epithelial Cells

Cold DMEM/F12, phenol red-free, 2× Pen/Strep = minimal medium (MM).

Phosphate-buffered saline.

Collagenase A: Make 100 mg/ml in PBS, and store aliquots at −20 °C.

Trypsin solution 0.25 %.

Dispase: Make 5 mg/ml in PBS, filter sterilize (0.22 μm), and store aliquots at −20 °C.

Deoxyribonuclease 1 (DNase): Make 1 mg/ml in PBS, filter sterilize (0.22 μm), and store aliquots at −20 °C.

Cell strainer 40 μm.

Sterile forceps.

Sterile scalpels.

Sterile chopping board.

10 cm cell culture dishes.

15 and 50 ml conical base tubes.

5.4 Components for Lentiviral Transduction of Mammary Cells

Single cells from reduction mammoplasty.

Cell culture medium (according to individual lab preference).

Viral stock.

Phosphate-buffered saline.

0.05 % trypsin/EDTA.

6-Well plates.

5 % CO_2, 37 °C incubator. Use 5 % O_2 for primary cultures.

5.5 Components for RCL Test

Viral suspension.

HIV genomic RNA (if available).

293T/17 cells (ATCC CRL-11268).

Dulbecco's modified Eagle medium, 10 % FBS.

Phosphate-buffered saline.

0.05 % trypsin/EDTA.

Trizol LS.

RNeasy kit.

6-Well plates.

5 % CO_2, 37 °C incubator.

Reagents for routine molecular biology

Superase inhibitor, 20 U/μl.

DNase I (RNase-free) 10 U/μl.

Restriction buffer M (Roche 11417983001).

DNase/RNase-free water.

10 % SDS.

Phenol/chloroform/isoamyl alcohol.

NaOAc 3 M pH 5.5.

Glycogen 20 mg/ml.

Ethanol 70 and 100 % (molecular biology grade).

Oligo-dT 0.5 mg/ml.

dNTPs (10 mM each).

Superscript II (reverse transcriptase, first-strand buffer, DTT).

Sybr Green qPCR master mix 2× (Life Technologies 4344463).

Forward primer PAXpolF: tggcagaaaacagggagatt.

Reverse primer PAXpolR: tgcccctgcttctgtatttc.

qPCR machine.

6 Methods

Follow national biosafety level 2 guidelines when working with lentiviral vectors. If you are unsure what to do you are almost certainly not legal, so seek advice on local regulations from more experienced colleagues before starting the project. *See* **Note 1** for additional information on biosafety of lentiviral vectors.

6.1 Production of Lentiviral Particles

293T cells grow rapidly and detach easily. Coating the dishes with polylysine helps to prevent the cells falling off the dish during medium changes. The protocol below differs from some classic protocols in that cells are plated 3 days before transfection. This is designed for a plate on Friday–transfect on Monday–harvest on Wednesday strategy. Despite the relatively high density at the time of transfection, the yields are excellent. 293T cells should be maintained in DMEM and 10 % FCS and split 1:10 twice a week. Take care always to passage the stock plates before the medium is exhausted. Replace the cultures at least every 3 months from frozen stocks that have been checked for mycoplasma. If none of the vectors contains GFP it is helpful to set up an additional transfection with GFP to check the efficiency of transfection.

1. Coat tissue culture plates with polylysine by briefly pipetting 5 ml of polylysine onto 10 cm plates.

2. Plate 2×10^6 293T cells per 10 cm dish 3 days before transfection.
3. On the day of transfection, replace the medium with 5 ml DMEM and 10 % FCS. Cells should be about 80 % confluent when transfected (*see* **Note 7**).
4. For each 10 cm plate, prepare the following plasmid cocktails in 1.5 ml Eppendorf tubes:

   4 μg pMD2.G (VSV-G viral envelope)

   10 μg psPAX2 (packaging construct)

   10–20 μg of your expression vector, adjusted according to the size of the plasmid (10 μg <7,000 bp, 15 μg 7,000–10,000 bp, 20 μg >10,000 bp)

   Add sterile water to 450 μl.
5. Add 50 μl $CaCl_2$ to the plasmid cocktails and mix thoroughly. Prepare 15 ml Falcon tubes containing 500 μl 2× HeBS.
6. Add the plasmid cocktails drop by drop to the Falcon tubes containing the 2× HeBS while shaking them on a vortexer at low speed.
7. Wait for 5 min to allow the precipitate to form.
8. Add the precipitate to the cells by pipetting it drop by drop, trying to homogeneously cover the whole plate. Ensure even spreading of the precipitate by gently swirling the dish. Return the dish to the 37 °C 5 % CO_2 incubator.
9. 6–14 h after transfection, remove the medium and replace it with 8 ml OptiMEM 20 mM HEPES.
10. 38–46 h after starting the transfection, harvest the medium, which now contains lentiviral particles. Centrifuge at 2,500 rpm for 3 min to remove debris, and then filter with a 0.22 μm syringe filter. The titer will drop if the medium becomes very acid, so it is not worth waiting an extra day before harvesting the virus in the hope that the yield will go up.
11. Optional: To concentrate the virus 10- to 100-fold, use a Vivaspin column (*see* **Note 7**). This is only possible if you used serum-free medium (OptiMEM) as described above (if you use FCS the filter will concentrate unwanted proteins from the serum and become clogged). Before you embark on extensive centrifugation of virus, check that you have taken reasonable steps to contain aerosols that might be released by leakage of viral supernatant.
12. Aliquot virus in freezing vials and store at −80 °C.

6.2 Titration of Lentiviral Vectors

Cells differ in their infectability, so viral titers are only strictly valid on the cell line used to calculate the titer. Since it is often not possible to perform a titration on the cells you are most interested

in, you need to bear in mind that there may be a systematic error when you do the experiment (the effective multiplicity of infection [moi] may be higher or lower than you intended). *See* **Note 5** for more information on calculating viral titers.

6.2.1 Titration by Antibiotic Selection

This is the simplest approach. It only gives a rough idea of the titer but this is good enough for most experiments. A dilution series is performed and the titer is based on finding the first well with no dead cells after antibiotic treatment. This well is conventionally taken to have been infected at an moi of 1. This approach works best for antibiotics that kill fairly quickly, in particular puromycin, blastomycin, and hygromycin.

1. Plate cells at a relatively low density to ensure that they can be left for a week without becoming overgrown. For MCF7 use 1×10^5 cells per well in 6-well plates, one plate per virus to be titered.
2. Infect cells. The following day, prepare six Eppendorf tubes each with a final volume of 1 ml medium containing:
   A. 1 μl virus
   B. 10 μl virus
   C. 100 μl virus
   D. 100 μl virus (control for toxicity of virus)
   E. No virus (control for toxicity of virus)
   F. No virus (control for antibiotic efficacy)
3. Replace the medium on the cells with the 1 ml dilutions in the Eppendorfs.
4. Incubate for 6 h, then remove the medium, and add 2 ml of fresh medium.
5. Antibiotic selection: 48 h after infection, remove medium and add 2 ml of fresh medium containing antibiotic to wells A, B, C, and F. Add 2 ml of fresh medium without antibiotic to wells D and E.

   The concentration of antibiotic required depends on the cells, so before testing the virus you should titrate the antibiotic to find the concentration that kills uninfected cells in a reasonable time—for MCF7 it is likely to be around 2 μg/ml puromycin, 200 μg/ml hygromycin, 5 μg/ml blasticidin, 750 μg/ml G418, and 1 mg/ml zeomycin. The time to kill 100 % of the cells should be around 3 days for puromycin, 5 days for blasticidin and hygromycin, 10 days for zeomycin, and 14 days for G418.
6. Calculate viral titer. Observe the cells and score them when there is obvious death in well F. This will be 2–3 days for puromycin, and up to 1 week for the other antibiotics. G418 is so slow that it may be hard to interpret the results because the

cells are too confluent. The goal is to find the well with the lowest amount of virus giving no death. Compare wells D and E to check that death is due to antibiotic rather than a direct toxic effect of the virus.

Titer (infectious particles/ml) = number of cells at infection/volume of virus in ml in the first well with no death.

If you used the amounts above, the titers will be:

$1 \times 10^5 / 0.001 = 1 \times 10^8$ infectious particles/ml if there is no death in well A

$1 \times 10^5 / 0.01 = 1 \times 10^7$ infectious particles/ml if there is no death in well B

$1 \times 10^5 / 0.1 = 1 \times 10^6$ infectious particles/ml if there is no death in well C

Good titers are 10^7–10^8 infectious particles/ml in unconcentrated viral supernatant. This approach will slightly underestimate the titer (*see* **Note 5** for the reason why).

6.2.2 Titration by Flow Cytometry

It is possible to titer viruses accurately by flow cytometry provided they express a fluorescent protein such as GFP. It is the percentage of cells positive not the intensity of expression that matters.

1. Plate 1×10^5 MCF7 cells per well in 6-well plates, one plate per virus to be tested. Seed two additional wells that will not be infected, so you can use one to count the exact number of cells at the time of infection and the other as a negative control to set the flow cytometer gates.
2. Infect cells. The day after plating the cells, prepare Eppendorf tubes containing serial twofold dilutions of virus. In the first tube mix 64 μl virus with 1,934 μl medium. Then set up five tubes containing 1 ml medium and make serial dilutions by transferring 1 ml sequentially to each tube.
3. Remove the medium from the cells and add 1 ml of each virus dilution per well. Harvest one uninfected well to count the number of cells at the moment of infection (this lets you correct for the plating efficiency and for cells that have divided since they were plated).
4. Incubate for 6 h, then remove the medium, and add 2 ml of fresh medium.
5. Three days after infection, aspirate the medium, add 0.5 ml trypsin/EDTA to each well, including the control uninfected well, and incubate at 37 °C until the cells detach.
6. Add 1 ml medium to neutralize the trypsin, pipette up and down to ensure that the cells are dissociated, and then transfer the suspension to 5 ml polypropylene FACS tubes.

7. Pellet the cells by centrifuging for 5 min at 1,500 rpm and discard the supernatant.

   Optional: If your flow cytometry facility does not accept cells recently transduced with level 2 viruses, kill residual virus by resuspending the pellet in 0.5 % formaldehyde in PBS and incubating at room temperature for 5 min. Then pellet the cells again by centrifuging for 5 min at 1,500 rpm and discard the supernatant. Note that formaldehyde is compatible with GFP fluorescence but may abolish the fluorescence of other markers.

8. Resuspend the cells in 200 µl of PBS, store them at 4 °C, and perform flow cytometry within a few hours. Use the uninfected control well to set the gate for background fluorescence.
9. Record the percentage of infected cells in each well.
10. In Excel, make a table with the volume of virus in ml in one column and the percentage of fluorescent cells in another column. Add a column called "moi" in which you enter a formula for the "negative log of the fraction of cells not infected." The formula should look like this:

$$= -\mathrm{LN}\left(\left(100 - \mathrm{POS}\right) / 100\right)$$

   where POS refers back to the column with the percentage of fluorescent cells, and LN() takes the natural log.

   The "moi" column now contains the moi achieved with the specified amount of virus.

11. Make a graph with volume of virus in ml on the x-axis and "moi" on the y-axis. Exclude any obvious outliers (they may occur at the most extreme virus concentrations), then invite Excel to draw a straight line through the points, and ask it to display the slope and intercept of the line. The viral titer in infectious units per ml is given by

$$\mathrm{titer} = \left(\mathrm{slope} \times \mathrm{cell\ number}\right) / \left(1 - \mathrm{intercept}\right)$$

    where cell number is the number of cells present in the well at the time of infection. *See* **Note 5** for additional information on calculation of titers.

6.2.3 Titration by p24 ELISA

It is possible to titer lentiviral vectors by ELISA for p24, a capsid protein derived from the gag polyprotein. This approach measures the amount of p24 in pg, which depends on the number of physical virus particles. The ratio of infectious units to physical particles (typically 1 in 100 to 1 in 1,000) is used to assess the quality of viruses, for example to detect batch-to-batch variation in the quality of preps destined for clinical use. Since the quality of typical

academic lab virus preps is highly questionable, it is necessary to make some very large assumptions when extrapolating from physical titers to infectious titers. The approach is only useful if you have a burning desire to know the titer and there is no other way to do it (no antibiotic marker, no fluorescent marker, no transgene that can be detected in transduced cells by IF or IHC). When forced to measure physical titers we use the Innotest HIV Antigen mAb P24 ELISA kit (#80563, http://www.fujirebio-europe.com) according to the manufacturer's instructions.

6.3 Isolation of Mammary Epithelial Cells

The protocol can conveniently be split into two parts separated by the freezing of the organoids.

1. Place reduction mammoplasty tissue on chopping board.
2. Remove yellow fatty tissue by scraping it off with a scalpel.
3. Shear and chop the remaining tissue using two scalpels until it reaches a mushy consistency.
4. Add 1 g tissue to 10 ml MM + 100 μl Collagenase in 50 ml tube.
5. Incubate at 37 °C with agitation (roller) for 3–16 h.
6. Spin at 1,400 rpm (~400 × *g*) for 4 min.
7. Wash pellet twice with warm PBS and 2 % FCS.
8. Resuspend pellet ("organoids") in 2 ml freezing medium (10 % DMSO, 90 % FBS; or Cryo3).
9. Aliquot into cryotubes and freeze in isopropanol box (Mr. Frosty, Nalgene) at −80 °C overnight and then transfer to liquid nitrogen.
10. Thaw organoids and transfer to 15 ml tube containing 4 ml prewarmed MM medium.
11. Spin at 1,400 rpm (~400 × *g*) for 1 min.
12. Eliminate the supernatant carefully.
13. Add 500 μl prewarmed trypsin 0.25 % and resuspend organoids.
14. Incubate for 2 min at room temperature.
15. Pipette the organoid suspension repeatedly against the tube wall for 1 min (the suspension becomes viscous because of DNA released by dead cells).
16. Add 1 ml prewarmed Dispase and 50 μl DNase. Filter sterilize Dispase immediately before use because Dispase granules precipitate with cells and are toxic if present in the culture medium.
17. Pipette the cell suspension repeatedly against the tube wall for 2 min (aggregates should dissolve and the suspension should become clear; if not, add 50 μl of DNase and pipette for 1 more minute).

18. Pass cells through a 40 μm cell strainer into a new 15 ml tube.
19. Spin at 1,400 rpm (~400 × *g*) for 3 min and remove the supernatant.
20. Resuspend cells in the selected culture medium, count cells, and plate as appropriate.
21. Incubate in a 37 °C, 5 % CO_2, 5 % O_2 incubator.

6.4 Infection of Mammary Epithelial Cells

The protocol below describes infection at an moi of 10, but it is often helpful to test a range of multiplicities, in case the titer was wrong or the cells are unusually sensitive to the virus. Always include a mock-infected well to check the efficiency of the antibiotic selection and an infected well that is not selected in antibiotic to check for toxicity of the virus. We normally grow primary cells in 5 % O_2 but if using established cell lines this is not necessary. The viral suspension is in serum-free medium (OptiMEM). At commonly achieved titers (>10^7 IU/ml) this means <10 % of the medium in an infection will be OptiMEM. If you are using special media (for example mammosphere or WIT medium) whose composition you do not wish to modify even transiently, concentrate the virus by Vivaspin (**step 10** of the lentiviral production protocol) and reduce the time of infection. If you do not achieve the expected results, *see* **Notes 3–6** for possible reasons. For other options *see* **Note 7**.

1. Trypsinize cells. Stain with trypan blue and count the living cells with a hemocytometer.
2. For infection in suspension, plate 3×10^5 cells per 35 mm well in 1 ml of medium. Immediately add 3×10^6 infectious units of virus (for an moi of 10).
3. For infection of adherent cells, plate 3×10^5 cells per 35 mm well in 1 ml of medium. The following day when the cells have adhered to the plastic, add 3×10^6 infectious units of virus (for an moi of 10).

   Infection in suspension is more effective but if you are worried about viability or toxicity it is easier to work out what is going on if the cells have adhered before they are assaulted with virus.
4. Incubate at 37 °C in a 5 % CO_2, 5 % O_2 incubator for at least 6 h, then replace the medium with 2 ml of fresh medium, and continue incubation at 37 °C, 5 % CO_2, 5 % O_2.
5. Add antibiotics (*see* **Note 6**). If the viruses carry antibiotic selection genes, add fresh medium containing antibiotics for selection 2 days after infection (if the vector contains a strong promoter [e.g., SV40] driving the expression of the antibiotic resistance gene it is possible to add the antibiotics already on day 1 after infection). The concentration required depends on

the cells, so you should perform a titration to find the concentration of antibiotic that kills uninfected cells in a reasonable time—it is likely to be around 1 μg/ml puromycin, 100 μg/ml hygromycin, 2 μg/ml blasticidin, 300 μg/ml G418, and 1 mg/ml zeomycin. The time to kill 100 % of the cells should be around 3 days for puromycin, 5 days for blasticidin and hygromycin, 10 days for zeomycin, and 14 days for G418.

6.5 Replication-Competent Lentivirus Test

See **Note 2** for a discussion of possible mechanisms leading to the formation of replication-competent lentivirus (RCL). The protocol below is used to test concentrated virus stocks but the supernatant of any cells could be tested if required. The goal is to show that infected cells do not release replication-competent viruses. In some jurisdictions you may be asked to perform an RCL test before removing cells from the level 2 lab. It is rarely done now because RCL has not emerged as a significant problem after over a decade of widespread use of lentiviral vectors. It is also extremely difficult to prove a negative (not a single replication-competent virus present in a prep containing 10^9 replication-incompetent viruses). Furthermore, proving that an RCL test is truly effective requires the use of live virus as a positive control. In principle, this virus should contain VSV G instead of the normal envelope gene but this would be a monster that no one should deliberately create, least of all in the pursuit of biosafety. It would require level 3 containment and would expose large numbers of non-virologists to a wholly unjustifiable risk of contracting AIDS or worse. We compromise by using pure HIV RNA from our colleagues as a positive control, but if you do not have access to this you can use psPAX2 plasmid, which will at least allow you to confirm that the qPCR works.

1. Infect 293T cells. This approach will detect recombinant viruses that can infect 293T cells (we assume that a recombinant would use VSV G instead of the normal envelope gene, which is not present in the vectors). To detect viruses using the normal envelope, Escarpe et al. (ref. 6) recommend using the C8166-45 cell line.
2. Plate 5×10^4 293T cells per well in 12-well tissue culture plates in 400 μl final volume of DMEM and 10 % FCS medium.
3. Immediately add 100 μl of viral supernatant to infect the cells as they adhere.
4. Remove virus from cells after 6 h.
5. Wash the cells twice with fresh medium.
6. Incubate at 37 °C 5 % CO_2 for 6 days.
7. Split each well into 35 mm wells in 1 ml medium per well.
8. Incubate at 37 °C 5 % CO_2 for 6 days.

9. Harvest the medium (supernatant) containing putative RCL.
10. Mix 1 ml of supernatant with 500 µl Trizol LS.
11. Incubate for 5 min at room temperature.
12. Add 100 µl chloroform, and vortex for 15 s.
13. Incubate for 3 min at room temperature.
14. Centrifuge for 15 min at 4 °C, 12,000×*g*.
15. Transfer the upper phase to a new tube, add 600 µl of ethanol 70 %, and vortex to mix.
16. Load the mixture on an RNeasy Mini spin column.
17. Centrifuge for 15 s. Discard the flow-through.
18. Add 500 µl Buffer RPE and centrifuge for 15 s. Discard the flow-through.
19. Add 500 µl Buffer RPE and centrifuge for 2 min.
20. Place the spin column in a new 2 ml collection tube and centrifuge for 1 min.
21. Place the spin column in a new 1.5 ml collection tube and add 30 µl RNase-free water.
22. Wait for 1 min and then centrifuge for 1 min to elute the RNA.
23. To treat with DNase I, to each 30 µl RNA prep add:

1 µl	Superase inhibitor
5 µl	Roche restriction buffer M
13 µl	RNase-free water
1 µl	DNase I (RNase-free) 10 U/µl

24. Incubate at 37 °C for 30 min to digest DNA.
25. Add 1 µl 10 % SDS.
26. Add 50 µl phenol/chloroform/isoamyl alcohol.
27. Vortex, and spin for 10 min.
28. Take the upper phase and add:

4 µl	NaOAc 3 M pH 5.5
1 µl	Glycogen
120 µl	Ethanol 100 %

29. Put on dry ice for 5 min, spin for 20 min, and discard the supernatant.
30. Add 100 µl ethanol 70 %, spin for 5 min, and discard the supernatant.
31. Dry the pellet for 3 min, and add 10 µl RNase-free water.
32. Put on ice for 5 min to resuspend the RNA then store at −80 °C

33. To reverse transcribe add 1 µl oligo-dT to 5.25 µl RNA from supernatant or positive control.
34. Heat to 65 °C for 10 min, then chill on ice, and spin briefly.
35. Prepare the reaction mix:

2 µl	5× first-strand buffer
1 µl	100 mM DTT
0.5 µl	dNTPs (10 mM each)
0.25 µl	Superscript II reverse transcriptase

36. Add 3.75 µl of the reaction mix to the 6.25 µl of RNA/oligo-dT mix.
37. Incubate for 1 h at 46 °C and then store at –80 °C.
38. Perform quantitative PCR. Set up standard Sybr Green qPCR reactions using PAXpolF and PAXpolR primers according to your normal protocol with 40 cycles and annealing at 60 °C. The product length is 94 bp. You should get no signal after 40 cycles in the absence of the positive control template.

7 Notes

1. *General safety issues*

   Modern lentiviral vectors are classified in most jurisdictions as level 1 or level 2. Importantly, the viral particles used to transduce target cells contain no complete gene coding for HIV proteins. Furthermore, in common with all retroviruses, HIV vector particles have a lipid envelope that renders them sensitive to inactivation by simple detergents. Thanks to their fragility, lentiviruses can only be transmitted by direct contact with penetration, for example by needle stick injury. In the lab, this means avoiding the use of glass or needles. Otherwise, good microbiological practice, as commonly applied in level 2 tissue culture labs, provides adequate protection. The conditions where retroviral vectors have been demonstrated to produce malignant transformation in humans are known thanks to gene therapy experiments on children with severe combined immunodeficiency (SCID). It is inconceivable that these conditions could ever be met in a normal laboratory, even as a deliberate criminal act. Specifically, patients were treated with drugs to depress their already deficient immune response, their hematological stem cells were infected in massive numbers ex vivo, and their immune system was regenerated entirely from virally transduced cells. The goal of the protocol was to give the transduced cells the maximum encouragement to engraft and expand clonally. Crucially, the patients were defenseless against foreign

antigens because the only cells that could mount an immune response were the transduced cells themselves. One-quarter of the patients developed leukemia [7]. Gene therapy has also taught that a normally functioning immune system is extremely effective at eliminating transgenes, even if they differ by only a single amino acid from a patient's own version of the gene. In a laboratory accident, all integrated vectors are likely to express antibiotic resistance genes or fluorescent protein genes in addition to the experimental transgene, virtually guaranteeing the rapid immune killing of infected cells.

The rules for working in level 2 labs are specified by national authorities. Two sensible precautions when hiring new staff are to exclude people who are either immune deficient or suffer from skin diseases that impair the barrier function of the skin, the former because they are defenseless against foreign antigens and could, if HIV positive, propagate defective viruses, the latter because their underlying condition makes them easier to infect (and is incidentally likely to be made worse by wearing gloves all day, so they will probably spend long periods banned from the level 2 lab).

It is good practice to inactivate viral suspensions under the laminar flow hood by collecting them after use in a beaker containing disinfectant (for example, 1 % Virkon), and then waiting for 15 min before aspirating them to the waste bottle. Avoid centrifuging cells or medium containing concentrated virus; if you use a centrifuge make sure that the rotor has an aerosol-tight lid and never use polystyrene tubes that can shatter easily. An underappreciated route of infection is contact with the eyepieces of microscopes; this happens because the first act after putting petri dishes on the microscope stage is to adjust the separation of the eyepieces—hence if medium has slopped over the side of the dish it will promptly find its way onto the eyepieces. The solution is to wear safety glasses.

Two situations stand out as requiring careful thought. The first is injection of concentrated virus into live animals. Sharp needles and sudden movement are the perfect recipe for disaster. Good anesthesia mitigates the risk, but the most effective measure is to ask operators to spell out exactly what they would do if they were to stab themselves. The second is inclusion of multiple transgenes in a single vector. This has become fashionable, in particular thanks to the development of picornaviral 2A sequences as tools to express multiple proteins from a single mRNA. It is now easy, at least in principle, to produce single vectors expressing a full complement of transforming oncogenes and shRNAs. The chance of accidentally transforming a cell when each vector expresses a single oncogene is vanishingly small because the probabilities are multiplicative; the chance if it requires only a single event is dramatically increased.

Group leaders should be alert to this difference and discourage postdocs or students from making single-hit vectors unless there is a compelling reason.

2. *RCL*

Recombination between vector and packaging plasmids leading to the creation of RCL is the major theoretical safety concern when working with lentiviral vectors. To reduce this risk, the helper genes are split between two ("second generation") or three ("third generation") plasmids. In normal academic use, the quantities of virus produced are too small for RCL to be a problem. Attempts to produce RCL have failed in tests scaled up to 1.4×10^{10} transducing units [6].

Detecting RCL in the context of lentiviral vector production is not as easy as it sounds. Simple arithmetic shows that the number of molecules of plasmid DNA transfected into lentiviral packaging cells is around 10^{12}. This makes it pointless to test the viral supernatant itself. There is no way so many copies of contaminating plasmid DNA could be brought down to <10 in a reasonable time by any simple process. The protocol we use tests for viral RNA in the supernatant of infected cells. It is based on qPCR, since it is relatively easy to assess the sensitivity of qPCR assays on control DNA or purified HIV RNA templates, and qPCR machines are readily available in modern research labs. It is not perfect because it does not use replication-competent virus as a positive control, but this is a price most non-virologists would be willing to pay. In our experience it is better than some commonly used gel-based PCR assays, whose sole aim seems to be to get a negative result (data not shown). A full RCL assay based on ELISA for p24 and intended for testing of clinical grade virus preps is described in ref. 6.

A more plausible situation where RCL could arise in normal use would be transduction of a cell line that was already contaminated with wild-type HIV. Care should therefore be taken when using primary tissue samples that have not been screened for HIV. If you use biopsies from patients who are not routinely screened for HIV, you should consider testing the biopsies for HIV before using them (anonymously, of course). Outside professional virology labs, cell lines contaminated with wild-type HIV should be destroyed immediately (they are automatically classified as level 3). Since the packaging signal in the vector is placed upstream of the active promoter in SIN vectors, the packaging signal is not present in transcripts produced from integrated vector genomes. Hence, the simple presence of wild-type virus is not sufficient to package vector genomes; to transcribe the packaging signal the proviral vector DNA must either be integrated in a site where it can be transcribed from an upstream cellular promoter or recombine with integrated wild-type proviral DNA through the region between U5 and the

packaging signal. A hybrid virus arising in this situation would most likely resemble a classic retroviral oncogene-encoding virus. Propagation of such defective viruses typically requires the presence of a helper wild-type virus. This in turn requires the use of high titers to prevent loss of the recombinant through competition with the wild-type virus. Trying to assess the risk posed by such a recombinant virus pales to insignificance compared to the very real risk posed by the wild-type virus in the mixture.

3. *Plasmid problems*

Recombination between the LTRs leading to deletion of the intervening vector sequences is occasionally a problem during production of lentiviral plasmids. One situation where it is almost guaranteed is when there is a toxic gene in the vector. The classic example is a Gateway Destination vector: the *ccdB* gene is used to kill bacterial cells that have taken up the parental vector after a clonase reaction. Special strains containing a *gyrA* mutant that confers resistance to *ccdB* are used to produce Gateway Destination vectors, but it is still necessary to select for the *cat* (chloramphenicol resistance) gene that is adjacent to *ccdB* in the plasmid. Gateway *ccdB* cassettes are deliberately toxic, but even banal inserts may be mildly toxic in lentiviral plasmids. When this occurs the transformed bacteria may be noticeably temperature sensitive. The solution is to grow bacteria at 30 or 32°C at all steps from cloning to maxiprep. Another precaution commonly taken to prevent recombination is to use bacteria deficient in recombination enzymes, for example stbl3. Toxicity seems to be strain dependent, so if you have problems it is worth simply trying other commonly used bacterial strains (DH10B, stbl2, stbl3, etc.).

Recombination should not be a problem with existing plasmids. It is more likely to occur when constructing new plasmids. One solution is to use Gateway cloning, which eliminates the gel purification and ligation steps in conventional cloning. If you do use conventional cloning it is worth checking the wavelength of your UV light box. Most labs now use 315 nm UVB to purify DNA fragments, despite Maniatis' injunction to use 365 nm UVA. UVB specifically damages DNA, which reduces the number of colonies ~100-fold and triggers a DNA damage response that increases the risk of recombination. Finally, to avoid caramelizing the medium it may help to reduce the duration or temperature of the autoclave cycle used to prepare the media (we use 110 °C for 2 min because our autoclave takes so long to cool down).

When constructing lentiviral vectors it is important to delete polyA signals from transgenes. To produce the virus, the packaging cell has to transcribe all the way to the end of the 3′-LTR. If the RNA is cleaved at an internal polyA site, the

3′-LTR sequences will be deleted, preventing reverse transcription of the complete viral RNA. This will give a dramatically reduced viral titer. Apart from that, the commonest cause for low titers is simply that the insert is too big. It is easy to get titers of 10^8 infectious units/ml in unconcentrated supernatant when the total size of the vector is 6.5 kb, but becomes increasingly difficult when the size exceeds 8 kb. Hence it is a good idea to delete 5′- and 3′-untranslated regions from transgenes. This can be done cheaply by Gateway cloning of orf clones from http://plasmid.med.harvard.edu/PLASMID/.

4. *Interferon induction*

The interferon system blocks translation, degrades mRNA, and arrests the cell cycle, phenomena that can easily dwarf whatever effects you may be trying to study. We previously reported that lentiviral shRNA vectors can trigger an interferon response [8]. This is a transient phenomenon, which occurs soon after infection, probably from a convergence of multiple factors. We originally reported it with shRNA vectors but we have also seen it with ordinary polII expression vectors. Whether you see it depends to a great extent on how you look. Gene set enrichment analysis (GSEA) of microarray data using the Broad GSEA server (http://www.broadinstitute.org/gsea/) is a remarkably effective tool to detect it, but simple qPCR for an interferon-stimulated gene (ISG) like OAS1 also works well and is less expensive (primers: aggtggtaaagggtggctcc and acaaccaggtcagcgtcagat).

It is normal for cells to fight viruses by activating the interferon system, and lentiviruses are no exception. A growing number of steps in the lentiviral life cycle are known to be recognized as alien by the host cell: the viral capsid is recognized by TRIM5 immediately following cell entry [9]; SAMHD1 destroys nucleotides to prevent reverse transcription of viral RNA [10]; the reverse-transcribed DNA is mutated by APOBEC3G to scramble the viral sequence [11]; and MX2 blocks nuclear import [12]. The genes used by lentiviruses to block these responses are the very genes that are deleted in lentiviral vectors, so it should come as no surprise that interferon responses are occasionally seen following lentiviral vector infections.

Depending on the type of transgene being expressed it is also possible for the foreign transcript to be mistaken for a viral RNA, leading to activation of the interferon system through the mechanisms, such as PKR (EIF2AK2), that defend the cell against RNA viruses. This probably explains the interferon induction we reported with the U6 promoter [13]. An important theoretical advantage of polII-driven miRNA vectors over polIII-driven shRNA vectors is that saturation of Drosha should just lead to the accumulation of superfluous noncoding

polII transcripts; they are unlikely to be mistaken for intruders or to otherwise offend the cell. In contrast, shRNAs produced by polIII promoters skip the Drosha step. Saturation of Dicer leads to the accumulation of bizarre small RNAs that could very easily be mistaken for small viruses.

Besides these biological explanations, there is a technical explanation that probably accounts for the sporadic nature of the problem. Production of lentiviral vectors requires transfection of packaging cells with at least three plasmids. If any one of them is contaminated with bacterial endotoxin, the packaging cells themselves will release interferon, leading to the production of a viral suspension contaminated with both endotoxin and interferon. This is why it is important to use "endotoxin-free" maxiprep kits to purify lentiviral plasmids.

Once the proviral DNA has been integrated into the host genome, there are few clues to inform the cell that it harbors a new virus. Hence interferon responses are a nuisance if cells must be used immediately after infection, but of little or no importance once cells have been passaged. For this reason, it is infinitely preferable to design experiments such that biological measurements can be delayed until the cells have been passaged and any antibiotic selection is complete. Otherwise, the effect one is trying to measure can easily be confounded by a mixture of interferon effects and antibiotic-induced death. For toxic proteins, this usually means using inducible vectors.

5. *Viral titers*

The precise viral titer is rarely important in routine lab experiments. A more important question is whether you want the cells to contain only a single copy of the provirus or you want to have multiple copies. If the former, it is worth erring on the low side by using an moi of 0.1–0.2. This presupposes that you will be able to select transduced cells, by either antibiotic treatment or FACS for fluorescent proteins. Reasons to use multiple copies include needing to achieve high-level expression of a transgene, or wanting to avoid big differences between individual cells if a few proviruses are silenced. A classic situation where multiple copies may be required is the use of shRNA expressed from polIII promoters (H1 or U6) because a single copy frequently gives very poor silencing.

Viral infection obeys Poisson's law. In its simplest form this states that the moi is 1 virus per cell when one-third of the cells are not infected. The critical parameter is the fraction of cells that are not infected, which is equal to $1/e$ or 37 % when cells are infected at an moi of 1. This is because Poisson's law states that $P(k) = e^{-m} \times m^k/k!$, where m is the multiplicity of infection, k is the number of integrated proviruses per cell after infection, and P means probability. When $m = 1$ and $k = 0$, the probability that a cell contains no virus $P(0) = e^{-1} \times 1^0/0! = e^{-1}$. It is easy to estimate

the fraction of cells with $k=0$: they are the unstained cells in flow cytometry or the cells that die in antibiotic. Poisson's law can also be used to calculate a few other (mildly) interesting numbers. At an moi of 3, 5 % of cells will contain no virus, and 22 % of cells will contain three viruses. This probably corresponds to the commonly used yardstick of "no death with antibiotic"—from which we can surmise that people using the titration by antibiotic selection approach will mildly underestimate the titer. If it is not possible to apply any selection, it is worth knowing that at an moi of 5 there will be 0.67 % of cells uninfected, whereas at an moi of 10 there will only be 0.0045 % of cells uninfected. If cells divide daily, it will take about a week for uninfected cells to overgrow the culture in the former case but over 2 weeks in the latter case. What this tells you is that infection without selection gives you a very narrow window of time to test tumor-suppressor genes before the uninfected cells overgrow the culture, even if you use an moi of 10. Much higher multiplicities can be used to get around this problem, but they commonly lead to nonspecific toxicity or wildly unphysiological levels of transgene expression.

6. *Unwelcome surprises*

Antibiotic resistance does not guarantee that the transgene is expressed. To work out whether the transgene is expressed people normally perform a Western blot, but this can hide a multitude of sins. In particular, a transgene expressed in only 10 % of the cells will give a nice band on a Western. To find out how many cells express the transgene it is possible to do immunofluorescence (IF) on coverslips, immunohistochemistry (IHC) on plastic dishes, or flow cytometry with antibodies against your protein. One could imagine that resistance to antibiotic should guarantee successful expression of a transgene. Sadly, this is not the case when the transgene and marker are expressed from different promoters. Antibiotic resistance means the DNA has been successfully integrated, but for a transgene that is even mildly toxic, there is always a good chance that its promoter will be silenced.

Lentiviruses use complex alternative splicing to express their own genes efficiently. Their predilection for arcane splicing carries over into lentiviral vectors [14]. It can generate perplexing results, for example generating fusion proteins between a transgene and GFP in a downstream expression cassette. The only clues in one case we studied were that the transgene ran too high on a protein gel and GFP became nuclear. Subsequent investigation revealed that the vector had found a splice donor site a few nucleotides before the 3′-end of the transgene, and spliced it to a cryptic acceptor site in the murine PGK promoter that was used to express GFP.

7. *Optional variants*

Production of lentiviral particles, **step 3**: Addition of 25 μM chloroquine to the medium before transfection is commonly used to prevent acidification of endosomes that have taken up DNA. If done, prepare the transfection mixes without delay because chloroquine is toxic to the cells.

[Chloroquine (Sigma C6628): 2,000× stock contains 50 mM chloroquine in water; filter sterilize (0.22 μm) and store at 4 °C for 1 month or freeze at −20 °C.]

Production of lentiviral particles, **step 11**: More extensive concentration of virus is possible by ultracentrifugation or by using kits such as Millipore Fast-Trap or System Biosciences PEG-it.

Infection of mammary epithelial cells: Addition of polybrene 8 μg/ml to medium during infection of target cells was always done with retroviral vectors. It neutralizes charge leading to better receptor binding. It seems not to be necessary with VSV G pseudotyped lentiviral vectors. [Polybrene (hexadimethrine bromide, Sigma H9268): 1,000× stock contains 80 mg polybrene in 10 ml water; filter sterilize (0.22 μm) and store at 4 °C for 1 month or freeze at −20 °C.]

Acknowledgements

We thank former members of the lab, in particular Stephan Duss, for help in developing these protocols and the French Cancer Ligue ("Equipe Labellisee Ligue Contre le Cancer 2011") for financial support.

References [1]

1. Naldini L, Blomer U, Gallay P, Ory D, Mulligan R, Gage FH, Verma IM, Trono D (1996) In vivo gene delivery and stable transduction of nondividing cells by a lentiviral vector. Science 272(5259):263–267
2. Naldini L, Blomer U, Gage FH, Trono D, Verma IM (1996) Efficient transfer, integration, and sustained long-term expression of the transgene in adult rat brains injected with a lentiviral vector. Proc Natl Acad Sci U S A 93(21):11382–11388
3. Zufferey R, Dull T, Mandel RJ, Bukovsky A, Quiroz D, Naldini L, Trono D (1998) Self-inactivating lentivirus vector for safe and efficient in vivo gene delivery. J Virol 72(12):9873–9880
4. Dull T, Zufferey R, Kelly M, Mandel RJ, Nguyen M, Trono D, Naldini L (1998) A third-generation lentivirus vector with a conditional packaging system. J Virol 72(11):8463–8471
5. Duss S, Andre S, Nicoulaz AL, Fiche M, Bonnefoi H, Brisken C, Iggo RD (2007) An oestrogen-dependent model of breast cancer created by transformation of normal human mammary epithelial cells. Breast Cancer Res 9(3):R38
6. Escarpe P, Zayek N, Chin P, Borellini F, Zufferey R, Veres G, Kiermer V (2003) Development of a sensitive assay for detection of replication-competent recombinant lentivirus in large-scale HIV-based vector preparations. Mol Ther 8(2):332–341

[1] Additional useful information can be found on http://tronolab.epfl.ch/lentivectors and http://www.addgene.org.

7. Hacein-Bey-Abina S, Hauer J, Lim A, Picard C, Wang GP, Berry CC, Martinache C, Rieux-Laucat F, Latour S, Belohradsky BH, Leiva L, Sorensen R, Debre M, Casanova JL, Blanche S, Durandy A, Bushman FD, Fischer A, Cavazzana-Calvo M (2010) Efficacy of gene therapy for X-linked severe combined immunodeficiency. N Engl J Med 363(4):355–364. doi:10.1056/NEJMoa1000164
8. Bridge AJ, Pebernard S, Ducraux A, Nicoulaz AL, Iggo R (2003) Induction of an interferon response by RNAi vectors in mammalian cells. Nat Genet 34(3):263–264
9. Pertel T, Hausmann S, Morger D, Zuger S, Guerra J, Lascano J, Reinhard C, Santoni FA, Uchil PD, Chatel L, Bisiaux A, Albert ML, Strambio-De-Castillia C, Mothes W, Pizzato M, Grutter MG, Luban J (2011) TRIM5 is an innate immune sensor for the retrovirus capsid lattice. Nature 472(7343):361–365. doi:10.1038/nature09976
10. Lahouassa H, Daddacha W, Hofmann H, Ayinde D, Logue EC, Dragin L, Bloch N, Maudet C, Bertrand M, Gramberg T, Pancino G, Priet S, Canard B, Laguette N, Benkirane M, Transy C, Landau NR, Kim B, Margottin-Goguet F (2012) SAMHD1 restricts the replication of human immunodeficiency virus type 1 by depleting the intracellular pool of deoxynucleoside triphosphates. Nat Immunol 13(3):223–228. doi:10.1038/ni.2236
11. Mangeat B, Turelli P, Caron G, Friedli M, Perrin L, Trono D (2003) Broad antiretroviral defence by human APOBEC3G through lethal editing of nascent reverse transcripts. Nature 424(6944):99–103. doi:10.1038/nature01709
12. Kane M, Yadav SS, Bitzegeio J, Kutluay SB, Zang T, Wilson SJ, Schoggins JW, Rice CM, Yamashita M, Hatziioannou T, Bieniasz PD (2013) MX2 is an interferon-induced inhibitor of HIV-1 infection. Nature 502(7472):563–566. doi:10.1038/nature12653
13. Pebernard S, Iggo RD (2004) Determinants of interferon-stimulated gene induction by RNAi vectors. Differentiation 72(2–3):103–111
14. Moiani A, Paleari Y, Sartori D, Mezzadra R, Miccio A, Cattoglio C, Cocchiarella F, Lidonnici MR, Ferrari G, Mavilio F (2012) Lentiviral vector integration in the human genome induces alternative splicing and generates aberrant transcripts. J Clin Invest 122(5):1653–1666. doi:10.1172/JCI61852

Chapter 9

The Transplantation of Mouse Mammary Epithelial Cells into Cleared Mammary Fat Pads

Marisa M. Faraldo, Marina A. Glukhova, and Marie-Ange Deugnier

Abstract

The transplantation of mammary epithelial cells into the cleared fat pad allows their growth and differentiation in their normal physiological environment. This technique involves the grafting of tissue fragments or isolated cells into the mammary fat pads of prepubertal mice from which the endogenous epithelium has been surgically removed. Such transplantation assays are particularly useful for the analysis of morphogenetic potential and stem cell activity in normal mammary epithelium and breast tumors. We describe here the main steps in the transplantation of epithelial fragments and isolated cells from mouse mammary glands and the various approaches currently used to evaluate the regeneration and self-renewal properties of mammary stem cells.

Key words Transplantation, Outgrowth, Mammary fat pad, Mouse, Stem cell

1 Introduction

The mammary epithelium has a remarkable repopulation capacity, as shown by the replenishment of the mammary fat pad with new secretory tissue during each pregnancy in normal conditions and, experimentally, in transplantation assays. The transplantation technique makes use of the fact that before puberty, the growth of the mammary epithelium is very limited (Fig. 1). This important observation led deOme and coworkers, several decades ago, to use the prepubertal fat pad cleared of the endogenous epithelium as a physiological environment for tissue transplantation [1]. After several weeks, the transplanted fragments expand to fill the entire fat pad and display normal differentiation in response to hormonal stimulation (Fig. 1). Moreover, the outgrowths obtained can be successfully retransplanted into a new host, and further serially transplanted indicating the presence of a stem cell population capable of self-renewal [2]. However, the self-renewal potential of normal mammary stem cells is limited, and only tissue fragments or cells isolated from mammary malignant or premalignant lesions can be perpetually regrafted [3].

Maria del Mar Vivanco (ed.), *Mammary Stem Cells: Methods and Protocols*, Methods in Molecular Biology, vol. 1293,
DOI 10.1007/978-1-4939-2519-3_9,

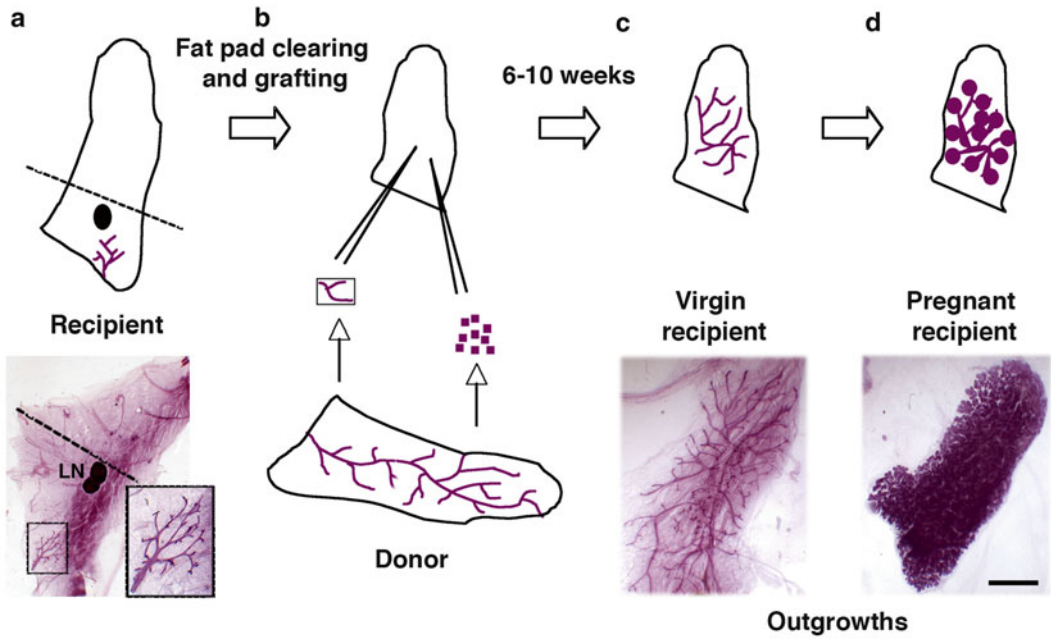

Fig. 1 Transplantation of mouse mammary epithelium fragments or isolated cells into the cleared mammary fat pad. The portion of the fat pad containing rudimentary mammary gland is excised, as indicated by the *dotted lines* (**a**) and a mammary epithelium fragment or isolated cells are grafted into the remaining fat pad (**b**). For outgrowth analysis, the recipient mouse mammary fat pads are dissected 6–10 weeks after transplantation and whole-mount preparations are stained (**c** and **d**). For the induction of lobulo-alveolar development and lactogenic differentiation in the grafted epithelium, the recipient mouse should be mated. The microphotographs presented in the *lower panels* show a rudimentary mammary gland dissected from a 3-week-old mouse (**a**) and mammary outgrowths developed in virgin (**c**) and pregnant (**d**) hosts. *LN* lymph node. Bar, 4 mm in (**a**) and (**c**); 6 mm (**d**)

The recent development of flow cytometry-based separation techniques has made it possible to examine the regenerative capacities of luminal and basal cell populations purified from the mammary epithelium [4–6]. These studies have shown that, in normal mammary glands, only the basal cell population is capable of regeneration, consistent with the presence of functional multipotent stem cells in the basal layer of the mammary epithelium [4–6]. Similarly, the fractionation of breast tumor cells on the basis of their expression of various surface markers has permitted to identify the tumor-initiating cells, the cell populations able to initiate a new tumor [7, 8].

Most of the cell surface markers used to separate stem cell- or progenitor-enriched cell populations from the mammary epithelium, breast tumors, or tumor cell lines are adhesion molecules, such as integrins, EpCAM, CD24, and CD44. This suggests that adhesion to neighboring cells and the ECM may create the stem cell microenvironment or niche required for the maintenance of the functional stem cell population. Laminins are the major components of the mammary basement membrane, and the transplantation of

sorted cells suspended in Matrigel, a defined basement membrane preparation, significantly increases the take rate for outgrowths, probably by increasing the survival of transplanted cells and enhancing early steps in morphogenesis, such as cell polarization [9].

Mammary transplantation techniques make it possible to compare stem cell activity in mammary gland specimens originating from two different donors, such as wild type and mutant. For such comparisons, the specimens to be compared are transplanted into contralateral fat pads of the same mouse, so that the regenerative potential of the tissues or cells examined is evaluated under the same physiological conditions.

Different transplantation protocols can be used to address the specific question of mammary stem cell activity. Serial transplantations are carried out to evaluate the self-renewal capacity of stem cells present in the tested cell populations or tissue fragments. Normal mammary tissue fragments can be successfully retransplanted five or six times [2], whereas the regenerative potential of sorted normal basal cells appears to be exhausted after only two transplantations [10]. These observations clearly indicate the importance of tissue architecture and of the adhesion molecules responsible for intercellular and cell-ECM interactions in the maintenance of mammary stem cell activity.

Limiting dilution transplantations are performed to estimate the frequency of active stem cells ([11]; http://bioinf.wehi.edu.au/software/elda/index.html). In this case, single-cell suspensions are serially diluted and transplanted into the cleared fat pads of the host mice. The frequency of mammary regenerating cells can be calculated from the rates of successful outgrowth formation for each dilution. The reported frequency of regenerating cells in the mammary basal compartment varies between studies, depending on mouse strain, genetic background, details of tissue digestion, cell sorting, and transplantation protocols, but it does not exceed 5 % for wild-type mammary epithelium [4–6, 9, 10].

Finally, the co-transplantation of two cell populations (for example wild-type and mutant cells) can be useful, making it possible to compare their repopulation capacities in conditions of competition. These experiments require the presence of a genetic marker (GFP, lacZ, etc.) in at least one of the populations compared, for estimation of the relative contribution of each population to the outgrowth [10, 12, 13].

2 Materials

2.1 Preparation of Mammary Epithelial Cells and Fragments for Transplantation

1. Scissors and forceps for tissue dissection.
2. Scalpels.
3. CO_2-independent medium.

4. DNase I solution: Prepare a 10 mg/mL solution and store aliquots at −20 °C.
5. EDTA (Versen) solution: 1 % w/v in PBS w/o Ca^{2+}, Mg^{2+}. Prepare 0.25 % trypsin/0.1 % Versen solution in PBS.
6. Ammonium chloride solution.
7. Sterile cell strainer, 40 μm nylon mesh.
8. Trypan blue solution 0.4 %.
9. Growth-factor reduced Matrigel (BD Biosciences).
10. Dissecting microscope with transmitted illumination.
11. Digestion solution: Weigh the required amount of digestion enzymes and keep at 4 °C until use. Dilute 3 mg/mL collagenase, 100 U/mL hyaluronidase in CO_2-independent medium complemented with 5 % FCS, and 2 mM L-glutamine.
12. Dispase solution: 5 % FCS and 5 mg/mL dispase in CO_2-independent medium.

2.2 Animal Surgery

1. Dissecting microscope with direct illumination.
2. Fiber-optic light source.
3. Electric thermocautherizer (Harvard Apparatus).
4. Corkboard (about 20 cm square).
5. Rubber or hard-tissue band, 0.5 cm wide.
6. Anesthetic solution: 0.4 mg/mL xylazine, 8 mg/mL ketamine, 30 μg/mL flunitrazepam in PBS. This solution is stable at 4 °C for several months (*see* **Note 1**).
7. Eye gel (Lacrinorm 0.2 %).
8. 1 mL syringe and 25-gauge syringe needles.
9. Scissors, 110 mm, S/S.
10. Round-nosed dressing forceps (skin forceps, tissue forceps).
11. Dissecting forceps (jeweler's type).
12. Iris scissors, angle to side, 90–100 mm, S/S.
13. Cotton swabs.
14. Hamilton syringe, 25 μL.
15. Sterile PBS and water.
16. 9 mm wound clips, clipping machine, and clip remover. Alternatively, braided absorbable suture Vicryl (6-0) with a multipass curved micro-needle (Johnson & Johnson).
17. Heating lamp.
18. Three-week-old female mice, weighing 8–10 g (*see* **Notes 2** and **3**).

2.3 Outgrowth Analysis

1. Glass histology slides.
2. Dissection material (scissors, forceps).
3. Methacarn fixation solution (methanol:chloroform:acetic acid/6:3:1).
4. Carmine Alum solution (Stem Cell Technologies Cat #7800).
5. 70, 95, and 100 % ethanol.
6. Xylene or methyl salicylate.

3 Methods

3.1 Clearing the Fat Pad

1. Rinse the operating table surface with 70 % ethanol.
2. Inject 100 μL anesthetic solution intraperitoneally into 3-week-old female recipient mice; the mice will be anesthetized within about 2 min and will remain so for at least 1 h.
3. Put the mouse on a corkboard, ventral side up, and attach the hind legs to the corkboard with the rubber band, tightly enough to fix the animal in place but not so tightly as to hamper blood circulation.
4. Apply eye gel to prevent eye dryness, as the blinking reflex is inhibited by anesthesia.
5. Swab the inguinal area of the mice with 70 % ethanol.
6. Grasp the skin above the pelvis with forceps, lifting it up from the abdomen. Make a midline incision starting just above the pelvis and extending over 1–1.5 cm from the pubis to the sternum (Fig. 2). Take care not to pierce the peritoneum and damage the abdominal musculature.
7. From this middle incision, make two oblique incisions towards the hind legs, ending at about the midpoint between nipples 4 and 5 (Fig. 2).
8. Lift up the skin with the forceps and pull the body wall with the cotton swab to expose fad pad no. 4 (Fig. 2); pin the skin to the board with a 25G needle.
9. Under the microscope, cauterize the arteries of nipple no. 4 leading to the node and margins of the fifth gland, to prevent ingrowth.
10. With the scissors, carefully excise the proximal part of the fat pad in one piece, including the lymph node, making clean and precise cuts, starting from the nipple (Fig. 2, *see* **Note 4**).
11. Clear the contralateral fat pad (*see* **Note 5**).

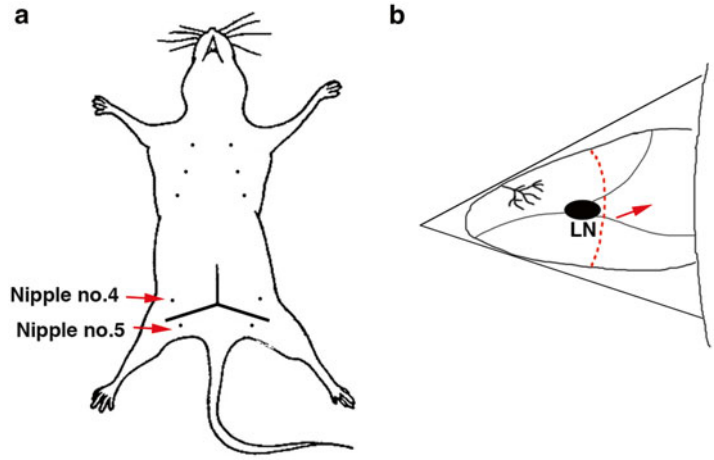

Fig. 2 Preparation of the mammary fat pad cleared of endogenous epithelium. One ventral midline incision, 1–1.5 cm long, starting a few mm above the pelvis, and two lateral incisions ending between the nipples of the glands 4 and 5 are made (**a**), and the endogenous epithelium is excised, as indicated by the *dotted line* (**b**). The *arrow* in (**b**) indicates the site of transplantation. *LN* lymph node

3.2 Preparation and Transplantation of Mouse Mammary Epithelial Fragments

1. Dissect gland no. 4 from the donor mouse; spread it onto a glass histology slide and cover it with a drop of CO_2-independent medium.
2. Under a dissecting microscope with transmitted illumination, locate the primary duct and the downstream secondary ducts.
3. Using a scalpel, cut tissue fragments of about 1 mm^3 in volume and containing epithelial ducts; steep the dissected fragments in CO_2-independent medium at 4 °C until transplantation (*see* **Notes 6–8**).
4. Make a small pocket in the middle of the cleared fat pad with iris scissors with an angled tip. The pocket should be deep enough to contain the tissue to be grafted, but care should be taken not to cut through the fat pad completely.
5. Insert a piece of donor epithelium into the pocket with the dissecting forceps. Hold the pocket with the skin forceps to keep it closed as you remove the dissecting forceps, so that the inserted tissue remains in place.

3.3 Preparation of Single Mouse Mammary Cells

1. Prepare 15 mL of digestion solution per sample.
2. Dissect both no. 4 glands, remove the lymph nodes, and put the glands on ice in a 100 sterile Petri dish with 500 μL CO_2-independent medium, to prevent the tissue from drying out (*see* **Note 9**).

3. Mince the tissue, first with curved scissors and then with two scalpels, one in each hand, for at least 5 min, until a homogenous paste is obtained (*see* **Note 10**).
4. Transfer the minced tissue to digestion solution.
5. Incubate for 90 min at 37 °C with shaking (150 rpm). Midway through the incubation, shake the tube vigorously to favor dissociation.
6. Transfer the samples to 15 mL tubes and centrifuge for 5 min at 450 × *g*.
7. Discard the upper fat layer and supernatant. Wash the pellet in 15 mL of CO_2-independent medium and centrifuge the tubes for 5 min at 450 × *g*.
8. Resuspend the pellet in 1 mL of trypsin/Versen solution prewarmed to 37 °C and pipette up and down with a 1,000 μL tip for 1 min.
9. Add 8 mL of CO_2-independent medium containing 5 % FCS and centrifuge for 5 min at 450 × *g*.
10. Carefully remove the supernatant, and resuspend the pellet in dispase solution, 2 mL per sample.
11. Add DNase I solution to a final concentration of 0.1 mg/mL. Incubate at 37 °C for 5 min.
12. Add 10 mL of CO_2-independent medium containing 5 % FCS and centrifuge for 5 min at 450 × *g*.
13. Resuspend in 1 mL of cold ammonium chloride solution and centrifuge for 5 min at 450 × *g* (*see* **Note 11**).
14. Resuspend in 1 mL of CO_2-independent medium and filter the cell suspension through a nylon mesh cell strainer with 40 μm pores inserted into a 50 mL tube. Wash the filter with 8 mL of medium.
15. Transfer to a 15 mL tube and centrifuge for 5 min at 450 × *g*.
16. Resuspend the pellet in 1 mL of CO_2-independent medium.
17. Label mammary cells in single-cell suspensions as described elsewhere, and proceed with flow cytometry separation ([4, 6] and other chapters in this book). Alternatively, unsorted mammary cells can be used for transplantation [14].

3.4 Injection of Mammary Epithelial Cells into Cleared Fat Pads

1. Check cell viability by staining with trypan blue and correct cell density accordingly.
2. Prepare the required amount of 25 % growth factor-free Matrigel, by diluting it with CO_2-independent medium (*see* **Note 12**).
3. Prepare the required cell dilutions by resuspending cells in 25 % Matrigel, such that 10 μL cell aliquots can be used for

transplantation (*see* **Note 13**). Try to avoid making bubbles during resuspension of the cells.

4. Using a 25 μL Hamilton syringe, inject 10 μL of cell suspension into the middle of the cleared fat pad (*see* **Notes 14** and **15**). Place the syringe in an oblique position, such that 1–2 mm of the tip penetrates the fat pad, without passing all the way through it. After inoculation, the injected liquid forms a bolus, visible under the fat pad (*see* **Note 16**).
5. Place the skin in its original position and then inject cells into the contralateral fat pad (*see* **Note 5**).

3.5 Closing/Revival of Mouse

1. Use forceps to bring the opposing margins of the skin together, and close with wound clips. Take care not to attach the abdominal wall to the skin. Two clips are normally sufficient to close the midline incision, with one clip required for each lateral oblique incision (*see* **Note 17**).
2. Ear-tag the mouse.
3. Place the mouse on a paper towel in a clean cage and place the cage under a heating lamp until the mouse comes round. The lamp should just warm the mouse, and care should be taken to avoid burning the skin. Give water and food to mice when awaken.
4. The wound clips should be removed after 2–3 weeks.

3.6 Outgrowth Analysis

Typically, outgrowth analysis is performed 6–10 weeks after transplantation (*see* **Note 18**).

1. Euthanize the mouse and place it, on its back, on a corkboard, fixing the limbs in position with needles.
2. Spray the mouse with 70 % ethanol. Make an incision along the longitudinal axis, and a lateral incision between nipples 4 and 5.
3. Using forceps, lift up the skin and gently pull the body wall with the cotton swab until the transplanted fat pad is exposed. The fat pad generally remains stuck to the skin, but it may, in some cases, be attached to the peritoneum.
4. Carefully dissect the transplanted fat pad. For this purpose, pull up the fat pad with tissue forceps, while cutting the transparent membrane attaching the gland to the skin, with sharp fine scissors.
5. Spread the removed fat pad out on a glass histology slide. Make the gland as flat as possible and wait for 5 min, to allow the tissue to stick well to the slide. Fix with MethaCarn for 6–18 h.
6. Place slides in 70 % ethanol for 20 min. Rinse twice with distilled water.

7. Stain with carmine alum overnight at room temperature.
8. Dehydrate the tissue by immersion in successive baths of 70, 95, and 100 % ethanol, for 20 min per bath.
9. Clear in xylene or methyl salicylate until the tissue becomes translucent. For examination and imaging under the dissecting microscope, place the slide in a glass Petri dish with some xylene or methyl salicylate. Peel the tissue off of the glass slide for embedding in paraffin, sectioning, and analysis by standard immunohistological methods.

4 Notes

1. A simple xylazine/ketamine solution has anesthetic properties, but we recommend the addition of flunitrazepam, as it significantly improves the efficacy of anesthesia and the tranquility of the mice during surgery.
2. Use 3-week-old female mice weighing 8–10 g each. Poor outgrowth development is frequently observed in smaller females. However, females weighing more than 12 g should not be used, to prevent the ingrowth of the remaining endogenous epithelium, as the mammary gland may be more developed in larger females.
3. Compound-mutant donor mice often have a mixed genetic background, making the use of syngeneic host mice impossible. Immunodeficient (nude or Scid) mice are used in such cases, to prevent graft rejection.
4. Not all protocols entail removal of the lymph nodes during fat pad clearance. However, whole-mount carmine staining of the removed gland fragments shows that in some 3-week-old animals, the epithelium can reach the lymph node. We therefore recommend staining the removed fat pad fragments in carmine alum, as described in Subheading 3.6, to check for cleared margins.
5. When fragments (or cell populations) from different donors are compared (for example, wild-type and mutant epithelia), they should be transplanted into contralateral fat pads of the same animal. This makes it possible to monitor their growth in the same hormonal environment.
6. In some mouse strains and in aged animals, the fat pad containing gland no. 4 may be thick, making it difficult to dissect out epithelial fragments. Gland no. 3 can be used instead, in such cases.
7. In our experience, keeping fragments in CO_2-independent medium at 4 °C for up to 2 h does not affect their morphogenetic

capacity. Some authors report freezing mammary epithelial fragments in 10 % DMSO according to a classical cell freezing protocol. Frozen fragments can be stored in liquid nitrogen until transplantation, with a minimal decrease in transplantation efficiency (>85 % efficiency) [15].

8. In serial transplantations of epithelial fragments, it is important to use fragments obtained from the center of the outgrowth. Mammary fragments dissected from any part of the mammary tree can give rise to new mammary tissue, but, when serially transplanted, the peripheral ducts may undergo senescence earlier, probably because they have been through more cell divisions [16].
9. For the preparation of a single-cell suspension from virgin mouse mammary glands, we recommend pooling the fourth and fifth glands from at least three or four virgin animals.
10. Some protocols suggest using a tissue chopper (Mcllwain Tissue Chopper, Mickle Laboratory Engineering Co. Ltd.) for mincing the tissue [14].
11. The volume of ammonium chloride solution used should be adapted to the size of the pellet; please follow the manufacturer's instructions.
12. The use of Matrigel for cell injection is optional. However, Matrigel significantly increases outgrowth formation and is particularly recommended when working with small numbers of cells. For example, it has been reported that the transplantation of 75 cells in the absence of Matrigel yields successful reconstitution in 45 % of cases, whereas the addition of 50 % Matrigel increases this percentage to 87.5 % [9].
13. For evaluation of the frequency of repopulating stem cells in limiting dilution transplantations, it is necessary to transplant cells at a minimum of four to five different dilutions. Such dilutions are required, when not all transplanted samples give rise to outgrowths, so that stem cell frequency can be calculated, taking into account the proportion of transplanted fat pads without outgrowths. In our hands, in a typical limiting dilution experiment performed with sorted mammary basal cells from mice of mixed 129SV/C57BL6 genetic background in the presence of 25 % Matrigel, between 5 and 150 cells are transplanted [10]. Increasing the number of dilutions and the number of transplanted fat pads per dilution increases the accuracy of the estimate.
14. We prefer to inject 10 μL aliquots, to prevent cell loss during injection.
15. Always use the same syringe for the injection of a given population and, in limiting dilution experiments, start with the most dilute samples. When two different cell populations are

injected, we use two different syringes to avoid the need to rinse the syringes between injections.

16. Formation of a "bolus" in the place of injection is a sign of successful cell inoculation into the fat pad. On the contrary, if some liquid is visible after removal of the syringe, one can doubt of the efficacy of the injection.
17. Given the fragility of the skin in nude mice, we prefer to stitch up the incision with absorbable sutures (6–7 stitches per mouse) rather than using wound clips. It is always a good idea, in any case, to have some suture available to close the peritoneum if it is accidentally pierced.
18. When very small numbers of cells are transplanted, complete growth may take up to 10–12 weeks. By contrast, the outgrowths develop more rapidly if tissue fragments, rather than sorted cell populations, are transplanted. For the visualization of terminal end buds, the bulbous structures present at the tips of growing ducts, the outgrowths, should be analyzed earlier, before the recipient fat pad is completely filled with the transplanted epithelium. Typically, for grafted wild-type mammary epithelium, terminal end buds can be found in the outgrowths 4–5 weeks after the transplantation of epithelial fragments and 6–7 weeks after the transplantation of sorted mammary basal cells.

Acknowledgements

This work was supported by *La Ligue Nationale Contre le Cancer (Equipe Labelisée 2009, 2013)* and a grant from *Agence Nationale de la Recherche* ANR-08-BLAN-0078-01 to MAG. MAG is *Directeur de Recherche*, MAD and MMF are *Chargé de Recherche* at the *Institut National de la Santé et de la Recherche Médicale (INSERM)*.

References

1. Deome KB, Faulkin LJ Jr, Bern HA et al (1959) Development of mammary tumors from hyperplastic alveolar nodules transplanted into gland-free mammary fat pads of female C3H mice. Cancer Res 19(5):515–520
2. Daniel CW, Deome KB, Young JT et al (1968) The in vivo life span of normal and preneoplastic mouse mammary glands: a serial transplantation study. Proc Natl Acad Sci U S A 61(1):53–60
3. Medina D (2000) The preneoplastic phenotype in murine mammary tumorigenesis. J Mammary Gland Biol Neoplasia 5(4): 393–407
4. Shackleton M, Vaillant F, Simpson KJ et al (2006) Generation of a functional mammary gland from a single stem cell. Nature 439(7072):84–88
5. Sleeman KE, Kendrick H, Robertson D et al (2007) Dissociation of estrogen receptor expression and in vivo stem cell activity in the mammary gland. J Cell Biol 176(1):19–26
6. Stingl J, Eirew P, Ricketson I et al (2006) Purification and unique properties of mammary epithelial stem cells. Nature 439(7079):993–997
7. Al-Hajj M, Wicha MS, Benito-Hernandez A et al (2003) Prospective identification of

tumorigenic breast cancer cells. Proc Natl Acad Sci U S A 100(7):3983–3988

8. Shipitsin M, Polyak K (2008) The cancer stem cell hypothesis: in search of definitions, markers, and relevance. Lab Invest 88(5):459–463
9. Vaillant F, Lindeman GJ, Visvader JE (2011) Jekyll or Hyde: does Matrigel provide a more or less physiological environment in mammary repopulating assays? Breast Cancer Res 13(3):108
10. Chiche A, Moumen M, Petit V et al (2013) Somatic loss of P53 leads to stem/progenitor cell amplification in both mammary epithelial compartments, basal and luminal. Stem Cells 31:1857–1867
11. Hu Y, Smyth GK (2009) ELDA: extreme limiting dilution analysis for comparing depleted and enriched populations in stem cell and other assays. J Immunol Methods 347(1–2):70–78
12. Van Keymeulen A, Rocha AS, Ousset M et al (2011) Distinct stem cells contribute to mammary gland development and maintenance. Nature 479(7372):189–193
13. Zeng YA, Nusse R (2010) Wnt proteins are self-renewal factors for mammary stem cells and promote their long-term expansion in culture. Cell Stem Cell 6(6):568–577
14. Smalley MJ (2010) Isolation, culture and analysis of mouse mammary epithelial cells. Methods Mol Biol 633:139–170
15. Dunphy KA, Tao L, Jerry DJ (2010) Mammary epithelial transplant procedure. J Vis Exp (40). doi:10.3791/1849
16. Daniel CW, Young LJ (1971) Influence of cell division on an aging process. Life span of mouse mammary epithelium during serial propagation in vivo. Exp Cell Res 65(1): 27–32

Chapter 10

Humanization of the Mouse Mammary Gland

A. Wronski, L.M. Arendt, and Charlotte Kuperwasser

Abstract

Although mouse models have provided invaluable information on the mechanisms of mammary gland development, anatomical and developmental differences between human and mice limit full understanding of this fundamental process. Humanization of the mouse mammary gland by injecting immortalized human breast stromal cells into the cleared murine mammary fat pad enables the growth and development of human mammary epithelial cells or tissue. This facilitates the characterization of human mammary gland development or tumorigenesis by utilizing the mouse mammary fat pad. Here we describe the process of isolating human mammary stromal and epithelial cells as well as their introduction into the mammary fat pads of immunocompromised mice.

Key words Human-in-mouse model, Humanization, Human mammary epithelial cells, Stroma, Mammary gland, Mammary gland biology

1 Introduction

The mammary gland is a unique tissue that partially develops during embryogenesis and matures further as the female progresses through sexual maturity and reproduction. Animal models, in particular mouse models, have been heavily used to elucidate the intricate regulatory networks of hormones and growth factors which underpin our current understanding of the development of the mammary gland [1, 2]. However, key differences exist between human and mouse mammary gland, which impedes the applicability of mouse models [3, 4]. These include structural differences between the functional units of the human terminal ductal lobular unit and the mouse lobular-alveolar unit in addition to the composition of the stroma in the human and mouse gland. In the mouse as in the human, the stroma consists of large deposits of adipose tissue in addition to fibrous connective tissue. However, the arrangement of the two tissue types differs between human in mouse. In human glands, the adipose tissue is generally found in large pools and the mammary epithelial cell structures are

Maria del Mar Vivanco (ed.), *Mammary Stem Cells: Methods and Protocols*, Methods in Molecular Biology, vol. 1293,
DOI 10.1007/978-1-4939-2519-3_10,

interspersed with connective tissue. In the mouse, the connective tissue still surrounds the mammary epithelial structures; however, the adipose tissue is more diffuse throughout the gland [4]. These differences between human and mouse mammary glands prohibit the growth of human mammary epithelial cells when introduced into mouse mammary glands [5, 6]. To more closely model the stromal environment of the human breast, a human-in-mouse model was developed. Humanization of the mouse mammary gland by introducing immortalized human mammary stromal cells allows for the implantation of normal human mammary cells or tissue and facilitates the study of human mammary gland development or tumorigenesis [7–10]. Importantly, this model also enables study of the effect of the stromal environment on gland development as well as tumorigenesis [11]. This protocol outlines the methodology of isolating and creating immortalized human mammary stromal and epithelial cells for use in this model, as well as the surgical procedures for clearing and humanizing the mouse mammary gland and introduction of human mammary epithelial cells into the humanized gland.

2 Materials

2.1 Isolation of Primary Mammary Fibroblasts and Epithelial Cells

1. Primary Reduction Mammoplasty Tissue (*see* **Note 1**).
2. Organoid Media (OM): DMEM-Hams F12 (50/50 mixture) supplemented with 10 % calf serum, recombinant human insulin, (10 μg/mL), recombinant human EGF, (10 ng/mL), hydrocortisone, (0.5 μg/mL), 1 % antibiotic/antimycotic (*see* **Note 2**).
3. Digestion Media: Organoid Media supplemented with collagenase (3 mg/mL) and hyaluronidase (600 μg/mL).
4. Surgical scissors and blades (*see* **Note 3**).
5. Rotating incubator at 37 °C.
6. Red blood cell lysing buffer (Sigma-Aldrich, Cat# R7757).
7. Tabletop centrifuge.
8. Wash buffer: 5 % calf serum in PBS.
9. Freezing Media: Organoid Media supplemented with 10 % DMSO and 5 % Calf Serum.
10. DNAse (Roche, Cat# 10104159001, stock at 5 mg/mL).
11. 0.40 μM cell strainer (BD Biosciences, Cat # 352340).

2.2 Cell Culture

1. hTERT Lentiviral particles (*see* **Note 4** for alternative methodology).
2. Reduction Mammoplasty Stromal Media (referred to as RMF media): DMEM (high glucose) supplemented with 10 % fetal calf serum and 1 % antibiotics/antimycotics.

3. 1,000× stock of protamine sulfate (5 mg/mL) or Polybrene (hexadimethrine bromide) (8 mg/mL).
4. Trypsin–EDTA solution (0.05 %).
5. Phosphate buffered solution (PBS).
6. Biosafety cabinet and cell culture incubator.
7. Hemocytometer or cell counter.
8. Low adherent 24 well plates.
9. Bleomycin sulfate (2 mU/mL).
10. 10 mL syringes and 18G needles.
11. Sterile PBS with 0.1 % Bovine Serum Albumin (BSA) solution.

2.3 Animal Surgery

1. Hair clippers or hair removal cream.
2. Petrolatum Ophthalmic Ointment (*see* **Note 5**), we use Puralube Vet Ointment (Dechra NDC 17033-211-38).
3. Betadine solution (1 % iodine).
4. Sterile polyester tipped applicators or cotton swabs.
5. Autoclips and Autoclip Remover.
6. Hamilton removable needle syringe; 100 μL (*see* **Note 6**), Cat# 80630.
7. Hamilton needles 22/22″/2S (Cat# 7758-01).
8. 70 % Ethanol or alcohol swabs.
9. Syringes and needles (approximately 27G).
10. Access to anesthetic (e.g., isofluorane), preferably via an anesthesia machine.
11. Heated surgical pads with nose cones for delivery of anesthesia and/or heating pads.
12. Analgesic (e.g., Buprenex).
13. Surgical saline.
14. Sterile surgical scissors (we use FST Cat #14001-12).
15. Sterile surgical forceps (we use FST Cat# 11050-10 and 11052-10).
16. 3 week old NOD-SCID female mice (Strain: NOD.CB17-Prkdcscid/J; JAX Stock #: 001303).
17. Matrigel solution (BD Biosciences, Cat # 354234).
18. Collagen I, rat tail solution (BD Biosciences, Cat # 354236, at 2 mg/mL *see* **Note 7**).
19. Trimethoprim and Sulfamethoxazole (Septra) solution.

3 Methods

3.1 Isolation of Primary Human Mammary Stromal Cells and Epithelial Cells

Primary human tissue is a potential biohazard and risk assessment and proper biosecurity containment practices as ascertained by your Institutional Biosafety Committee should be followed. *See* **Note 8** for recommendations from the Center of Disease Control (CDC).

1. In Biosafety Cabinet, chop tissue with surgical scissors and/or razors until finely minced. (approximately 5 mm^2 pieces). This should take between 30 and 60 min depending on the volume and composition of tissue.
2. In 15 mL tubes, add 10 mL of digestion media and minced tissue, leaving ~1 cm gap at the top to facilitate movement of liquid and enable homogenization. Seal tubes with Parafilm.
3. Rotate tubes at 37 °C in incubator overnight (approximately 12–16 h), or until tissue slurry is a homogenous color throughout with no tissue chunks (*see* **Note 9**).
4. Centrifuge tubes at $9 \times g$ for 1 min. This will result in three layers forming, an upper oil/fat layer, a middle aqueous layer containing stromal cells, and a semisolid organoid pellet.
5. Remove oil/fat layer using a plastic suction pipette (*see* **Note 10**).
6. Transfer the middle stromal fraction to 50 mL Falcon tubes. Combine stromal fractions from multiple tubes if they are from the same patient sample. Centrifuge tubes for 5 min at $300 \times g$. Aspirate and discard supernatant.
7. Add 2 mL of Red Blood Cell Lysing Buffer to both organoid and centrifuged stromal pellets. (You may combine organoid pellets into 15 or 50 mL tubes if they are from the same patients, ensuring that you can add at least 5 mL of liquid on top for **Step 9**) Mix all tubes.
8. Incubate tubes for 2 min at room temperature.
9. Add 5 mL of wash buffer to each tube and centrifuge at $300 \times g$ for 5 min.
10. Aspirate and discard supernatant.
11. Repeat **steps 9** and **10**. Cell fractions can now be cultured as described below or frozen for later use.
12. To freeze: Resuspend cells in freezing media (*see* **Note 11**) and allow to cool down slowly using an isopropanol-based cooling chamber or insulate in cloth to slow down cooling process. Allow to freeze in −80 °C before placing in liquid nitrogen for long-term storage.

The epithelial-cell containing (organoid) fraction is termed the collagenase pellet (required for Subheading 3.4), whereas the fibroblast/stromal fraction is termed the stromal pellet (required for Subheading 3.2).

3.2 Generation of Immortalized Stromal (RMF-EG) Cells

Cells from primary human tissue and generation of human viruses constitute a biosafety hazard. Risk assessments should be carried out in conjunction with the appropriate Biosafety Committee approval in addition to the utilization of proper biosafety containment procedures.

1. Thaw or use stromal fraction pellet as generated in Subheading 3.1
2. Plate cells onto 100 mm × 20 mm (growth area of 60 cm^2) plates in RMF media and allow stromal cells (*see* **Note 12**) to adhere to plastic (1 h minimum).
3. Wash cells with PBS and apply 0.05 % trypsin. Incubate in 37 °C cell culture incubator for approximately 5 min or until cells are no longer adhered to plate. Quench trypsin with RMF media and pellet cells at 335 × *g* for 5 min. Aspirate and discard supernatant.
4. Resuspend cells in RMF media and count cells using cell counter or hemocytometer.
5. Plate 1×10^5 cells per well in a 6 well plate, including one well as an uninfected control (*see* **Note 13**).
6. Allow cells to adhere for several hours or overnight prior to infection.
7. Pipette 1–10 μL of hTERT viral particles(as directed by manufacturer) with 1× Polybrene or protamine sulfate media to facilitate infection per well. Do not add virus to uninfected control well; however, do add Polybrene, protamine sulfate, or hexadimethrine bromide.
8. Allow to infect overnight and re-feed the cells with RMF media (without additives) 24 h post-infection.
9. Wash cells with PBS and apply 0.05 % trypsin. Incubate in 37 °C cell culture incubator until cells are no longer adhered to plate. Quench trypsin with RMF media and pellet cells at 335 × *g* for 5 min. Aspirate and discard supernatant.
10. Plate each well into a 10 cm plate with RMF media containing the appropriate antibiotics to select for addition of hTERT (*see* **Note 14**).
11. Change the media every 2 days until all uninfected control cells are dead. We term RMF cells immortalized with hTERT-GFP, RMF-EG cells. Expand cells to ~80 % confluency.

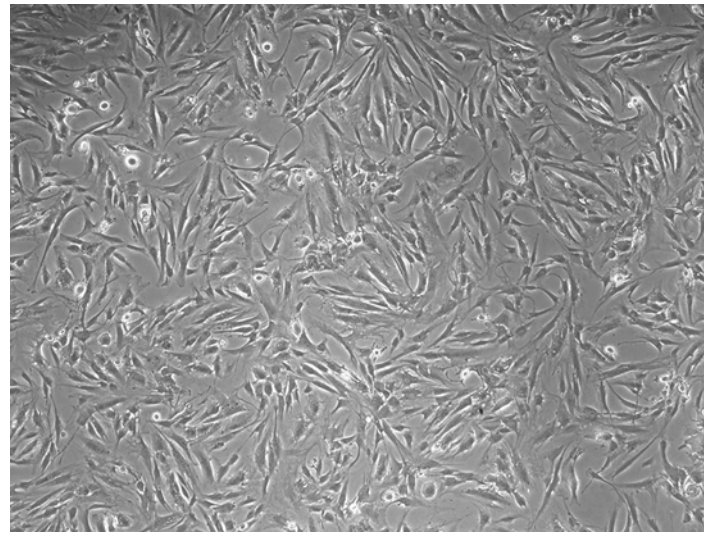

Fig. 1 Immortalized human stromal cells. Bright-field image of confluent RMF-EG (immortalized stromal) cells, isolated from human reduction mammoplasty tissue

Freeze portion for later use (*see* **Note 15**), split 1:3 or use for humanizing. Do not allow cells to reach confluency. An example of near confluent RMF-EG cells is given in Fig. 1.

For cell number requirements for injection of RMF-EG cells for humanization and primary material, *see* **Note 16**.

3.3 Humanizing of Mammary Fat Pads

All animal procedures require permission from your animal ethics board. Conduct surgery in sterile conditions and using aseptic technique.

1. 24 h prior to surgery, add 2 mU/mL bleomycin sulfate to the media of half of the RMF-EG cells to be used for humanizing glands and incubate for 30 min, then change media to RMF media.

   On the day of surgery:

2. Wash bleomycin-treated and untreated RMF-EG cells with PBS and apply 0.05 % trypsin. Incubate in 37 °C cell culture incubator until cells are no longer adhered to plate. Quench trypsin with RMF media and pellet cells at $335 \times g$ for 5 min. Aspirate and discard supernatant.
3. Count cells using cell counter or hemocytometer. Each gland requires 2.5×10^5 cells of bleomycin treated RMF-EG cells and 2.5×10^5 untreated RMF-EG cells. Prepare enough for at least 2 extra mice (i.e., 4 glands). Co-mix treated and untreated cells, pellet, and resuspend in 25 μL of RMF media per gland prepared. Keep on ice until ready to inject.

   For surgery:

4. Disinfect surgical area, including anesthetic box and heated surgical pads
5. Prepare all required tools and materials including preparing the anesthesia machine, turning on bead sterilizer (if required) and warming pads.
6. Place animal to be operated upon in the induction chamber of the anesthesia machine and apply gas flow to approximately 1–3 % if using isofluorane as the anesthetic. Closely monitor the animals to ensure they do not fall too deeply into anesthesia (*see* **Note 17**).
7. When the animal no longer has a toe pinch reflex (i.e., does not respond to pinching of the toe), it is in a surgical plane of anesthesia.
8. Apply ophthalmic ointment to eyes and place animal in lateral recumbency (*see* Fig. 2a) on a heated surgical station in a nose cone to continue administration of anesthesia.
9. Shave a 3 cm square area starting 1 cm below the spine and extending ventrally to the level of the level of the kneecap and over the abdomen starting 1 cm from the rib cage and extending caudally to the leg (Fig. 2a). Apply Betadine solution to the whole area.
10. Turn mouse over and repeat **Step 8** on other side.
11. Wipe the Betadine solution off with an alcohol wipe, sterilizing the area. You may be able to see the darkened spot of the lymph node through the skin (Fig. 2a). If you cannot see it, move the leg up and down, the lymph node should also move.
12. Make a small incision (approximately 2 cm) over the surface of the lymph node (Fig. 2b). The lymph node should be present at the level of the kneecap. Expose the lymph node, and with the scissors, cut the mammary gland immediately dorsal to the

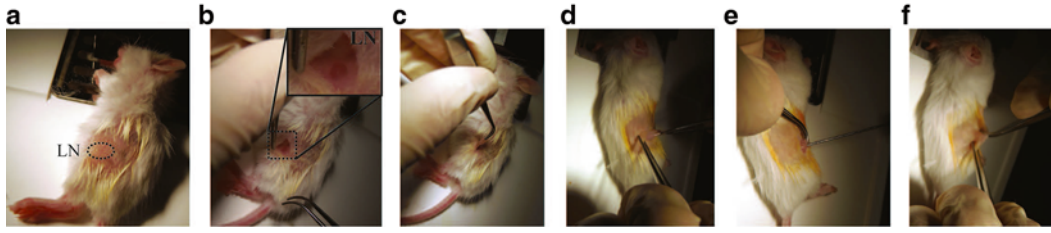

Fig. 2 Surgical steps for humanizing mammary fat pad. (**a**) Mouse in lateral recumbency under anesthesia with example of area to be shaved for incision. Approximate location of lymph node, which may be visible under the skin, is indicated. (**b**) Incision for clearing of mammary fat pad and identification of the lymph node (magnified in inset). Incision was made larger than required to adequately visualize the lymph node. (**c**) Retraction of the mammary lymph node in preparation for excision. (**d**) Retraction of remaining mammary fat pad tissue to prepare for injection. (**e**) Injection of RMF-EG cells into mammary fat pad using a Hamilton syringe. (**f**) Tenting of skin to facilitate placement of wound clips to close incision site

lymph node (Fig. 2c). Gently retract the mammary gland containing the lymph node, and with the forceps, free the mammary gland from the skin and abdomen. Using the scissors, excise the mammary gland near the nipple, removing the lymph node and endogenous epithelium.

13. Gently pull the remaining fat pad tissue away from the skin to prepare to inject into it (Fig. 2d).
14. Mix RMF-EG solution and using Hamilton Syringe draw up 25 μL of cells. Carefully slide syringe into outstretched fat pad taking care not to pierce through the tissue. Slowly inject the cells into the gland (Fig. 2e), ensuring the cells are not leaking out of the gland. A small bolus should form at the site of injection. Slowly withdraw the syringe, twisting as you exit to stem leakage from the injection site.
15. Tuck tissue back under the skin and pull skin together, forming a tent (Fig. 2f). Clip wound closed using autoclips.
16. Turn mouse over and repeat **steps 10–15** to inject second gland.
17. Inject 100 μL of saline subcutaneously to aid hydration and recovery. Administer analgesic as per ethics protocol.
18. Place animal back into cage under heat lamp and monitor for recovery.
19. Check welfare of animals as required by your animal ethics protocol. Ensure surgical clips remain in place and replace if they get torn off or displaced. Remove clips after approximately 10 days or as stipulated by your animal ethics protocol. Mice are given antibiotics (we use sulfamethoxazole) in their drinking water for 2 weeks post-surgery.
20. Properly humanized glands look pale/white when the incision site is reopened for injection of further material in the humanized gland. Hematoxylin and Eosin staining of a humanized fat pad is depicted in Fig. 4a.
21. Allow cells to humanize gland for 2 weeks before injecting normal HMECs or organoids for further study.

3.4 Preparation of Human Mammary Epithelial Cells (HMECs)

Tumor organoids, xenograft tissue or HMECs can be injected into the humanized stroma. *See* (refs. [7, 8, 10]). This is an example using primary HMECs.

On the day of surgery:
Allow Matrigel to thaw on ice

1. Thaw vial of collagenase pellet generated as per Subheading 3.1
2. Resuspend cells in 10 mL RMF media and plate on a 10 cm plate. Incubate for 1–2 h at 37 °C in tissue culture incubator. The fibroblasts will adhere, whereas the epithelial organoids will float in culture (Fig. 3a, b).

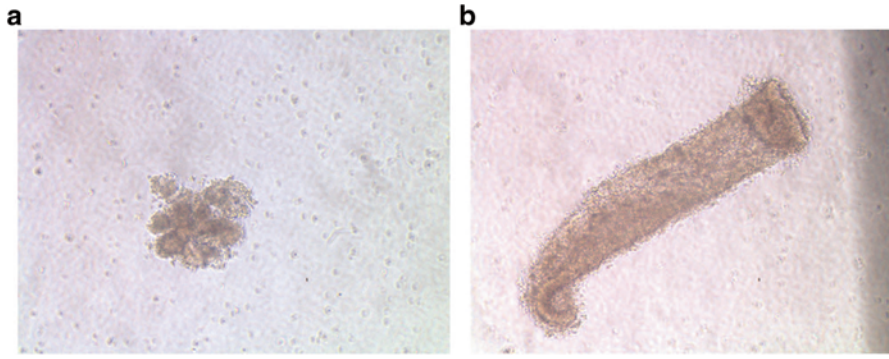

Fig. 3 Human mammary epithelial cell organoids. (**a** and **b**) Bright-field images of human mammary epithelial cells floating in culture under adherent conditions. Note the degree of cell clumping

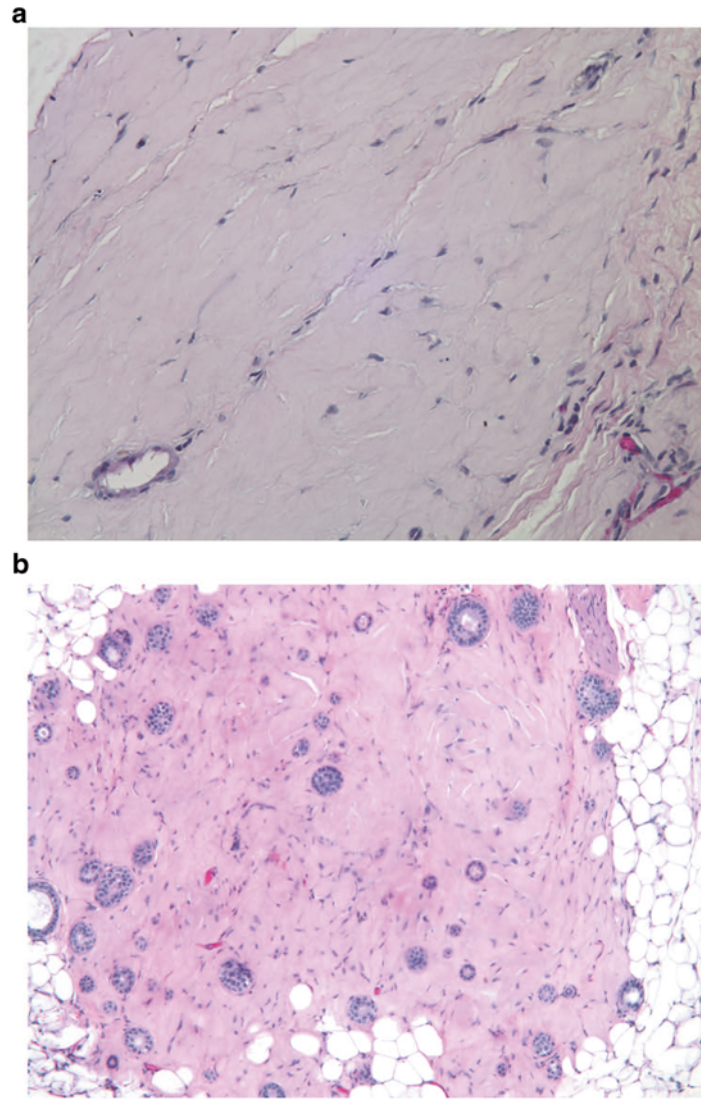

Fig. 4 Hematoxylin and Eosin (H and E) staining of humanized mammary gland. (**a**) H and E stained humanized mammary fat pad prior to injection of HMECs. (**b**) H and E staining of humanized mammary gland injected with human mammary epithelial cells indicative of normal human mammary gland architecture

3. Collect media containing non-adherent cells into a 50 mL tube, wash plates with 10 mL of PBS and add to 50 mL tube. Centrifuge cells at 233 × *g* for 5 min. If you wish to use the remaining stromal cells, feed adherent stromal cells on 10 cm plate with 10 mL RMF media and culture until near confluency and then freeze or use as necessary.
4. Aspirate and discard supernatant and resuspend pellet in 10 mL of cold PBS/0.1 % BSA solution. Homogenize pellet by passing it through an 18G needle eight to ten times.
5. Centrifuge organoids at 233 × *g* for 5 min. Discard supernatant.
6. Resuspend pellet in 2 mL 0.05 % trypsin–EDTA. Pipette solution with a 1 mL pipette vigorously for 1 min to break up organoids. Incubate at 37 °C for 5 min. Pipette solution vigorously for another 1 min then incubate again at 37 °C for 5 min.
7. Mix with a 1 mL pipette to break up cell clumps. Inactivate trypsin by adding 10 mL RMF media and 100 μL DNAse to digest DNA from dead cells.
8. Mix by pipetting then filter through a 0.45 μm filter into a 50 mL conical tube.
9. Wash the filter with an additional 10 mL of RMF media.
10. Centrifuge filtered cells and media at 233 × *g* for 5 min and resuspend pellet in RMF or HMEC media. Count cells (*see* **Note 18**) with cell counter or hemocytometer. Each gland to be injected requires 1×10^5 HMECs.
11. Keep cells on ice prior to injection.
12. Wash RMF-EG cells (not bleomycin treated) with PBS and apply 0.05 % trypsin. Incubate in 37 °C cell culture incubator until cells are no longer adhered to plate. Quench trypsin with RMF media and pellet cells at 335 × *g* for 5 min. Aspirate and discard supernatant.
13. Count RMF-EG cells

For each gland, you require 2.5×10^5 RMF-EG cells combined with 1×10^5 HMECs/gland. Combine the appropriate number of each cell type and pellet cells (we suggest preparing cells for at least 2 extra injections).

14. Aspirate and discard supernatant and resuspend in 30 μL per gland of a 1:1 solution of collagen and Matrigel.
15. Keep on ice until ready to inject.

3.5 Injection of Material for Further Study

1. Disinfect surgical area, including anesthetic box and heated surgical pads.
2. Prepare all required tools and materials including preparing the anesthesia machine, turning on bead sterilizer (if required) and warming pads.

3. Place animal to be operated upon in anesthesia machine and apply gas flow as appropriate. Closely monitor the animals to ensure they do not fall too deeply into anesthesia (*see* **Note 17**).
4. When the animal no longer has a toe pinch reflex (i.e., does not respond to pinching of the toe or webbing of the foot), it is deep enough under and should not sense pain.
5. Apply ophthalmic ointment to eyes and place animal in lateral recumbency (*see* Fig. 2a) on a heated surgical station in a nose cone to continue administration of anesthesia.
6. Shave area as described above (Fig. 2a) from the knee of the animal towards the rib cage and dorsally toward the spine. Apply Betadine solution to the whole area.
7. Turn mouse over and repeat **Step 8** on other side.
8. Wipe the Betadine solution off with an ethanol wipe, sterilizing the area.
9. Make a small incision dorsal to the scar tissue from the previous humanization incision.
10. Using your forceps, gently retract the humanized mammary gland away from the skin to prepare for injection, similar to Fig. 2d. The humanized area will have a white color in comparison to surrounding tissue.
11. Briefly agitate the cell mixture to be injected and aspirate 30 μL into the Hamilton Syringe (*see* **Note 6**).
12. Carefully thread the syringe into the outstretched humanized gland and inject the cells into the gland. Ensure you do not push through the gland with the syringe and there are no leaks. You should observe a bolus where the cells have been injected if successful.
13. Tuck the tissue under the skin and pull skin together over the top, forming a tent (Fig. 2f). Clip wound closed using autoclips.
14. Turn mouse over and repeat **steps 9–13** to inject second gland (*see* **Note 19**).
15. Administer analgesic as per ethics protocol.
16. Place animal back into cage under heat lamp and monitor for recovery.
17. Check welfare of animals twice a day for 3 days. Ensure surgical clips remain in place and replace if they get torn off or displaced. Remove clips after approximately 10 days or as stipulated by your animal ethics protocol. Mice are given antibiotics in their drinking water (we use sulfamethoxazole) for 2 weeks post-surgery.
18. Allow glands to grow for approximately 8 weeks before removing and assaying gland development and growth by whole-mount, staining, or sectioning. An example of Hemaotoxylin and Eosin staining is displayed in Fig. 4.

4 Notes

1. Human breast reduction tissue should be obtained in accordance with the regulations of the Institutional Review Board.
2. We suggest a combination of 10,000 U/mL penicillin G, 10 mg/mL streptomycin sulfate and 25 μg/mL amphotericin B, such as Corning Cellgro Cat# 30-004-CI.
3. We alternate between using several techniques, based on personal preference. Some find it easier to loosen the tissue by chopping it with large surgical scissors and then slice it with a scalpel blade, while others prefer to use large razors blades mounted on hemostat forceps.
4. You can also generate your own hTERT lentiviral particles using plasmids readily available from Addgene (pBABE-hTERT plasmid, either in hygromycin (Addgene Plasmid #1773) or puromycin (Addgene Plasmid # 1771)) and 293 T cells (ATCC #CRL-3216). Detailed instructions and protocols are available on http://www.addgene.org/lentiviral/.
5. Anesthesia reduces the blink reflex, leading to drying out of the eyes.
6. We use a 100 μL syringe as we find it easier to work with.
7. To make up 2 mg/mL of collagen, follow instructions for the "Alternate Gelation Procedure for BD Collagen I, rat tail" enclosed in the product manual on the BD Website: http://www.bdbiosciences.com/ptProduct.jsp?prodId = 362369. Check pH using a pH test strip and adjust pH to ~7–7.5 by adding either sterile NaOH or HCl as necessary.
8. Appendix H—Working with Human, NHP and Other Mammalian Cells and Tissues from the Biosafety in Microbiological and Biomedical Laboratories (BMBL) 5th Edition. http://www.cdc.gov/biosafety/publications/bmbl5/BMBL5_appendixH.pdf
9. If liquid still contains large chunks of tissue after incubation, it is most likely that the tissue was not chopped finely enough in **Step 1** or too much tissue was placed in each tube, inhibiting enzymatic dissociation. Ensure tissue is finely minced prior to incubation and that the liquid can move freely when rotated.
10. Use of plastic suction pipettes greatly reduces the possibility of skin penetration by biohazardous sharps, thereby reducing the potential of the spread of blood-borne pathogens.
11. We do not count the number of cells, as this is does not give an accurate representation of the number of viable cells, rather

divide the cells in a third of the number of 15 mL tubes that were used in **step 2**, i.e., 25 tubes would equal roughly 8 tubes to be cryopreserved.

12. This selection method enriches for fibroblasts, adipocytes and pre-adipocytes. These cells are difficult to distinguish in culture, because adipocytes and pre-adipocytes lose their lipid droplets when grown on plastic. Stromal cells proliferate more rapidly than contaminating epithelial cells, particularly in the presence of serum, and outcompete any remaining epithelial cells.
13. Optimization may be required to achieve ideal cell confluency of ~70 % on day of infection.
14. The amount of antibiotic used may need to be optimized to balance cell toxicity and selection. Working concentration for puromycin range from 0.2 μg/mL to 5 μg/mL whereas Hygromycin B is used from 50 μg/mL to 500 μg/mL.
15. To minimize the number of population doublings and genetic variation between experiments, we generally do not use a sample of non-immortalized RMF cells for more than a month. We suggest once a stable population of cells is created to expand and freeze a large number of vials for later use.
16. Humanization (Subheading 3.3) requires at least 1–15 cm plate of RMG-EG cells at 80 % confluency (Fig. 1) per animal. Primary material (e.g., HMECs) to be injected into the humanized gland are also co-mixed with RMF-EG cells (Subheading 3.4) and requires at least 2×10^5 cells per mouse.
17. Aim for a medium anesthesia, or plane 2 in which muscles are relaxed, yet respiration still occurs. Monitor animal for continuous albeit slow breathing and reduce dosage of anesthesia if animal cannot respirate due to paralysis of the diaphragm and intercostal muscles. See http://www.ahc.umn.edu/rar/anesthesia.html for more details.
18. It is very difficult to estimate cell number as not all of the cells may be viable. Thus, to ensure you have enough cells to inject into animals, greatly over-compensate by plating as many cells as possible.
19. As many cells get trapped in the hub of the needle—we do not wash out the syringe for every injection, only washing the syringe out by pumping water through the n between samples. We inject the positive control last to avoid contamination.

References

1. Hennighausen L, Robinson GW (2005) Information networks in the mammary gland. Nat Rev Mol Cell Biol 6(9):715–725
2. Smith BA, Welm AL, Welm BE (2012) On the shoulders of giants: a historical perspective of unique experimental methods in mammary gland research. Semin Cell Dev Biol 23(5):583–590, http://dx.doi.org/10.1016/j.semcdb.2012.03.005
3. Gusterson BA, Stein T (2012) Human breast development. Semin Cell Dev Biol 23(5):567–573, http://dx.doi.org/10.1016/j.semcdb.2012.03.013
4. Parmar H, Cunha GR (2004) Epithelial-stromal interactions in the mouse and human mammary gland in vivo. Endocr Relat Cancer 11(3):437–458
5. Sheffield LG, Welsch CW (1988) Transplantation of human breast epithelia to mammary-gland-free fat-pads of athymic nude mice: influence of mammotrophic hormones on growth of breast epithelia. Int J Cancer 41(5):713–719
6. Outzen HC, Custer RP (1975) Growth of human normal and neoplastic mammary tissues in the cleared mammary fat pad of the nude mouse. J Natl Cancer Inst 55(6):1461–1466
7. Kuperwasser C, Chavarria T, Wu M, Magrane G, Gray JW, Carey L, Richardson A, Weinberg RA (2004) Reconstruction of functionally normal and malignant human breast tissues in mice. Proc Natl Acad Sci U S A 101(14):4966–4971. doi:10.1073/pnas.0401064101
8. Keller PJ, Arendt LM, Skibinski A, Logvinenko T, Klebba I, Dong S, Smith AE, Prat A, Perou CM, Gilmore H, Schnitt S, Naber SP, Garlick JA, Kuperwasser C (2012) Defining the cellular precursors to human breast cancer. Proc Natl Acad Sci U S A 109(8):2772–2777. doi:10.1073/pnas.1017626108
9. Proia TA, Keller PJ, Gupta PB, Klebba I, Jones AD, Sedic M, Gilmore H, Tung N, Naber SP, Schnitt S, Lander ES, Kuperwasser C (2011) Genetic predisposition directs breast cancer phenotype by dictating progenitor cell fate. Cell Stem Cell 8(2):149–163. doi:10.1016/j.stem.2010.12.007
10. Proia DA, Kuperwasser C (2006) Reconstruction of human mammary tissues in a mouse model. Nat Protoc 1(1):206–214
11. Arendt LM, Rudnick JA, Keller PJ, Kuperwasser C (2010) Stroma in breast development and disease. Semin Cell Dev Biol 21(1):11–18. doi:10.1016/j.semcdb.2009.10.003

Chapter 11

Lineage Tracing in the Mammary Gland Using Cre/lox Technology and Fluorescent Reporter Alleles

Renée van Amerongen

Abstract

Lineage tracing using Cre/lox technology has become a well-established technique to study the contribution of different (stem) cell populations to organ development and function. When used in the mammary gland, it forms a valuable addition to the already existing experimental toolbox and an important alternative to other readouts measuring stem cell potential, such as the fat pad transplantation assay.

Here I describe how to set up and analyze an in vivo lineage tracing experiment using tamoxifen-inducible Cre/lox technology, highlighting the specific challenges that the investigator faces when employing this method and interpreting the results in the mammary gland.

Key words Lineage tracing, Mammary gland stem cells, Tamoxifen, Whole mount, Confocal microscopy

1 Introduction

Owing to its unique developmental properties, the mouse mammary gland is an excellent model system to study various biological processes associated with tissue growth and regeneration. Located immediately below the skin and well outside the body cavity, it offers easy access. Moreover, it is a non-essential organ, thus allowing relatively straightforward experimental manipulation. More important than these practical considerations, however, are its morphological and functional characteristics. Biologically speaking, the mammary gland is a very dynamic tissue that undergoes dramatic changes in cell proliferation and differentiation during the life span of an organism [1].

The adult mouse mammary gland is composed of a bilayered, ductal epithelium that lies embedded in the stromal tissue of the fat pad (Fig. 1). This elaborate ductal network forms during puberty, when rapid branching morphogenesis causes the rudimentary mammary epithelium to grow out and invade the entire length of the fat pad. During pregnancy, a second wave of tissue expansion

Maria del Mar Vivanco (ed.), *Mammary Stem Cells: Methods and Protocols*, Methods in Molecular Biology, vol. 1293,
DOI 10.1007/978-1-4939-2519-3_11,

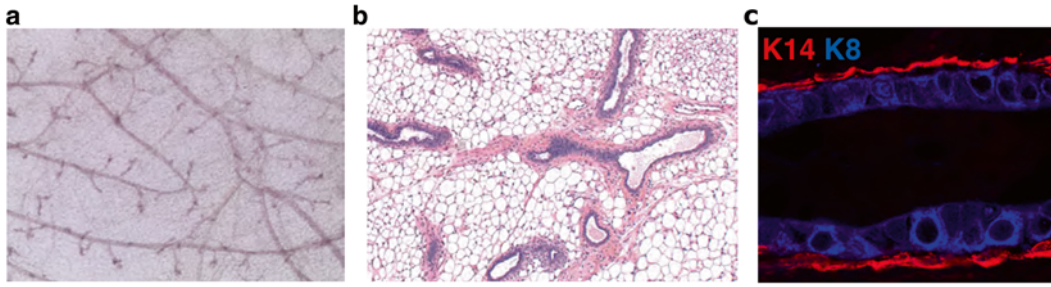

Fig. 1 Macroscopic and microscopic appearance of the mouse mammary gland. (**a**) Whole-mount picture of a carmine stained mouse mammary gland reveals a branched ductal network. (**b**) Tissue section of a hematoxylin/eosin stained mouse mammary gland reveals how the ductal epithelium lies embedded in the stromal tissue of the fat pad, which consists mostly of adipocytes. (**c**) Cross section of the mouse mammary epithelium revealing the bilayered appearance of the epithelium following immunofluorescent detection of basal, K14-positive (*red*) and luminal, K8-positive (*blue*) cells

occurs, this time associated with the formation and terminal differentiation of milk-producing alveoli. After lactation, these alveolar structures regress in a process called involution, when massive tissue remodeling takes place and the gland is essentially restored to a pre-pregnancy state.

Both developmental and cancer biologists have long been fascinated by these dynamic growth properties and in particular by the identity of the underlying stem and progenitor cell populations. As a result, a wide variety of experimental techniques exist to probe mammary cell behavior and function [2]. These include the prospective isolation of distinct cell populations based on the combinatorial expression of defined cell-surface markers by fluorescence-activated cell sorting (FACS) [3, 4] and their subsequent transplantation into the cleared fat pad [5]. First devised in the late 1950s, this transplantation assay remains a robust and powerful method to test the regenerative capacity of putative stem cell populations. However, it is important to realize that it requires cells to be taken out of their natural environment. In contrast, dedicated in vivo lineage tracing studies are designed to track cell fate in situ. Importantly, a direct comparison of the two experimental approaches has revealed important differences between the normal developmental potential tested by lineage tracing and the regenerative potential displayed by the same cell population upon transplantation [6, 7].

In this chapter I provide stepwise instructions for setting up and analyzing an in vivo lineage tracing experiment using genetically engineered mouse models and Cre/lox technology. This includes breeding of the required compound genotypes, initiation and duration of the trace, processing of the mammary gland for histological analysis, and 3D reconstruction using the Fiji software program. I specifically focus on the practical considerations related to tamoxifen-inducible Cre driver lines and (multicolor) fluorescent reporter alleles.

2 Materials

2.1 Compound Mutant Mice

Given the amount of time and money involved with long-term, in vivo lineage tracing analyses, selection of the genetically engineered mouse strains with which to perform the experiment is the most crucial step of the entire experiment. Ample time should be dedicated to making this decision. Ultimately the choice is up to the investigator, as it will depend on the specific research question. Although alternatives exist (*see* **Note 1**), the most straightforward and flexible approach is to make use of the tried and tested Cre/lox technology [8, 9].

In this scenario, the first mouse strain (hereafter referred to as the "Cre driver") should express the Cre recombinase protein in the cell population of interest (i.e., the cell population of which the investigator wishes to study the developmental fate). Spatial control is provided by the promoter and enhancer sequences used to drive Cre expression (*see* **Note 2**). Modified versions of the Cre protein (Cre^{ER}, Cre^{ERT}, or Cre^{ERT2}, *see* **Note 3**) in addition offer temporal control, allowing the investigator to decide the onset of Cre recombinase activity and thus the developmental time point at which the tracing experiment is initiated. In most cases, this is recommended (*see* **Note 4**). The Jackson mouse repository offers a large selection of (inducible) Cre strains (http://cre.jax.org/index.html). Practical considerations and pitfalls associated with selecting the appropriate Cre driver are discussed elsewhere [10, 11]. Ultimately, however, investigators may feel the need to generate novel Cre driver lines, as these will be best suited to address their specific research question. This falls out of the scope of the current chapter.

The second mouse strain (hereafter referred to as the "reporter") needs to meet two criteria. First, it should contain a conditional, Cre-inducible reporter allele that will "switch" from state A to state B in the presence of Cre-recombinase activity. This marks the cell population of interest (*see* **Note 5**). Second, after Cre-mediated recombination, expression of the marker gene itself should be driven by a constitutively active promoter, such that all cells in the lineage can be visualized at any given time point. Multiple Cre/lox technology based reporter lines are available from the Jackson mouse repository (http://jaxmice.jax.org/list/xprs_creRT1805.html). The simplest versions are binary OFF/ON switches, such as the trustworthy *Rosa26-lacZ* reporter [12]. More sophisticated reporters, such as the *Rosa26-mTmG* line [13], allow cells to be visualized both before and after recombination by switching on the expression of a different fluorescent protein. Yet other reporters, such as the *Rosa26-Confetti* line [14] are specifically suited for studying the clonal outgrowth of individual stem cells. Again, the choice of reporter will depend on the specific

research question to be addressed (*see* **Note 6**). Some characteristics of the three reporter lines mentioned above, pertaining to their use for lineage tracing in the mammary gland, are compared in Table 1.

As an example, the remainder of this protocol will assume the presence of the following mouse strains:

1. *Axin2-Cre^{ERT2}* (available from Jackson labs, stock #018867): a tamoxifen-inducible Axin2-Cre^{ERT2} allele [6] that marks Wnt/β-catenin responsive cells based on their expression of the negative feedback target gene *Axin2*.
2. *Rosa26-mTmG* (available from Jackson labs, stock #007676): a Cre-inducible reporter allele that marks all cells in the animal with a membrane-bound dTomato (mT) fluorescent protein prior to recombination. Cells that recombine the reporter allele lose mT expression and gain expression of a membrane-bound eGFP (mG) fluorescent protein.
3. *Axin2-Cre^{ERT2}*;*Rosa26-mTmG* double-heterozygous mice (*see* **Note 7**) in which the actual lineage tracing experiment is performed (Fig. 2).

2.2 Inducing Tamoxifen-Mediated Recombination

1. Gloves.
2. Tamoxifen solution: Dissolve tamoxifen (Sigma, *see* **Note 8**) at 5–20 mg/ml in 90 % corn oil (Sigma) and 10 % ethanol. A standard stock of 10 mg/ml tamoxifen consists of 10 mg tamoxifen, 900 μl corn oil, and 100 μl ethanol (*see* **Note 9**).
3. Corn oil control solution: Mix 900 μl corn oil and 100 μl ethanol.
4. Nutator mixer or tube roller.
5. Two 3 ml syringes.
6. Two 22 μm syringe filters.
7. Two 1.5 ml or 2 ml eppendorf tubes.
8. Two 1 ml BD™ slip-tip syringes with 26 G × 5/8 in. subQ needles.

2.3 Harvesting the Mammary Glands

1. Euthanasia chamber.
2. Dissection pad.
3. Spray bottle with 70 % ethanol.
4. 6–8 Pushpins.
5. One pair of surgical scissors.
6. One eppendorf tube.
7. One pair of Dumont No. 5 forceps.
8. Two pairs of fine (Iris or Graefe) forceps.
9. Four pieces of 3 mm Whatman paper, 4 cm × 1 cm each.

Table 1
Comparison of the *Rosa26-lacZ* (generated by the lab of Phil Soriano [12]), *Rosa26-mTmG* (generated by the lab of Liqun Luo [13]) and *Rosa26-Confetti* (generated by the lab of Hans Clevers [14]) reporter lines

Strain	Official name	Jackson strain	Before Cre	After Cre
Rosa26-lacZ	B6.129S4-Gt*(ROSA)26Sortm1Sor*/J	003474	Unlabeled	lacZ
Rosa26-mTmG	B6.129(Cg)-*Gt(ROSA)26Sortm4(ACTB-tdTomato,-EGFP)Luo*/J	007676	dTomato	EGFP
Rosa26-Confetti	B6.129P2-Gt*(ROSA)26Sortm1(CAG-Brainbow2.1)Cle*/J	017492	Unlabeled	CFP, GFP, YFP, or RFP
Strain	Detection	Advantages	Disadvantages	
Rosa26-lacZ	– Enzymatic detection of β-galactosidase activity by X-gal staining	– Sensitive and robust – Allows early detection (24 h after Cre) – Allows co-staining with structural markers by IHC – Permanent record of X-gal stained tissue slides	– No direct detection of recombined cells in unfixed material – Not suited for confocal analysis – Not well suited for live-cell sorting by FACS	
Rosa26-mTmG	– Direct fluorescence – anti-GFP staining (IHC or IF)	– Both dTomato en EGFP are membrane bound, which nicely visualizes the cell outlines and provides free structural information – Well suited for whole-mount confocal analysis –Well suited for FACS analysis	– Earliest detection in the mammary gland at 48 h after Cre – No permanent record (unless stained with anti-GFP by IHC)	
Rosa26-Confetti	– Direct fluorescence	– Allows individual cell clones to be discriminated with more certainty – Allows “re-switching” of already recombined cells – Suited for whole-mount confocal analysis	– Recombination in the mammary gland is very inefficient – No permanent record	

Each line has its own advantages and disadvantages. Abbreviations: *IF* immunofluorescence; *IHC* immunohistochemistry; *FACS* fluorescence-activated cell sorting

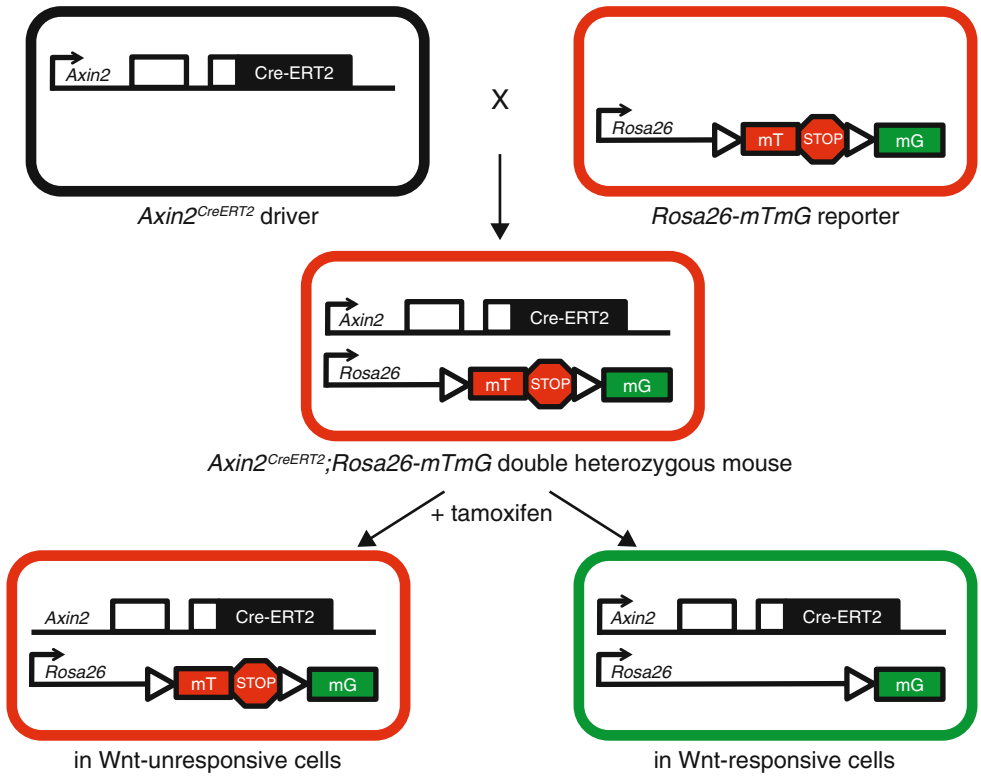

Fig. 2 Lineage tracing with the *Axin2-Cre* ^{ERT2} driver and the *Rosa26-mTmG* reporter. Schematic depicting the genetic principle behind Cre/lox-mediated lineage tracing. After crossing *Axin2-CreERT2* and *Rosa26-mTmG* mice (*top*), double-heterozygous offspring will express the Cre recombinase in all Axin2-positive, Wnt/β-catenin responsive cells (*middle*). However, owing to the presence of an ERT2 moiety, the Cre recombinase will be inactive. Therefore, prior to tamoxifen administration, all cells in the animal will be *red*, due to expression of a membrane-bound dTomato, which is expressed from the *Rosa26* reporter allele. The administration of tamoxifen will result in a pulse of Cre-activity in Axin2-positive, Wnt/β-catenin responsive cells, which in turn will recombine the *Rosa26-mTmG* reporter allele. This results in a switch from membrane-bound dTomato to membrane-bound GFP expression in Wnt-responsive cells, but not in Wnt-unresponsive cells (*bottom*). Because the switch is genetic, it is permanent and will remain present for the remainder of the life span of the recombined cell. In addition, it will be passed on to the cell's offspring, allowing its lineage to be traced

10. Glass vial with 10 % neutral buffered formalin (4 % paraformaldehyde).
11. Aluminum foil.

2.4 Whole-Mount Confocal Analysis of Fluorescent Reporter Alleles

1. Nutator mixer or tube roller.
2. Phosphate buffered saline (PBS) solution.
3. 30 % Ethanol: 30 ml ethanol in 70 ml PBS.
4. 50 % Ethanol: 50 ml ethanol in 50 ml PBS.
5. 70 % Ethanol: 70 ml ethanol in 30 ml deionized H_2O.
6. 100 % Ethanol.

7. Glass vial with methylsalicylate (*see* **Note 10**).
8. Single concave microscope slide (14 mm diameter).
9. #1.5 Coverslip.
10. Nail polish.
11. Confocal microscope with 488 nm and 561 nm laser lines for *Rosa26-mTmG* or with 458 nm, 488 nm, 514 nm, and 561 nm laser lines for *Rosa26-Confetti* (*see* **Note 11**).
12. Acetone.
13. Kleenex tissues.
14. Glass vial with paraffin.
15. Paraffin for refreshing.
16. Hybridization oven.
17. Embedding cassette.
18. Computer with Fiji software (downloadable from http://fiji.sc/Fiji).

3 Methods

3.1 Inducing Cre-Mediated Recombination

1. Design the appropriate lineage-tracing experiment (Fig. 3).
2. Breed *Axin2-Cre^{ERT2}*;*Rosa26-mTmG* double-heterozygous mice, which carry both the Cre-driver and the reporter allele, by intercrossing the *Axin2-Cre^{ERT2}* and the *Rosa26-mTmG* strains. I usually cross a heterozygous *Axin2-Cre^{ERT2}* male to a homozygous *Rosa26-mTmG* female. Half of the offspring will be double-heterozygous (*see* **Note 12**).
3. Genotype the mice by PCR (*see* **Notes 13–15**).
4. Divide the mice into experimental cohorts (*see* **Notes 16–19**).
5. Prepare the tamoxifen and the corn oil control solution. It is best to always prepare these fresh. Remember to wear gloves when handling tamoxifen!
6. Incubate the solution on a nutator or tube roller. Tamoxifen will take some time to dissolve.
7. Filter the solutions through a 22 μm syringe filter into an eppendorf tube (*see* **Note 20**).
8. When you are ready to inject the mice, fill a 1 ml syringe attached to a subQ needle with each of the solutions (*see* **Note 21**).
9. Remove all air bubbles by holding the syringe vertically, pulling down on the plunger and flicking the syringe with your fingers to force the air to the top.
10. Insert the plunger to let all air escape.
11. Put down the syringe and open the mouse cage.

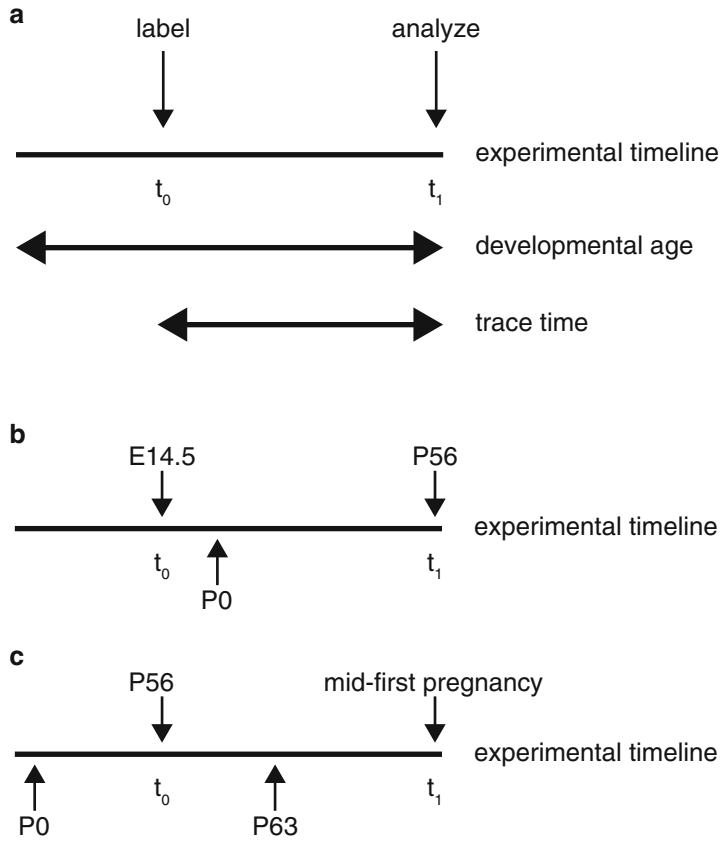

Fig. 3 Experimental setup of an in vivo lineage tracing experiment. (**a**) Timeline depicting the two critical time points of a lineage tracing experiment. Using an inducible system, Cre-mediated recombination can occur at any time of choice. The time point at which the cells are labeled following tamoxifen administration (t_0) represents the onset of the actual tracing experiment. The trace can be stopped for analysis at any time point greater than 24 h (the minimum amount of time for reporter activity to be detectable) after tamoxifen administration (t_1). (**b**) The trace can be started prior to birth by administering tamoxifen to pregnant mothers. As an example, recombination can be induced in E14.5 embryos, after which the mice are traced through puberty and analyzed as adults at 8 weeks (56 days, P56) of age. (**c**) Alternatively, the trace can start at any time after birth. As an example, recombination can be induced at P56, after which the cells are analyzed at mid-pregnancy

12. Holding it by the tail, lift the mouse that is to be injected out of the cage.
13. Lower the mouse onto the wire rack of a cage lid and let it grab hold of the bars.
14. With the thumb and index finger of your other hand, firmly grab the loose skin at the back of its neck and pull back to secure its head.

15. Turn the mouse over and secure its tail between your fourth finger or pinky and the palm of your hand. Slightly tilt your hand, such that the head of the mouse is lower that its abdomen. Your other hand should now be free again (*see* **Note 22**).
16. Pick up the syringe and gently insert it into the lower right quadrant of the abdomen at an approximately 30-degree angle (*see* **Note 23**).
17. Pushing down on the plunger, inject the required amount of tamoxifen (*see* **Notes 24–27**).
18. Pull back the syringe. Dispose of it immediately if you are done injecting and a sharps container is within reach. Alternatively, put down the syringe and dispose of it in a sharps container after you have finished injecting all mice and the animals have been returned to the cage (*see* **Note 28**).

3.2 Tracing

1. In the first few days after administering tamoxifen, check on the mice regularly to ensure there are no ill side effects of tamoxifen administration.
2. Wait for the desired amount of trace time to pass (*see* **Note 29**). If required, set up timed-matings to trace the contribution of your cell population of interest to alveoli formation during pregnancy.

3.3 Analyzing the Trace Experiment by Whole-Mount Confocal Microscopy

1. Transfer the mouse to a euthanasia chamber.
2. Start the flow of CO_2 to euthanize the animal (*see* **Note 30**).
3. Confirm that the animal is dead.
4. Spray the mouse with 70 % ethanol and pin it to a dissection pad.
5. Cut off a piece of tail and store it in an Eppendorf tube at –20 °C to confirm the genotype of the animal by PCR at a later time point.
6. Remove the mammary glands as shown in Fig. 4, working as described in **steps 7–18** (*see* **Note 31**).
7. Using a pair of forceps to hold the skin, make an incision along the ventral midline with a pair of sharp scissors. The mammary glands are located outside the peritoneum, so try to leave it intact when you cut open the skin.
8. Moving from the midline towards the hind limb, make an incision between the fourth and the fifth mammary gland. This should result in an incision that is at an approximate 45-degree angle to the incision along the ventral midline made in **step 7**. Be careful not to cut any blood vessels.
9. Moving from the midline towards the front limb, make another incision at a 45-degree angle to the incision along the ventral midline. Be careful not to cut any blood vessels (*see* **Note 32**).

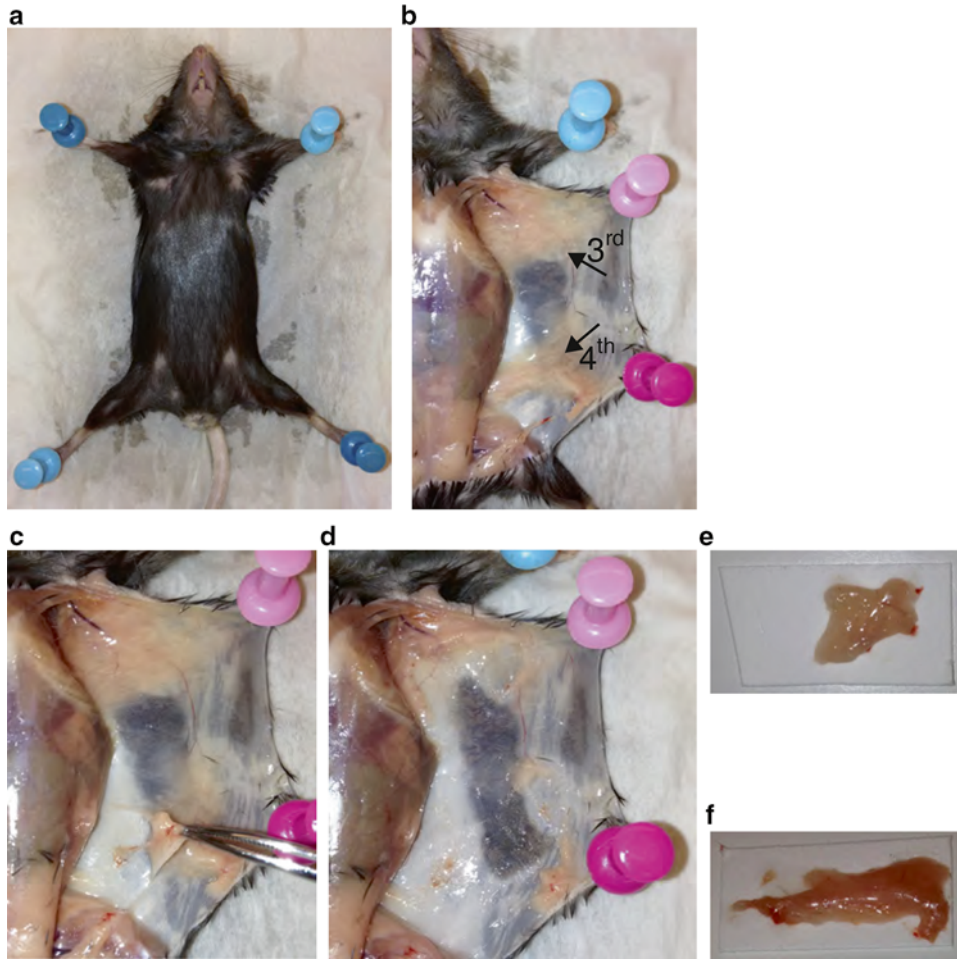

Fig. 4 Isolation of the third and fourth mammary gland as described in Subheading 3.3, **steps 1–18**. (**a**) Image showing the secured animal on a dissecting pad, as described in **step 4**. (**b**) Image showing that both the third and the fourth mammary gland (*arrows*) can be easily accessed after following **steps 7–10**. (**c**) Image showing how to remove the fourth mammary gland by following **steps 12–14**. (**d**) Image showing the skin after both the third and the fourth mammary gland have been removed. (**e–f**) Image showing the third (**e**) and the fourth (**f**) mammary gland after isolation and transfer to a piece of 3 mm Whatman paper

10. Using one pair of fine forceps to hold the peritoneum and a second pair of fine forceps to grab the skin, peel the skin flap in between the upper and lower incisions away from the peritoneum and pin it down to the dissection pad. The third and the fourth mammary glands should now be exposed.
11. Repeat **steps 7–10** on the contralateral side.
12. Using one hand to grab the most distal tip (i.e., closest to the spine) of the fourth mammary gland with a pair of fine (or Dumont no. 5) forceps.

13. Holding a pair of scissors in your opposite hand, gently cut away the fine connective tissue that attaches the mammary gland to the skin, starting at the distal tip and progressing towards the nipple.
14. As you cut away the connective tissue, gently pull the mammary gland upwards.
15. Cut off the mammary gland close to the nipple.
16. Position the mammary gland on a piece of 3 mm Whatman paper and use a pair of Dumont no. 5 forceps to stretch it out as well as possible (*see* **Note 33**).
17. Repeat **steps 12–16** for the fourth mammary glad on the contralateral side.
18. Remove the third pair of mammary glands in a similar fashion (*see* **Note 34**).
19. Process the mammary glands for whole-mount confocal microscopy as shown in Fig. 5, working as described in **steps 20–34**.
20. Transfer the pieces of Whatman paper with the mammary glands to a vial with 10 % neutral buffered formalin (*see* **Note 35**).
21. Wrap the vial in aluminum foil and fix the mammary glands by incubating them on a nutator or tube roller for up to 1 h at room temperature (*see* **Note 36**).
22. Peel away the pieces of Whatman paper and replace the formalin solution with PBS.
23. Incubate on a nutator or tube roller for 15 min at room temperature (*see* **Note 37**).
24. Replace the PBS solution with 30 % ethanol and incubate on a nutator or tube roller for 15 min at room temperature.
25. Replace the 30 % ethanol solution with 50 % ethanol and incubate on a nutator or tube roller for 15 min at room temperature.
26. Replace the 50 % ethanol solution with 70 % ethanol and incubate on a nutator or tube roller for 15 min at room temperature.
27. Replace the 70 % ethanol solution with 100 % ethanol and incubate on a nutator or tube roller for 15 min at room temperature.
28. Replace with fresh 100 % ethanol and incubate on a nutator or tube roller for another hour at room temperature (*see* **Note 38**).
29. Transfer the mammary glands to a fresh vial with methylsalicylate, cover it in aluminum foil and incubate on a nutator or tube roller for up to 1 h, or until the mammary glands are sufficiently cleared (*see* **Note 39**).
30. Use a pair of fine forceps to lift the cleared mammary glands from the vial.

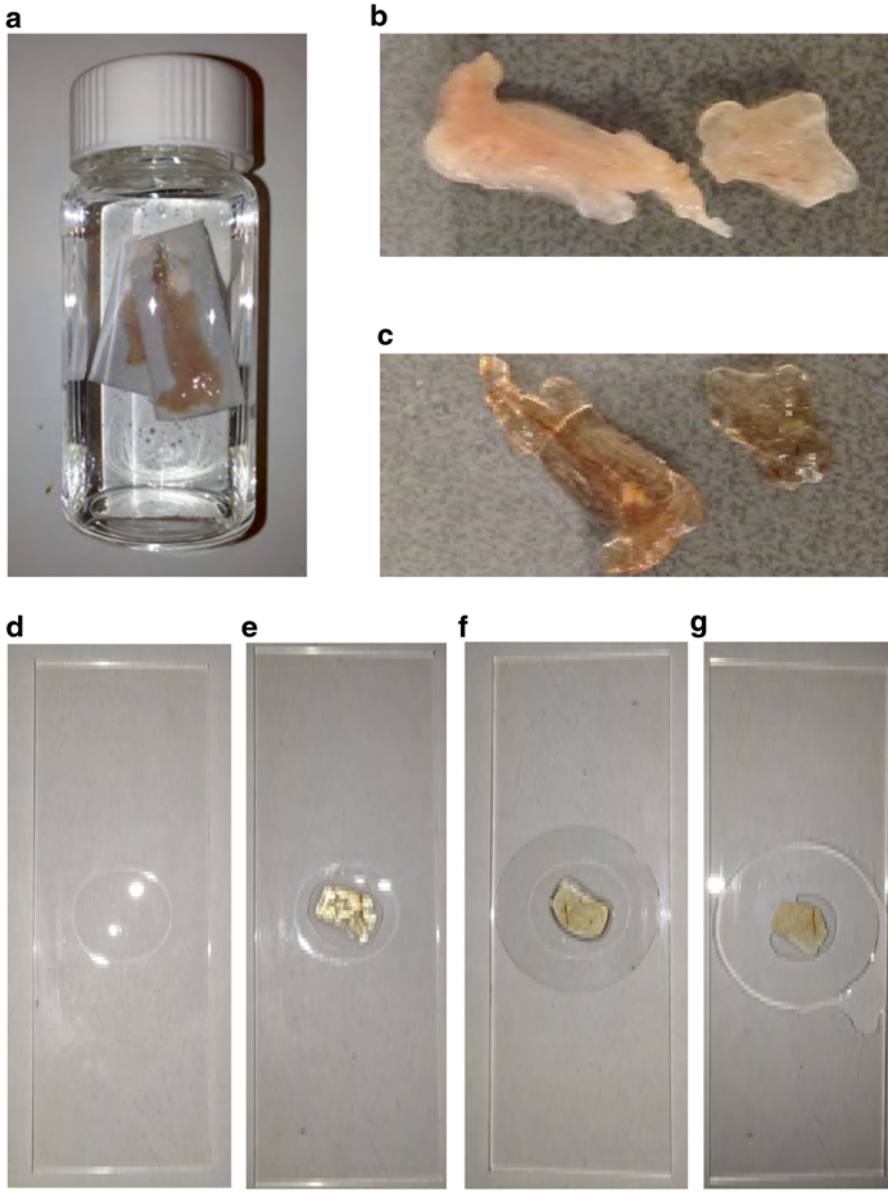

Fig. 5 Processing the mammary glands for confocal microscopy as described in Subheading 3.3, **steps 19–33**. (**a**) Image showing the isolated mammary glands in a glass vial with formalin fixation solution. (**b**) Image showing the mammary glands after fixation, prior to clearing. (**c**) Image showing cleared mammary glands following fixation, dehydration, and incubation in methylsalicylate. (**d**) Image showing a 14 mm concave microscope slide. (**e**) Same as in (**d**) with a trimmed piece of cleared mammary gland tissue. (**f**) Same as in (**e**) with a coverslip positioned onto the specimen. (**g**) Same as in (**f**) after carefully exerting pressure on the coverslip to flatten the tissue, while simultaneously removing excess methylsalycilate

31. Using a pair of scissors, cut a piece that will fit in the opening of a concave microscope slide (*see* **Note 40**).
32. Position the piece in the middle of the 14 mm diameter circle and add a drop of methylsalicylate from the incubation vial.
33. Cover the mammary gland with a coverslip and (wearing gloves) gently press down on the coverslip to flatten the tissue and remove excess methylsalicylate.
34. Wipe away the excess methylsalicylate with a Kleenex tissue (*see* **Note 41**).
35. Seal the coverslip with nail polish.
36. Let the nail polish dry completely before taking your samples to the confocal microscope (*see* **Note 42**).
37. Mount the slide on the stage of the confocal microscope.
38. Use a 488 nm laser line to excite the membrane-bound GFP and a 568 laser line to excite the membrane-bound dTomato (*see* **Note 43**).
39. Image the endogenous fluorescence signal using a 20x/0.7NA objective. If applicable, record a Z-stack (*see* **Note 44**).
40. When you are done, remove your slide from the microscope stage and switch off the microscope (the following **steps 41–46** are optional).
41. To process the cleared glands for paraffin embedding, remove the coverslip from the microscope slide using a bit of acetone and a Kleenex tissue.
42. Transfer the mammary gland to a glass vial with molten paraffin.
43. Incubate in a hybridization oven at 60 °C for 1 h.
44. Refresh the paraffin.
45. Incubate overnight in a hybridization oven at 60 °C.
46. Embed the mammary gland in a tissue cassette for future paraffin sectioning (*see* **Note 45**).

3.4 Constructing a 3D Picture of Labeled Alveoli Using Fiji

1. Download Fiji software from http://fiji.sc/Fiji and install the software on your computer.
2. Import the source files from your confocal microscopy experiment and visualize your Z-stack with Image 5D (*see* **Notes 46** and **47**).
3. Select 'Color' and assign colors to each of your channels.
4. If required, select Image → Adjust → Brightness/Contrast and adjust the sliders to improve the signal to noise ratio (*see* **Note 48**).
5. Select Plugin → Image 5D → Image 5D stack to RGB.

6. To make a three-dimensional reconstruction, follow **steps 8–11**.
7. To make a maximum projection, follow **steps 12–14**.
8. Make sure the RGB stack window is selected.
9. From the menu select Plugins → 3D viewer and press 'OK'.
10. Make sure the ImageJ 3D viewer window is selected.
11. From the menu, select View → Record 360 degrees rotation.
12. Make sure the RGB stack window is selected.
13. From the menu select Image → Stacks → Z-project.
14. Choose the appropriate projection (usual Maximum Intensity or Average Intensity will be the right option) and press 'OK'.

4 Notes

1. Another approach would be to use FLP/FRT technology. However, the number of available mouse strains based on Cre/lox technology far exceeds the collection of existing FLP/FRT lines.
2. Most available Cre drivers are conventional transgenic lines, meaning that the transgene cassette (comprising the Cre recombinase gene and the selected promoter and enhancer sequences driving its expression) has randomly integrated into the genome. As a result, Cre expression is unlikely to completely recapitulate the expression pattern of the original gene from which the promoter and enhancer sequences are derived. In addition, it is important to realize that not all strains with the same name carry an identical transgene insertion as individual founder lines or independent transgenic constructs may have been shared within the scientific community. Cre knock-in alleles, in which the Cre recombinase is targeted to the locus of interest, are more likely to faithfully recapitulate the endogenous gene expression pattern. Regardless, it is recommended that investigators do not solely rely on the published literature describing the Cre expression pattern. Few if any lines have been exhaustively characterized and ideally, Cre activity in each line should be carefully assessed in both spatial and temporal terms prior to commencing the actual lineage tracing experiment.
3. When using a straight (i.e., non-inducible) Cre allele, the first cells to express the recombinase will be labeled. For instance, K14-Cre first becomes active in the developing embryo. This results in labeling of $K14^+$ cells in the embryonic mammary bud and precludes the specific interrogation of $K14^+$ cells in the postnatal mammary gland. Modified versions make use of a Cre-ER fusion gene, in which the Cre recombinase has been

fused to a moiety of the estrogen receptor (ER), thereby rendering the Cre recombinase inactive in the absence of estrogen analogues [15]. Later generations contain specific point mutations in the ER portion of the fusion gene (Cre^{ERT} [16] or Cre^{ERT2} [17, 18]), which greatly reduce sensitivity to circulating endogenous estrogens. This tightens the system by eliminating leakiness, while simultaneously allowing the induction of Cre recombinase activity by the administration of the synthetic estrogen analog tamoxifen.

4. Alternatives to this system already exist and as the experimental methodologies continue to be refined, more will undoubtedly become available in the future. For instance, lineage tracing can also be performed using a three-component system comprising a tissue-specific rtTA driver, a tetO-Cre recombinase and a floxed reporter allele. Each system has its own advantages and disadvantages, but the use of more than two alleles greatly complicates mouse breeding.
5. Cre-inducible reporter alleles usually contain a so-called stop cassette, which is flanked by loxP sites and which prevents transcription of the downstream marker gene. Upon recombination of the reporter allele, the stop cassette is excised and the marker gene is expressed. Genetic recombination is irreversible. Therefore, the mark not only remains present for the remainder of the cell's life span but it is also passed on to all of the cell's offspring. It is this property that allows lineage tracing.
6. A more sophisticated reporter does not necessarily represent a better choice. For instance, compared to *Rosa26-mTmG*, the *Rosa26-Confetti* reporter recombines less efficiently in the mammary gland. Thus, whereas the *Rosa26-mTmG* reporter can be used to label cells at all stages of embryonic and postnatal mammary gland development in combination with the *Axin2CreERT2* driver, in my hands use of the *Rosa26-Confetti* reporter is effectively limited to puberty.
7. It is recommended to backcross the Cre driver and reporter lines to the same genetic background (usually C57/B6 or FVB), owing to differences in mammary gland development between individual mouse strains. The reporter lines listed in Table 1 can be maintained as a homozygous stock on a C57/B6 background without any breeding problems. Whether the same holds true for the Cre driver will depend on the specific strain. I prefer to keep the $Axin2^{CreERT2}$ mice as a heterozygous stock on a C57/B6 background. Even though the $Axin2^{CreERT2}$ allele is not leaky, I always maintain separate stocks of the driver and reporter lines, intercrossing them only as required. The presence of a single copy of the reporter allele is sufficiently sensitive to perform lineage-tracing experiments in the mammary gland.

8. Tamoxifen is a structural estrogen analog and is classified as a carcinogen. Gloves should be worn when handling and weighing the product.
9. Tamoxifen is notoriously difficult to dissolve. Including 10 % ethanol helps to get the tamoxifen into solution. Instead of corn oil, it is also possible to dissolve the tamoxifen in oil that is fit for human consumption (e.g., sunflower oil bought in the supermarket).
10. Methylsalicylate (also known as oil of wintergreen) is toxic upon ingestion. Inhalation and contact with the skin should be prevented. It has a very penetrant smell and even when the stock bottle is opened in the fume hood it is impossible to prevent the smell from entering the lab. It has, however, long been used as a clearing agent and in my hands, after testing many different methods, it gives the best results for whole-mount confocal microscopy. The commercially available clearing agent Focus Clear (Cedarlane Labs) gives good results as well, but it is very expensive.
11. Given the cost associated with purchasing a confocal microscope, the average investigator will most likely have little choice with respect to the equipment that is available for use. He/She is advised to talk to a local expert, who can help with the appropriate settings. In the past we used a Leica SP5 equipped with 3 HyD detectors and 2 PMTs, which is user friendly and offers the benefit of having a slider rather than fixed-width bandpass filters. The latter is particularly useful for multi-color reporter (e.g., *Rosa26-Confetti*) imaging. We are currently using a Nikon A1 to detect endogenous fluorescence of the *Rosa26-mTmG* and the *Rosa26-Confetti* reporter alleles and we have also observed endogenous fluorescence on a Carl Zeiss LSM510.
12. As an investigator, you are both ethically and scientifically responsible. Make sure that all animal experiments are approved by your local animal welfare committee prior to starting and always adhere to the local guidelines.
13. Always genotype your mice, even if you "know" what the genotype is supposed to be! It is almost inevitable that at some point or another animals will be switched (either because they are put in the wrong cage, or because their mark is misread), especially when you are breeding large numbers of mice and/or multiple strains. It is better to catch a mistake early on than after many months (or years) of crossing. I genotype the *Axin2-Cre*^{ERT2} mice using the forward primer RVA283 (5′CGATGCAACGAGTGATGAGGTTC3′) and the reverse primer RVA282 (5′GCACGTTCACCGGCATCAAC3′), with

an annealing temperature of 58 °C and a total of 35 cycles. This results in a Cre-transgene specific product of approximately 350 base pairs. I genotype the *Rosa26-mTmG* mice using the three-primer PCR posted on the Jackson labs website for this strain. Primers RVA284 (or oIMR7318, 5′CTC TGCTGCCTCCTGGCTTCT3′), RVA285 (or oIMR7319, 5′CGAGGCGGATCACAAGCAATA3′), and RVA286 (or oIMR7320, 5′TCAATGGGCGGGGGTCGTT3′) give a band of 330 base pairs for the wild-type *Rosa26* locus and a band of 250 base pairs for the *Rosa26-mTmG* allele. This PCR can also be run with an annealing temperature of 58 °C and a total of 35 cycles. Primers RVA284, RVA285, and RVA286 can also be used to genotype the *Rosa26-Confetti* mice.

14. It is easiest to genotype the mice around the time they are weaned (approximately postnatal day 21, P21) and to also give each of the animals a unique identifier at this point (e.g., earclip). Collect a piece of tail, toe or ear tissue (according to local guidelines) and lyse the tissue. The easiest way to get DNA out, is to lyse your samples in Viagen tail lysis buffer (use approximately 100–200 μl per sample) supplemented with 100 μg/ml proteinase K. Following overnight incubation at 55 °C, inactivate the proteinase K by heating the samples to 85 °C for 15–45 min. You can now directly use 1–10 μl the lysate as input for your genotyping PCR. Alternatively, you can follow a DNA isolation protocol that uses homemade lysis buffer [19]. Using the commercial lysis buffer is faster, but more expensive. There is no difference in the quality of the DNA in terms of performance in the PCR.
15. This only holds for traces that are started in postnatal animals. If you start an embryonic trace (e.g., as outlined in Fig. 3b) you can only genotype the experimental animals after they are born. When you initiate a trace in early postnatal animals (e.g., P14, but in reality anything prior to weaning), it is often unpractical to genotype the mice beforehand as well. In these cases it is advisable to set up your breeding schemes in such a way that your litters have a high chance of containing double-heterozygous mice, but remember that not all strains perform well as breeders when they are homozygous.
16. Like any experiment, a lineage-tracing analysis should be well controlled. A technical positive control will usually be difficult (if not impossible) to obtain, since it would require an independent Cre-driver that is known to work in your tissue of interest. If possible, use a different tissue from the double-heterozygous mice in which you initiate the trace as a positive control at the time of analysis. For instance, *Axin2-Cre*^{ERT2} also marks intestinal stem cells. Because Cre-mediated recombination in the

intestine is far more efficient than in the mammary gland, I often check if my experiment has worked by isolating a piece of intestine from tamoxifen-injected double-heterozygous *Axin2-Cre^{ERT2};Rosa26-mTmG* mice and quickly score that under a fluorescent microscope.

17. As a negative control, inject double-heterozygous *Axin2-Cre^{ERT2};Rosa26-mTmG* mice with corn-oil control solution. This will allow you to ascertain if your Cre allele is leaky. Because animal numbers are often limiting, it is virtually impossible to take this control along in every experiment. However, leakiness should ideally be tested for every Cre strain for each experimental protocol (i.e., breeding scheme and age of analysis) at least once at the outset of the experiment.
18. To be sure that the fluorescence signal you are scoring in your analysis is real, you can take along a littermate that does not carry the Cre-allele, but which is heterozygous for the *Rosa26-mTmG* allele. This is especially important when you are just getting started and still need to become familiar with the pattern of clonal outgrowth that you will see and/or if you are analyzing the mammary gland by FACS analysis. If you are truly performing clonal tracing analyses (i.e., each mammary gland will only contain a few positive clones), the majority of the tissue will in fact be an intrinsic negative control and individual (or patches of) labeled cells will be easy to identify in an otherwise unrecombined epithelium.
19. For the correct interpretation of your tracing experiments, proper biological controls are essential. For instance, when you are studying the contribution of mammary stem cells to turnover of the mammary epithelium during multiple rounds of pregnancy, lactation and involution, be sure to trace nulliparous and primiparous mice as well. Given the biological variation between individual mice, it is best to always use littermates of the multiparous mice you are tracing and, when the mice are not in a mating scheme, to house these females in the same cage as much as possible.
20. Filter sterilizing may not always be required and most likely depends on the quality of the oil you use to dissolve the tamoxifen. When using corn oil, I always do it as a precaution, after experiencing problems with injecting unfiltered corn oil at some point. Be careful when exerting pressure on the syringe, as the solutions will be very viscous.
21. This protocol will assume that tamoxifen is administered by means of an intraperitoneal injection. Alternatively, oral gavage may be used. This is a matter of personal preference.
22. Find out what is most comfortable. Either inject with your dominant hand and hold the mouse with the other, or vice versa.

23. Injecting at a shallow angle in this quadrant minimizes the chance of damaging internal organs, such as the liver, small intestine, caecum, and bladder. If you want to make sure you are in the right spot, you can always aspirate a small volume prior to injecting. If the aspirate is green/brown, yellow, or red, you have penetrated the intestine, bladder, or blood vessels and you should not inject. However, as long as you do not insert the needle too deep (i.e., up until about 0.5 cm) this should not be a problem.
24. A tamoxifen inducible system offers experimental control over the onset, but also the extent of recombination. This is particularly important when the lineage-tracing experiment is designed to label stem cells. To be able to track clonal outgrowth, Cre-mediated recombination should be sporadic. This ensures that labeled cell clusters really are the clonal offspring of a single recombination event in an individual stem cell. Theoretically, each mammary gland should thus contain a single cell clone. In practice however, it means that there should be sufficient space (i.e., stretches of unlabeled tissue) between labeled patches of tissue. This can be achieved by lowering the amount of tamoxifen that is injected. I often get asked what the half-life of tamoxifen is following injection as it will circulate in the animals for some time following injection. In practice, however, it is very well possible to label even fast-dividing cells (e.g., in the intestinal crypt [6, 20] or the developing embryo [21]) by essentially causing a pulse of Cre-activity.
25. In my experience (at least with the *Axin2-Cre^{ERT2}* mice), tamoxifen-mediated recombination in the mammary gland is far less efficient than in other tissues. For instance, in the skin [22] and the intestine [6], which also contain Wnt-responsive stem cells, we can inject as little as 0.1–0.2 mg tamoxifen per 25 g of body weight into adult mice and still score a sufficient number of clones. By comparison, recombination in the mammary gland requires 4 mg tamoxifen per 25 g of body weight in adult mice. This translates to administering 200 μl of a 20 mg/ml tamoxifen solution into an 8–10-week-old mouse. The amount of tamoxifen that is to be injected will vary depending on the experiment (e.g., if clonal labeling is not required, more tamoxifen can be injected), the reporter that is used (e.g., using the same amount of tamoxifen, recombination is far less efficient in *Axin2-Cre^{ERT2};Rosa26-mTmG* mice than in *Axin2-Cre^{ERT2};Rosa26-Confetti* animals) and the Cre driver.
26. The absolute amount of tamoxifen (as well as the total injection volume) should always be adjusted for the age and weight of the mice. For instance, when inducing sporadic recombination in P14 animals, I try to inject at most 1–2 mg tamoxifen

in a total volume of 100 µl. Injecting tamoxifen at this age can result in a growth deficit. The animals will eventually catch up, but it may require them to stay with the mother for a bit longer. Extra care should be taken when inducing recombination in the developing embryo by injecting tamoxifen into pregnant animals. I prefer to use a low stock concentration (i.e., a tamoxifen solution of 2–5 mg/ml) and try to inject no more than 0.5 mg tamoxifen in total. Even so, the injection of tamoxifen into pregnant females can induce termination of the pregnancy and/or delivery problems. This can be avoided by co-injecting progesterone [21].

27. Please be aware that tamoxifen is a mixed estrogen agonist/antagonist, meaning that it can either mimic or counteract the effects of estrogen in different tissues. Since the mammary gland is particularly sensitive to estrogen, it is important to be aware of potential side effects. For instance, we have observed that even a single injection of tamoxifen prior to or during puberty (at concentrations below those reported in the literature) can delay mammary gland outgrowth [23]. Although the tissue eventually catches up, this is something to keep in mind. This is a downside of using tamoxifen-mediated Cre/lox recombination for lineage-tracing experiments in the mammary gland, but at present this remains the most flexible, informative and widely used system of choice.
28. Never recap a used needle.
29. To interpret the outcome of a long-term tracing experiment, it is advisable to collect samples at (i.e., set up dedicated tracing experiments for) various time points along the way. First, you will always want to determine which cells first recombine the reporter allele (i.e., your starting population) by performing a short term tracing experiment. The *Rosa26-lacZ* reporter will allow you to analyze the mammary gland as early as 24 h after tamoxifen administration, whereas the GFP signal in the *Rosa26-mTmG* cannot be detected robustly until 48 h after tamoxifen administration. Second, if you are interested in tracing stem cells, it is important to note that (even when you are using a driver that is known to label stem cells, such as *Axin2-Cre*^{ERT2}) not all labeled cells are indeed stem cells. To qualify as a stem cell, a cell needs to meet two criteria: It has to give rise to differentiated offspring and it has to survive turnover of the tissue. The only way to be sure that the mammary epithelium has completely turned over is by tracing cells through a complete round of pregnancy, lactation and involution. Here too, it will be helpful to have some analytical time points along the way (e.g., prior to pregnancy, mid-pregnancy, mid-lactation, mid-involution, post-involution).

30. Please follow the local guidelines for euthanizing animals.
31. There are many ways in which a lineage tracing experiment can be analyzed. This includes FACS analysis, but also various histological analyses. The remainder of the protocol will describe analysis by whole-mount confocal analysis, which allows 3D reconstruction of labeled structures.
32. Accidentally hitting a blood vessel is more likely to occur near the front limbs than near the hind limbs. Try to prevent it by not cutting too far away from the midline.
33. The idea is to fix the mammary gland in such a way that it stays flat. Another way to achieve this is by stretching the mammary gland on a glass slide, covering it with a second glass slide and fixing this "sandwich" in a 50 ml Falcon tube. This works well, but uses a lot more formalin.
34. The boundaries of the third mammary gland are not as well defined as the fourth mammary gland, so isolating it may feel a bit intuitive at first. It is closely associated with the first and second mammary gland. In addition, there is a high chance of collecting some muscle tissue and of hitting blood vessels, both of which may obscure a whole-mount preparation. On the up side, the third mammary gland is a lot flatter than the fourth, which helps for whole-mount confocal microscopy.
35. You can use glass scintillation counter vials that hold up to 25 ml for processing multiple glands together, or smaller snap cap glass vials that hold up to 4 ml for processing an individual gland.
36. As little as 15 min may be enough. In fact, if you are interested in analyzing the *Rosa26-mTmG* reporter by whole-mount confocal microscopy, you can omit the formalin fixation step altogether and transfer the isolated mammary glands directly to 100 % ethanol. Because the GFP and dTomato are membrane bound, their signal will be preserved. Importantly, this will not work for the *Rosa26-Confetti* reporter, which does require formalin fixation. Therefore, it is safest to include this step for all fluorescent reporters.
37. Formalin should be disposed of as toxic waste. Please follow local guidelines.
38. It is important that the tissue is completely dehydrated prior to transfer into methylsalicylate, otherwise the clearing will not work.
39. Use approximately 5 ml per mammary gland. Provided that the mammary glands are properly dehydrated, clearing will become apparent within 15 min.
40. For the third mammary gland it is often sufficient to trim the edges. For the fourth mammary gland, I usually cut straight through the lymph node. This separates the proximal from the

distal portion of the gland and still allows the lymph node to be used for orientation. After this, trim the edges of the fat pad and remove excess pieces of tissue from the top or bottom.

41. At this point, there should be a continuous ring of methylsalicylate surrounding the concave opening. If you see any air pockets, this means the specimen either needs to be flattened further or is too thick. In the latter case, you can remove the tissue and use pair of scissors to trim it until it does fit. The entire dimple holding the tissue does not need to be filled with methylsalicylate, but to prevent the tissue from drying out, it is best to only mount the specimen immediately prior to microscopic analysis.
42. At this point, I usually dry the slides in the dark (i.e., in a drawer). There is no need to switch off the overhead lights during any of the previous steps. The fluorescent signal will not be quenched.
43. For the *Rosa26-Confetti*, use 458 nm (for CFP), 488 nm (GFP), 514 nm (YFP), and 561 nm (RFP) laser lines.
44. This is the most difficult part of the procedure. It takes time and patience to get a feel for the appearance of the whole-mount tissue under the microscope. I usually scan the tissue through the eyepiece, using a UV lamp and a GFP filter. With the *Rosa26-mTmG* reporter, this gives you just enough cell outlines to see where you are in the tissue. Using the focus knob to move up and down, you will be able to discern epithelial branches and blood vessels surrounded by adipocytes. After a while, you will be able to identify GFP-positive cell clusters based on their increased intensity. Finding labeled cells with the *Rosa26-Confetti* reporter takes more effort, because you no longer have the information of the cell outlines provided by the membrane-bound dTomato, but can be done as well. Using a 20x/0.7 NA objective should give you enough working distance to make a Z-stack through an entire alveolar cluster as shown in Fig. 6.
45. The described protocol is compatible with paraffin embedding of the cleared mammary glands. The same labeled cell clusters can thus be imaged as whole mounts and on tissue sections in combination with other markers. During the processing for paraffin embedding, the dTomato signal is always lost. This frees up a channel for co-staining with antibodies directed against structural markers. Sometimes, the GFP signal will be preserved, but it is advisable to detect recombined cells with an anti-GFP antibody (I like the Abcam chicken-anti-GFP, ab13790). The downside of using methylsalicylate cleared samples for paraffin embedding is that it precludes heat-induced epitope retrieval (HIER) as the tissue tends to come off the slide. However, on paraffin sections from *Rosa26-mTmG*

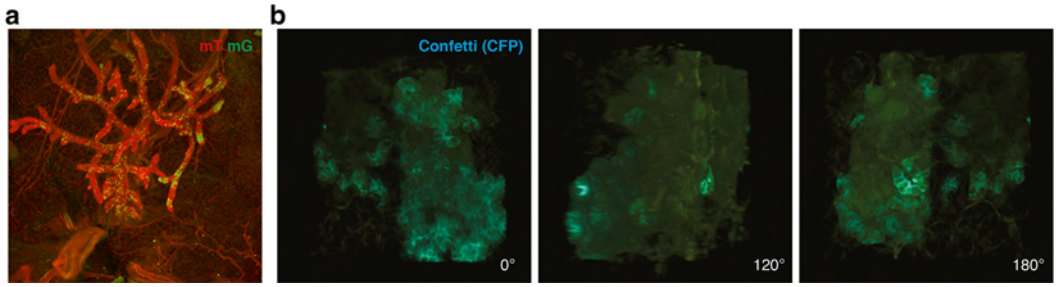

Fig. 6 Whole-mount confocal microscopy images after processing in Image J. (**a**) Maximum Z-projection of a whole-mount *Axin2-CreERT2;Rosa26-mTmG* mammary gland showing recombined (mG, *green*) and unrecombined (mT, *red*) cells (168 slices, imaged on a Leica SP5 confocal microscope using a 20x/0.7NA objective). For this particular experiment, the trace was initiated at E13.5 and the mammary glands were isolated at P8. Prior to puberty, the ductal network is small and an entire epithelial tree fits into the frame of view when using a 20× objective. (**b**) Snapshots from a movie showing the 3D rotation of a reconstructed alveolar cluster of a whole-mount *Axin2-CreERT2;Rosa26-Confetti* mammary gland demonstrating the clonal outgrowth of recombined (CFP, *blue*) cells (107 slices, 1024 × 1024 pixels, imaged on a Leica SP5 confocal microscope using a 20x/0.7NA objective and a 4× zoom). For this particular experiment, the trace was initiated at P42 and the mammary glands were isolated at E14.5 of the first pregnancy

mammary gland samples that are processed for whole-mount confocal microscopy with methylsalicylate but without including the formalin fixation step (*see* **Note 36**), you can often use antibodies that would normally require HIER on regular formalin-fixed paraffin-embedded sections (including the anti-GFP antibody mentioned above). You should test which conditions are optimal for your antibodies. Alternatively, you can always process one mammary gland for whole-mount confocal microscopy and the contralateral gland for formalin fixation and paraffin embedding, thus allowing HIER and colocalization studies by confocal microscopy.

46. When using a Leica SP5 confocal microscope, you can simply drag the *.lif file into the Fiji toolbar. You will then be presented with the option to 'View as Image 5D'. Choose this option. For other microscopes, the images may open as a stack. In that case, select Plugin → Image 5D → Stack to Image 5D and proceed as described.
47. If you happen to only be able to import individual *.tif files, wait for all the files in your stack to import. Then select Image → Stacks → Images to Stacks. Make sure the resulting stack is selected and choose Image → Hyperstacks → Stacks to Hyperstacks. Assign the correct number of channels (c) and sections (z). For Display Mode select 'Color'. Make sure that the resulting hyperstack is selected and choose Plugins → Image 5D → Stack to Image 5D and proceed as described.
48. Be careful when adjusting the sliders and try to prevent image adjustments as much as possible.

Acknowledgements

RvA is supported by the Dutch Cancer Society (KWF cancer research career award, 2013-6057) and by a MacGillavry fellowship from the University of Amsterdam. I thank my ex-colleagues and Roel Nusse at Stanford University (USA) for discussions and feedback during the experimental stages of this work, Lauran Oomen and Lenny Brocks at the Netherlands Cancer Institute in Amsterdam (the Netherlands) for help with the Leica SP5, Ronald Breedijk, and Erik Manders for help with analyzing samples on the Nikon A1, Ji-Ying Song for the image depicted in Fig. 1b and Amber Zeeman for comments on the manuscript and the image depicted in Fig. 1a.

References

1. Watson CJ, Khaled WT (2008) Mammary development in the embryo and adult: a journey of morphogenesis and commitment. Development 135(6):995–1003. doi:10.1242/dev.005439, 135/6/995 [pii]
2. Smith BA, Welm AL, Welm BE (2012) On the shoulders of giants: a historical perspective of unique experimental methods in mammary gland research. Semin Cell Dev Biol 23(5):583–590, 10.1016/j.semcdb.2012.03.005 S1084-9521(12)00047-X [pii]
3. Shackleton M, Vaillant F, Simpson KJ, Stingl J, Smyth GK, Asselin-Labat ML, Wu L, Lindeman GJ, Visvader JE (2006) Generation of a functional mammary gland from a single stem cell. Nature 439(7072):84–88. doi:10.1038/nature04372, nature04372 [pii]
4. Stingl J, Eirew P, Ricketson I, Shackleton M, Vaillant F, Choi D, Li HI, Eaves CJ (2006) Purification and unique properties of mammary epithelial stem cells. Nature 439(7079):993–997. doi:10.1038/nature04496, nature04496 [pii]
5. Deome KB, Faulkin LJ Jr, Bern HA, Blair PB (1959) Development of mammary tumors from hyperplastic alveolar nodules transplanted into gland-free mammary fat pads of female C3H mice. Cancer Res 19(5):515–520
6. van Amerongen R, Bowman AN, Nusse R (2012) Developmental stage and time dictate the fate of Wnt/beta-catenin-responsive stem cells in the mammary gland. Cell Stem Cell 11(3):387–400. doi:10.1016/j.stem.2012.05.023, S1934-5909(12)00342-6 [pii]
7. Van Keymeulen A, Rocha AS, Ousset M, Beck B, Bouvencourt G, Rock J, Sharma N, Dekoninck S, Blanpain C (2011) Distinct stem cells contribute to mammary gland development and maintenance. Nature 479(7372):189–193, 10.1038/nature10573, nature10573 [pii]
8. Akagi K, Sandig V, Vooijs M, Van der Valk M, Giovannini M, Strauss M, Berns A (1997) Cre-mediated somatic site-specific recombination in mice. Nucleic Acids Res 25(9):1766–1773, gka289 [pii]
9. Sauer B, Henderson N (1988) Site-specific DNA recombination in mammalian cells by the Cre recombinase of bacteriophage P1. Proc Natl Acad Sci U S A 85(14):5166–5170
10. Smedley D, Salimova E, Rosenthal N (2011) Cre recombinase resources for conditional mouse mutagenesis. Methods 53(4):411–416, 10.1016/j.ymeth.2010.12.027. S1046-2023(10)00310-5 [pii]
11. Murray SA, Eppig JT, Smedley D, Simpson EM, Rosenthal N (2012) Beyond knockouts: cre resources for conditional mutagenesis. Mamm Genome 23(9–10):587–599. doi:10.1007/s00335-012-9430-2
12. Soriano P (1999) Generalized lacZ expression with the ROSA26 Cre reporter strain. Nat Genet 21(1):70–71. doi:10.1038/5007
13. Muzumdar MD, Tasic B, Miyamichi K, Li L, Luo L (2007) A global double-fluorescent Cre reporter mouse. Genesis 45(9):593–605. doi:10.1002/dvg.20335
14. Snippert HJ, van der Flier LG, Sato T, van Es JH, van den Born M, Kroon-Veenboer C, Barker N, Klein AM, van Rheenen J, Simons BD, Clevers H (2010) Intestinal crypt homeostasis results from neutral competition between symmetrically dividing Lgr5 stem cells. Cell 143(1):134–144, S0092-8674(10)01064-0 [pii]. 10.1016/j.cell.2010.09.016
15. Metzger D, Clifford J, Chiba H, Chambon P (1995) Conditional site-specific recombination in mammalian cells using a ligand-dependent chimeric Cre recombinase. Proc Natl Acad Sci U S A 92(15):6991–6995

16. Feil R, Brocard J, Mascrez B, LeMeur M, Metzger D, Chambon P (1996) Ligand-activated site-specific recombination in mice. Proc Natl Acad Sci U S A 93(20): 10887–10890
17. Feil R, Wagner J, Metzger D, Chambon P (1997) Regulation of Cre recombinase activity by mutated estrogen receptor ligand-binding domains. Biochem Biophys Res Commun 237(3):752–757, S0006-291X(97)97124-2 [pii] 10.1006/bbrc.1997.7124
18. Indra AK, Warot X, Brocard J, Bornert JM, Xiao JH, Chambon P, Metzger D (1999) Temporally-controlled site-specific mutagenesis in the basal layer of the epidermis: comparison of the recombinase activity of the tamoxifen-inducible Cre-ER(T) and Cre-ER(T2) recombinases. Nucleic Acids Res 27(22):4324–4327, gkc656 [pii]
19. Laird PW, Zijderveld A, Linders K, Rudnicki MA, Jaenisch R, Berns A (1991) Simplified mammalian DNA isolation procedure. Nucleic Acids Res 19(15):4293
20. Barker N, van Es JH, Kuipers J, Kujala P, van den Born M, Cozijnsen M, Haegebarth A, Korving J, Begthel H, Peters PJ, Clevers H (2007) Identification of stem cells in small intestine and colon by marker gene Lgr5. Nature 449(7165):1003–1007, nature06196 [pii]. 10.1038/nature06196
21. Nakamura E, Nguyen MT, Mackem S (2006) Kinetics of tamoxifen-regulated Cre activity in mice using a cartilage-specific CreER(T) to assay temporal activity windows along the proximodistal limb skeleton. Dev Dyn 235(9):2603–2612. doi:10.1002/dvdy.20892
22. Lim X, Tan SH, Koh WL, Chau RM, Yan KS, Kuo CJ, van Amerongen R, Klein AM, Nusse R (2013) Interfollicular epidermal stem cells self-renew via autocrine Wnt signaling. Science 342(6163):1226–1230. doi:10.1126/science.1239730
23. Shehata M, van Amerongen R, Zeeman AL, Giraddi RR, Stingl J (2014) The influence of tamoxifen on normal mouse mammary gland homeostasis Breast Cancer Res 16:411

Chapter 12

Modeling the Breast Cancer Bone Metastatic Niche in Complex Three-Dimensional Cocultures

Rebecca Marlow and Gabriela Dontu

Abstract

Despite advances in early detection, prevention and treatment of breast cancer, the mortality of breast cancer patients did not decrease considerably in the last years. Metastatic breast cancer remains incurable. There is compelling evidence that dissemination of breast cancer cells at distant sites is an early event. At the time of detection and diagnosis, patients have disseminated breast cancer cells in the bone marrow. Only in half of these patients the disseminated cells proliferate and generate metastases, typically in 3–5 years for ER negative breast tumors and 10–15 years for ER positive breast tumors. In other patients metastases never develop. The ability to predict which patients will develop metastases and to devise strategies to interfere with this process hinges on understanding the mechanisms underlying growth at the metastatic site. In turn, this requires novel experimental systems that model in vitro the survival, dormancy and proliferation of disseminated cancer cells.

We have established such experimental systems that model the bone microenvironment of the breast cancer metastatic niche. These systems are based on 3D complex cultures of human bone marrow stromal cells and breast cancer cell lines in collagen biomatrices. We identified conditions in which cancer cells are dormant, and conditions in which they proliferate and we validated the results in vivo. Dormant cancer cells were able to proliferate upon transfer into supportive microenvironment or upon manipulation of signaling pathways that control dormancy. These experimental systems will be instrumental in screening new compounds for metastasis studies and particularly in studying the pathways that control cellular dormancy. We provide in this chapter detailed protocols for these complex 3D coculture systems.

Key words Breast cancer, Metastasis, Three-dimensional culture, Complex coculture system

1 Introduction

In many cancers, the main cause of death is metastatic spread. Bone is one of the most frequent sites of metastasis particularly for breast and prostate tumors, but also other cancers, such as lung, kidney, and thyroid cancers [1, 2]. There is compelling evidence that systemic dissemination of cancer cells is an early event, usually occurring before detection of the primary tumor [3]. Disseminated tumor cells (DTC) survive in a state of cell cycle arrest for long periods of time, a phenomenon defined as "cellular dormancy"

Maria del Mar Vivanco (ed.), *Mammary Stem Cells: Methods and Protocols*, Methods in Molecular Biology, vol. 1293,
DOI 10.1007/978-1-4939-2519-3_12,

[3–5]. Despite their significance for progression and outcome of disease, these aspects of cancer biology are relatively under-investigated, mostly due to lack of in vitro experimental systems and scarcity of in vivo models.

Reasoning that the complex interactions between cancer cells and the microenvironment are most likely critical for cellular dormancy and proliferation, we established in vitro models of DTC based on co-cultivation of breast cancer cells (BCC) with bone marrow derived (BM) cells in a 3D-collagen biomatrix. We identified conditions in which BCC are dormant ("inhibitory niche") and conditions in which they proliferate ("supportive niche") [6]. We define cellular dormancy as cell cycle arrest of cancer cells [7]. Cell cycle arrest of BCC in our experimental system is reversible either by changing the microenvironment or by inhibiting signaling pathways previously shown to have role in dormancy [6]. Upon xenotransplantation in immunodeficient mice, tumors developed only from 3D-biomatrix bearing BM stromal cells that represented the "supportive niche" and not from those bearing stromal cells that represented the "inhibitory niche." Importantly, BCC recovered from the "inhibitory niche" were bone-fide dormant cells, because they retained their ability to reenter the cell cycle [6]. These experimental systems will be instrumental for investigating the mechanisms that control dormancy of cancer cells, and for developing strategies to target these cells or prevent their "re-awakening" during disease progression. Figure 1 describes the 3D complex coculture system and its applications.

2 Materials

2.1 For Generating Collagen Biomatrix Discoids for 3D Coculture

1. Collagen biomatrix. Gelfoam™ from Pfizer—(6 sheets/box).
2. Single metal hole-punch (sterilized either by autoclaving or soaking in 70 % Ethanol).
3. Sterile scalpels (22 blade).
4. Sterile forceps.
5. 15 cm tissue culture plates.
6. 10 cm tissue culture plates.
7. 50 ml Falcon tubes.

2.2 For Cell Plating

1. Ultra-low attachment 96-well plates (CoStar).
2. Yellow tips (200 µl).

2.3 For Plate Reader Readings

1. µClear white 96-well plates (Greiner).

2.4 Medium Used for 3D Cocultures

1. DMEM-F12 (Gibco) supplemented with 5 % fetal bovine serum (FBS) and antibiotic/antimycotic (Invitrogen).

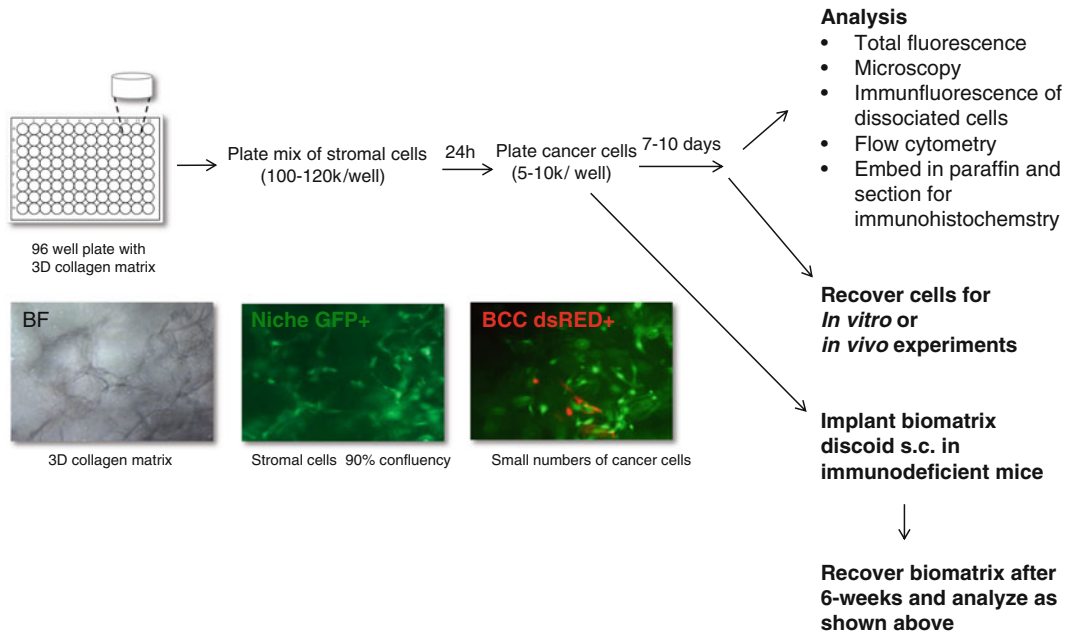

Fig. 1 In vitro models of bone metastatic niche—experimental setup. Bone marrow derived stromal cells are plated in 96-well plates containing collagen biomatrix discoids. Stromal cells are plated at high density in order to reach sub-confluency rapidly. Cancer cells are subsequently plated in small numbers, to mimic the low density of disseminated cancer cells. Proliferation of cells is followed by microscopy and total fluorescence reading. Intact biomatrices containing cells or dissociated cells are analyzed or used in additional experiments (BF, Brightfield, GFP, Green Fluorescent protein, BCC, Breast Cancer Cells, s.c. subcutaneous)

2.5 Dissociation of 3D Cocultures

1. Collagenase/hyaluronidase solution (07912 Stem Cell Technologies).

2.6 Cell Lines

Unless otherwise stated media were obtained from Invitrogen. Suppliers are denoted by ().

All cell lines were infected with lentivirus constructs to express fluorescent proteins of choice. Generally BM cells were labeled with GFP and BCC with dsRED.

Cell Line	Supplier	Media	Notes
Primary bone marrow stromal cells (BMSC)	(Lonza) 2 M-302	(StemCellTech) Myelocult 05150	1. The medium is complete (i.e., do not add FBS) but does require hydrocortisone and antibiotic/antimycotic (Invitrogen) 2. Split cells at 1:2 or 1:3 dilution. 3. Use only to passages 6–8 after (cell morphology changes after more passages) 4. Use 5× trypsin (0.5 % trypsin) for splitting)

(continued)

Cell Line	Supplier	Media	Notes
Human umbilical vein endothelial cells (HUVEC)	(Lonza) C2517A	(Lonza) EGM-2 CC-3162 EGM-2 BulletKit (CC-3156 and CC-4176)	1. EGM-2 kit is complete medium—add antibiotic/antimycotic 2. Require gelatin-coated flasks for propagation. Coat for ~5–10 min at 37 °C with gelatin solution (Sigma) before plating (wash with PBS twice) 3. Use only to passages 6–8 after (cell morphology changes after more passages)
Bone marrow stromal cells (HS-5)	(ATCC) CRL-11882	DMEM 10 % FBS	
Human fetal osteoblasts (hFOB)	(ATCC) CRL-11372	DMEM/F12 10 % FBS G418 (Invitrogen)	
SUM159	In House	F12 5 % Insulin Hydrocortisone	
MCF7 BT474 ZR75-1 MDA-453	In House	DMEM 10 %	
T47D	In House	RPMI 10 % Insulin	
MDA-231	In House	DMEM 10 %	
MDA-231 1833 BoM 4175 LM2	*	DMEM 10 %	1. Organ specific metastatic sub-clones obtained through collaboration with Sloan Kettering Memorial Cancer Center.

3 Methods

All manipulations should take place under sterile conditions. When plate reading, ensure that lids remain on the 3D cocultures. Figure 2 shows an example layout of a typical experiment.

3.1 Cutting Collagen Biomatrix into Discoid Pieces for Coculture

1. Using a 15 cm tissue culture (TC) plate as a sterile surface, open the envelope containing the collagen biomatrix and place it into the plate lid using sterile forceps.
2. Cut (using the sterile scalpel) the collagen biomatrix into strips ~2 cm in width. Use the lid as a cutting surface and place strips into plate for safe-keeping.
3. Cut these strips into ~4 cm pieces.
4. Using the scalpel cut these into half lengthways so you have 2 pieces of half the thickness (~3 mm).

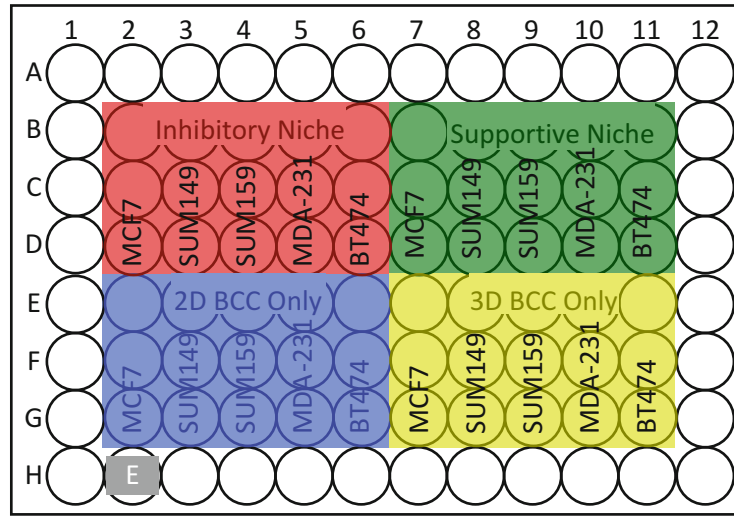

Fig. 2 Example layout in 96-well plate of experiment to monitor proliferation of multiple breast cancer cell lines cocultured in the Supportive and Inhibitory Niche. Experimental setup is optimal in one single 96-well plate thus avoiding plate-to-plate differences in readings. A discoid of collagen biomatrix that has been saturated but not seeded with cells is used as a background reading for control purposes (*grey* well (E)). Routinely triplicate wells (3 per condition) or quintlicate wells (5 per condition) are used. An average reading of these wells is used for further analysis All wells in the 96-well plate should be incubated with medium to avoid evaporation loss and to include background readings

5. Cut discoids using the sterile hole punch (~5 mm in diameter) for use in the 96-well cocultures.
6. Collect the discoids into a 50 ml falcon tube.
7. Using sterile forceps, place the collagen biomatrix discoids into ultra-low 96-well plates for performing the experiment or in sterile tube for storage. UV irradiate overnight.

3.2 Plating Supportive and Inhibitory Niche Cultures

1. Place the collagen biomatrix discoids into the required number of wells using sterile forceps. Use an ultra-low attachment plate for plating stromal cells.
2. UV-irradiate this plate for a minimum of 1 h.

3.2.1 Setting up 3D Cocultures

3. Using a multichannel pipette, place 200 µl of DPBS (Dulbecco's phosphate buffered saline without Ca^{+}/Mg^{+}) into each well to wet the discoids.
4. Leave for at least 15 min to ensure it is fully saturated.
5. Remove the liquid using a multichannel pipette.

3.2.2 Plating Bone Marrow Cells

Please note that the medium used for all 3D cocultures is DMEM-F12 5 % FBS + antibiotic/antimycotic, and incubation is at 37 °C with 5 % CO_2.

1. Trypsinize cells.
2. Resuspend cells into 1 ml of medium and count plating.
   (a) Supportive Niche—BMSC—100,000 BMSC cells per well (in 15 μl of medium).
   (b) Inhibitory Niche—BMCL—120,000 cells in total per well (in 15 μl of medium) (40,000 cells of each cell line (HS-5, hFOB, and HUVEC)).
3. Plate cells into the center of each collagen biomatrix disc.
4. Leave in the incubator for 2 h to enable diffusion of cells and medium by capillary action.
5. Add 200 μl medium per well and leave overnight.

3.3 Plating Breast Cancer Cells

1. Move collagen biomatrices from the ultra-low plates to the new clear-bottomed white plates for the plate reader using sterile forceps.
2. Resuspend cells into 1 ml of medium and count.
3. Get cells to the required concentration (one million cells per ml).
   (a) For breast cancer cells plating is done at 10,000 cells per well in 10 μl of media, onto the Supportive Niche (BMSC) or Inhibitor Niche (BMCL). This requires a cell concentration of one million cells per ml.
4. Add 10 μl of cell suspension onto the plated biomatrix discs.
5. Leave in the incubator for 2 h to enable plating by capillary action.
6. Add 200 μl media per well and leave overnight.
   - For 2D monoculture controls—plate 5,000 cells per well (5 μl).
   - For 3D monoculture controls—plate 50,000 or 100,000 cells per well depending on the experimental setup.
     – Use the same procedure as for the BM cells except use the μClear plates along with plating into the Supportive or Inhibitory Niches.

3.4 Total Fluorescence Reading and Microscopy

1. Prepare plates to move 3D cocultures into.
2. Pick up the collagen biomatrix with sterile forceps and move into the new plate.
3. Use a yellow tip to gently move all into the center of the well.
4. Add 200 μl of media to each well. Add media also to all empty wells to help with evaporation loss and Empty well controls.
5. Read on the plate reader. Fluorescent plate reader FLUOStar Omega (BMG Labtech Firmware 1.32, Software 1.20).

Fluorescent intensity is read using bottom optic readings with orbital averaging of 3 mm, GFP 485 nm/520 nm dsRED 544 nm/590 nm, E2-Crimson 610 nm/650 nm (excitation nm/emission nm).

6. After 24 h, remove 100 μl of medium from each well and replace with 100 μl fresh medium.
7. Read again on the plate reader and perform microscopic examination. Photograph each condition if required.
8. Repeat at 24-h intervals.

3.5 Analysis

1. Subtract the reading of the well containing empty collagen biomatrix and medium (background fluorescence) from all the other readings. For 2D readings subtract a well containing medium only.
2. Reading are normalized to the first reading 24-h after BCC plating. Following readings are then expressed as a fold increase of this reading (1.

3.6 Dissociation of Cocultures in Biomatrix

1. Remove medium from wells.
2. Add 50 μl of dissociation solution per well (Collagenase/Hyaluronidase).
3. Incubate for 5 min at 37 °C.
4. Observe dissociated cocultures under the microscope. If you observe dissociated single cells then stop the reaction by adding 200 μl of medium per well.
5. Spin down the plate and remove the supernatant. Resuspend in required medium volume for downstream processing.

4 Advantages, Limitations, and Potential Applications of the Bone Metastatic Niche Experimental Systems

The models we established facilitate studies of dynamic interactions between cancer cells and several cell types present in the bone marrow stroma. As with any experimental system, they have limitations: the lack of cell components such as osteocytes, osteoclasts, immune cells, neural cells, mineralized bone, and extracellular matrix components.

We aimed to reproduce in vitro the high ratio between bone marrow cells and DTC observed in patients. We also aimed to make these systems amenable to a variety of readout assays, such as microscopy, total fluorescence reading, immunohistochemistry of sectioned biomatrix, flow cytometry and IF analysis of cells recovered from 3D-biomatrix. Different cell components of the coculture can be manipulated individually or recovered as live cells for further analysis.

These assays are quantitative and can be adapted for small or medium-throughput screening studies using RNA interference, antibody or small molecule inhibitors, therefore permitting an exploratory approach in the study of DTC and dormancy and in identifying targets for anti-metastatic therapy.

References

1. Patel LR, Camacho DF, Shiozawa Y, Pienta KJ, Taichman RS (2011) Mechanisms of cancer cell metastasis to the bone: a multistep process. Future Oncol 7:1285–1297. doi:10.2217/fon.11.112
2. Weilbaecher KN, Guise TA, McCauley LK (2011) Cancer to bone: a fatal attraction. Nat Rev Cancer 11:411–425. doi:10.1038/nrc3055, nrc3055 [pii]
3. Husemann Y et al (2008) Systemic spread is an early step in breast cancer. Cancer Cell 13: 58–68.doi:10.1016/j.ccr.2007.12.003,S1535-6108(07)00372-8 [pii]
4. Fehm T, Muller V, Alix-Panabieres C, Pantel K. Micrometastatic spread in breast cancer: detection, molecular characterization and clinical relevance. Breast Cancer Res 10 Suppl 1, S1, doi:bcr1869 [pii] 10.1186/bcr1869 (2008).
5. Aguirre-Ghiso JA (2007) Models, mechanisms and clinical evidence for cancer dormancy. Nat Rev Cancer 7:834–846. doi:10.1038/nrc2256, nrc2256 [pii]
6. Marlow R et al (2013) A novel model of dormancy for bone metastatic breast cancer cells. Cancer Res. doi:10.1158/0008-5472.CAN-13-0991
7. Klein CA (2011) Framework models of tumor dormancy from patient-derived observations. Curr Opin Genet Dev 21:42–49. doi:10.1016/j.gde.2010.10.011, S0959-437X(10)00189-9 [pii]

Chapter 13

Mammary Cancer Stem Cells Reinitiation Assessment at the Metastatic Niche: The Lung and Bone

Marc Guiu, Enrique J. Arenas, Sylwia Gawrzak, Milica Pavlovic, and Roger R. Gomis

Abstract

Mammary cancer stem cells (MCSC) have been operationally defined as cells that re-form secondary tumors upon transplantation into immunodeficient mice. Building on this observation, it has also been suggested that MCSCs are responsible for metastasis as well as evasion and resistance to therapeutic treatments. MCSC reinitiating potential is usually tested by implantation of limited amounts of cells orthotopically or subcutaneously, yet this poorly recapitulates the metastatic niche where truly metastatic reinitiation will occur. Herein, we describe the implantation of small amounts of MCSC selected populations in the bone (intra tibiae injection) and the lung (intra thoracic injection) to test for their metastatic reinitiation capabilities.

Key words Mammary stem cells, Metastasis, Reinitiation, Xenograft models, Breast cancer

1 Introduction

Cancer stem cells (CSCs) have been the subject of intensive discussion and investigation leading to a continuous evolution of the concept over that period. The concept was based on the thought that malignant cell populations are organized as unidirectional cellular hierarchies. Among those, CSCs constitute unique subsets of cells that have the exceptional ability to perpetuate the growth of a malignant cell population indefinitely [1–4]. Thus, this population recapitulated the naturally existing features of cellular populations within tissues that account for its plasticity and growth cycles, for example the mammary gland. In each menstrual cycle, the mammary gland is subjected to substantial growth [5]. Similarly, during pregnancy, there is both a tenfold increase in the number of alveoli per lobule as well as de novo formation of lobules by lateral budding from existing terminal ducts [6]. These cellular dynamics led to postulate the existence of a population of precursor cells in the adult human breast that are capable of giving rise to new lobules.

Maria del Mar Vivanco (ed.), *Mammary Stem Cells: Methods and Protocols*, Methods in Molecular Biology, vol. 1293,
DOI 10.1007/978-1-4939-2519-3_13,

To date, several markers have been described in the literature and are used for the identification of human mammary stem cells (MaSC). For instance, increased aldehyde dehydrogenase (ALDH-1) activity was associated with a population of human mammary epithelial cells, which do not show estrogen receptor (ER) expression [7, 8]. Moreover, CD49+ and EpCAM+ low markers are usually being used to sort human mammary epithelial cells [9]. Of note, the MaSC are present in mammary ducts and lobule, whereas progenitor cells are prevalent in the terminal ductal lobules [10]. These data suggested that a candidate stem cell zone resides in ducts that are enriched in generally quiescent SSEA-4^{hi}/$K5^{+}$/$K6a^{+}$/$K15^{+}$/Bcl-2^{+}cells. On the contrary, the more abundant proliferating progenitors are found outside this region and are often surrounded by laminin-2/4 [10]. Moreover, new evidence suggested that the stem cell zone in ducts is defined by $K19^{+}$/$K14^{+}$ giving rise to $K19^{+}$/$K14^{-}$, $K19^{-}$/$K14^{-}$, and $K19^{-}$/$K14^{+}$ lineage-restricted progenitors [11]. In addition, RANK/RANKL signaling was involved in proliferation and maintenance of normal and cancer breast stem cells. In mouse models, mammary glands of RANK- and RANKL-deficient mice develop normally during sexual maturation, but fail to form lobulo-alveolar structures during pregnancy due to defective proliferation and increased apoptosis of mammary epithelium [12]. Interestingly, RANK/RANKL signaling has also recently been proposed to be an important component in mammary carcinogenesis, specifically in the maintenance of breast cancer stem cells and potentially metastasis [13–15]. The distribution and function of mammary stem cells, as well as breast cancer stem cells in mature mammal remains to be fully elucidated.

Interest on mammary stem cells has increased by their potential role in breast tumorigenesis [16]. Different breast cancer stem cells populations have been identified such as CD44+/CD24- [16], CD49f+[17, 18], or ALDH [19]. Interestingly, the MCSCs have been suggested to be less sensitive to cell cycle inhibition than the bulk of the tumor cells that they generate, in part due to either asymmetric division or slow cycling profile [20]. As a result, a mammary tumor may appear to be eradicated, but it is known that in a subset of patients recurrence will happen years or decades post primary tumor excision, a process that is suggested to be led by the rare invisible populations of MCSCs survived. Interactions of the MCSC and their microenvironment (metastasis niches) may also contribute to resist the treatment and disease dissemination [21–24].

These clinical important matters call for methodologies to investigate how MCSCs promote metastasis reinitiation. Most recent works have relied on the operational detection of cells with CSCs properties by assessing its ability of generating and propagating a malignant cell population, identified and characterized in an experimental setting. Much of this work uses transplanted immunodeficient mice to characterize the ability of MCSCs to

regenerate malignant outgrowths that look like the initial breast cancer. To this end, we have set up an experimental approach to test metastasis reinitiation both at the bone and the lung metastatic niches. This approach focuses only on the metastatic reinitiation process in a reductionist attempt to score the contribution of specific genes and functions to this process obviating earlier functions such as intravasation, survival in transit, and extravasation that needed to be accomplished through the multistep process that a cancer cell must undertake for metastatic accomplishment.

2 Materials

Prepare all solutions and reagents in sterile conditions using laminar flow hood. Prepare and store all reagents at room temperature (unless indicated otherwise).

2.1 Cell Culture Components

1. Cell culture grow medium: DMEM/F-12 supplemented with 10 % FBS. Store at 4 °C.
2. Media Supplements: 1 % L-glutamine (200 mM), 1 % penicillin–streptomycin, 10 % fetal bovine serum (FBS). Stored at –20 °C. Add to media cells and then store the mix at 4 °C (*see* **Note 1**).
3. Phosphate Saline Buffer (PBS).
4. Trypsin–EDTA Solution: 0.05 % Trypsin and EDTA (1:5,000) in PBS. Store at –20 °C (*see* **Note 2**).
5. Growth Factor Reduced Matrix Basement Membrane (Becton Dickinson, BD). Store at –20 °C (*see* **Note 3**).

2.2 Fluorescence Activated Cell Sorting Components

1. Staining Buffer: PBS 1× + 0.02 % BSA.
2. Washing Sorting Buffer: PBS 1× + 0.02 % BSA or if cells are sticky add 3 mM EDTA.

2.3 Antibodies

1. Antibodies to detect Breast Cancer Stem Cells: CD44-PE (BD Pharmingen), CD24-PERCP-CY5.5 (BD Pharmingen) and CD49f-PE-Cy5 (BD Pharmingen). All incubations at 4 °C for 30 min in dark.

2.4 Cells Inoculation In Vivo

Oncology animal models (when using human cancer cells) must be based on the use of immunodeficient animals, which require special conditions of maintenance. These animal models are maintained in the animal house barrier area (SPF) including HEPA filtered air conditions.

1. Immunodeficient mice: Balb C/Nude mice (*see* **Note 4**) or NOD SCID mice (*see* **Note 5**), 5 week old.
2. Anesthesia mix: Mix 1 ml Ketamine (100 mg/ml), 0.5 ml Xilacine (20 mg/ml), 8.5 ml NaCl 0.009 g/ml solution pH 6.

3. Buprenorphine (100 μl/mice from 0.01 mg/dl solution) (*see* **Note 6**).
4. Betadine solution.
5. Ethanol 70 %.
6. Deionized water (H_2Od).
7. 10 μl Hamilton syringe.
8. 28G/15 mm/pst4 Hamilton Needle.
9. 27G syringe needle.
10. 25G syringe needle and 1 ml syringe.
11. Blades.
12. 5/0 black silk.
13. Sterile material surgery: surgical scissors, blunt forceps, hemostatic clamps, needle holder.

2.5 In Vivo Imaging System

1. IVIS system (Xenogen-Caliper).
2. Luciferin solution: 15 mg/ml Beetle luciferin, potassium salt with NaCl 0.009 g/ml solution pH 6 (*see* **Note 7**).
3. Insulin (30G) syringe.

3 Methods

Carry out all cell culture procedures in a flow laminar hood and at room temperature unless otherwise indicated.

3.1 Cell Culture Establishment

1. Culture cell lines with the proper medium. All cells must stably express the *luciferase* gene. In the case of MCF7, T47D, MDA-MB-231, or BT474, DMEM/F-12 or indicated ATCC media supplemented with FBS, P/S, and L-glutamine will be used. Grow cells until 70 % confluence.

3.2 Fluorescence Activated Cell Sorting (FACS)

1 Collect cells: wash once with 1× PBS and trypsinize 5–10 min at 37 °C (*see* **Note 2**).

2 Block trypsin activity with double the amount of growth media and transfer into a 50 ml Falcon.

3 Spin down at 1,200 rpm for 5 min.

4 Wash the pellet once with 1× PBS.

5 Split cells using staining buffer (200 μl) into 15 ml Falcon tubes (one per condition). Conditions: Non Stained cells (Blank control), single staining (CD24, CD44, CD49f) and double staining (CD24 and CD44). In the case of multiple staining, always assess Fluorescence Minus One (FMOs) controls (*see* **Note 8**), which are all staining minus one of the fluorophores.

6 Staining: add 1:100 dilution (*see* **Note 9**) of all antibodies (i.e., case 2 μl for 200 μl). Number of cells range: up to 10^8 per condition (*see* **Note 8**).

7 Incubate tubes at 4 °C for 30 min in dark.

8 Wash cells twice with washing sorting buffer (rinse totally the tube; *see* **Note 10**).

9 Resuspend pellet with 200 μl depending on the number of cells (*see* **Note 11**).

10 Add 3 μl of 200 mg/ml DAPI or propidium iodide as viability staining.

11 Sort population of interest with a sorting machine (i.e., Sorting using FACS Aria (BD), *see* **Note 12**).

12 Sort cells in media without supplements.

3.3 Reinitiation Metastatic Potential Assessment

1. The day before remove the growth factor reduced (GFR) Matrigel vial from the −20 or −80 °C freezer, place the vial in a refrigerator at 4 °C.
2. Cells are sorted and spin down for 5 min at room temperature.
3. Resuspend pellet in Matrigel. Add 1:1 Matrigel–PBS 1× and mix gently but well (*see* **Note 13**). Material must be kept cold to avoid gelling when mixing the cells.
4. Keep the cells solution cold at all times.
5. Cells injection in live mouse (to be executed in the animal facility. Must comply with the Institutional Review Board committee approval): secure the animals as needed according to the experimental plan minimizing its use and following the 3Rs whenever possible (Replacement, Reduction, and Refinement). Subsequently, prepare the mice for injection using the standard approved protocols for anesthesia.
6. Mix the cells gently before loading the chilled syringe. The cells will settle by gravity and the tube of cells must be gently shaken to obtain a homogeneous mixture devoid of bubbles before injection. Syringes and needles to be used should be kept on ice until needed to prevent Matrigel polymerization.
7. To assess metastasis reinitiation at specific tissues, cells should be injected at the organ site. In order to evaluate metastatic potential of all cell population, different numbers of cells have to be injected (limiting dilution assay: 100, 500, 1,000, 2,000, 5,000, 10,000) (see below).

3.3.1 Intrathoracic Injections

1. Anesthetize mice with 10 μl anesthesia mix/g mouse delivered via intraperitoneal injection.
2. Wait until mice are completely anesthetized (*see* **Note 14**).
3. Place the mice in left lateral decubitus position.

4. Clean thoroughly the surgical area with betadine solution (*see* **Note 15**).
5. Made a small skin incision approximately on the lateral dorsal axillary line, 1.5 cm above the lower rib line just below the inferior border of the scapula.
6. Move carefully the muscles using blunt forceps.
7. Hydrate surgical area with NaCl solution.
8. Inject 40 μl of cell suspension using 25G needle syringe into the left lateral thorax.
9. Suture back skin using 5/0 black silk.
10. Inject subcutaneously 100 μl of Buprenorphine solution.
11. Confirm the inoculation by bioluminescent imaging (*see* below).
12. The mice will wake up in 20–30 min. Keep mice warm.

3.3.2 Intratibiae Injections

1. Cells are sorted and spin down for 5 min at room temperature.
2. Resuspend the cellular pellet in PBS up to 5 μl total volume/injection.
3. Keep the cells solution cold at all times.
4. Anesthetize mice with 10 μl anesthesia mix/g mouse delivered via intraperitoneal injection.
5. Wait until the mice are completely anesthetized (*see* **Note 14**).
6. Made 1 cm skin incision on the antero-medial part of the leg.
7. Put the muscles aside using blunt forceps.
8. Drill the bone using a 27G syringe needle.
9. Hydrate surgical area with NaCl solution.
10. Take out the drilling syringe needle from the bone and inject immediately 5 μl of cell suspension using Hamilton syringe with 28G Hamilton needle.
11. Suture back skin using 5/0 black silk.
12. Inject subcutaneously 100 μl of Buprenorphine solution.
13. Confirm the inoculation by bioluminescent image.
14. The mice will wake up in 20–30 min. Keep the mice warm.
15. Wash 5× 28G needle-Hamilton syringe with ethanol 70 % (*see* **Note 16**).
16. Wash 5× 28G needle-Hamilton syringe with H_2Od.

3.4 Bioluminescent Imaging

1. Mice are anesthetized as described above.
2. Place the mice in lateral decubitus position.
3. Inject 50 μl luciferin solution (*see* **Note 7**).

4. Place mice inside IVIS machine system in lateral decubitus position in intrathoracic injections or ventral position in intratibiae injections.
5. Acquire image. Conditions for acquiring luminescent images:
   - Photographic image time exposure: 0.2 s.
   - Photographic image binning exposure: Medium.
   - Photographic image focus: 8.
   - Luminescent image exposure time: 1 min.
   - Luminescent image binning exposure: Medium.
   - Field of view: D position (18.5 cm from camera).
6. Take pictures every week to score the reinitiation capability of the putative MCSC to generate a metastatic lesion at a distant niche.
7. Quantify according to the users manual and plot the luminescent values as a function of time (*see* **Note 17**).

4 Notes

1. Supplements are required in cells growth media for their survival. Stick to ATCC instructions for each cellular population as requirements might vary.
2. Time exposure to trypsin is important in order to collect intact cells. Normally 5–10 min at 37 °C is sufficient. However, adhesion to the plate will depend on the cell type and confluence. Thus, incubation time should be prolonged until cells are unattached as per visual confirmation under the microscope.
3. Growth Factor Reduced Matrix is necessary to recover cells when inoculated in vivo in a hostile tissue.
4. Balb C/Nude mice are athymic mice, hair, thymus, and T-cells deficient.
5. NOD SCID mice are athymic mice with severe immunodeficiency due to improper T-cells and B-cells development. Natural Killer (NK) cells; macrophage and granulocyte numbers and function are reduced.
6. Buprenorphine is a semisynthetic derivative of thebaine, one of the most chemically reactive opium alkaloids. Buprenorphine is used for pain management in mice, and is the favored analgesia if available.
7. Luciferin is the substrate for the luciferase enzymatic reaction expressed in cells injected. When the reaction occurs luminescent light appears and we can capture and measure with IVIS system.

8. Each FMO and double staining should be done using the same amount of cells in order to compare the signals strength.
9. Each antibody in every laboratory ideally should be titrated for each cell line to obtain the most reliable results.
10. Wash extensively the pellet in order to remove all remaining non-bound antibodies, which may interfere in FACS analysis.
11. Volume suspension is extremely important to increase the yield of sorting. If cell suspension is too murky, the yield of sorting will decrease and can generate clumps in the machine.
12. To obtain greater number of viable cells after sorting use sorting tips of >100 μm. Speed sorting is crucial to obtain higher yield and to minimize cell damage. More than 5,000 events/s is not recommended. Sorter machine should have been calibrated according to manufacturer instructions.
13. Be sure the dispersed material is cold when Matrigel is added. The matrix is very viscous and difficult to pipette accurately. It is recommended that when filling the pipette you pipette up and down several times to coat the inside of the pipette and then eject the Matrigel several times to empty the pipette as much as possible. If you are using a plastic tip micropipette, cut the tip to create a larger bore for faster and more accurate pipetting.
14. Remember that anesthesia effect in full only lasts 10–15 min when planning the experiment.
15. The surgical area must be cleaned to prevent any possible infection.
16. It is necessary to clean thoroughly the Hamilton's syringe and needle to prevent any salt precipitation.
17. Usually, 24–48 h post inoculation there is a dramatic reduction in luciferase activity, which eventually will return as a function of the MCSC ability to reinitiate a lesion at the distant metastatic niche.

Acknowledgement

M.P, S.G., and E.J.A. are supported by "La Caixa" PhD fellowship program. R.R.G. was supported by the Institució Catalana de Recerca i Estudis Avançats. Support and structural funds were provided by the BBVA foundation, Generalitat de Catalunya (2014 SGR 535) and the Spanish Ministerio de Ciencia e Innovación (MICINN) (SAF2013-46196) to R.R.G.

References

1. Husemann Y, Geigl JB, Schubert F, Musiani P, Meyer M, Burghart E, Forni G, Eils R, Fehm T, Riethmuller G et al (2008) Systemic spread is an early step in breast cancer. Cancer Cell 13:58–68
2. Cameron MD, Schmidt EE, Kerkvliet N, Nadkarni KV, Morris VL, Groom AC, Chambers AF, MacDonald IC (2000) Temporal progression of metastasis in lung: cell survival, dormancy, and location dependence of metastatic inefficiency. Cancer Res 60:2541–2546
3. Psaila B, Lyden D (2009) The metastatic niche: adapting the foreign soil. Nat Rev Cancer 9: 285–293
4. Hynes RO (2009) The extracellular matrix: not just pretty fibrils. Science 326:1216–1219
5. Potten CS, Watson RJ, Williams GT, Tickle S, Roberts SA, Harris M, Howell A (1988) The effect of age and menstrual cycle upon proliferative activity of the normal human breast. Br J Cancer 58:163–170
6. Russo J, Russo IH (2004) Development of the human breast. Maturitas 49:2–15
7. Ginestier C, Hur MH, Charafe-Jauffret E, Monville F, Dutcher J, Brown M, Jacquemier J, Viens P, Kleer CG, Liu S et al (2007) ALDH1 is a marker of normal and malignant human mammary stem cells and a predictor of poor clinical outcome. Cell Stem Cell 1:555–567
8. Liu S, Ginestier C, Charafe-Jauffret E, Foco H, Kleer CG, Merajver SD, Dontu G, Wicha MS (2008) BRCA1 regulates human mammary stem/progenitor cell fate. Proc Natl Acad Sci U S A 105:1680–1685
9. Eirew P, Stingl J, Raouf A, Turashvili G, Aparicio S, Emerman JT, Eaves CJ (2008) A method for quantifying normal human mammary epithelial stem cells with in vivo regenerative ability. Nat Med 14:1384–1389
10. Villadsen R, Fridriksdottir AJ, Ronnov-Jessen L, Gudjonsson T, Rank F, LaBarge MA, Bissell MJ, Petersen OW (2007) Evidence for a stem cell hierarchy in the adult human breast. J Cell Biol 177:87–101
11. Petersen OW, Polyak K (2010) Stem cells in the human breast. Cold Spring Harb Perspect Biol 2:a003160
12. Fata JE, Kong YY, Li J, Sasaki T, Irie-Sasaki J, Moorehead RA, Elliott R, Scully S, Voura EB, Lacey DL et al (2000) The osteoclast differentiation factor osteoprotegerin-ligand is essential for mammary gland development. Cell 103:41–50
13. Schramek D, Sigl V, Penninger JM (2011) RANKL and RANK in sex hormone-induced breast cancer and breast cancer metastasis. Trends Endocrinol Metab 22:188–194
14. Gonzalez-Suarez E, Jacob AP, Jones J, Miller R, Roudier-Meyer MP, Erwert R, Pinkas J, Branstetter D, Dougall WC (2010) RANK ligand mediates progestin-induced mammary epithelial proliferation and carcinogenesis. Nature 468:103–107
15. Tarragona M, Pavlovic M, Arnal-Estape A, Urosevic J, Morales M, Guiu M, Planet E, Gonzalez-Suarez E, Gomis RR (2012) Identification of NOG as a specific breast cancer bone metastasis-supporting gene. J Biol Chem 287:21346–21355
16. Al-Hajj M, Wicha MS, Benito-Hernandez A, Morrison SJ, Clarke MF (2003) Prospective identification of tumorigenic breast cancer cells. Proc Natl Acad Sci U S A 100:3983–3988
17. Shackleton M, Vaillant F, Simpson KJ, Stingl J, Smyth GK, Asselin-Labat ML, Wu L, Lindeman GJ, Visvader JE (2006) Generation of a functional mammary gland from a single stem cell. Nature 439:84–88
18. Pece S, Tosoni D, Confalonieri S, Mazzarol G, Vecchi M, Ronzoni S, Bernard L, Viale G, Pelicci PG, Di Fiore PP (2010) Biological and molecular heterogeneity of breast cancers correlates with their cancer stem cell content. Cell 140:62–73
19. Gopalan A, Yu W, Sanders BG, Kline K (2013) Eliminating drug resistant breast cancer stem-like cells with combination of simvastatin and gamma-tocotrienol. Cancer Lett 328:285–296
20. Caussinus E, Gonzalez C (2005) Induction of tumor growth by altered stem-cell asymmetric division in Drosophila melanogaster. Nat Genet 37:1125–1129
21. Kim MY, Oskarsson T, Acharyya S, Nguyen DX, Zhang XH, Norton L, Massague J (2009) Tumor self-seeding by circulating cancer cells. Cell 139:1315–1326
22. Kii I, Nishiyama T, Li M, Matsumoto K, Saito M, Amizuka N, Kudo A (2010) Incorporation of tenascin-C into the extracellular matrix by periostin underlies an extracellular meshwork architecture. J Biol Chem 285:2028–2039
23. von Holst A (2008) Tenascin C in stem cell niches: redundant, permissive or instructive? Cells Tissues Organs 188:170–177
24. Oskarsson T, Acharyya S, Zhang XH, Vanharanta S, Tavazoie SF, Morris PG, Downey RJ, Manova-Todorova K, Brogi E, Massague J (2011) Breast cancer cells produce tenascin C as a metastatic niche component to colonize the lungs. Nat Med 17:867–874

Chapter 14

Nanomechanical Characterization of Living Mammary Tissues by Atomic Force Microscopy

Marija Plodinec and Roderick Y.H. Lim

Abstract

The mechanical properties of living cells and tissues are important for a variety of functional processes in vivo, including cell adhesion, migration, proliferation and differentiation. Changes in mechano-cellular phenotype, for instance, are associated with cancer progression. Atomic force microscopy (AFM) is an enabling technique that topographically maps and quantifies the mechanical properties of complex biological matter in physiological aqueous environments at the nanometer length scale. Recently we applied AFM to spatially resolve the distribution of nanomechanical stiffness across human breast cancer biopsies in comparison to healthy tissue and benign tumors. This led to the finding that AFM provides quantitative mechano-markers that may have translational significance for the clinical diagnosis of cancer. Here, we provide a comprehensive description of sample preparation methodology, instrumentation, data acquisition and analysis that allows for the quantitative nanomechanical profiling of unadulterated tissue at submicron spatial resolution and nano-Newton (nN) force sensitivity in physiological conditions.

Key words Atomic Force Microscopy, Sensitivity, Spatial resolution, Mechanobiology, Cells, Extracellular matrix, Living mammary tissues, Human breast biopsies, Diagnosis, Disease

1 Introduction

Living tissues exhibit remarkable physical properties as defined by the complex interplay between cellular and extracellular elements that exert a "tug-of-war" of forces that resist compression and adapt to changes in the microenvironment [1]. This is directly coupled to gene regulation and protein expression, cellular development, motility, proliferation and differentiation (i.e., cell "fate") that altogether define tissue mechano-functionality [2–4]. Mechanical factors that affect cell fate include the rigidity and topology of the extracellular matrix (ECM) [5], substrate adhesion, cell deformability within tissues as a result of mechanical loading, and shear stresses associated with corresponding fluid flow [4]. In this way, changes in cell cytoarchitecture and the ECM during cancer development and progression are manifested in the

Maria del Mar Vivanco (ed.), *Mammary Stem Cells: Methods and Protocols*, Methods in Molecular Biology, vol. 1293,
DOI 10.1007/978-1-4939-2519-3_14,

corresponding nanomechanical responses [6, 7]. This link between the functional changes and the mechanobiology of cells and tissues is not only fundamental for our understanding of tissue specific functions in vivo but may provide potential diagnostic and prognostic markers as well [8]. But how does one measure these properties reliably and efficiently, under physiological conditions found in vivo? For starters, single cell and tissue level experimentation must be bridged to obtain a length-scale dependent understanding of mechanobiological properties. Indeed, this is where atomic force microscopy (AFM) [9] as a technique can break new ground.

The principle of AFM operation is very similar with that of a gramophone. Typically, the AFM uses a ~10 nm-sharp tip (i.e., "probe" or "tip") at the end of a flexible cantilever that directly contacts and probes the surface corrugations of an underlying sample. This is known as "contact" mode and represents a standard mode of AFM operation used for biological applications. Here, a laser is reflected off the back of an AFM cantilever as it raster scans across a sample. In this manner, deflections that arise from surface features are monitored using a photodiode detector, as the applied force on the sample is kept constant by a piezoelectric scanner. The signals associated with the cantilever deflection or the vertical piezoelectric-scanner displacement can be used to generate a three-dimensional image of the sample surface. Another key feature of the AFM involves measuring the nanomechanical properties of biological samples under aqueous conditions. Instead of raster-scanning as is done during imaging, the AFM tip applies a local compressive force and reports the resulting material deformation in the form of a force curve.

Several AFM studies of living cells have been undertaken to examine the direct correlation between malignancy and cell deformability using various cell lines [6, 10–14]. In 2007, a key study by Cross et al. uncovered a softening in primary cells obtained from pleural effusions of human patients [15]. Nevertheless, these findings have been disputed due to: (1) a lack of the natural 3D tissue context, and (2) insufficient measurements/analysis to account for intracellular heterogeneities. As this highlights, investigating entire tissue segments with sub-cellular resolution would provide a more comprehensive understanding of such mechanical changes because biological tissues contain different cellular phenotypes with differing roles in tissue homeostasis [16]. Other techniques, such as bulk rheology [17], tissue elastosonography [18], or even AFM tips modified with colloidal probes [19], typically suffer from poor spatial resolution and low force sensitivity, which are necessary to address these mechano-cellular effects at the nanoscale.

To bridge this gap we have developed an AFM-based apparatus known as ARTIDIS ("*Automated and Reliable Tissue Diagnostics*") that measures and spatially correlates local nanomechanical properties

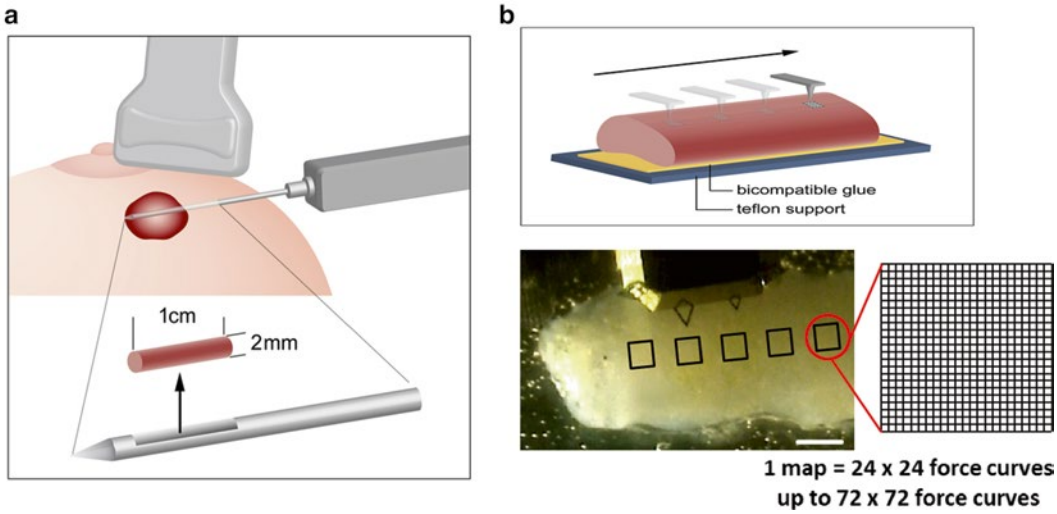

Fig. 1 Testing human breast biopsies by ARTIDIS. (**a**) Schematic representation of an ultrasound guided biopsy from a patient with a suspicious lesion. (**b**) Multiple stiffness maps (20×20 μm^2), each consisting of 24×24 indentation measurements are recorded at up to 20 different sites across the entire specimen in a systematic manner (*top*). "Birds-eye" view of an oriented, immobilized biopsy in Ringer's Complete solution with the cantilever in position (*bottom*). For better visualization, *square insets* in the image illustrating stiffness maps are not drawn to scale. Scale bar, 500 μm. Modified with permission from Nature Nanotechnology [20]

across entire unadulterated tissues in close to native physiological conditions. In the case of human and murine breast cancer tissues, ARTIDIS provides unprecedented spatial resolution and sub-kilopascal (kPa) stiffness sensitivity that is able to distinguish individual cells from their surrounding extracellular matrix (ECM) [20]. An ARTIDIS assay uses a ~10 nm-sharp AFM tip that collects ~10,000 force measurements (i.e., indentations) that are spatially distributed across a biopsy surface within 3 h. Therefore, each indentation effectively measures the stiffness of local structures (e.g., ECM, cancer cells, etc.) that lie under the tip (Fig. 1). In this manner, one obtains a quantitative biopsy-wide nanomechanical profile or signature that is strongly correlated to tissue status and health [20]. Another key advantage of ARTIDIS is the automatization process that markedly reduces user input and increases experimental throughput without compromising data quality, spatial resolution, and force sensitivity.

This chapter, illustrated using human mammary tissue as an example, provides detailed instructional tips, methods and protocols that are beneficial for resolving the mechanical properties of native biological tissues by ARTIDIS, and may be applicable to other AFM systems. Moreover, we note that the guidelines presented here are not only limited to mammary tissues but can be applied to a large variety of soft tissues (i.e., cartilage [21], lung, liver, prostate, and lymph nodes) and 3D tissue cultures [22].

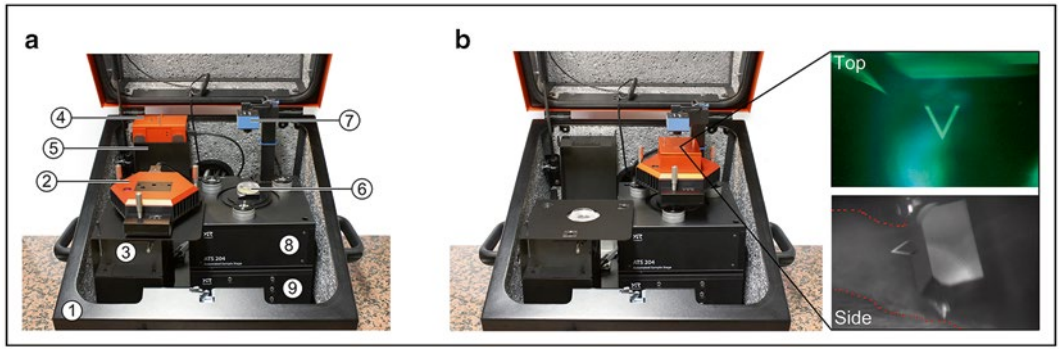

Fig. 2 Basic components of the ARTIDIS AFM System. (**a**) Open acoustic housing (1) where the scan head (2) is standing on a parking station (3) and a camera (4) on its holder (5). A cell culture dish containing the sample (6) imaged by a "birds-eye" camera (7) and mounted on top of the Automated Sample Stage (8) that allows for movement in the *x*-, *y*-, and *z*-direction. This is placed on top an active Isostage Table (9) for vibration isolation. (**b**) In a measurement-ready configuration, the scan head with a mounted AFM probe in a cantilever holder (CantiClip, not seen here) is placed on the sample stage. The camera—mounted on top of the scan head—provides the top and side views of the sample that is beneath the cantilever (*red dashed lines*)

2 Materials

2.1 Reagents

1. Fresh Tissue sample (*see* **Note 1**).
2. Ringer solution with 5 % glucose (*see* **Note 2**). Sterile isotonic Ringer lactate solution with 5 % glucose is prepared from 6.00 g NaCl, 0.40 g KCl, 50 g anhydric glucose, 0.27 g $CaCl_2$, 3.20 g lactic acid, and finally by adding 1.0 liter (l) of cooled sterile water. The prepared solution can be stored up to 1 year at 4 °C. Prior to each tissue measurement, add one tablet of protease inhibitors (Complete, EDTA free, Roche) per 50 ml of Ringer solution (henceforth known as "Ringer Complete"). Ringer Complete can be stored up to maximum of 14 days at 4 °C (however, it is recommended to prepare it fresh prior to experiment).
3. Protease inhibitor cocktail (Complete, Roche Switzerland).
4. Indian Ink/Tissue Dye (e.g., CDI's Tissue Marking Dye, Cancer Diagnostics Inc., USA).
5. Formalin solution 10 %, neutral buffered (Sigma Aldrich, Switzerland).
6. RNA stabilization reagent (e.g., RNAlater, Qiagen Netherlands).
7. Epoxy Two Component Glue, 5 min hardening time (*see* **Note 3**, Harz, Germany or similar).

2.2 Equipment

1. ARTIDIS (Nanosurf AG, Switzerland) equipped with a 100 μm piezo element (Fig. 2)[1].

[1] May not be applicable to other AFM systems.

2. *AFM cantilevers* used are DNP-S10 D with a nominal stiffness of 0.06 N/m (Bruker, USA, *see* **Note 4**).
3. Sterile scalpel for cutting and preparing tissue.
4. Plastic tweezers for cantilever handling and mounting AFM probes onto the cantilever holder ("CantiClip", *see* **Note 5**).
5. Metal tweezers for handling and mounting the sample.
6. Cell culture dishes (35 Diameter, e.g., Tissue Culture Dish 40, TPP Switzerland).
7. Lint free tissue paper (e.g., *Kimtech Science Precision Wipes*, Kimberley-Clark Professional).

3 Methods

3.1 Sample Preparation

Prior to experimentation, samples need to be attached to a substrate (Culture dish bottom) to ensure solid contact during the entire measurement. Loose samples that swim around in buffer are inappropriate. For this purpose, we suggest using two-component 5 min epoxy glue. Sample preparation should be performed as follows:

1. Post-excision, the tissue must be immediately transferred to the Ringer Complete solution and kept at 4 °C until an experiment commences (*see* **Note 6**).
2. Dissect the sample into 1–3 mm thick slices. It is imperative to dissect the two sides in a manner that is as parallel and smooth as possible for high quality measurements. When the contamination by fascia, mucin or floating debris is present, it should be removed by sample washing with Ringer's Complete.
3. Unused tissue pieces can be saved in a RNA stabilization reagent for later RNA extraction and consequently gene expression profiling.
4. Put two similar sized droplets of epoxy resin and the hardener respectively, on the lid of a TPP dish (Fig. 3a).

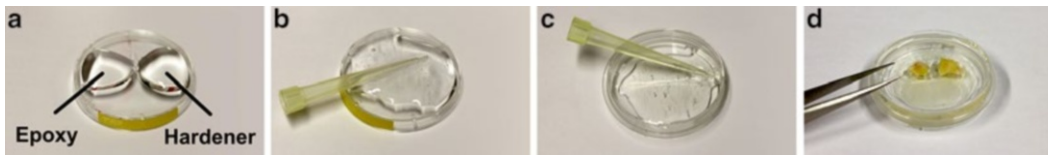

Fig. 3 Preparing tissues for AFM experiments. For ARTIDIS measurements, the sample needs to be attached to a hard substrate during the entire measurement. For that purpose we use two-component epoxy glue (5 min hardening time). (**a**) Two droplets of epoxy resin and hardener on the lid of a TPP culture dish. (**b**) Both components are mixed using a 200 μl pipette tip. (**c**) A thin layer of epoxy glue is applied onto the bottom a TPP dish. (**d**) Tissue samples are gently laid on top of the epoxy layer once it is hard enough and does not mix with buffer

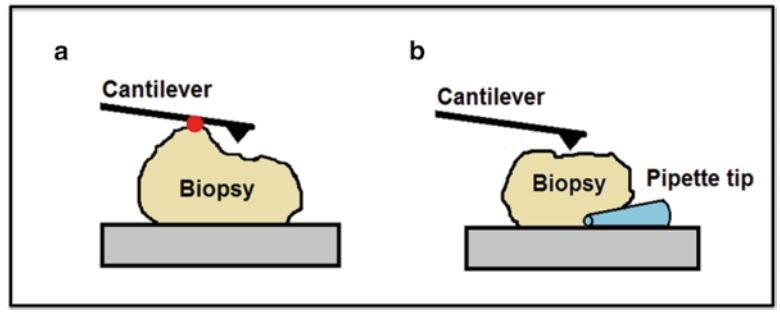

Fig. 4 Avoiding measurement artifacts caused by surface waviness. Surfaces are often rough on a macroscopic scale (waviness). This can cause problems (**a**) when the cantilever touches the biopsy before the probe, yielding image artifacts and unidentifiable AFM force curves. A simple solution to this problem is illustrated in (**b**) where one can level the tissue surface with an object (e.g., pipette tip) to ensure that the AFM probe makes proper contact with the biopsy

5. Use a 200 μl pipette tip to mix thoroughly both components (Fig. 3b).
6. Allow the epoxy to harden sufficiently for 1.5–2 min such that it will not mix with the Ringer Complete (*see* **Note 7**). Next, apply a thin layer of epoxy glue onto the bottom of a TPP dish (Fig. 3c). Take the tissue sample out of the original tube filled with Ringer Complete using tweezers and dry briefly the bottom side using a lint-free tissue paper.
7. As soon as the epoxy is hard enough, gently lay the tissue sample on top of the epoxy layer in the TPP dish using tweezers (Fig. 3d). Pay attention that the sample does not sink too deep into the glue. Therefore, the epoxy layer should be either thinner than the tissue sample or viscous enough.
8. Pipette tips can also be inserted below the sample if it is visually uneven and tilted with respect to the AFM probe (Fig. 4). This "levelling" procedure ensures that the AFM tip makes proper contact with the specimen during measurement and not the cantilever or the chip itself.
9. *Optional washing step* (*see* Subheading 3.2, **step 2**): Gently add Ringer Complete at the side of the dish until the sample is covered completely. Then, aspirate the buffer again.
10. Gently add some buffer at the side of the dish at least until the sample is covered completely. In general, it is better to apply more solution to protect the tissue from buffer evaporation. However, do pay attention that the liquid does not spill onto the scan head electronics when the AFM probe dips.
11. Place the sample-mounted TPP dish onto the ARTIDIS sample stage and perform the measurement.

3.2 ARTIDIS: Force Spectroscopy Mode[2]

1. Turn all Hardware components (Fig. 2) on and open the ARTIDIS "LoginScreen". Select the appropriate user and sample. Continue in "ARTIDIS Core".
2. Mount the DNP-S10 Chip on the grooveless cantilever holder (called "CantiClip") using plastic tweezers (*see* **Note 5**) and place the CantiClip onto the scan head. Place the scan head with the Canticlip onto the parking station and open the "Laser Signal" window. Align the laser and photo diode in air.
3. Calculate the cantilever spring constant using the thermal tune function (SPM Parameters → Probe/Tip → Cantilever spring constant: Calibrate) (*see* **Notes 8** and **9**). Average the calculations over 1,000 thermal tune measurements to obtain consistent results and enter the final value in the "ARTIDISCore".
4. Using a pipette, add a drop of Ringer Complete onto the glass of the CantiClip to avoid bubble formation. Realign the laser and photo diode in the Ringer Complete-filled TPP dish on the parking station. Move the TPP dish to the sample mount, retract the Z-stage fully using the Stage Control Unit (SCU) and place the scan head on. Measure the deflection sensitivity on the dish using setpoint of 1 Volt (V) to minimize damage to the AFM probe when contacting the hard TPP substrate (*see* **Notes 10–12**).
5. Remove the scan head again and position the prepared sample onto the sample mount. If the surface of the sample is tilted, the gradient must align with the cantilever, so that the highest area points to the user. This minimizes the risk of the cantilever touching the sample (*see* Fig. 4).
6. Adjust camera settings (focus and exposure), obtain an optical image and place the scan head back. Let the cantilever equilibrate for 20 min (*see* **Note 13**).
7. Define measurement settings. Standard values are as follows: map scan size 20–50 μm (make sure to adjust the pixel size accordingly to maintain the same resolution through different measurements), 32 × 32 pixel resolution (Note: each pixel is a force measurement), defined force setpoint at 1.8 nN, piezo ramp size of 12 μm (*see* **Note 14**), and indentation velocity of 16 μm/s. For high-resolution measurements it is recommended to increase to 64 × 64 or higher to resolve cellular and extracellular components. Double check the General Settings, use the nPoint piezo and an appropriate retract distance of for example 1,500 μm when moving from one spot to the other.

[2] May not be applicable to other AFM systems.

8. Select the areas to be measured by creating multiple maps that cover the sample in a defined spatial manner (for details see Fig. 1). Use the 'Add multiple Spots' function for this. Make sure that all macroscopically distinguishable areas have at least three spots measured and select at least 15–20 spots per sample.
9. Start automated measurement (*see* **Notes 15** and **16**).

3.3 Post-AFM Processing of Tissue Specimens

After each measurement, the sample should be post-processed. It can be easily removed from the epoxy by gently applying tweezers to pull the sample off the substrate. This includes:

1. Gene expression profiling: place the sample in the RNA stabilization reagent and store at −20 °C, or snap-freeze the sample and store it at −80 °C until further processing.
2. Histology/Immunohistochemistry staining (*see* **Note 17**).
3. Scanning Electron Microscopy: Post AFM samples should be fixed in a mixture of 2.5 % formaldehyde/2.5 % glutaraldehyde (Electron Microscopy Sciences) in 0.1 M sodium cacodylate buffer (Electron Microscopy Sciences) for 1 h at room temperature (RT), after which they should be placed in a fresh fixative and incubated overnight at 4 °C.

3.4 Force Curve Processing

This section describes how data (e.g., elastic or Young's modulus) is extracted from force-indentation curves by processing raw loading/unloading curves using "ARTIDISReader" analysis software.[3] It is important to note that when using ARTIDIS these procedures are fully automated and thus not directly visible to the user, however the protocols, as listed below, can be fully accessed by the user if required or applied to data collected by other AFMs.

The raw curve is recorded as a cantilever deflection c_d [V] versus piezo distance p_d [m]. The maximum cantilever deflection is controlled by the setpoint and the piezo distance is defined by the ramp size (*see* Subheading 3.2, **step 7**). The name force-indentation curve indicates that the *y*-axis c_d needs to be transformed from Volts to Newton units. The *x*-axis p_d, is transformed to indentation, h [m], which accounts for (subtracts) the bending of the cantilever (Fig. 5). Only the transformed curve or more specifically, the unloading part of the transformed curve is used for the calculation of the Young's modulus. This is because loading curves include both plastic and elastic deformation that cannot be distinguished,

Fig. 5 (continued) contact region, whereas the indentation-depth h (**b**) is the distance between the contact point and the maximum deflection of the cantilever for the maximum force applied (setpoint). Slope stiffness S (**c**) is simply the linear fit to the upper 50 % of the force-indentation curve

[3] May not be applicable to other AFM systems.

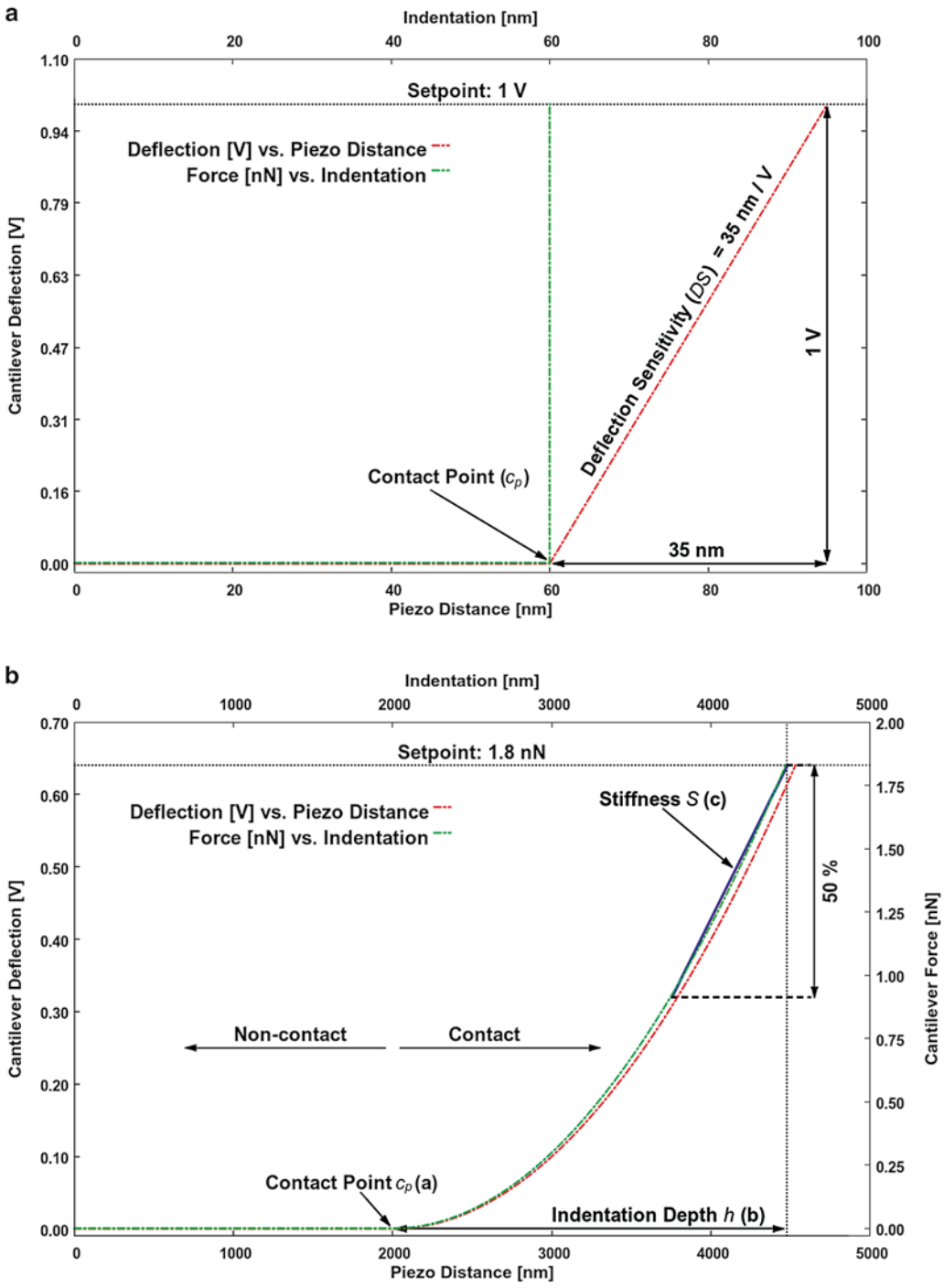

Fig. 5 Force curve data conversion. (**a**) The slope of an unloading portion of the force curve measured on an infinitely stiff (plastic) TPP dish with a setpoint of 1 V is used to determine the deflection sensitivity (DS) of the measuring AFM probe (calibration). The force curve conversion is performed by cantilever bending subtraction from the *z*-piezo distance (*green curve*, *upper x-axes*). The slope becomes vertical due to zero indentation into the infinitely stiff sample. (**b**) Subsequently, the calibrated probe (spring constant; $k = 0.06$ N/m) is used for measuring force curves on a soft tissue. By applying the Hooke's Law (Eq. 2), the setpoint is transformed to force (F) = 1.8 nN (*right y-axes*) and the force-piezo distance to force-indentation curve by subtracting the cantilever bending from the *z*-piezo distance. Here the contact point cp (**a**) separates the non-contact and

whereas the unloading curves represent only the (visco)-elastic recovery of the material when the load is released [23, 24].

The transformation of the force curve is performed as follows:

1. The non-contact region (called "baseline", *see* Fig. 5b) in certain raw curves may be tilted. To correct the tilt, ARTIDISReader calculates a linear fit of the baseline which is then subtracted from the complete curve which sets the baseline to 0 V. For this algorithm to work correctly, the baseline needs to be at least 20 % of the full piezo displacement recorded in a measurement.
2. Hooke's law states that:

$$F(\mathrm{N}) = k(\mathrm{N/m}) \times d(\mathrm{m}) \tag{1}$$

   In an AFM setup, k is the spring constant of the cantilever and d its deflection. But, the AFM measures d in Volts (c_d) on the photodiode. Using the deflection sensitivity (DS) [m/V] (*see* Subheading 3.2, **step 4**), one can relate the deflection of the cantilever to the applied force and hence transform the y-axis from Volt to Newton (change from the left to the right y-axes in Fig. 5a) in the following manner:

$$F(\mathrm{N}) = k(\mathrm{N/m}) \times c_\mathrm{d}(\mathrm{V}) \times \mathrm{DS}(\mathrm{m/V}) \tag{2}$$

3. Nevertheless, a force-piezo-distance curve still underestimates the stiffness of a sample, because it contains the stiffness of a sample and the cantilever bending.
4. The piezo distance to indentation (h) transformation removes bending of the cantilever (soft cantilever contribution). Here, the contact region appears contracted (*see* Fig. 5a) because it reveals only the indentation and stiffness of the sample.

$$h(\mathrm{m}) = p_\mathrm{d}(\mathrm{m}) - c_\mathrm{d}(\mathrm{V}) \times \mathrm{DS}(\mathrm{m/V}) \tag{3}$$

5. Values calculated from the force-indentation curve in Fig. 5b are: (a) cp, the contact point where the force curve crosses the zero of the x-axis, (b) h [m], the indentation depth as given by the distance on the x-axis between cp and the point of maximum cantilever deflection; and (c) slope stiffness S [N/m] is defined as the slope of the upper 50 % of the force-indentation curve.
6. The Young's (E) modulus [Pa] or "contact stiffness" is calculated according to Oliver and Pharr theory [23] based on the slope stiffness and the contact area A_c [21, 25].

$$E = \sqrt{n} \,/\, 2(1-U^2)S \,/\, \sqrt{(A_c(h))} \tag{4}$$

The Oliver & Pharr model requires the indentation-depth for calculating the contact area Ac. Other models as Hertz and Sneddon

are less suited for soft visco-elastic biological materials because of the lack of plastic deformation in the force regimes probed in biological tissue experiments. The contact area *Ac (h)*, for a given tip angle θ is the projection of the contact area of a 4-sided pyramid with the indentation-depth being the pyramid height:

$$A_c(h) = [(2htan[(\theta)]]^2 \quad (5)$$

The Poisson ratio ν is chosen as 0.5, hence there is no change in sample volume when it is compressed [26]. Indeed, this is physically meaningful since tissues and cells mostly consist of water that is incompressible.

3.5 Data Analysis

Recorded data thereafter can be compared across many samples and conditions using "ARTIDISReader"*. A display of calculated data is critical for sample evaluation, which can be shown in three ways as illustrated for healthy and malignant breast tissue (Figure 6). Please note that data can be visualized in the following manner (calculated according to Subheading 3.4):

1. *Maps* are 2D arrays of data collected in **step 7** of Subheading 3.2. The *x*- and *y*-axes are the width and length of a scanned area and the *z*-axes represents the channel values in color-coded fashion.
   (a) Maps allow us to correlate Young's modulus values (stiffness) with local tissue features, for example a soft cell embedded in a stiff matrix (Fig. 6a, top and bottom).
   (b) Using ARTIDISReader, a user can load an arbitrary number of force maps by clicking 'Open Force Curves'. In general, stiffness maps contain quantitative information about sample stiffness. However, they are more useful in terms of visualization rather than providing comprehensive statistical information. Therefore it is more beneficial to combine them with histograms or bar charts.
2. *Histograms* contain ("bin") all values of a map, or multiple maps. On the *x*-axes are the bins of a given width (e.g., 200 Pa, from 0 to 20 kPa). The first bin will then be from 0 to 199, the next from 200 to 399 and so on. Every stiffness value that falls within one bin increases the count of that bin by one. Therefore the *y*-axes represent the "count" of bins or a frequency of certain stiffness values (*see* **Note 18**). This is also a simple way to check the statistics of sample stiffness. For example, for soft samples, the bins at low stiffness values will have large counts.
   (a) Histograms show the distribution of stiffness across an individual tissue specimen. Post-AFM, histological sections provide specific immunohistochemical information that can be directly related to light microscopy overview images of the measured sample.

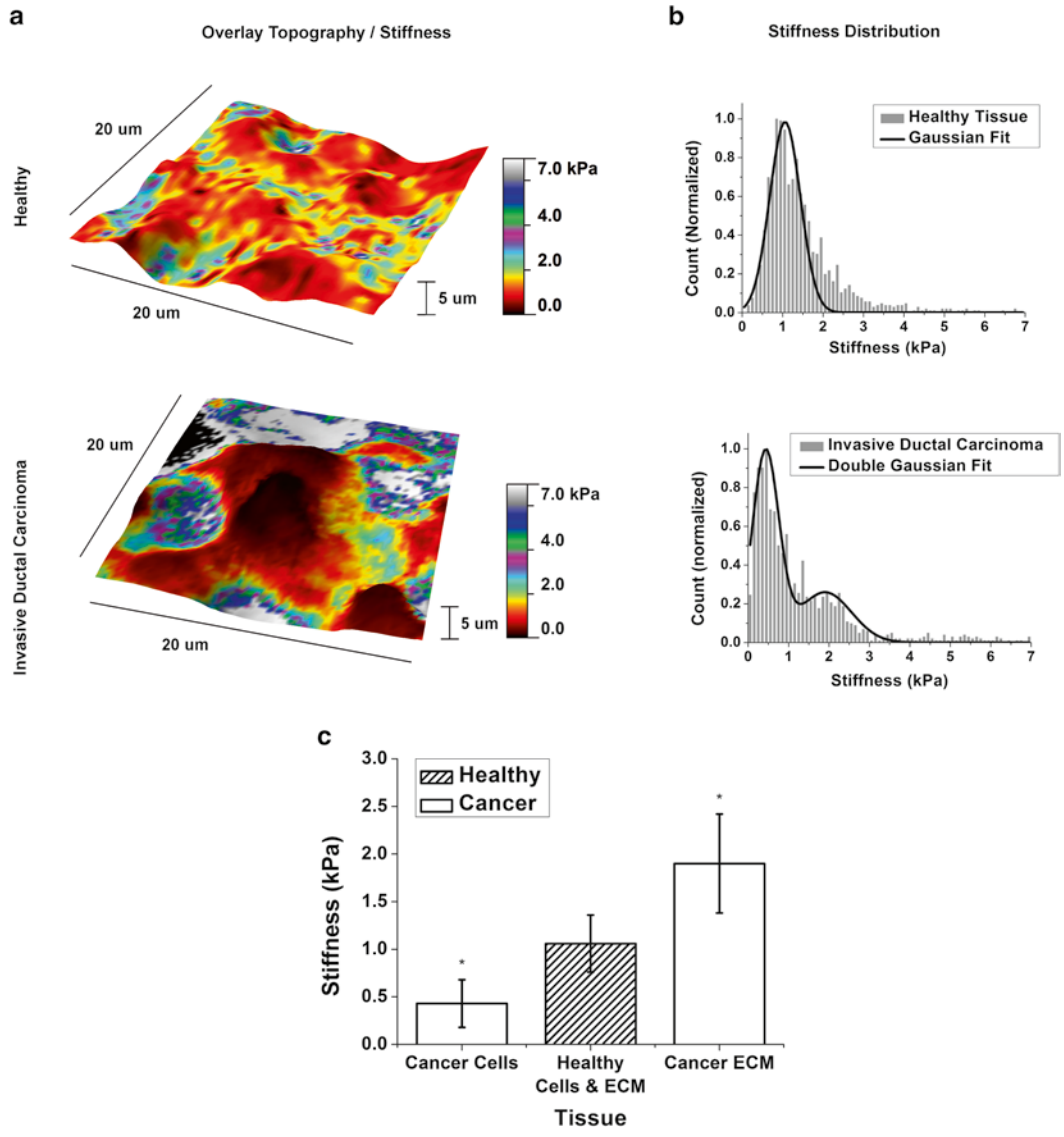

Fig. 6 The nanomechanical signature of human mammary tissues. (**a**) Representative four-dimensional (4D) maps of a healthy and invasive ductal carcinoma showing three-dimensional topology (72 × 72 pixels, 5,184 indentations) overlaid with stiffness (Young's modulus; color scale). Data are plotted in the Gwyddion image analysis software using plane levelling and mean fitting (radius 5 pixels). Healthy tissue exhibits both cellular and extracellular components of similar stiffness (~1 kPa) (*top*). In contrast, an invasive ductal carcinoma reveals approximately twofold softer cellular components (~0.5 kPa) surrounded by the stiff extracellular matrix (~2 kPa) (*bottom*). (**b**) Biopsy-wide histogram of the healthy tissue exhibits unimodal Gaussian distribution with small local variations in tissue stiffness (1.06 ± 0.25 kPa) (*top*). An invasive ductal carcinoma exhibits bimodal stiffness distribution with a characteristic soft peak for malignant cells (Young's Modulus = 0.43 ± 0.25 kPa) and a second stiffer peak denoting the extracellular matrix (1.90 ± 0.55 kPa with an exponential decay) (*bottom*). (**c**) Bar chart representing the average stiffness (Young's modulus) values were obtained by fitting the Gaussian distribution to histograms in (**b**). Error bars represent average ± S.D. The statistical significance was tested at $*P = 0.05$

(b) The user can also merge calculated stiffness data into a global histogram (the sum of all histograms per individual sample). In the case of patient biopsies this is referred as a biopsy-wide histogram. This is pertinent when comparing stiffness data between multiple specimens/patients (Fig. 6b, top and bottom).

(c) Global (biopsy-wide) histograms are created in ARTIDIS-Reader by selecting samples or experiments and then clicking 'Optimize Selection' or 'Compare Selection'.

(d) Predominantly biopsy-wide histograms follow bell-shaped Gaussian distributions where the maximum of the peak represents a mean stiffness value and the width of the distribution correspond to its standard deviation. Fitting is performed using the 'Fitting Tool' that can create a Gaussian fit with up to three peaks per histogram. However, since the fitting parameters depend on the distribution's appearance for a given specimen, in specific cases statistical probability functions other than Gaussian can be applied as well.

3. *Bar Charts* are another way of presenting quantitative sample stiffness distributions. Mean values and standard deviations of the Gaussian fit are used to efficiently compare dozens or hundreds of single histograms by plotting the mean value on the *y*-axes against the sample name on the *x*-axes (Fig. 6c). They are created automatically from the Gaussian fit in the ARTIDISReader when working with the 'Compare Selection' in Subheading 3.5.2c.

4 Notes

1. The involvement of a physician or pathologist may be required for handling human tissue samples. Also, appropriate S2 safety standards and ethical permissions should be ensured for handling and experimenting with human and murine tissue samples.
2. Sterile Ringer lactate solution with 5 % glucose can be commercially obtained as an infusion package from Braun (Germany) or similar providers.
3. Do NOT use tissue adhesives for wound repair (as for example 3 M Vetbond or Histoacryl)! They penetrate into the tissue and can irreversibly alter its mechanical properties.
4. It is critical to select the appropriate probe for each AFM experiment. There are two critical parameters that define the AFM probe: (1) cantilever spring constant and (2) tip radius of curvature. The cantilever spring constant determines the sensitivity of the AFM to the mechanical properties of the sample. Tip radius defines the image quality and resolution

during scanning. Silicon-nitride cantilevers with spring constant values ranging from 0.01 to 0.06 N/m are typically used for imaging and mechanical testing of biological material because these probes are sensitive to forces in the picoNewton (pN) and nanoNewton (nN) range. Also, the tip geometry (i.e., pyramidal, flat, conical, rounded, spherical) is a crucial parameter to consider in AFM applications. High-resolution probes (10–20 nm) are optimized for measuring local properties of the sample at the nanometer scale.

5. Never use sharp metal tweezers when mounting the AFM probe onto the cantilever holder because the CantiClip lens might be permanently damaged.
6. Breast tissue can be kept for up to 3 days in a Ringer Complete solution at 4 °C, without deterioration of RNA bands [20].
7. Keep a small amount of mixed glue outside the TPP to check the hardening process.
8. It is important to experimentally determine the spring constant (e.g., by thermal noise) and the sensitivity of each cantilever before starting AFM experiments. Measured spring constants can differ from nominal manufacturer values and are crucial for accurate force control on the sample.
9. On the DNP-S10 chips, the "D" cantilever is the softest ($k = 0.06$ N/m), hence the longest and thinnest of the four levers. Make sure that this lever is in the middle of the CantiClip holder and its lens. For easier handling remove the neighboring cantilever by touching it with tweezers. Here a magnifying glass is helpful.
10. Ensure that the CantiClip has a clean lens by washing it with soap, water and ethanol if necessary. Poor laser alignment significantly reduces curve quality. Therefore, the laser must be optimally focused on the cantilever.
11. For the "D" cantilever on the DNP-S10 chip the optimal cantilever frequency should be between 18 and 20 kHz with a Q-factor of 30–34. If the baseline shows a sinusoidal pattern with a period of about 600 nm, the laser light is passing the cantilever. In this case center the laser correctly. Note: .nid files do not store deflection sensitivity values. These need to be user-recorded.
12. Be aware that air bubbles may interfere with the laser path through the CantiClip lens to the photodiode. They can be removed by lifting the scan-head and reinserting it back to the liquid. Another way is by gently applying the buffer drop to the side and flushing the bubbles away.
13. Allow the prepared sample to equilibrate with the environment temperature. Differences in temperature between the cooled sample solution and the instrumentation will cause set-point

drift, changing the force applied to the sample. This can lead to erroneous results. It is recommended to prepare the sample before setting up the AFM.

14. The non-contact region or force-curve baseline needs to be at least 20 % of the complete piezo-distance for proper tilt correction (Subheading 3.4, **step 4**).
15. The software will send an e-Mail notification if the measurement was interrupted by an error. Try to determine the cause of the error and repeat the relevant steps. The prevalent cause arises from a loss of laser signal when the cantilever crashes into the sample or impurities and bubbles contaminating the AFM tip.
16. It is recommended to replenish the Ringer Complete solution every 2.5 h when extensive experiments are planned.
17. Stain the side of the sample that has not been measured with Indian ink and let it set for a minute. Remove excess with blotting paper, afterwards fix the sample in formalin solution and store at 4 °C overnight. Then proceed with the standard protocol by applying steps of ethanol dehydration and paraffinization.
18. Always use the same bin-width for histograms that you want to compare.

Acknowledgments

This work is funded by the Commission for Technology and Innovation (CTI) Project 11977.2 PFNM-NM; ARTIDIS 'Automated and Reliable Tissue Diagnostics' awarded to R.Y.H.L. in partnership with Nanosurf AG.

The authors thank Christian Räz, Christophe A. Monnier and Philipp Oertle for their contributions to this manuscript.

Competing financial interests: The University of Basel has filed patents on the technology and intellectual property related to this work based on the inventions of M.P. and R.Y.H.L.

References

1. Hoffman BD, Crocker JC (2009) Cell mechanics: dissecting the physical responses of cells to force. Annu Rev Biomed Eng 11:259–288
2. Janmey PA, McCulloch CA (2007) Cell mechanics: integrating cell responses to mechanical stimuli. Annu Rev Biomed Eng 9:1–34
3. Mammoto T, Mammoto A, Ingber DE (2013) Mechanobiology and developmental control. Annu Rev Cell Dev Biol 29(29):27–61
4. Mammoto T, Ingber DE (2010) Mechanical control of tissue and organ development. Development 137:1407–1420
5. Plodinec M, Schoenenberger CA (2010) Spatial organization acts on cell signaling: how physical force contributes to the development of cancer. Breast Cancer Res 12:308
6. Chasiotis I, Fillmore HL, Gillies GT (2003) Atomic force microscopy measurement of cytostructural elements involved in the nanodynamics of tumour cell invasion. Nanotechnology 14:557–561
7. Coughlin MF, Bielenberg DR, Lenormand G, Marinkovic M, Waghorne CG, Zetter BR, Fredberg JJ (2013) Cytoskeletal stiffness,

friction, and fluidity of cancer cell lines with different metastatic potential. Clin Exp Metastasis 30:237–250

8. Wirtz D, Konstantopoulos K, Searson PC (2011) The physics of cancer: the role of physical interactions and mechanical forces in metastasis. Nat Rev Cancer 11:512–522
9. Binnig G, Quate CF, Gerber C (1986) Atomic force microscope. Phys Rev Lett 56:930–933
10. Fuhrmann A, Staunton JR, Nandakumar V, Banyai N, Davies PCW, Ros R (2011) AFM stiffness nanotomography of normal, metaplastic and dysplastic human esophageal cells. Phys Biol 8
11. Bastatas L, Martinez-Marin D, Matthews J, Hashem J, Lee YJ, Sennoune S, Filleur S, Martinez-Zaguilan R, Park S (2012) AFM nano-mechanics and calcium dynamics of prostate cancer cells with distinct metastatic potential. Biochim Biophys Acta 1820:1111–1120
12. Cross SE, Jin YS, Lu QY, Rao JY, Gimzewski JK (2011) Green tea extract selectively targets nanomechanics of live metastatic cancer cells. Nanotechnology 22:215101
13. Lekka M, Wiltowska-Zuber J (2009) Biomedical applications of AFM, Nano 2008: 2nd national conference on nanotechnology. J Phys Conf Ser 146:012023
14. Darling EM, Zauscher S, Block JA, Guilak F (2007) A thin-layer model for viscoelastic, stress-relaxation testing of cells using atomic force microscopy: do cell properties reflect metastatic potential? Biophys J 92:1784–1791
15. Cross SE, Jin YS, Rao J, Gimzewski JK (2007) Nanomechanical analysis of cells from cancer patients. Nat Nanotechnol 2:780–783
16. Paszek MJ, Weaver VM (2004) The tension mounts: mechanics meets morphogenesis and malignancy. J Mammary Gland Biol Neoplasia 9:325–342
17. Levental KR, Yu HM, Kass L, Lakins JN, Egeblad M, Erler JT, Fong SFT, Csiszar K, Giaccia A, Weninger W, Yamauchi M, Gasser DL, Weaver VM (2009) Matrix crosslinking forces tumor progression by enhancing integrin signaling. Cell 139:891–906
18. Krouskop TA, Wheeler TM, Kallel F, Garra BS, Hall T (1998) Elastic moduli of breast and prostate tissues under compression. Ultrasonic Imaging 20:260–274
19. Lopez JI, Kang I, You WK, McDonald DM, Weaver VM (2011) In situ force mapping of mammary gland transformation. Integr Biol UK 3:910–921
20. Plodinec M, Loparic M, Monnier CA, Obermann EC, Zanetti-Dallenbach R, Oertle P, Hyotyla JT, Aebi U, Bentires-Alj M, Lim RY, Schoenenberger CA (2012) The nanomechanical signature of breast cancer. Nat Nanotechnol 7:757–765
21. Loparic M, Wirz D, Daniels AU, Raiteri R, VanLandingham MR, Guex G, Martin I, Aebi U, Stolz M (2010) Micro- and nanomechanical analysis of articular cartilage by indentation-type atomic force microscopy: validation with a gel-microfiber composite. Biophys J 98: 2731–2740
22. Blache U, Silvan U, Plodinec M, Suetterlin R, Jakob R, Klebba I, Bentires-Alj M, Aebi U, Schoenenberger CA (2013) A tumorigenic actin mutant alters fibroblast morphology and multicellular assembly properties. Cytoskeleton 70:635–650
23. Oliver WC, Pharr GM (1992) An improved technique for determining hardness and elastic-modulus using load and displacement sensing indentation experiments. J Mater Res 7:1564–1583
24. Hay JL, Oliver WC, Bolshakov A, Pharr GM (1998) Using the ratio of loading slope and elastic stiffness to predict pile-up and constraint factor during indentation. Fundamentals of nanoindentation and nanotribology vol. 522. pp. 101–106
25. Plodinec M, Loparic M, Suetterlin R, Herrmann H, Aebi U, Schoenenberger CA (2011) The nanomechanical properties of rat fibroblasts are modulated by interfering with the vimentin intermediate filament system. J Struct Biol 174:476–484
26. Mahaffy RE, Park S, Gerde E, Kas J, Shih CK (2004) Quantitative analysis of the viscoelastic properties of thin regions of fibroblasts using atomic force microscopy. Biophys J 86: 1777–1793

Chapter 15

Mathematical Modelling as a Tool to Understand Cell Self-renewal and Differentiation

Philipp Getto and Anna Marciniak-Czochra

Abstract

Mathematical modeling is a powerful technique to address key questions and paradigms in a variety of complex biological systems and can provide quantitative insights into cell kinetics, fate determination and development of cell populations. The chapter is devoted to a review of modeling of the dynamics of stem cell-initiated systems using mathematical methods of ordinary differential equations. Some basic concepts and tools for cell population dynamics are summarized and presented as a gentle introduction to non-mathematicians. The models take into account different plausible mechanisms regulating homeostasis. Two mathematical frameworks are proposed reflecting, respectively, a discrete (punctuated by division events) and a continuous character of transitions between differentiation stages. Advantages and constraints of the mathematical approaches are presented on examples of models of blood systems and compared to patients data on healthy hematopoiesis.

Key words Mathematical model, Population dynamics, Structured population models, Stem cell dynamics, Ordinary differential equation

1 Why Do We Need Mathematical Models?

Stem cell processes have multiscale character. Cell division and differentiation are controlled by extracellular signals, originating from the environment or from other cells and from intracellular networks. Due to the new technologies of biological data collection an enormous amount of information on a molecular and cellular scale has become available and much has been learned about the molecular components involved in signal transduction during normal and pathological development. However, there exists a gap between molecular knowledge and its integration into macroscopic phenomena that is observable at the tissue level. Much remains unknown about the interaction of components such as genes, epigenetic modifiers, and proteins in health and disease. Due to their multiscale and interactive character these

Maria del Mar Vivanco (ed.), *Mammary Stem Cells: Methods and Protocols*, Methods in Molecular Biology, vol. 1293,
DOI 10.1007/978-1-4939-2519-3_15,

processes are difficult to explain by purely conceptual models. A new paradigm of systems biology calls for tools such as mathematical modelling and analysis to deal with spatial and temporal multiscale aspects. The focus is now shifting towards understanding how different components are integrated into networks and translated to a process observable at the macroscopic scale of a tissue or a whole organism. This can be accomplished using rigorous mathematical techniques.

2 How to Model a Cell Production System?

Cell production systems are self-renewing cell populations that maintain a continuous supply of differentiated functional cells to various parts of a living organism. Since blood is among the simplest and most accessible mammalian tissue systems, its dynamics attracted the attention of biologists and mathematicians a long time ago [15], *see* Ref. [38] for a review on blood systems biology. There exist many different models and approaches to address questions of healthy hematopoiesis and development of blood cancers. Despite differences depending on the type of cells considered, common elements can be found in all cell production systems and their models. Therefore, mathematical methods and models presented in this paper have widespread importance and can be further extended and applied to different systems.

Mathematical models have a long history of applications to biological and medical problems. Depending on the question of interest, different mathematical approaches can be chosen. Large cell populations can be modelled by differential equations describing the change of cell counts over time. Depending on the structure of the considered population and on spatial effects, either ordinary or partial differential equations are applied. A necessary assumption for the application of differential equations is that a given event happens to each individual of a given subpopulation with the same probability (subpopulations behave as a "well mixed tank"). If cell populations can be divided into a finite number of discrete subpopulations, as it can be done in the hematopoietic system, and if spatial interactions can be neglected, a system of ordinary differential equations (ODEs) is obtained, e.g. [16, 18, 21, 25]. In case of a continuum of individual states, partial differential equations of the transport type [7, 30] or delay differential equations can be used [1, 2]. If interactions of cells in space are important, partial differential equations describing change of cell concentrations in time and space can be formulated [39]. To incorporate stochastic effects, branching processes [14] or individual based models can be applied [19, 28, 29]. Individual based models are valid for small populations but become computationally intensive in case of large numbers of individuals.

In this chapter we focus on mathematical modelling of hierarchical cell production systems using systems of ordinary and delay differential equations. We refer to models of healthy hematopoiesis proposed and analyzed in Refs. [8, 21, 26, 32] and extended to account for development of leukemia in Ref. [33] and clonal selection in acute myeloid leukemia in Ref. [35]. Similar models have been applied to describe dynamics of divergent systems such as neurogenesis [40], olfactory system [16, 18], myelodysplastic syndromes [36] as well as to model dynamics of stem cell-initiated cancers, see, e.g., [27, 39]. The aim of this chapter is to present a mathematical approach to describe dynamics of self-renewing and differentiating cell populations, to explain basic mathematical concepts to non-mathematicians and to highlight possibilities of mathematical modelling.

3 How to Model Growth of a Population Using Differential Equations

Let us consider a population of cells $u(t)$ at time t. To describe its time dynamics, we apply an *ODE*

$$\frac{d}{dt}u(t) = f(u(t)), \tag{1}$$

complemented by initial data

$$u(0) = u_0. \tag{2}$$

The equation means that an instantaneous change of the population (or change of the population size per unit of time) is given by a (possibly nonlinear) function f. Hence, f should account for factors that influence this change such as proliferation, cell death, migration, and transformation. The equation is completed by initial data (2) describing initial size of the population, which is given by a value u_0.

The function f and the data u_0 are called *model ingredients*. Certainly, in models describing population dynamics $u_0 \geq 0$. Finding appropriate form of f is the main task of mathematical modelling. It requires not only understanding of biological processes under consideration but also a reasonable estimation, which components of the complex process should be taken into account, and which may be neglected.

Remark 3.1. *The shorthand notation for Eq. 1 is* $\dot{u} = f(u)$.

It is important to see that the variable u does not need to be a one-dimensional (scalar) value but may also be a vector $u=(u_1, u_2, \ldots, u_n)$ describing n different populations or subpopulations and ingredients of the system undergoing time evolution, e.g.

nutrients or signalling molecules. In the vector case, also $f(u)$ is a vector $(f_1(u_1,\ldots,u_n), f_2(u_1,\ldots,u_n),\ldots, f_n(u_1,\ldots,u_n))$ accounting for interactions between different components of the model, such as competition, feedback, and cooperativity.

A model of the form (1)–(2) can be used to accomplish two rather different tasks:

(1) For a given f, in particular a given set of parameters and a given initial condition u_0, compute or approximate a solution $u(t)$ in time points $t>0$; or estimate its qualitative properties, e.g. long-term behavior.

(2) Having data on time dynamics of $u(t)$ (i.e., values in different time points) compute or estimate parameters that are used to construct f.

The latter type of problems are called *inverse problems*. In the remainder of the chapter, we focus on the problems of type (1).

In general, due to possible nonlinearities in f, it is not possible to find a solution analytically, i.e. to find an exact representation of u as a function of time. There are two ways out. One is to apply numerical methods to approximate u, i.e. calculate values of u in subsequent time point and plot the resulting curve. Such methods are implemented and available as software packages (ODE solvers). The other way is to study qualitative behavior of solutions, i.e. apply mathematical tools to investigate how solutions of the model behave depending on initial data and model parameters.

Mathematical theory of ODEs is well developed and provides tools for the investigation of the dynamics of the models. When studying the time dynamics of a population, we would like to know if (and when) it is growing and declining and if it can stabilize at some *equilibrium* point, where "point" refers to a population constant in time. We may then investigate existence and stability of *stationary solutions* of the model (also called steady states), i.e. search for solutions $u(t)$, which stay constant in time. We denote these by $\overline{u}$. Hence, the values of $\overline{u}$ are trajectories with time derivative equal to zero. The form of the differential equation gives us immediately the implicit formula for $\overline{u}$,

$$f(\overline{u}) = 0,$$

which can be solved explicitly in many cases, even if the time-dependent equation cannot be solved. Clearly, the steady state equation may have several solutions and a question of their stability arises. Mathematical analysis requires a precise notion of stability. Roughly speaking, the equilibrium is *stable* if any solution starting close to this equilibrium stays in its neighborhood; it is *asymptotically stable* if it converges to an equilibrium for large times and it is *unstable* if it is not stable. We may speak about *local stability* if we analyze only the behavior of solutions in the neighborhood of

equilibria and *global stability*, if any initial population converges to this equilibrium, even the ones starting far away. Classical methods of mathematical analysis allow to study stability and destabilization of stationary solutions depending on the structure and parameters of the right-hand side function f. The destabilization of a certain equilibrium may lead to unbounded growth of solutions, convergence to another equilibrium or emergence of oscillations. In multidimensional systems very complex dynamics may be observed.

We illustrate the above concepts on two basic examples of ODE models describing growth dynamics of a population. The examples involve a simple form of the right-hand side function f and describe the resulting dynamics.

Example 3.2. *Linear ODE,* $f(u) = au$.

The equation describes the situation in which a change of population in time unit is linear in its current size. The solution of this equation can be calculated. We obtain

$$u(t) = u_0 e^{at}.$$

Clearly, for positive initial data $u_0 > 0$, for $a > 0$ it describes exponential growth, whereas for $a < 0$ solutions decline exponentially to zero, *see* Fig. 1 for numerical solutions. If $u_0 = 0$, the solution stays constant equal to zero. Hence, $\bar{u} = 0$ is a stationary solution of the model. For $a \neq 0$ this stationary solution is unique, since it is the only solution $\bar{u}$ such that $f(\bar{u}) = 0$. The stability of $\bar{u} = 0$ depends on the value of the growth parameter a. For $a > 0$, it is unstable, while for $a < 0$ it is globally asymptotically stable.

Furthermore, in case of $a = 0$, we obtain a stationary solution for any initial data, i.e. the population always stays constant in time.

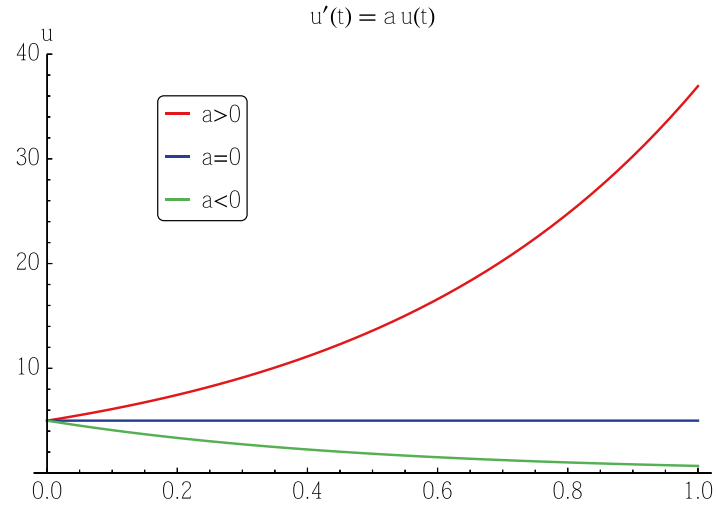

Fig. 1 Solutions of the model of exponential growth with different growth coefficients

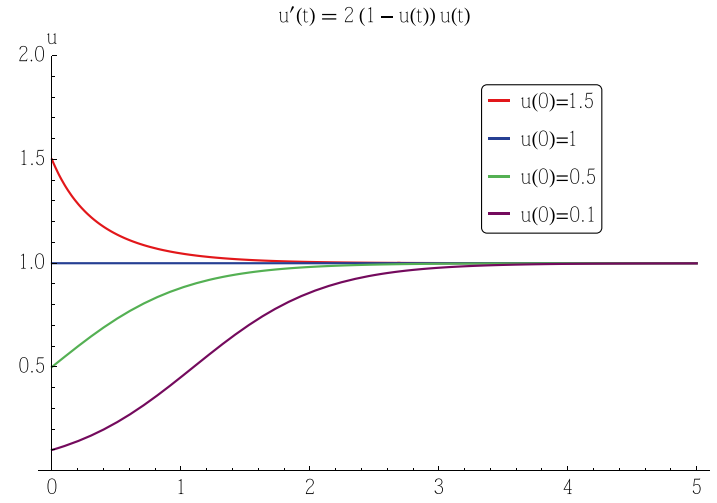

Fig. 2 Solutions of the logistic growth model with different initial data

It is a degenerated case and we observe infinitely many stationary solutions, although none of them is asymptotically stable, since a small perturbation always leads to a new stationary solution. Such models can be used to describe, for example, a population of bacteria proliferating without constraints.

Example 3.3. *Logistic ODE with* $f(u) = au(K - u)$. *Here, we restrict ourselves to positive parameters* $a > 0$ and $K > 0$.

This equation describes a growth with a saturation effect. It is also called the Verhulst model. The constant K models a carrying capacity of the population. Simulations of the model are presented in Fig. 2.

The equation can be also solved explicitly. We obtain

$$u(t) = \frac{Ce^{at}}{1 + \frac{C}{K}e^{at}},$$

where $C = \frac{Ku_0}{K - u_0}$ is a constant depending on the initial data. To understand the long time dynamics of the model, we set $t \to +\infty$ and see that if $u_0 > 0$, then $u(t) \to K$. It means that, independent of the initial data, for long times the size of population tends to the carrying capacity value, as long as the initial size of population is positive.

The long time dynamics can also be deduced without calculating the explicit formula for the solution. Setting $f(\bar{u}) = 0$, we calculate the two stationary solutions $\bar{u}_1 = 0$ and $\bar{u}_2 = K$. Changes of $f(u)$ in the neighborhood of $\bar{u}_1$ and $\bar{u}_2$ indicate that $\bar{u}_1 = 0$ is always unstable (solutions diverge away from zero), and that $\bar{u}_2 = K$ is a

globally asymptotically stable equilibrium. Indeed, since the right-hand side of the equation is strictly positive for $0 < u < K$, the equation describes a situation, in which the size of the population grows as long as it is smaller than K. If we set initially $u > K$, then the right-hand side is negative and the population decays as long as u does not reach the value K.

In case of more complicated models, especially when considering systems of equations, stability of stationary solutions can be investigated using classical tools of mathematical analysis such as *linear stability analysis* for local properties and *Lyapunov functions* for global dynamics. Such methods have been applied to the stem cell models which we present in the next section.

4 Multi-compartment Models of Cell Differentiation

4.1 Compartmental Structure

One established method of modelling of hierarchical cell systems is to use ODEs describing dynamics of cells at different maturation stages and transitions between the stages. Such a model choice is based on the classical understanding of the hematopoietic system, with all lineages originating from the hematopoietic stem cells (HSC) that give rise to different discrete populations of progenitor cells producing mature blood cells [10, 12, 13]. For simplicity the model is restricted to one cell lineage.

We assume that the system consists of n differentiation stages, corresponding to n subpopulations, denoted by u_i, $i = 1, \ldots, n$. Since the system is based on an ordered sequence of different maturation states, so-called compartments, we call it *multi-compartment*. To describe time evolution of cell populations, $u_i(t)$, $i = 1, \ldots, n$ for $t \geq 0$, we apply ODEs of the form (1)–(2). Equations for the cell counts follow from an accepted model of cell cycle which is treated as a well-mixed tank, from which cells may either enter division or death and the length of cell cycle is equally distributed among individuals. Since the hematopoietic system consists of large numbers of cells (of the order of 10^9 leukocytes per liter blood) differential equations are a suitable tool to describe the processes of interest [12, 17].

The main step in building our model is the construction of specific functions $f(u) = f(u_1, \ldots, u_n) = (f_1(u_1, \ldots, u_n), \ldots, f_n(u_1, \ldots, u_n))$. The model is based on the assumption that dynamics of each compartment are determined by its growth due to self-renewing proliferation and differentiation of cells from the previous compartment and cell death. The whole process is regulated by feedback mechanisms based on the assumption that there exist signalling molecules (cytokines) which regulate differentiation and proliferation processes. The intensity of the signal is denoted by $s(t)$. We assume that it depends on the level of mature cells, $s(t) = s(u_n(t))$. The specific

choice of this feedback function and its derivation is presented in the next subsection.

The concentration of the stem cell population at time t is denoted by $u_1(t)$ and the concentration of signalling molecules by $s(t)$. The time evolution of the cell system is described by the system of ODEs

$$\begin{aligned} \frac{du_1(t)}{dt} &= h_1(s(t), u_1(t)), \\ \frac{du_2(t)}{dt} &= h_2(s(t), u_2(t)) + g_1(s(t), u_1(t)), \\ &\vdots \quad \vdots \quad \vdots \\ \frac{du_n(t)}{dt} &= h_n(s(t), u_n(t)) + g_{n-1}(s(t), u_{n-1}(t)). \end{aligned} \tag{3}$$

The term $g_i(s(t), u_i(t))$ denotes the inflow of cells from the maturation stage i to the maturation stage $i + 1$ due to differentiation. Since we neglect any de-differentiation events we assume that $g_i(s(t), u_i(t))$ is nonnegative. The term $h_i(s(t), u_i(t))$ denotes a change of $u_i(t)$ that is caused by processes taking place at the ith stage of maturation. If the gain of cell counts caused by proliferation and self-renewal is stronger than the loss caused by differentiation or death, then $h_i(s(t), u_i(t))$ is positive. Otherwise $h_i(s(t), u_i(t))$ is negative. Since mature cells do not proliferate, the term $h_n(s(t), u_n(t))$ accounts only for cell death and is therefore negative (Fig. 3).

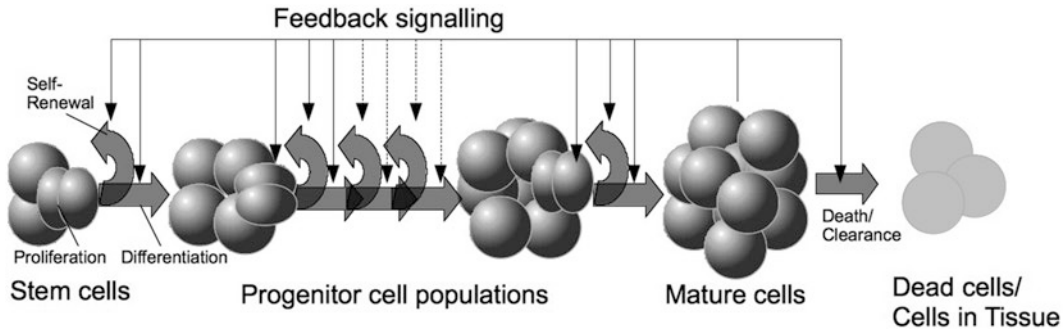

Fig. 3 Schematic illustration of the model assumptions: within a tissue, a cell population (or cell lineage) consists of several differentiation stages (compartments). Cell counts in each compartment change due to proliferation leading to self-renewal and differentiation, and cell death. Cell self-renewal and differentiation are regulated by signalling feedback. Mature cells do not divide and ultimately die. The system is regulated through a signalling feedback depending on mature cell count

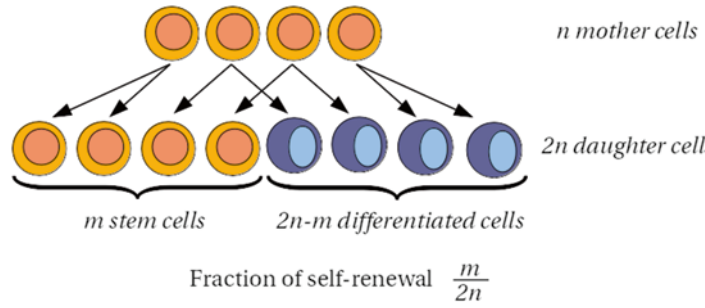

Fig. 4 Illustration of the fraction of self-renewal which is the fraction of daughter cells that belong to the same sub-population as the mother cell

4.2 Modelling of Cell Kinetics

To parameterize functions g_i and h_i, we introduce the following specification of the model ingredients:

- *Proliferation rate*, describing how often a cell divides per unit of time.
- *Fraction of self-renewal*, describing the fraction of daughter cells returning to the compartment occupied by the mother cells (Fig. 4).
- *Death rate*, describing how many cells die per unit of time.

For simplicity, we assume that under healthy conditions proliferating cells do not die and that post-mitotic mature blood cells die at a constant rate.

We remark that the fraction of self-renewal is the probability that a daughter cell belongs to the same sub-population as the mother cell.

In general, these three modelling ingredients may change during the maturation process due to feedback signal. Denote the proliferation rate of the subpopulation of type i at time t by p_i, the fraction of self-renewal by a_i and the death rate by d_i. Then, the count of dividing cells per unit of time t is given by $p_i(t)u_i(t)$. The fraction $a_i(t)$ of daughter cells stays undifferentiated. Therefore, the influx to cell population i after cell division is given by $2a_i(t)p_i(t)u_i(t)$ and the flux to the next cell compartment is given by $2(1 - a_i(t))p_i(t)u_i(t)$. The outflux due to death at time t is given by $d_i(t)u_i(t)$. In summary we can specify

$$\begin{aligned} h_i(t) &= (2a_i(t)-1)p_i(t)u_i(t) - d_i(t)u_i(t), \quad \textit{for} \quad 1 \le i \le n-1, \\ g_i(t) &= 2(1-a_{i-1}(t))p_{i-1}(t)u_{i-1}(t), \quad \textit{for} \quad 1 \le i \le n-1, \\ h_n(t) &= -d_n(t)u_n(t). \end{aligned}$$

This leads to the model proposed in Ref. [21].

4.3 Modelling of Signalling Feedback

An important aspect of the modelling is the description of regulatory mechanisms. It is known that the dynamics of cell proliferation and differentiation are controlled by extracellular signaling molecules. The mechanistic nature of these processes remains to be fully elucidated. Different plausible regulatory feedbacks lead to different nonlinearities in the model equations. The models may help to explain which types of interactions lead to stable homeostasis and to efficient reconstitution after a large perturbation or to elucidate the robustness of the system with respect to different regulatory modes.

Motivated by clinical data, we concentrate on cases where feedback signalling depends only on the level of mature cells [31]. We focus on one kind of feedback signal, e.g., G-CSF, which is the major regulator of granulopoiesis [23]. We assume that $a_i(t)$ and $p_i(t)$ depend solely on the feedback signal at time t, i.e., $a_i(t) \equiv a_i(s(t))$ and $p_i(t) \equiv p_i(s(t))$.

Assuming that signalling molecules are secreted by specialized cells at a constant rate α and degraded proportionally to the level of mature cells u_n and at a constant rate β, we obtain the following differential equation for the dynamics of the concentration of signalling molecules, denoted by $S(t)$:

$$\frac{d}{dt}S(t) = \alpha - \mu S(t) - \beta S(t) u_n(t). \tag{4}$$

Based on studies of cytokine kinetics during infections or injuries, we assume that the time scale of cytokine dynamics is much shorter than that of the cell cycle. As a result we obtain a quasi-stationary approximation of $S(t)$ given by a solution of the equation

$$0 = \alpha - \mu S(t) - \beta S(t) u_n(t).$$

Rescaling $s(t) := \frac{\mu}{\alpha} S(t)$ and $k := \frac{\beta}{\mu}$ results in a formula for signal intensity s:

$$s := s(u_n(t)) = \frac{1}{1 + k u_n(t)},$$

which is between 0 and 1, as a result of rescaling.

The above expression reflects the heuristic assumption that the signal intensity achieves its maximum in absence of mature cells and decreases asymptotically to zero if the level of mature cells increases. Another qualitatively similar regulatory function is based on exponential dependence of the signal intensity on mature cell counts, $s(v) = e^{-\text{const} \cdot u_n}$, similar to that in the well-known Lasota–Wazewska model, see, e.g., [37], where the authors developed a mathematical model describing red blood cell population dynamics.

A similar regulatory mechanism has been proposed in Refs. [16, 18] to describe cell proliferation in mammalian olfactory epithelium and applied in Ref. [39] in context of cancer development.

Different plausible regulatory feedback mechanisms are possible and their efficiency can be tested within our mathematical framework. Hypothesis 1 assumes that differentiation is governed by enhancing the rate of proliferation only, while in Hypothesis 2 it is the ratio of the rate of self-renewal to the rate of differentiation that is regulated by external signals. Consequently, two different regulatory modes are considered:

(H1) Regulated $p_i(s) = \dfrac{p_{i,\max}}{1 + ku_n}$ and constant a_i;

(H2) Constant p_i and regulated $a_i(s) = \dfrac{a_{i,\max}}{1 + ku_n}$.

Using methods of local and global stability analysis, it has been found that stable regulation of the cell differentiation system can be achieved under both hypotheses (each leading to a different mathematical model) and that there is a range of parameters and variant feedbacks with the same qualitative outcome [8, 26, 32]. However, numerical simulations of the model solutions demonstrate that the regulation of self-renewal fractions is more efficient and the homeostasis can be achieved in the clinically relevant time scale [21]. Regulation of the rates of proliferation (H2) is not sufficient for that purpose. The results of simulations of both models calibrated to the individual patients data in Ref. [8] are presented in Fig. 5.

Choosing different regulatory feedback we can test another biological hypothesis proposing that overproduction of mature cells might cause inhibition of differentiation to avoid oversupply from stem cell compartment. The fraction of differentiation in absence of the regulation is given by $1 - ai$. Introducing the dependence of the fraction of differentiation on the signal intensity, we obtain

(H3) $(1 - a_i)(s) = \dfrac{1 - a_{i,\max}}{1 + ku_n}$

as the regulated fraction of differentiation. It has been shown in Ref. [8] that this control mechanism, although intuitively plausible, is inefficient and can lead to unbounded growth of the stem cell population.

In summary, model analysis and simulation suggest that the regulation of the self-renewal is an important mechanism for efficient blood reconstitution. Similar conclusions have been drawn using the models of multistage cell lineages applied to regeneration and maintenance of the mouse olfactory epithelium [16, 18]. It has further inspired studies on possible role of regulation of fraction of cell renewal in cancer development, see, e.g., [27, 33, 35, 39].

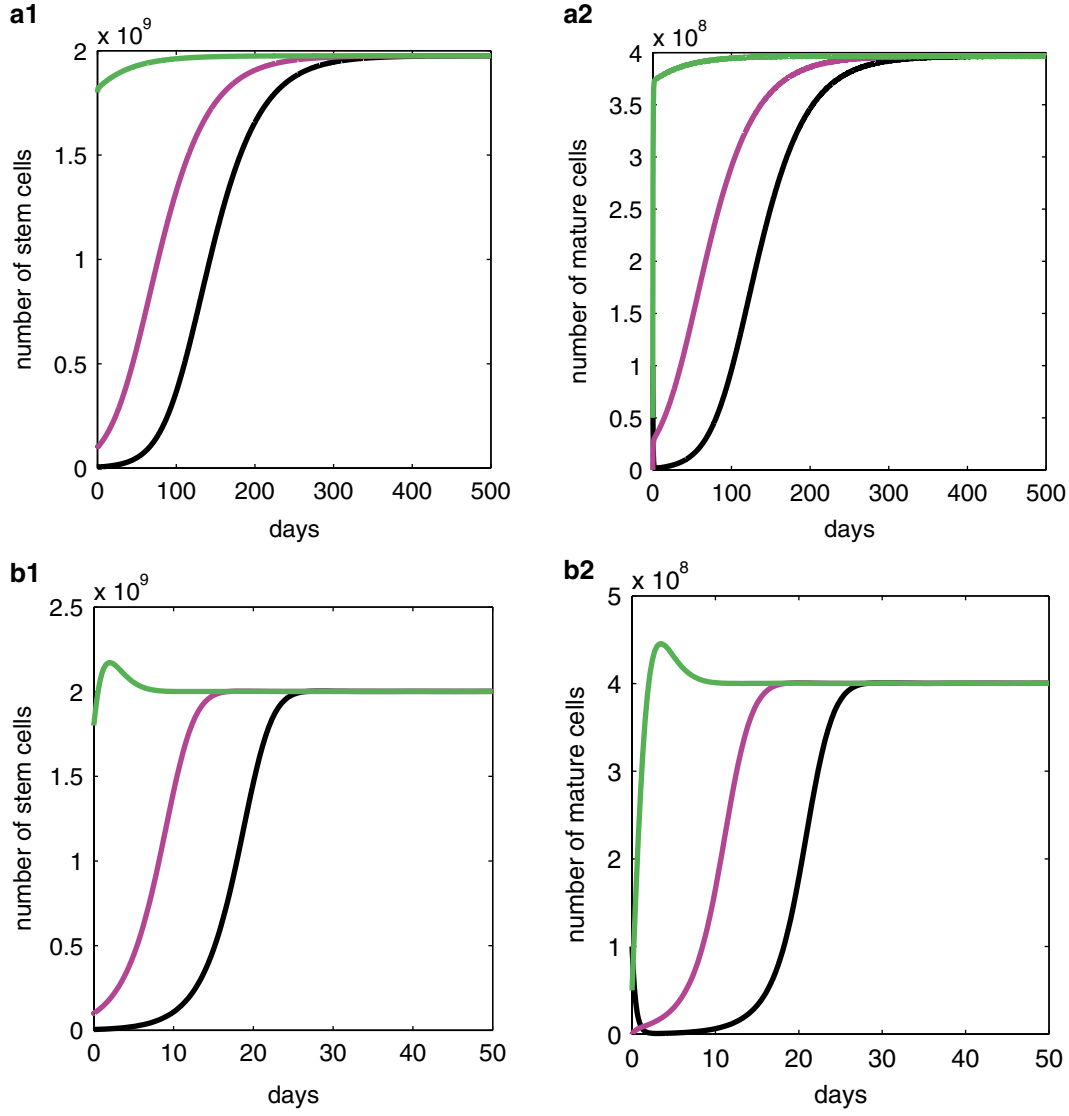

Fig. 5 Simulated solutions of the models with regulated fraction of self-renewal (*lower panel*) versus regulated proliferation (*upper panel*) with different initial conditions (depicted with different colors). The model has been calibrated based on patients' data. Every solution converges to the positive equilibrium. We observe that the regulation of self-renewal fractions leads to a much faster convergence of the solutions to the stable positive equilibrium than the regulation of the division rate. We also note that the solutions of the model with regulated fraction of self-renewal may exhibit overshoot over the steady state value, which are dynamics that are observed in the data obtained from patients during hematopoietic reconstitution after bone marrow transplantation

4.4 Model Reduction: Two- and Three-Compartments

In some cases, the model can be reduced to its basic version, consisting of two equations describing coupled dynamics of undifferentiated and mature cells. As shown in Refs. [8, 26], two-compartment models may capture the reconstitution dynamics of the multi-compartment cell population and can be fitted to the patients' data. This allows to reduce the complexity of the differentiation process to focus on key mechanisms governing the process. It may be also useful when extending the model to account for additional cell types, e.g. in modelling of a competition between healthy and cancer cells.

With three compartments the number of parameters rises and one can observe an increased dependence of the dynamics on the quantitative choices of the parameters. We can identify a parameter range where the unique strictly positive steady state is stable and show that there exists an instability region. The instability may lead to emergence of sustained oscillations. Analysis of the three-compartment model has been carried out in Ref. [26]

4.5 Model Applications and Extensions

The multi-compartmental models have been calibrated based on the data obtained from patients with multiple myeloma after high-dose chemotherapy and stem cell transplantation [20, 34] (Fig. 6). They were further applied to simulate treatment of large patient groups with random interindividual variation [34]. This allowed to develop a model-based methodology for using averaged clinical trial data to estimate responses of individual patients.

The multi-compartment models can be further extended in different directions, among others to address the role of continuous transitions in cell differentiation [2, 7] or to account for replicative senescence [22]. The models have been applied to investigate mechanisms of leukemia development [33]. Models of multi-compartment structure taking into account a multiclonal character of leukemia have been recently studied in Ref. [35].

5 Structured Population Models

In the previous sections we have applied a system of ODEs to model the hierarchical structure of a cell population. Each equation describes a discrete differentiation stage. However, there are indications that the differentiation process is more plastic and that it also involves transitions which are continuous. As an example, cell differentiation without cell divisions is observed during neurogenesis. To describe such a process, we can use the framework of structured population models that applies transport equations [7, 30] and delay differential equations [1, 2]. Note that also multi-compartment

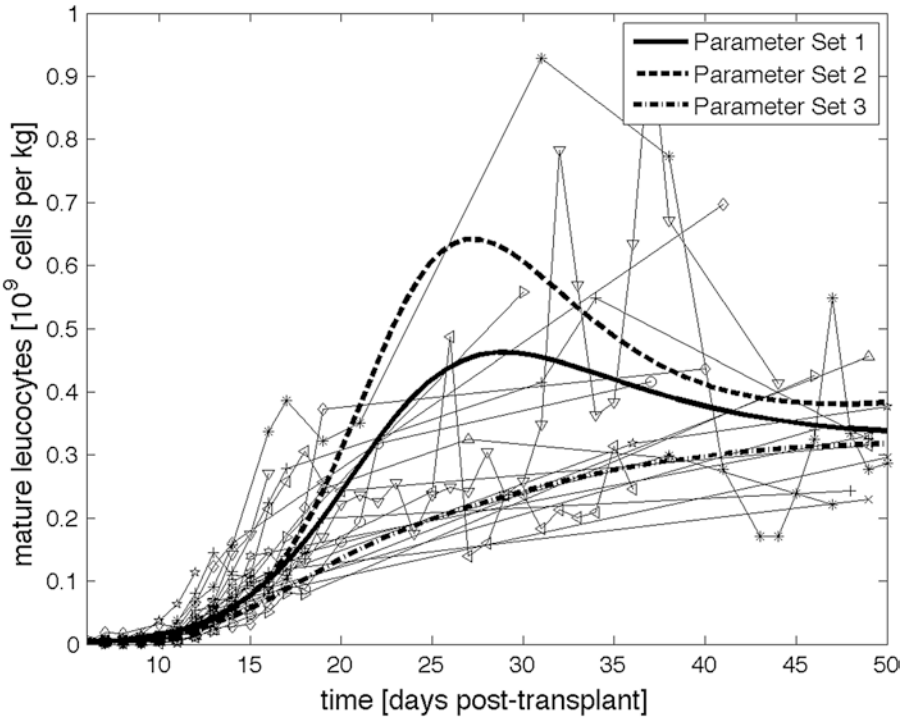

Fig. 6 Application of the multi-compartment model (3) with regulated fractions of self-renewal to blood cell regeneration after stem cell transplantation. The model allows reproducing observable dynamics (peripheral blood cell counts) based on the underlying cellular processes (*thick lines*: sample simulations for three different sets of parameters, *thin lines*: patient data). Please note the heterogeneity of individual patients responses

models incorporate structure in the sense of different behavior of different cells. We here use the word structure in the historical sense where structured populations refer to individual bookkeeping over a continuum of individual stages [3, 5, 6, 24].

5.1 Delay Differential Equation Model

In this section we focus on the description in the framework of delay differential equations. The model we describe in this section was developed and motivated in [2]. An example for a structured population model of cell differentiation in the form of partial differential equations can be found in [7].

We introduce a submodel for progenitor cells that mature through a continuum of stages. For the mathematical formulation and analysis, however, it is useful to start with a formulation of the dynamics of stem and mature cells.

In contrast to the two-compartment model, we here account for continuous maturation with a regulated time delay between commitment to the progenitor phase and full maturation. The regulated delay takes into account all feedback from mature cells that happens to all progenitor cells.

We start with the system of delay differential equations

$$w'(t) = q(v(t))w(t), \tag{5}$$

$$v'(t) = \beta(v(t-\tau(v_t)))w(t-\tau(v_t))f(v_t) - d_v v(t), \tag{6}$$

where w and v denote the number of stem cells and mature cells, respectively. In the following we discuss these equations in detail. For a given time course of development of mature cells $v(t)$, Eq. 5 describes the stem cell dynamics as in the two-compartment model if we define

$$q(v) = [2a(v) - 1]p(v) - d_w,$$

where q is the stem cell net growth rate, i.e., the rate at which the stem cell population changes due to division, self-renewal, differentiation, and death. We define the flow of cells at some level of maturity as the amount of cells passing through this level per time unit. Then, the flow of cells into the progenitor compartment at time θ is given as

$$\beta(v(\theta))w(\theta),$$

where $\beta(v) = 2[1 - a(v)]p(v)$ is the rate of inflow (Fig. 7, left).

Next, we call a *history* a function defined on a negative time interval $[-h, 0]$. For example, the history of the mature cell population may be a function ψ, such that $\psi(\theta)$, $\theta \le 0$, gives the number of mature cells $-\theta$ time units ago (Fig. 8). Moreover, we introduce a notation that is common in functional differential equations, *see* Ref. [9]. We define

$$v_t(\theta) := v(t+\theta), t \ge 0, \theta \le 0,$$

and similarly for w. Then, if t denotes the present, v_t denotes the history of the population density of mature cells at time t (Fig. 8).

Now we can model the inflow of cells into the mature cell compartment. We assume that a cell that neither divides nor dies, fully matures in a finite time, which we call the maturation delay. As in the compartmental model, we assume that the maturation process is regulated by feedback from mature cells.

As a consequence, the delay depends on the history of mature cells. We denote the delay by $\tau(\psi)$, which is the time it takes a committed progenitor cell to fully mature, given it neither dies nor divides, and that at the time of reaching full maturity it has experienced the regulation by a history ψ of mature cells.

Then $\tau(v_t)$ is the length of the progenitor phase, given that full maturity is reached at time t. Moreover $t - \tau(v_t)$ is the moment at which the progenitor phase is entered Fig. 9. Then

$$\beta(v(t-\tau(v_t)))w(t-\tau(v_t))$$

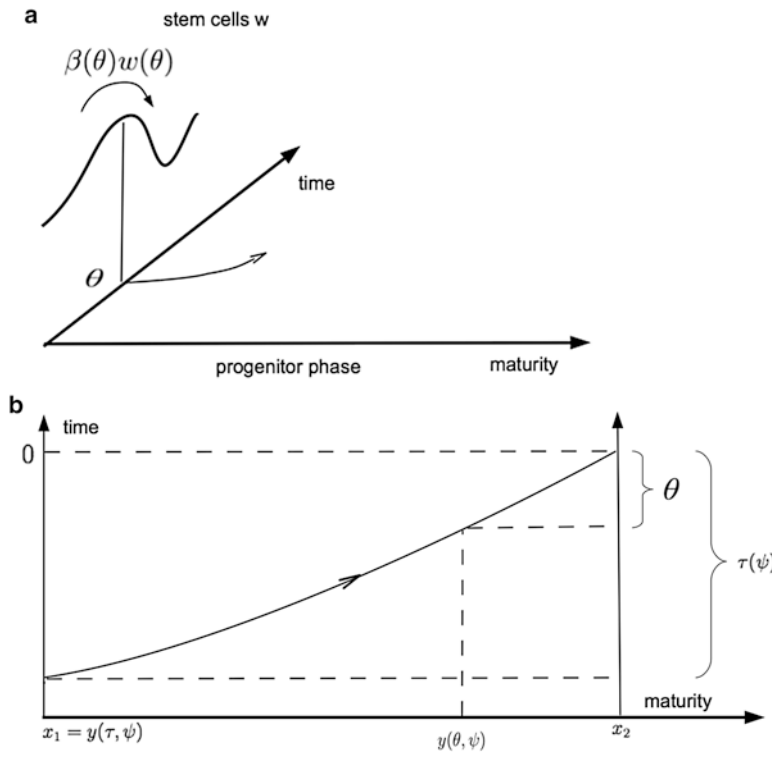

Fig. 7 (**a**) flow of stem cells into the progenitor compartment. (**b**) regulated maturation delay defined as the time to mature from x_1 to x_2

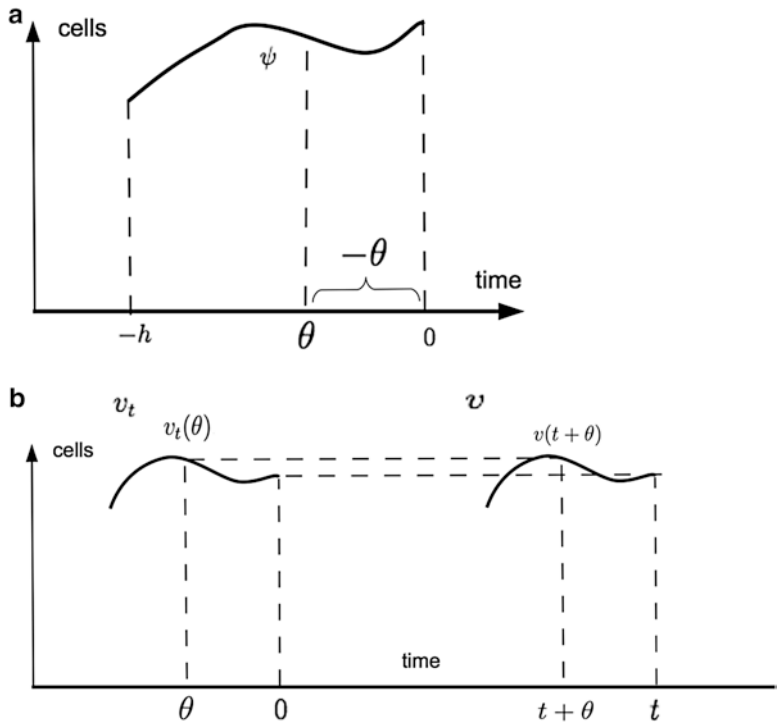

Fig. 8 (**a**) history of mature cells is a function ψ on a negative time interval $[-h, 0]$. (**b**) history v_t of mature cells at time t

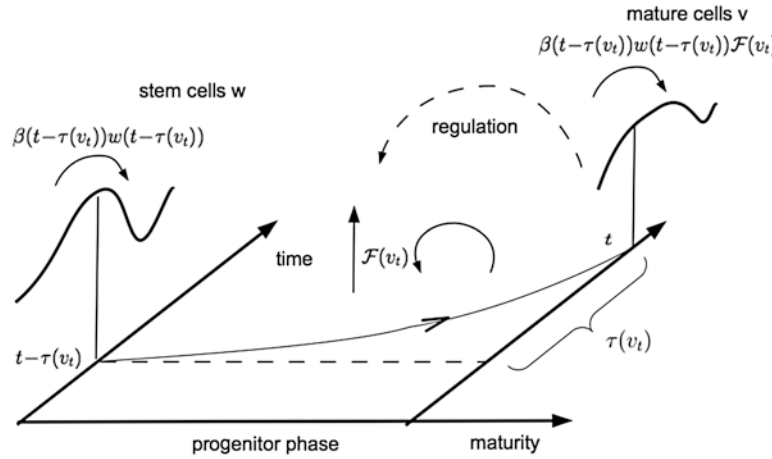

Fig. 9 Delayed inflow of stem cells into the progenitor compartment expressed via regulated progenitor population growth factor

is the inflow into the progenitor compartment of those stem cells that would fully mature at time t if cell counts did not change during the progenitor phase.

To account for the change in numbers, we define the *progenitor population growth factor* $F(\psi)$. It should be such that if (Ψ) is the flow of divided stem cells then $F(\psi)$ is the flow of cells entering the mature cell compartment $\tau(\psi)$ time units later. We conclude that

$$\beta(v(t-\tau(v_t)))w(t-\tau(v_t))F(v_t)$$

is the inflow of mature cells at time t (Fig. 9).

5.2 Specification of Delay

In the following we propose a model for the delay. Divided stem cells that have committed themselves to the progenitor phase enter this phase at a level x_1 of maturity and at level $x_2 > x_1$ they become mature cells, such that the interval $[x_1, x_2]$ represents a continuum of possible maturities (Fig. 7, right panel) for this and the exposition that follows. Suppose that we know a function $y(s,\psi)$ that gives the maturity at the time of $s>0$ time units *before* reaching full maturity, given that history ψ is experienced at full maturity. It holds $y(0,\psi) = x_2$ and we can define the delay $\tau = \tau(\psi)$ as the solution of the equation

$$y(\tau,\psi) = x_1.$$

We can specify y, if we are given a maturation rate $g(x,v)$ that describes the change of maturity of a progenitor cell at some point in time. This rate depends on the maturity $x \in [x_1, x_2]$ of the

progenitor cell and on the number v of mature cells. Then, we define $y(\theta) = y(\theta, \psi)$ through

$$y'(\theta) = -g(y(\theta), \psi(-\theta)), \theta > 0,$$
$$y(0) = x_2.$$

5.3 Specification of Progenitor Population Net Growth Factor

Suppose that we have a given net growth rate $d(x, v)$ of progenitor cells at maturity x regulated by a mature cell population v, where growth refers to changes in numbers of progenitor cells. Then we specify the progenitor growth factor via

$$F(\psi) = e^{\int_0^{\tau(\psi)} \delta(y(\theta,\psi),\psi(-\theta))d\theta}.$$

We can specify δ, if for the progenitor cells we have a proliferation rate $a(x, v)$ and a mortality rate $d(x)$. Then

$$\delta(x, v) = a(x, v) - d(x).$$

An example for a is

$$a(x, v) = \frac{\alpha(x)}{1 + k_\alpha v},$$

see Ref. [2].

5.4 Analysis of the Model

Well-posedness of the model has been analyzed in [2]. This means it is shown that for a certain choice of model ingredients, there exists a unique pair (w, v) that solves (5–6). In [2] we have also computed a formula that gives the density $u(t, \xi)$ of progenitor cells at time t and maturity ξ, such that $\int_x^y u(t, \xi)d\xi$ gives the number of progenitor in a desired interval of maturities $[x, y]$.

Models with a large number of compartments often do not have a unique nontrivial equilibrium, which makes them seem less appropriate for situations where one expects a unique equilibrium and all the more complicates their analysis. It is shown in [2] that the model presented here features a unique equilibrium and expressions for it are computed. As in previous sections we can ask whether cell populations starting close to an equilibrium state will go extinct, stabilize around the equilibrium or whether oscillations will emerge. More precisely, we can ask how dependencies of delays on feedback submodels influence the outcome of the above. Though there exist analytical tools [11] for the stability analysis of differential equations with state-dependent delay, their application to our model remains open.

Acknowledgements

PG was supported by the German Research Council (DFG) and the Spanish Ministry of Economy and Competitiveness under project MTM 2010-18318. AM-C was supported by the Collaborative Research Center, SFB 873 "Maintenance and Differentiation of Stem Cells in Development and Disease." The authors would like to thank Thomas Stiehl and Marcel Mohr for help in preparation of figures.

References

1. Adimy M, Crauste F (2012) Delay differential equations and autonomous oscillations in hematopoietic stem cell dynamics modeling. Math Model Nat Phenom 7(06):1–22
2. Alarcón T, Getto Ph, Marciniak-Czochra A, Vivanco MdM (2011) A model for stem cell population dynamics with regulated maturation delay. Discrete Continuous Dyn Syst B (Suppl):32–43
3. Diekmann O, Getto Ph (2005) Boundedness, global existence and continuous dependence for nonlinear dynamical systems describing physiologically structured populations. J Differ Equ 215:268–319
4. Diekmann O, van Gils S, Verduyn Lunel SM, Walther H-O (1995) Delay equations, functional-, complex-, and nonlinear analysis. Springer, New York
5. Diekmann O, Gyllenberg M, Huang H, Kirkilionis M, Metz JAJ, Thieme HR (2001) On the formulation and analysis of general deterministic structured population models II. Nonlinear theory J Math Biol 43:157–189
6. Diekmann O, Getto Ph, Gyllenberg M (2007) Stability and bifurcation analysis of Volterra functional equations in the light of suns and stars. SIAM J Math Anal 39(4):1023–1069
7. Doumic M, Marciniak-Czochra A, Perthame B, Zubelli J (2011) Structured population model of stem cell differentiation. SIAM J Appl Math 71:1918–1940
8. Getto Ph, Marciniak-Czochra A, Nakata Y, Vivanco MdM (2013) Global dynamics of two-compartment models for cell production systems with regulatory mechanisms. Math Biosci 245:258–268
9. Hale JK, Verduyn Lunel SM (1991) Introduction to functional differential equations. Springer, New York
10. Handin RI, Lux SE, Stossel TP (2003) Blood: principles and practice of hematology, 2nd edn. Lippincott, Phiadelphia
11. Hartung F, Krisztin T, Walther H-O, Wu J, Functional differential equations with state dependent delays: theory and applications. In: Handbook of differential equations: ordinary differential equations, vol 4. Elsevier, Amsterdam
12. Jandl JH (1996) Blood cell formation. Little, Brown and Company, Boston
13. Kaushansky K, Lichtman AM, Beutler LE, Kipps TJ, Prchal J, Seligsohn U (2010) Williams hematology, 8th edn. Mcgraw-Hill Professional, New York
14. Kimmel M, Axelrod DE (2002) Branching processes in biology. Springer, New York
15. Lajtha LG et al (1969) Kinetic properties of haemopoietic stem cells. Cell Prolif 2:39–49
16. Lander A, Gokoffski K, Wan F, Nie Q, Calof A (2009) Cell lineages and the logic of proliferative control. PLoS Biol 7:e1000015
17. Lansdorp PM (1998) Stem cell biology for the transfusionist. Vox Sang 74(Suppl. 2): 91–94
18. Lo W, Chou C, Gokoffski K, Wan F, Lander A, Calof A, Nie Q (2009) Feedback regulation in multistage cell lineages. Math Biosci Eng 6:59–82
19. Loeffler M, Roeder I (2002) Tissue stem cells: definition, plasticity, heterogeneity, self-organization and models - a conceptual approach. Cells Tissues Organs 171:8–26
20. Marciniak-Czochra A, Stiehl T (2011) Mathematical models of hematopoietic reconstitution after stem cell transplantation. In: Bock HG, Carraro T, Jaeger W, Koerkel S, Rannacher R, Schloeder JP (eds) Model based parameter estimation: theory and applications. Springer, Heidelberg

21. Marciniak-Czochra A, Stiehl T, Ho AD, Jäger W, Wagner W (2009) Modeling asymmetric cell division in hematopoietic stem cells—regulation of self-renewal is essential for efficient repopulation. Stem Cells Dev 18: 377–386
22. Marciniak-Czochra A, Stiehl T, Wagner W (2009) Modeling of replicative senescence in hematopoietic development. Aging (Albany NY) 1:723–32
23. Metcalf D (2008) Hematopoietic cytokines. Blood 111:485–491
24. Metz JAJ, Diekmann O (1986) The dynamics of physiologically structured populations. In: LNB, vol 68. Springer, New York
25. Michor F, Hughes TP, Iwasa Y, Branford S, Shah NP, Sawyers CL, Nowak MA (2005) Dynamics of chronic myeloid leukaemia. Nature 435:1267–1270
26. Nakata Y, Getto P, Marciniak-Czochra A, Alarcon T (2011) Stability analysis of multi-compartment models for cell production systems. J Biol Dyn. http://dx.doi.org/10.1080/17513758.2011.558214 [published online]
27. Rodriguez-Brenes IA, Wodarz D, Komarova NL (2013) Stem cell control, oscillations, and tissue regeneration in spatial and non-spatial models. Front Oncol 3:82
28. Roeder I, Kamminga LM, Braesel K, Dontje B, de Haan G, Loeffler M (2005) Competitive clonal hematopoiesis in mouse chimeras explained by a stochastic model of stem cell organization. Blood 105:609–616
29. Roeder I, Horn K, Sieburg HB, Cho R, Muller-Sieburg C, Loeffler M (2008) Characterization and quantification of clonal heterogeneity among hematopoietic stem cells: a model-based approach. Blood 112:4874–4883
30. Roeder I, Herberg M, Horn M (2009) An age structured model of hematopoietic stem cell organization with application to chronic myeloid leukemia. Bull Math Biol 71:602
31. Shinjo K, Takeshita A, Ohnishi K, Ohno R (1997) Granulocyte colony-stimulating factor receptor at various differentiation stages of normal and leukemic hematopoietic cells. Leuk Lymphoma 25:37–46
32. Stiehl T, Marciniak-Czochra A (2011) Characterization of stem cells using mathematical models of multistage cell lineages. Math Comput Model 53:1505–1517
33. Stiehl T, Marciniak-Czochra A (2012) Mathematical modelling of leukemogenesis and cancer stem cell dynamics. Math Model Nat Phenom 7:166–202
34. Stiehl T, Ho AD, Marciniak-Czochra A (2013) The impact of CD34+ cell dose on engraftment after stem cell transplantations: personalized estimates based on mathematical modeling. Bone Marrow Transplant. doi:10.1038/bmt.2013.138 [published online]
35. Stiehl T, Baran N, Ho AD, Marciniak-Czochra A (2014) Clonal selection and therapy resistance in acute leukemias: mathematical modelling explains different proliferation patterns at diagnosis and relapse. J R Soc Interface 11: 20140079. http://dx.doi.org/10.1098/rsif.2014.0079
36. Walenda T, Stiehl T, Braun H, Fröbel J, Ho AD, Schroeder T, Goecke T, Germing U, Marciniak-Czochra A, Wagner W (2014) Feedback signals in myelodysplastic syndromes: increased self-renewal of the malignant clone suppresses normal hematopoiesis. PLOS Comput Biol doi:10.1371/journal.pcbi.1003599
37. Wazewska-Czyzewska M (1984) Erythrokinetics radioisotopic methods of investigation and mathematical approach. Foreign Scientific Publications Dept. of the National Center for Scientific, Technical, and Economic Information, Springfield
38. Whichard ZL et al (2010) Hematopoiesis and its disorders: a systems biology approach. Blood 115:2339–2347
39. Youssefpour H, Li X, Lander AD, Lowengrub JS (2012) Multispecies model of cell lineages and feedback control in solid tumors. J Theor Biol 204:39–59
40. Ziebell F, Martin-Villalba A, Marciniak-Czochra A (2014) Mathematical modelling of adult hippocampal neurogenesis: effects of altered stem cell dynamics on cell counts and BrdU-labelled cells. J R Soc Interface 11: 20140144

Chapter 16

Mammary Stem Cells: A Clinician's View

José Schneider

Abstract

Mammary stem cells were identified and isolated more than a decade ago and, although much remains to be learned, a lot has been revealed about their properties and behavior. Yet there is a gap between the newly acquired knowledge and its successful clinical application. This chapter presented a critical view from the perspective of a clinician.

Key words Cancer stem cells, Breast cancer, Therapy

In 1964, when I was still a child, the Nobel Prize in Physics was awarded to Charles H. Townes, Nicolay G. Basov and Aleksandr M. Prokhorov for the invention of the laser beam. For decades afterwards, it was common in scientific research circles to comment as a joke that the Nobel Prize had been awarded for an invention which helped exploding dark-colored balloons inside light-colored ones, but had no further practical use whatsoever apart from its appearance as a magical weapon in science-fiction literature and the films derived from it. Well, several decades more had to pass, but who could imagine our present world without the laser beam! It is present in virtually every realm not just of science, but of our daily life as well, from CD-players to those handy pointers we all use during our slide presentations.

Why am I beginning a chapter on stem cells with these reminiscences? Because steps forward in fundamental knowledge always end up influencing our lives, no matter how much later the breakthrough takes place. Also, because it is rather common for some discoveries to be far ahead of their time, and we simply have to get accustomed to the appearance of new paradigms which shatter the existing ones. Times when such events take place are exciting for science, but they tend also to be difficult ones, because it belongs to human nature to stick to the prevalent body of knowledge, and this elicits some fierce resistance against the new one trying to advance. All this, I believe, is applicable to the whole new world that has opened up for us since the role of stem cells in

Maria del Mar Vivanco (ed.), *Mammary Stem Cells: Methods and Protocols*, Methods in Molecular Biology, vol. 1293,
DOI 10.1007/978-1-4939-2519-3_16,

disease, and not only in disease, has become evident during the last years. A whole new branch of Biomedicine based on the use of stem cells, Regenerative Medicine, is developing at fast pace, and the targets that can be envisaged, at least in theory, form the stuff of dreams for a clinician: organs that will not be rejected when transplanted, injured or severed nerves that will regenerate, cardiac muscle that will regenerate after an infarct, and even at a more modest level, autologous endothelium that will coat inert vascular grafts, autologous neural tissue that can be injected directly into the "substantia nigra" of Parkinson patients, just to talk about some experiences that are already ongoing as phase-I and even phase-II trials in some centers.

However, I do not want to give the impression that I am the typical clinician, ignorant of basic research facts, who day-dreams after half-grasping them. Indeed, I belong to the rather skeptical branch, because in my younger years I had the immense fortune to undergo specific training in Molecular Biology, and have been involved to various degrees of depth in basic research ever since, for the past 25 years. And it has been a sobering experience: It began it in 1988–1989, when I happily landed for a post-doc stage in one out of three laboratories in the world which possessed at that time an own model of multidrug-resistant cells overexpressing the MDR1 gene. We were about to conquer the Holy Grail of resistance to chemotherapy, or so we thought, an issue of immense importance to me, being a specialist in Gynecologic Oncology, absolutely frustrated by the results of ovarian cancer therapy. Now, a lot of papers and some two to three decades later, we all know that resistance to chemotherapy is not to be overcome by some magic weapon, and that, alas, it is not mediated by a single resistance gene as we then thought. In fact, the MDR1-gene now belongs to an ever-growing superfamily of ABC transporter genes (the last census speaks of 48 members), and they are by far not the only genes involved in resistance! What I want to say with all this is that I am well aware of the huge gap between the acquisition of new, even life-changing basic knowledge, and the moment of its successful clinical application, if it ever takes place. This said, I would now like to turn to my specific field of gynecological and breast cancer, and try to look optimistically, as far as possible, into the future. In a certain, let us call it "sentimental" way, I am somehow connected to the matter, since the first adult cancer stem cells (CSCs) to be identified in a solid tumor were breast cancer stem cells, back in 2003 [1], and one of my main fields of research over the past decades has been precisely breast cancer. Since then, several facts about cancer stem cells have consolidated, and they are mostly NOT reassuring for the clinician. First and foremost, tumors seem to regenerate from their extremely scant stem cell population after initial successful treatment, even if all remaining cells have been eliminated, and this is due to the fact that said stem

cells are intrinsically resistant against the effects of chemotherapy, and by extension radiotherapy, which conceptually is very similar to the former in its mechanism of action [2]. This characteristic of CSCs is in itself paradoxical, since one would expect an excellent response to chemotherapy from the most undifferentiated of cells to be found in a tumor, as stem cells by definition are. Unfortunately, stem cells in general, not only CSCs, MUST be weaponed against any external aggression, since only they guarantee the regeneration of damaged tissues from scrap, so to say. Tumor cells, and by extension CSCs, as the cunning opportunists they always are, just use this fundamental feature to their advantage. As a consequence, among other features, CSCs constitutionally express known chemotherapy resistance genes, such as one prominent member of the aforementioned ABC transporter superfamily, ABCG2 (also known as BCRP or Breast Cancer Resistance Protein gene). Ironically, ABCG2 is one among relatively few recognized universal stem cell markers [3]. And from bitter past experience with resistance-associated genes, especially those belonging to the ABC transporter family, we very well know that the expression of one of them almost never goes alone, and that if just one of them is expressed at a certain time, the first exposure to chemotherapy, or for that matter, any other external threat to the cell, almost immediately elicits the concomitant expression of many, if not all remaining members of the family, massively reinforcing the resistance mechanisms [4]. The corollary of all this is that CSCs almost never will be eliminated from the tumor cell pool by conventional means, i.e., basically chemotherapy or radiotherapy, or a combination of both. In fact, this is the now accepted reason why, sooner or later, most cancers not surgically eradicated at their most initial stages recur after therapy. On a purely theoretical basis, the way out of this dilemma would be the individual targeting of CSCs and their selective elimination. The idea is simple and elegant, but unfortunately unrealistic at the present stage. The first reason is that there still does not exist a generalized consensus on what is a stem cell and by which combination of markers "stemness" can unequivocally be defined. The very existence of CSCs has even been questioned in a revision on the subject with a telling title [5]. In other words, stem cells are not pitch-black sheep standing out from an immaculate flock of white sheep, but rather darker sheep within an otherwise somewhat dirty community containing perhaps some very clean individuals (the most differentiated cells) on its outer rim. In this context, to afford successful selective killing of just the undesired subjects is illusory, a biological argument that could well be extended to military strategy, as experience tells. Until we agree on a clear definition of what exactly is a cancer stem cell (at variation with less compromising terms such as "precursor cell"), and assuming that the definition will be applicable to CSCs underlying every tumor type (which is to assume quite a lot), we will not be

able to target them effectively and to eliminate them. In the meantime, the only way to mitigate the tumor-regenerating effects of CSCs is to impair their normal function to any possible extent, trying not to harm the normal cells as a collateral effect, which is not always easy. In fact, as already mentioned, CSCs, as tumor cells in general, use perfectly normal mechanisms of growth to their advantage, and to impair them means almost automatically to interfere with often vital functions of normal organs. For instance, it is well known that the Hedgehog, Wnt, and Notch signalling pathways are essential for the replication of CSCs, but the complete inhibition of these pathways, if at all possible, would most probably have a deleterious effect on the tumor-hosting patient. Firstly, there exist warning experiences from the past, such as how the complete blocking of the MDR1 gene product, P-glycoprotein, trying to revert resistance to chemotherapy, resulted in hepatic and renal failure of the patients, for the simple reason that the liver and the kidney used that same extrusion pump as an essential detoxifying mechanism [6]. And secondly, all molecular pathways leading to a common target, such as cell proliferation or apoptosis, are interconnected and function as reciprocal safety mechanisms, so that if one of them is impaired or completely blocked, the remaining tend to take over and thus keep the intended function largely intact. This goes so far that if a principal pathway is blocked, other parallel, even dormant ones are activated to compensate for the loss of function. This is well illustrated in the clinic by the resistance mechanisms which are elicited by the quite effective blocking of the tyrosine kinase pathway in cancer treatment, which is ultimately overcome by the tumor cells in almost every, if not every case [7].

However, I would not like to end on a negative note, and therefore I would like to stress an enormously positive fact, and derive from it the ideal wish list from the sight of a clinician.

The positive, indeed revolutionary fact I would like to stress is that through the recognition of the role of CSCs, our understanding about how a tumor develops, grows and becomes resistant to therapy has completely changed. Not only that, but for the first time we seem to have identified something that lies at the very core of oncogenesis and which provides us, at least in theory, with a target that might reveal itself as decisive if efficiently attacked. And herefrom my personal wish list to our dear colleagues from basic and translational research:

- Take the “mask” off CSCs, i.e., provide us with the means to identify them unequivocally, and once this is achieved.
- Develop targeted therapies able to completely eradicate CSCs without side effects for the host.

Admittedly, it is not an easy task, for all the reasons stated above, but who said this would be an easy journey!

References

1. Al Hajj M, Wicha MS, Benito-Hernández A, Morrison SJ, Clarke MF (2003) Prospective identification of tumorigenic breast cancer cells. Proc Natl Acad Sci U S A 100:15178–15183
2. Hu Y, Fu L (2012) Targeting cancer stem cells: a new therapy to cure cancer patients. Am J Cancer Res 2:340–356
3. Zhou S, Schuetz JD, Bunting KD, Colapietro AM, Sampath J, Morris JJ, Lagutina I, Grosveld GC, Osawa M, Nakauchi H, Sorrentino BP (2001) The ABC transporter Bcrp1/ABCG2 is expressed in a wide variety of stem cells and is a molecular determinant of the side-population phenotype. Nat Med 7:1028–1034
4. Gillet JP, Schneider J, Bertholet V, De Longueville F, Remacle J, Efferth T (2006) Microarray expression profiling of ABC transporters in Human Breast Cancer. Cancer Genomics Proteomics 3:97–106
5. Gupta PB, Chaffer CL, Weinberg RA (2009) Cancer stem cells: mirage or reality? Nat Med 15:1010–1012
6. Volm M (1998) Multidrug resistance and its reversal. Anticancer Res 18:2905–2917
7. Gainor JF, Shaw AT (2013) Emerging paradigms in the development of resistance to tyrosine kinase inhibitors in lung cancer. J Clin Oncol 31:3987–3996

Index

Maria del Mar Vivanco (ed.), *Mammary Stem Cells: Methods and Protocols*, Methods in Molecular Biology, vol. 1293,
DOI 10.1007/978-1-4939-2519-3, © Springer Science+Business Media New York 2015

P

R

S

T

V

W

X